The Role of BNIP3 in Proliferation and Hypoxia-Induced Autophagy: Implications for Cancer Therapy

by

Meghan Brianne Azad

A Thesis submitted to the Faculty of Graduate Studies of
The University of Manitoba
in partial fulfillment of the requirements of the degree of

DOCTOR OF PHILOSOPHY

Department of Biochemistry and Medical Genetics
Faculty of Medicine
University of Manitoba
Winnipeg, Manitoba, Canada

For Hussieni and my parents.
I could never have made it this far without you!

Abstract

Introduction: Autophagy is a regulated degradation pathway functioning in both cell survival and cell death. Its role in cancer is controversial since autophagy can be protective or destructive to tumor cells, depending on individual genetic signatures, stage of malignancy and treatment conditions. Hypoxia is a common feature of solid tumors, correlating with poor prognosis and chemoresistance. We have investigated autophagy in hypoxic cancer cells and examined the role of the hypoxia-inducible protein, BNIP3.

Methods: Multiple cancer cell lines were exposed to chronic hypoxia ($<1\%$ O_2) in the presence or absence of specific inhibitors for autophagy and apoptosis. Cell death was measured by membrane permeability assay, and autophagy was assayed by GFP-LC3 distribution, LC3 processing, electron microscopy, and acidic vacuole formation. BNIP3 was over-expressed by transient transfection, stably induced in a tetracycline-regulated expression system, or knocked down using siRNA. Whole brain morphology, cell proliferation, and hypoxic response were additionally studied in a BNIP3-null mouse model.

Results: Autophagic cell death was detected in hypoxic cancer cells, occurring independent of apoptosis through a mechanism involving BNIP3. BNIP3 itself induced autophagic cell death, and loss of BNIP3 protected against hypoxia-induced autophagy and cell death. Loss of BNIP3 also resulted in differential growth and cell cycle progression *in vitro*, and increased brain cellularity *in vivo* compared to wild type

controls. Potential mediators of resistance to BNIP3-induced cell death were identified using a novel model of BNIP3 resistance.

Conclusions: Taken together, these results support the emerging theory that autophagy represents an alternative cell death pathway that could be targeted in hypoxic and/or apoptosis-resistant tumors. We have specifically identified BNIP3 as a potential target molecule in this pathway. Finally, we have identified a possibly novel role for BNIP3 in brain development and cell cycle regulation.

These findings have important clinical applications given the potential for personalized cancer therapy based on individual tumor characteristics including autophagic capacity, hypoxic status, and BNIP3 activity.

Acknowledgements

This body of work could not exist without the support and guidance of some very special people. First, I would like to thank my supervisor, Dr. Spencer Gibson, for his mentorship during my six years as a graduate student. Under his guidance, I have learned a great deal about the trials and tribulations of academic research, including what it takes to persevere and succeed as an independent investigator.

I am grateful to my advisory committee members, Dr. David Eisenstat, Dr. Michael Mowat, and Dr. Leigh Murphy, who provided crucial guidance as my project changed directions time and again. Leigh has been especially influential in my career development, having patiently mentored me since I was an inexperienced (but eager) summer student with limited knowledge and clumsy technique. I would also like to thank my external examiner, Dr. Richard Hill, for his critical review of my thesis and for traveling to Winnipeg for my oral defense.

Over the years, I have been surrounded by many fantastic people at MICB and within the BMG department. In particular, I would like to acknowledge Nicolle Bristow and Bonnie Tighe (my labmates-turned-bridesmaids), Liz Henson-Hamanishi (my ultimate cheerleader), Brenda Kuschak (my trusted chocolate supplier and confidante), as well as Michelle Brown, Molly Pind, Nichola Wigle and fellow students Teralee Burton, Sara Beiggi, Evan Booy, Paula Espino, Francisco Mendoza and Ju-Yoon Yoon. I also received excellent technical assistance from Eileen McMillan-Ward, Ludger Klews and Yong Qiang Chen.

I would like to thank NSERC and the US Army Department of Defense Breast Cancer Research Program for my studentship funding, as well as the University and the Province of Manitoba for their generous annual top-up funds.

Lastly, I want to acknowledge my friends and family outside of the lab, who have provided invaluable support and encouragement to keep me going through the highs and lows of grad school. To Sam, thank you for your unwavering support – I know I can always count on you for a good laugh and an extra long lunch date! To my parents, thank you for being my biggest fans and for providing me with the foundation to be successful in all aspects of life. Thank you for being my sounding board, and for fostering my scientific curiosity even when I threw magnets at you or caused embarrassing confrontations with the school librarians. To my brothers, thank you for providing a welcome relief from school and science – your sense of humor keeps life in perspective and sometimes that is exactly what I need!

Finally, a huge thank you to my husband, Hussieni. You keep me focused, but you also push me to explore new possibilities. You inspire me to succeed, and you ease my doubts and fears. I couldn't have earned my new title without you!

Table of Contents

List of Tables

List of Figures

List of Abbreviations

3-MA	3-methyladenine
4E-BP1	eukaryotic translation initiation factor-4E-binding protein 1
AIF	apoptosis inducing factor
AMPK	adenosine 5'-monophosphate activated protein kinase
AO	acridine orange
Apaf-1	apoptotic peptidase activator 1
ATG	autophagy
AVO	acidic vesicular organelle
βgal	b-galactosidase
BAD	Bcl-2-associated death promoter
BAK	Bcl-2 homologous antagonist killer
BAX	Bcl-2-associated X protein
Bcl-2	B-cell lymphoma 2
Bcl-xL	Basal cell lymphoma-extra large
BCS	bovine calf serum
BH	Bcl-2 homology
BID	BH3 interacting domain death agonist
BIM	BH3-only protein Bcl-2 family member
BNIP	BCL2/adenovirus E1B 19kDa interacting protein
bp	base pairs
BrdU	5-bromo-2-deoxyuridine
BSA	bovine serum albumin
CAIX	carbonic anhydrase 9
CLU	clusterin
CM-H$_2$DCFDA	5,6-chloromethyl-2′,7′-dichlorodihydrofluofluorescein diacetate
CSC	cancer stem cell
DAPI	4',6-diamidino-2-phenylindole (fluorescent DNA stain)
ddH$_2$O	double distilled water
DCIS	ductal carcinoma in situ
DEVD-AFC	Asp-Glu-Val-Asp-7-amino-4-trifluoromethylcoumerin
DHE	dihydroethidium
DIABLO	Direct IAP Binding Protein with Low PI
DISC	death-inducing signaling complex
DMEM	Dulbecco's modified essential medium
DMSO	dimethyl sulfoxide
ds	double stranded
EBSS	Earle's Balanced Salt Solution
EDTA	ethylenediaminetetraacetic acid
EGFR	epidermal growth factor receptor
ER	endoplasmic reticulum
ERK	extracellular regulated kinases
FACS	fluorescence-activated cell sorting
FADD	Fas-associated protein with Death Domain

FBS	fetal bovine serum
FITC	fluorescein isothiocyanate
FKRH	forkhead transcription factor
FOXO	forkhead box class O
GAPDH	glyceraldehyde 3-phosphate dehydrogenase
GFAP	glial fibrillary acidic protein
GFP	green fluorescent protein
GLUT	glucose transporters
GTPase	guanosine triphosphate hydrolase
GOI	gene of interest
GRB2	growth factor receptor-bound protein 2
HDAC	histone deacetylase
HIF	hypoxia inducible factor
HMGB1	high mobility group box 1
HRE	hypoxia response element
HRP	horseradish peroxidase
HSP	heat shock protein
IF	immunofluorescence
IgG	immunoglobulin G
I/R	ischemia-reperfusion
JNK	Jun N-terminal kinase
kDa	kilodalton
KO	knock-out
LC3	light chain protein 3
Mcl-1	myeloid cell leukemia sequence 1
MAPK	mitogen-activated protein kinase
MEF	mouse embryonic fibroblast
MEK	MAPK and ERK kinase
mETC	mitochondrial electron transport chain
MPTP	mitochondrial permeability transition pore
mRNA	messenger ribonucleic acid
mTOR	mammalian target of rapamycin
MTT	3-(4,5-dimethylthiazol-2-yl)-2,5-diphenyl tetrasodium bromide
NF-L	68kDa light neurofilament subunit
NFκB	nuclear factor kappa-light-chain-enhancer of activated B cells
NIX	BCL2/adenovirus E1B 19kD-interacting protein 3-like
NO	nitric oxide
OCT	optimal cutting temperature
OMM	outer mitochondrial membrane
PAGE	polyacrylamide gel electrophoresis
PBS	phosphate buffered saline
PCD	programmed cell death
PCR	polymerase chain reaction
PDK1	phosphoinositide-dependent kinase 1
PE	phosphatidyl-ethanolamine
PEST	proline-glutamic acid-serine-threonine sequence

PI3K	phosphoinositide 3-kinase
PIP2	phosphatidylinositol 3,4-bisphosphate
PIP3	phosphatidylinositol 3,4,5-trisphosphate
PT pore	mitochondrial permeability transition pore
PTEN	phosphatase and tensin homolog
PUMA	p53 upregulated modulator of apoptosis
RA	rheumatoid arthritis
Rb	retinoblastoma
Rheb	Ras homolog enriched in brain.
RNAi	RNA interference
ROS	reactive oxygen species
rpm	revolutions per minute
RT	room temperature
RT-PCR	reverse transcription – polymerase chain reaction
S6K	S6 kinase
SDS	sodium dodecyl sulfate
siRNA	small interfering RNA
Smac	second mitochondria-derived activator of caspases
SOS	son of sevenless
SSAT	spermidine/spermine N1-acetyltransferase
STAT3	signal transducer and activator of transcription 3
TBE	Tris/Borate/EDTA
t-BID	truncated BH3 interacting domain death agonist
TO	Tet-ON
TR	tetracycline repressor
TBS	Tris-buffered saline
TM	transmembrane domain
TNF	tumor necrosis factor
TRAIL	tumor necrosis factor–related apoptosis-inducing ligand
TSC1/TSC2	tuberous sclerosis complex
UPR	unfolded protein response
UV	ultraviolet
VEGF	vascular endothelial growth factor
VHL	Von Hippel-Lindau
v/v	volume/volume
WB	Western blot
WT	wild-type
Z-VAD-fmk	N-benzyloxycarbonyl-Val-Ala-Asp(O-Me) fluoromethyl ketone

List of Copyrighted Material for which Permission was Obtained

Portions of the following copyrighted materials have been reproduced with permission:

1. Azad MB, Chen Y, Gibson SB. Regulation of autophagy by reactive oxygen species (ROS): implications for cancer progression and treatment. Antioxid Redox Signal. 2009 Apr; 11(4):777-90.

2. Azad MB, Chen Y, Henson ES, Cizeau J, McMillan-Ward E, Israels SJ, Gibson SB. Hypoxia induces autophagic cell death in apoptosis-competent cells through a mechanism involving BNIP3. Autophagy. 2008 Feb 16; 4(2):195-204.

3. Taylor RC, Cullen SP, Martin SJ. Apoptosis: controlled demolition at the cellular level. Nat Rev Mol Cell Biol. 2008 Mar; 9(3):231-41

4. MacFarlane M, Williams AC. Apoptosis and disease: a life or death decision. EMBO Rep. 2004 Jul; 5(7):674-8.

5. Edinger AL, Thompson CB. Death by design: apoptosis, necrosis and autophagy. Curr Opin Cell Biol. 2004 Dec; 16(6):663-9.

6. Coates JM, Galante JM, Bold RJ. Cancer Therapy Beyond Apoptosis: Autophagy and Anoikis as Mechanisms of Cell Death. J Surg Res. 2009 Aug 7. [Epub ahead of print]

Chapter 1: Introduction

1.1   Hallmarks of Cancer

Cancer is a major cause of morbidity and mortality in developed countries. Cancer development, or tumorigenesis, is a multistep process that involves the acquisition of multiple successive genetic, epigenetic or somatic alterations as a result of increasing genomic instability (1). Research over the last several decades has identified numerous cancer-related genes which are altered in human tumors and elicit cancer phenotypes in experimental models. Carcinogenesis frequently involves over-activation of oncogenes (such as *ras* and *bcl-2*) through dominant gain of function mutations, and/or inhibition of tumor suppressor genes (such as *p53* and *PTEN*) through recessive loss of function mutations (2). Together, these alterations enable cancer cells to acquire atypical characteristics including: self-sufficiency in growth signals, insensitivity to anti-growth signals, evasion of cell death, limitless replication potential, abnormal angiogenesis, evasion of the immune system, tissue invasion and metastasis (1). In addition to these "hallmarks of cancer", the tumor microenvironment is considered to be a critical factor in malignancy progression and metastasis (3).

The following sections will provide a detailed introduction to the concepts of hypoxia, autophagy, cell survival and cell death. Each will be discussed broadly as well as from the perspective of cancer progression and treatment. Finally, these topics will be re-examined to delineate the functional role of the Bcl-2 family member, BNIP3, in each context.

1.2   Hypoxia

Oxygen is essential for the development and growth of multicellular organisms. Mammals have therefore evolved a sophisticated network to maintain oxygen homeostasis, since either too much or too little oxygen can have detrimental effects (4). One of the critical aspects of this network is the ability to sense and respond to low-oxygen conditions (hypoxia), a physiological stress encountered during various pathologies including cancer, myocardial infarction, and stroke (5). While the atmosphere contains approximately 21% oxygen, the level in normal human tissue is closer to 5%, which is equivalent to a partial pressure (pO_2) of 38 mmHg (6). Physiological hypoxia results when tissue oxygenation falls below this level, and a complete lack of oxygen (in practice, below 0.02% or 1 mmHg) constitutes anoxia. Oxygen deprivation may be acute (minutes to hours) or chronic (hours to days). Both the level and duration of hypoxia are important determinants of the ensuing cellular response.

Hypoxia-mediated signaling pathways have been extensively studied in recent years, due to their prominent role in development and disease conditions. The cellular response to hypoxia can involve both acute mechanisms such as altered activity of existing proteins, as well as more global changes such as altered gene expression (4). A complete absence of oxygen (anoxia) will quickly result in cell death. By contrast, survival is possible in hypoxia (as little as 0.2% O_2) because cells will initially employ adaptive strategies; however, severe and prolonged hypoxia will ultimately lead to cell death. The precise mechanisms of hypoxia-induced cell death remain unclear as apoptosis, necrosis and autophagy have all been reported in response to hypoxic stress (7-9).

1.2.1 Hypoxia inducible factors (HIFs)

Mammalian cells respond to hypoxia by activating broadly-acting transcription factors, named "hypoxia inducible factors" (HIFs) (10). The HIF family comprises three members: HIF-1, HIF-2 and HIF-3. Of these, HIF-1 is widely considered to be the "master regulator" of hypoxic responses (11). HIFs bind to consensus hypoxia-responsive elements (HREs) in the promoter region of more than 100 hypoxia-inducible genes. The HIF transcription factors are heterodimers composed of two subunits, the oxygen-sensitive HIFα subunit, and the constitutively stable HIFβ subunit. As shown in Figure 1.1, HIF activity is regulated by the HIFα subunit, which under normoxic conditions is rapidly degraded, preventing dimerization (10). HIFs represent the functional link between oxygen sensors and effectors, as detailed below.

1.2.1.1 Regulation of HIFs by oxygen sensors

Eukaryotic cells have developed several mechanisms for sensing changes in oxygen tension. Of these, the best-characterized oxygen sensors are the mitochondrial electron transport chain (mETC), the prolyl hydroxylase family of enzymes (PHDs 1-3), and the factor inhibiting HIF-1 (FIH). Studies have shown that hypoxia paradoxically stimulates the release of reactive oxygen species (ROS) from complex III of the mETC, and that these oxidants can subsequently trigger multiple signaling pathways (12). Alternatively, FIH and/or PHD hydroxylases can be employed to sense changes in oxygen tension and stimulate diverse cellular responses. These enzymes require molecular oxygen for hydroxylation of conserved HIF residues (10). Mitochondria, FIH and PHDs are all

considered as integral members of the oxygen-sensing machinery, since all three are required for optimal hypoxic stabilization and activation of HIF-1α, as discussed below.

The original and simplest model of oxygen-sensing describes PHDs as direct oxygen sensors, since they require molecular oxygen for activity (13). Under normoxic conditions, PHDs hydroxylate HIF-1α at conserved proline residues in the HIF oxygen-dependent degradation domain. The hydroxylated residues are recognized by an E3 ubiquitin ligase (von Hippel-Lindau protein, pVHL), which targets HIF-1α for rapid degradation by the proteasome. Under hypoxic conditions, hydroxylation is limited by the absence of oxygen and HIF-1α can migrate to the nucleus, dimerize with HIF-1β and bind to target gene HREs to activate transcription (13). More recently, FIH was identified and shown to hydroxylate an asparagines residue in the C-terminal HIF transactivation domain, preventing transcriptional activation and providing a second level of control. Both PHDs and FIH are oxygen-dependent; however, PHDs become inactivated below 4% O_2, whereas lower levels are required to inactivate FIH. Consequently, some hypoxia-responsive genes are induced at higher levels of O_2 than others (14). This scenario begins to explain how varying degrees of hypoxia can elicit differential cellular responses. For example, maximal VEGF expression has been observed at 2% O_2, while maximal HIF-1α expression occurs at $0.2 - 1\%$ O_2 (15).

Recent evidence suggests that, although elegantly simple, the PHD/FIH model may not entirely explain the oxygen-dependent stabilization of HIF-1α, since oxygen levels are not sufficiently reduced in hypoxia to completely inhibit FIH and PHDs (12). While

hydroxylases are inarguably the proximal regulators of HIF-1α protein stabilization, it

now appears that the mETC also plays a role. The current prevailing theory asserts that

hypoxia stimulates ROS production from complex III of the mETC, and these ROS

subsequently prevent hydroxylation of HIF-1α by PHDs (12). Although several studies

have clearly demonstrated that mitochondrial ROS are required for hypoxic stabilization

of HIF-1α (16-18), more research is required in order to define the mechanisms by which

ROS affect PHD activity. In summary, FIH, PHDs and the mETC act as oxygen sensors

to co-operatively regulate the activation of HIF-1 in hypoxia (Figure 1.1).
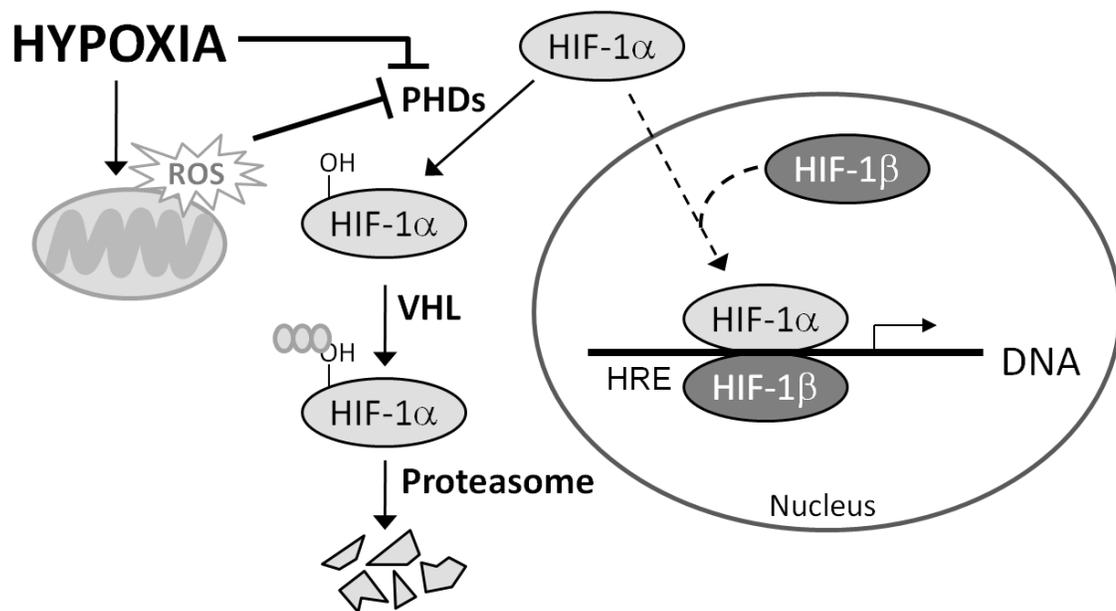
Figure 1.1 HIF-1 activation.
Under normoxic conditions, HIF-1α is rapidly hydroxylated by proline hydroxylases (PHDs), marking HIF-1α for ubiquitination by the Von Hippel Lindau (VHL) E3 ubiquitin ligase, and subsequent degradation by the proteasome. Under hypoxic conditions, PHDs are inhibited by hypoxia-induced mitochondrial ROS and hydroxylation is limited by the absence of oxygen. This stabilizes the HIF-1α protein, allowing for translocation to the nucleus and dimerization with HIF-1β. The HIF-1α/HIF-1β dimer is then able to bind to HIF-1 responsive elements (HREs) in the promoter region of target genes.

1.2.1.2 HIF-1 target genes

HIF-1 regulates more than 100 hypoxia-responsive genes, which are typically involved in three main survival strategies: energy conservation, induction of glycolysis, and induction of angiogenesis (19). Target genes include angiogenic factors such as vascular endothelial growth factor (VEGF) and erythropoietin (EPO), proliferation/survival factors such as insulin-like growth factor-2 (IGF-2) and transforming growth factor-α (TGF-α), as well as glucose transporters such as glucose transporter-1 (GLUT-1), and multiple glycolytic enzymes. HIF-1-mediated induction of these "adaptive" genes is typical in mild hypoxia; however, severe or sustained hypoxia can lead to HIF-1-dependent activation of pro-death genes, such as BNIP3, caspase-3, and p53 (20). This may be achieved through accumulation of ROS and subsequent activation of secondary HIF-1 co-factors. Thus, depending on the duration and severity of hypoxic stress, HIF-1 can mediate both pro-death and pro-survival responses through activation of target genes.

1.2.2   HIF-independent hypoxia signaling

Although HIFs are regarded as the "master regulators" of the hypoxic response, two additional signaling pathways have recently been implicated: signaling through the mammalian target of rapamycin (mTOR) kinase and signaling through activation of the unfolded protein response (UPR). mTOR signaling (described in section 1.5.3) integrates signals from a variety of stimuli to control cell growth and survival through changes in mRNA translation and metabolism. Hypoxia inhibits mTOR activation through several HIF-dependent and -independent mechanisms, leading to suppression of mRNA translation as a means of conserving energy during hypoxic stress (21). Through

mechanisms which remain poorly understood, hypoxia also disrupts endoplasmic reticulum (ER) homeostasis, causing accumulation of unfolded or misfolded proteins in the ER lumen. This in turn triggers the UPR, a signaling program that aims to either restore ER homeostasis or induce cell death (21). The UPR is initiated by ER "stress sensors", integral ER membrane proteins that signal luminal stress to the cytosol and nucleus, with the ultimate consequences of inhibiting overall mRNA translation, inducing protein maturation machinery, and stimulating the degradation and removal of toxic misfolded proteins. Although more research is required to fully characterize the complete spectrum of oxygen-sensitive signaling pathways, it is clear that HIFs, mTOR and the UPR are essential regulators of the hypoxic response.

1.2.3   Hypoxia in human development and disease

Hypoxia is a physiological stress encountered during development, and in various pathologies including myocardial infarction, stroke, neurodegeneration, and rheumatoid arthritis (5). The role of hypoxia in the pathophysiology of cancer will be discussed separately in the following section.

The mammalian embryo develops in a low-oxygen environment, where HIF plays an important role in controlling gene expression, cell behavior and morphogenesis of the embryo and placenta (22). In particular, HIF is an important mediator of heart development (23), migration of neural crest cells (24), and endochondrial bone formation (25). In addition, recent studies have implicated hypoxia and HIF-1 in controlling the pluripotency and differentiation of embryonic stem cells (26).

Besides its important role in development, hypoxia is a critical factor in the pathophysiology of several human disease conditions. Myocardial infarction, a leading cause of clinical heart failure and death, is characterized by acute hypoxia (ischemia) in the heart, caused by sudden occlusion of the coronary artery and resulting in cell death of cardiomyocytes (27). Similarly, ischemic stroke is characterized by acute hypoxic stress in the brain, leading to neuronal cell death (28). HIF-1 is an important regulator of the hypoxic response in both ischemic cardiomyocytes and ischemic neurons (27, 28).

Hypoxia also factors significantly in neurodegenerative disorders such as Alzheimer's disease, which is characterized by increased production of amyloid-β plaques in affected neurons. Periods of chronic hypoxia, arising from cardiorespiratory disorders, predispose individuals to Alzheimer's disease, and studies have shown that hypoxia increases production of amyloid-β in multiple cell types (29). HIF-1 is thought to be an important mediator of neurodegeneration in Alzheimer's disease (30).

Rheumatoid arthritis, an inflammatory disease of the synovial joints, is also characterized by chronic hypoxia (31). Dysfunctional neovascular networks fail to maintain tissue oxygen homeostasis, resulting in a profoundly hypoxic environment in affected joints. Repetitive cycles of hypoxia and reoxygenation in the rheumatoid joint promote chronic oxidative stress, leading to generation of tissue-damaging ROS (31).

Thus, hypoxia and HIFs play important roles in normal mammalian development, and factor prominently in the pathophysiology of numerous disease conditions, including myocardial infarction, stroke, neurodegeneration and rheumatoid arthritis. In addition,

8

hypoxia plays a significant role in the development and progression of solid tumors, as discussed in the following section.

1.2.3.1 Hypoxia in cancer

Hypoxia is a common feature of solid tumors, and the extent of tumor hypoxia correlates with neoplastic aggression, increased metastases, resistance to therapy and decreased overall patient survival (32). The mechanisms of hypoxia-mediated tumor progression and therapy resistance, including possible strategies for exploiting tumor hypoxia in novel therapeutic approaches, are detailed below.

Tumor hypoxia is the result of rapid cell proliferation, which causes the tumor to outgrow its vasculature (33). Although tumor hypoxia is often clinically defined as < 10 mmHg, the heterogeneous and dynamic tumor microenvironment produces many types of hypoxia, which differ in severity and duration (21). For example, tumor cells residing at the limits of oxygen diffusion (approximately 150 – 200 μm) from functional blood vessels are thought to be exposed to prolonged or chronic hypoxia (for hours to days). By contrast, tumor cells located adjacent to blood vessels may experience acute and fluctuating hypoxia (for minutes to hours) caused by disrupted perfusion of the abnormal tumor vasculature, which can recur and lead to "cycling hypoxia". Studies have shown that acute, chronic and cycling hypoxia have different biological consequences in tumor cells (6).

Limited delivery of oxygen and nutrients often causes necrosis in the interior regions of solid tumors, where the microenvironment can become anoxic. However, surrounding hypoxic tumor cells can adapt, survive and proliferate by exploiting the induction of HIF-1-mediated survival factors such as insulin-like growth factor 2 (IGF2, promotes cell survival), glucose transporter 1 (GLUT-1, increases glucose uptake), vascular endothelial growth factor (VEGF, promotes angiogenesis), hepatocyte growth factor receptor (c-Met, promotes invasion), and chemokine CXC motif receptor 4 (CXCR4, promotes metastasis) (34). The cellular response to hypoxia leads to sustained angiogenesis and genomic instability, contributing to further tumor cell transformation (33) . Tumor hypoxia additionally selects for gene mutations in regulators of cell proliferation, such as p53 and EGFR (epidermal growth factor receptor), thereby driving the evolution of the cancer cells towards increased malignancy (35, 36). Finally, acute and cycling hypoxia are major drivers of systemic metastasis, since they promote increased invasive capacity in hypoxic tumor cells (37, 38).

Recent studies have additionally implicated tumor hypoxia in the biology of cancer stem cells (CSCs) (39). CSCs represent a small population of tumor cells that are highly resistant to conventional therapies and, by definition, exhibit high metastatic potential. CSCs have been shown to reside in hypoxic niches within solid tumors, and like embryonic stem cells, CSCs are critically dependent on HIFs for survival and self-renewal. These observations provide a new mechanistic explanation for the contribution of hypoxia to tumor malignancy (39).

While HIF itself does not act as a classical oncogene, since it is not mutated in neoplastic cells, a variety of other factors that affect HIF stability are deregulated or inactivated in cancer (4). For example, the Von Hippel-Lindau protein (pVHL) is mutated in VHL disease, a hereditary cancer syndrome predisposing to a variety of benign and malignant neoplasms including: retinal and central nervous system hemangioblastomas, renal cell carcinoma, pheochromocytoma and pancreatic tumors. VHL tumors exhibit inactivation of the wild-type allele by allelic loss, mutation or methylation (40). Since pVHL is responsible for ubiquitination and proteasomal targeting of HIF-1α, loss of pVHL activity causes constitutive stabilization of HIF-1α independent of hypoxia. This leads to tumor development associated with deregulated angiogenesis due to up-regulation of HIF target genes, confirming the role of HIF in tumor progression (40).

Besides its role in tumor progression and malignancy, tumor hypoxia also contributes significantly to therapy resistance. Hypoxic regions of solid tumors exhibit a reduced response to radiotherapy due to a decrease in the oxygen free radicals required to cause DNA-damage and cell death (41). These regions also exhibit resistance to chemotherapy due to limited delivery of drugs via the circulation. Indeed, increased HIF-1α expression (a marker of tumor hypoxia) has been observed in multiple tumor types, where it is associated with increased aggressiveness, metastasis, treatment failure and increased mortality (34).

Although it is a major cause of therapy resistance, tumor hypoxia can also be exploited for therapeutic purposes. For example, several HIF-1 inhibitors have shown promising anti-tumor effects in clinical trials and mouse models of human cancer (34). In addition,

11

new "hypoxia-specific cytotoxins" are being developed to specifically target hypoxic

tumor cells, a strategy that involves administration of a nontoxic prodrug, which is

selectively activated under hypoxic conditions (42). A successful example of this

concept is Tirapazamine, a hypoxia-specific toxic radical that potentiates the antitumor

effect of radiation (43). Hypoxia-specific gene therapy approaches have also been tested,

involving the expression of pro-apoptotic proteins (such as BAX) under the control of

hypoxia-specific promoters (44). Thus, novel therapeutic strategies for exploiting tumor

hypoxia represent a promising new area of research in cancer chemotherapeutics.

The ability to detect regions of low-oxygen within solid tumors is essential to the study of

tumor hypoxia. HIF-1α and its downstream targets carbonic anhydrase IX (CAIX) and

GLUT-1 have been used as surrogate markers of hypoxia in various

immunohistochemical assays (45). These are considered markers of chronic hypoxia

because extended exposure to low oxygen levels is required to increase their expression

(6). Alternatively, when administered prior to tissue resection, 2-nitroimidazoles (such as

EF5 and pimonidazole) act as chemical markers of hypoxia since they are metabolically

reduced under hypoxic conditions to produce long-lived protein adducts that can later be

detected with specific antibodies (46). These "hypoxic probes" can be used in succession

(2 to 3 hours apart) to distinguish between acute and chronic hypoxia: co-localization of

both probes indicates chronic hypoxia, whereas mismatches reflect acute hypoxia where

oxygenation was altered between serial injections (6).

The methods described thus far are useful for detecting hypoxia in tissue samples *ex-vivo*;

however, there is a clinical need to measure tumor oxygenation *in vivo* as a treatment

planning tool. The current gold standard method involves direct measurement of oxygenation using polarographic oxygen electrodes; however, this method is invasive, subject to sampling errors, and useful only for tumors accessible to electrode placement (47). Recently there has been considerable interest in developing non-invasive imaging techniques for hypoxia detection (48). These include BOLD-MRI (blood oxygen level-dependent magnetic resonance imaging), dynamic contrast-enhanced MRI to measure tumor perfusion and vascularity, and PET (positron emission tomography) imaging to detect radio-labelled hypoxic probes. Thus, oxygen electrodes and non-invasive imaging techniques, as well as both molecular and chemical markers may be used to identify regions of acute and chronic tumor hypoxia.

In summary, hypoxia is a driving factor in cancer progression, contributing to tumor aggression and poor prognosis. Tumor hypoxia is a major cause of therapy resistance; however, new therapeutic approaches propose to exploit the hypoxic microenvironment for enhanced tumor cell-killing activity. The study of tumor hypoxia is facilitated by the use of chronic hypoxia markers such as CAIX and pimonidazole. Because hypoxic tumor cells are the most difficult to target effectively, it is important to understand the cell death mechanisms involved (and evaded) during sustained oxygen deprivation in order to develop better strategies to treat cancers.

1.3 Autophagy

Autophagy is the cellular pathway of "self digestion", a regulated lysosomal pathway for the degradation and recycling of long-lived proteins and organelles (49). During

autophagy, cytoplasmic constituents are sequestered into double-membraned autophagosomes, which are delivered to lysosomes and degraded. This process generates nucleotides, amino acids and fatty acids which are recycled for ATP generation and macromolecular synthesis. Genetic screening in yeast has identified more than 30 ATG (autophagy-related) genes required for autophagy, many of which have mammalian homologs (50). As discussed in the following sections, autophagy is involved in both survival and cell death, and is frequently altered in cancer. Indeed, recent studies suggest that autophagy plays a significant role in cancer progression and could be a target for treatment (51).

1.3.1 Regulation of autophagy

As shown in Figure 1.2, several upstream regulators and downstream effectors of autophagy have been characterized (52). The class III PI3K (phosphoinositide-3 kinase) complex including Beclin-1 (mammalian ATG6) is required for generation of preautophagosome structures (50). The mammalian target of rapamycin (mTOR), a nutrient-sensing kinase complex that regulates cell growth and survival, blocks autophagy during nutrient-rich conditions by inhibiting the ATG1 complex, which is involved in the initiation stages of autophagic activity (53). Accordingly, upstream activators of mTOR (such as class I PI3K and Akt) suppress autophagy while inhibitors of this pathway (such as rapamycin and PTEN) induce autophagy (54). Downstream of these regulatory pathways, additional ATG proteins function to build autophagosomes. The ATG5-ATG12 covalent protein complex and ATG8-phosphoethanolamine (PE) conjugates are essential components of the autophagosome membrane. Ubiquitin-like

14

reactions involving other ATG proteins generate these conjugates (55). For example, the

ATG4 cysteine protease cleaves ATG8 at the C-terminus in order to facilitate lipidation,

generating ATG8-PE, which is then recruited to autophagosome membranes. ATG4 is

also responsible for recycling ATG8 by cleaving PE at later stages of autophagy (55).

The discovery of ATG genes in yeast, and subsequently their mammalian homologs, has

greatly advanced our understanding of the molecular mechanisms involved in the

autophagy signaling pathway.
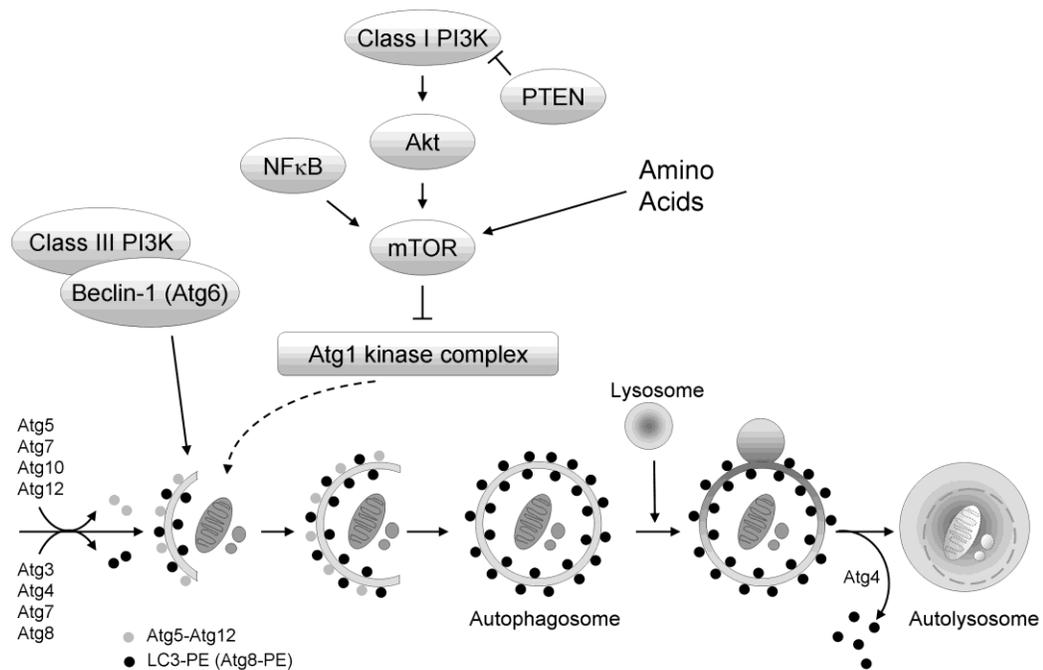
Figure 1.2 Regulation of autophagy.
Following external stimuli such as nutrient deprivation, mTOR is inhibited leading to induction of autophagy. Accordingly, autophagy is regulated by upstream factors in the mTOR pathway: autophagy is induced by PTEN and inhibited by class I PI3 kinase, Akt and NFκB.   The mTOR-regulated ATG1 complex is involved in autophagy initiation and the class III PI3 kinase complex including Beclin-1/ATG6 is required for generation of preautophagosome structures. The ATG5-ATG12 covalent protein complex and LC3/ATG8-phosphoethanolamine (PE) conjugates are essential components of the autophagosome membrane, and are generated by ubiquitin-like reactions involving other ATG proteins.   In particular, ATG4 mediates the initial lipidation of LC3/ATG8 as well as cleavage of LC3 from the autophagosome membrane at later stages of autophagy.   As elongation of the autophagosomal membrane occurs, cytoplasmic proteins and organelles are sequestered into double-membraned autophagosomes, which are delivered to lysosomes and degraded.

1.3.2   Selectivity of autophagy

Although autophagy is generally considered as a bulk degradation pathway, the process of packaging cytoplasmic components into autophagosomes may be selective or non-selective. *Mitophagy* refers to the selective elimination of mitochondria by autophagy (56). Evidence suggests that damaged mitochondria may express surface proteins and generate ROS to signal for autophagic degradation (56). *Pexophagy* is defined as the specific autophagic degradation of damaged or superfluous peroxisomes (57), and *xenophagy* describes autophagy selective for the degradation of intracellular bacteria or viruses (49). Most recently, selective autophagic degradation of protein aggregates has been described, occurring via the ubiquitin- and LC3-interacting protein, p62 (also known as A170/SQSTM1) (58). Characterized by a self-oligomerization domain and a ubiquitin-binding domain, p62 promotes the formation of ubiquitin-protein aggregates and inclusion bodies (59). Recently it was discovered that p62 directly binds to LC3 (mammalian ATG8), acting as a "shuttle protein" to transport ubiquitinated protein aggregates to autophagosomes for degradation (60).

1.3.3   Autophagy in homeostasis and survival signaling

Conserved from yeast to humans, autophagy occurs at low basal levels to maintain cellular homeostasis through cytoplasmic protein and organelle turnover. This has been demonstrated *in vivo* using the ATG7 knockout mouse model, where ATG7 was discovered to be essential for autophagosome formation, amino acid supply in neonates, and starvation-induced protein and organelle degradation (61). ATG7 deficiency also led to several striking cellular abnormalities, such as mitochondrial deformation and

accumulation of ubiquitin protein aggregates. Indeed, mice lacking ATG7 specifically in the central nervous system showed neurological defects, including abnormal clasping reflexes and decreased coordinated movement (62). These mice died within 28 weeks of birth due to massive neuronal loss in the cerebral and cerebellar cortices. Polyubiquitinated protein aggregates were found in surviving neurons as inclusion bodies, which increased in size and number over time. Together, these studies demonstrate that basal autophagy plays an important role in protein and organelle "quality control", and in maintaining normal neuronal function.

Apart from its homeostatic function, autophagy is also transiently induced as a survival response to various stress stimuli, such as nutrient deprivation (49) (Figure 1.3). Yeast mutants defective in any autophagy gene fail to survive nutrient starvation (63), and similar results have been obtained in plants (64). In mammalian cells, starvation induces autophagy to protect against apoptosis: if autophagy is blocked genetically by ATG-gene knockdown, or chemically by synthetic autophagy inhibitors, nutrient-deprived cells will undergo apoptosis (65). In addition, apoptosis-resistant cells which are growth factor-dependent can survive growth factor withdrawal for several weeks through induction of autophagy (rapid cell death occurs if ATG5 or ATG7 expression is blocked). Upon growth factor withdrawal, these cells lose their ability to take up extracellular nutrients but maintain ATP production from catabolism of intracellular substrates through autophagy (66).

The pro-survival role of starvation-induced autophagy has been confirmed in an animal model of ATG5-deficient mice (67). These mice are autophagy-deficient, and although

phenotypically nearly normal at birth, they cannot survive the early neonatal starvation period; they have reduced circulating amino acids and decreased cardiac ATP. The ATG5-deficient neonates die prematurely due to energy depletion caused by lack of autophagy. In another study, simulated ischemia-reperfusion (I/R) injury of wild-type cardiomyocytes *in vitro* impaired autophagy by inhibiting both the formation and downstream lysosomal degradation of autophagosomes (9). Overexpression of Beclin-1 increased autophagy following I/R injury and significantly reduced activation of pro-apoptotic BAX and induction of apoptosis, whereas knockdown of Beclin-1 increased BAX activation and apoptosis. Moreover, expression of a dominant negative mutant of ATG5 increased cell death after I/R, indicating that autophagy provides a protective mechanism against I/R injury. Thus, both *in vivo* and *in vitro* models confirm that autophagy contributes to cell survival functions in various physiological contexts.

1.3.4   Autophagic cell death

Although autophagy can function as a cytoprotective mechanism, it also has the capacity to promote or induce cell death (Figure 1.3). In some cases, autophagy may promote or activate apoptosis (68-70). Alternatively, death can occur through apoptosis-independent "autophagic cell death". As discussed in section 1.4, autophagic cell death or "programmed cell death type two" (PCD II) is characterized by morphological and molecular features that are distinct from apoptosis (PCD I) (70) (Figure 1.5). The underlying mechanism of autophagic cell death is excessive self-degradation, whereby autophagosomes degrade cellular components to a level where normal function is compromised and cell death occurs.

Prolonged autophagy leading to PCD II has been demonstrated under various conditions.

For example, treatment of glioma cells with arsenic trioxide (As_2O_3) induced autophagy

without apoptosis, and blocking autophagy resulted in decreased cell death (71). In

another study, over-expression of a short isoform of tumor suppressor p19ARF (smARF)

resulted in formation of autophagosomes and caspase-independent cell death. Upon

increased expression, smARF localized to mitochondria and reduced mitochondrial

membrane potential, causing increased ROS. Knock-down of *Beclin-1* and *ATG5*

reduced smARF-mediated cell death, indicating PCD II (72). A third study has found

that hydroxychloroquine induces autophagic cell death in human dermal fibroblasts (73).

Hydroxychloroquine induced cell death without DNA fragmentation or other apoptotic

morphology, instead triggering increased expression of the autophagy proteins Beclin-1

and LC3-II, along with formation of autophagic vacuoles. Autophagic cell death has also

been observed in astrocytes, where gangliosides were shown to induce cell death

characterized by LC3 processing and formation of autophagic vacuoles (74).

Ganglioside-induced cell death was inhibited by the autophagy inhibitor 3-

methyladenine, or by ATG6 knock-down, indicating PCDII. Finally, Kwon and

colleagues have recently identified a novel small molecule inducer of autophagy (which

they have called "autophagonizer") that exhibits cytotoxicity towards several cancer cell

lines through an autophagy-dependent, apoptosis-independent mechanism (75).

It has been suggested that PCD types I and II may converge at the mitochondrion where

membrane integrity is controlled by the Bcl-2 family of proteins, crucial regulators of

PCD (76) (see section 1.6). In support of this hypothesis, it has been shown that the anti-

apoptotic protein Bcl-2 also has anti-autophagic properties which are mediated through

19

direct interaction with the autophagy protein, Beclin-1 (77). Additionally, As_2O_3-induced

autophagy involves increased expression of the Bcl-2 family member BNIP3 (71). Upon

over-expression BNIP3 induces a caspase independent cell death that requires

mitochondrial localization, loss of membrane potential and increased ROS (78). Thus,

similar to apoptosis, mitochondria appear to regulate autophagic cell death.
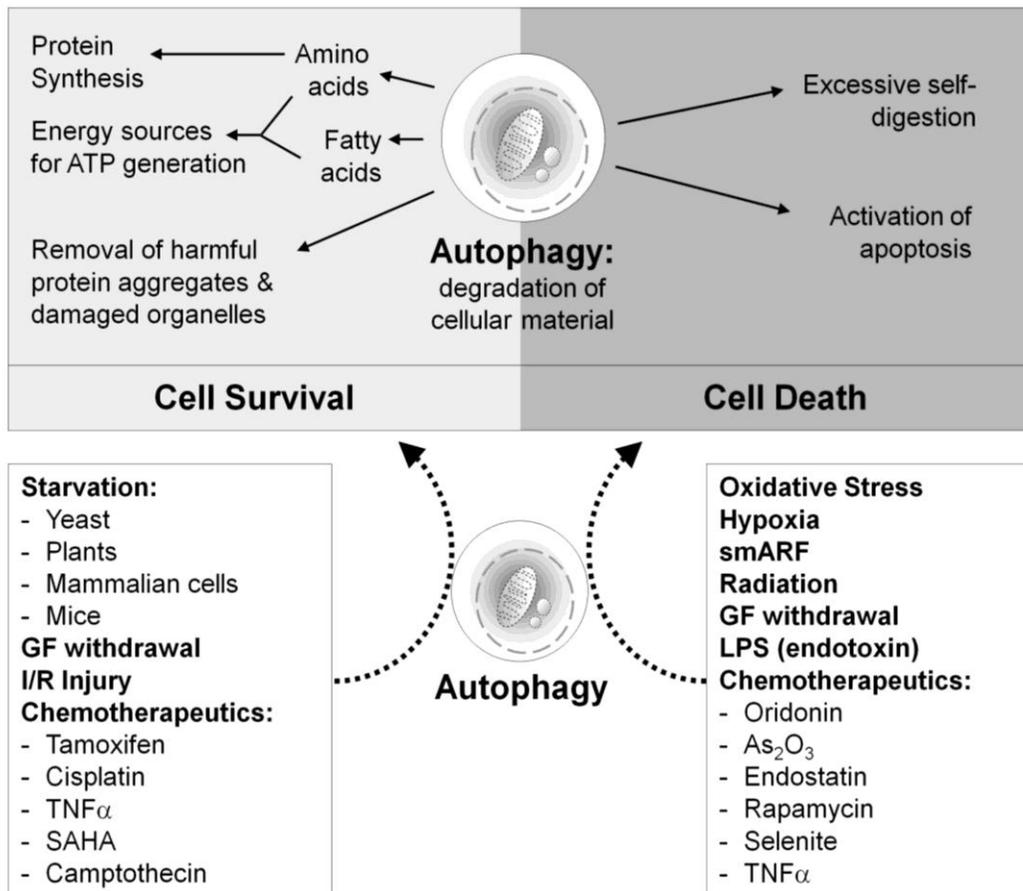
Figure 1.3 Dual role of autophagy in cell survival and cell death.
Autophagic degradation of cellular materials generates amino acids and fatty acids which can be used for protein synthesis and ATP generation during stressful conditions such as starvation. Autophagy also removes protein aggregates (which can trigger apoptosis) and damaged mitochondria (major source of apoptotic proteins and toxic ROS). However, prolonged autophagy can lead to cell death through excessive self-digestion or activation of apoptosis. Studies have demonstrated pro-survival autophagy in response to starvation in yeast, plants, mammalian cells and mouse models. Pro-survival autophagy has also been detected in response to growth factor (GF) withdrawal, ischemia / reperfusion (I/R) injury, and various chemotherapeutic drugs. Autophagic cell death has been observed in response to hypoxia, oxidative stress, radiation, GF withdrawal, lippopolysaccharide (LPS), overexpression of smARF, and various chemotherapeutic drugs.

1.3.5 Autophagy in human health and disease

As an essential mediator of cellular homeostasis, cell survival and cell death, autophagy plays a central role in human health and disease (79). Over the last decade, research has linked autophagy to aging, immunity, neurodegeneration, heart disease and cancer, as discussed below.

Several studies have shown that autophagy contributes to longevity and may be an important regulator of aging (80, 81). Aging is a universal phenomenon characterized by the progressive deterioration of cells and organs due to accumulated oxidative damage to DNA, proteins and organelles. Autophagy can counteract the aging process through continuous removal of damaged cellular components (80). Indeed, growing evidence indicates that the rate of autophagy declines with age, resulting in increased levels of oxidative stress (82). In addition, several independent reports indicate that autophagy is required for calorie restriction-mediated lifespan extension in *C. elegans*. These studies demonstrate that calorie restriction (modeled using the *eat-2* strain of feeding-defective mutants) can extend the average *C. elegans* adult lifespan by over 20% through inhibition of the TOR pathway. Notably, this longevity phenotype is completely suppressed when autophagy is inhibited by RNAi against Beclin-1 or the class III PI3K Vps-34 (83, 84). In *C. elegans*, autophagy appears to be essential for both normal dauer development (a stage of developmental arrest induced during starvation or over-crowding conditions) and for adult life-span extension (85). Most recently, Eisenberg and colleagues showed that autophagy regulates spermine-induced longevity in yeast, *C. elegans, Drosophila,* and

human cells, increasing lifespan up to four-fold (86). Thus, autophagy is an established regulator of aging and longevity in multiple species.

Autophagy is also an important regulator of innate and adaptive immunity (87). Many intracellular pathogens are engulfed and destroyed through autophagy as a host-defense mechanism. This type of autophagic innate immune response has been demonstrated for *Herpes simplex* virus (88), Group A Streptococci (89) and *Mycobacterium tuberculosis* (90), among others. Autophagy also contributes to adaptive immunity by regulating antigen presentation, as cytosolic microbial antigens are delivered to major histocompatibility complex (MHC) class II loading compartments by autophagosomes (91).

Many age-related neurodegenerative disorders reportedly involve defective autophagy (92). Neurodegeneration is often characterized by the accumulation of misfolded protein aggregates in affected brain regions. As described earlier, autophagy is necessary for the clearance of such protein aggregates, since neuron-specific disruption of autophagy in mice causes accumulation of protein aggregates accompanied by neurodegeneration (62). Autophagy has been specifically implicated in Huntington's and Parkinson's diseases, where enhanced autophagy in animal models of these disorders improves clearance of the aggregated proteins and reduces the symptoms of neurodegeneration (93, 94).

Autophagy also features prominently in the pathology of heart disease (95). In the healthy heart, autophagy is critical for maintaining normal cardiac function, as evidenced by the major cardiac dysfunction observed in ATG5-deficient mice (96). Similar to its

role in the brain, autophagy is also responsible for clearing potentially toxic protein aggregates in cardiomyocytes (97). During ischemia, autophagy promotes cardiomyocyte survival by maintaining energy homeostasis and by removing damaged mitochondria in order to reduce oxidative stress (98). However, excessive autophagy in the failing heart can lead to autophagic cell death and loss of cardiomyocytes (99).

In summary, autophagy is critically involved in various aspects of human health and disease, including aging, immunity, neurodegeneration and heart disease. With the recent explosion in autophagy research (100), many new therapeutic strategies targeting autophagy are being developed (95). The following section will specifically discuss the role of autophagy in cancer progression and treatment.

1.3.5.1 Autophagy in cancer

Due to its contradictory association with both survival and cell death, the role of autophagy in cancer is both complex and controversial (51, 101) (Figure 1.4). Several studies point towards a cancer-promoting role for autophagy, while others support an anti-cancer role for this self-digestion pathway. Accordingly, numerous studies purport the benefits of autophagy inhibition in cancer therapy, yet there is equally compelling evidence to support autophagy induction as a therapeutic approach.

In support of autophagy as a pro-cancer mechanism, it has been shown that tumor cells can exploit autophagy as a survival mechanism in the harsh tumor microenvironment, in order to sustain viability during periods of nutrient limitation, growth factor deprivation and metabolic stress (7, 65, 66). A recent study demonstrated that autophagy is required

23

for survival and anchorage-independent growth of tumorigenic DCIS (ductal carcinoma

in situ) cells, linking autophagy to breast cancer progression (102). In contrast, other

studies indicate that autophagy can function as a tumor suppression mechanism. Indeed,

cancer cells often display a reduced autophagic capacity compared to their normal

counterparts (103), suggesting that defective autophagy may play a role in malignant

transformation. In support of this theory, the autophagy gene Beclin-1 has been

identified as a haploinsufficient tumor suppressor in mice (104), and was shown to be

mono-allelically deleted in 40-75% of sporadic human breast, ovarian and prostate

tumors (105). Furthermore, the established tumor suppressors p53 and PTEN are known

to induce autophagy (106, 107) while the oncogenic proteins Bcl-2 and Bcl-xL interact

with Beclin-1 to inhibit autophagy (77, 108). In addition, activation of Akt (which is

increased in many cancers) leads to mTOR activation and blocks autophagy (109). The

mechanism by which autophagy inhibits tumorigenesis is unclear, but it may involve

"mitochondrial quality control": prevention of oxidative damage and mutagenesis though

the removal of damaged mitochondria, which are a major source of toxic ROS (51).

Recent evidence indicates that autophagy may also suppress tumorigenesis through

specific elimination of p62, an adaptor protein that promotes oxidative stress, genome

damage and tumorigenesis upon its accumulation (110).

As outlined above, autophagy can have entirely opposite consequences for tumor cells

depending on the circumstances: survival and tumorigenesis, or cell death and tumor

suppression. Accordingly, there is intense debate and conflicting evidence surrounding

the role of autophagy in cancer therapy (111-113). Many anticancer agents induce

autophagy, including tamoxifen, rapamycin, temozolomide, histone deacetylase (HDAC)

inhibitors, and ionizing radiation (114). However, it remains questionable whether the

observed autophagic response is a survival attempt by tumor cells, or a killing mechanism

of anticancer agents. For instance, studies have demonstrated the induction of autophagy

by cancer cells as a protective response to several therapies, including: tamoxifen (115),

camptothecin (116), cisplatin (117, 118), TNFα (119), perifosine (120), the HDAC

inhibitor suberoylanilide hydroxamic acid (SAHA) (121), the alkylating agent

cyclophosphamide (115), the proteasome inhibitor MG-132 (122), the BH3-mimetic

GX15-070 (123), and laser phototherapy (124). Many of these agents exhibit increased

cytotoxicity when autophagy is inhibited, prompting clinical trials to test the therapeutic

efficacy of combining autophagy inhibitors with existing anti-cancer drugs (112).

On the contrary, autophagy has been shown to enhance or directly mediate the

cytotoxicity of other cancer therapies including acadesine/AICAR (125), resveratrol

(126), valproic acid (127), arsenic trioxide (71), temozolomide (128), endostatin (129),

ascorbate (130), silibinin (131), imiquimod (132), and photodynamic therapy (133, 134).

Conflicting reports indicate that radiation toxicity may be enhanced or inhibited by

autophagy in different tumors, suggesting that further research is required before

manipulation of autophagy can be clinically applied as a radio-sensitizing strategy (135,

136). In summary, autophagy appears to differentially antagonize or enhance the

cytotoxicity of various cancer therapies. There is a growing consensus that, since many

tumors are characterized by defects in apoptosis, induction of autophagic cell death

represents a promising alternative therapeutic approach (109).
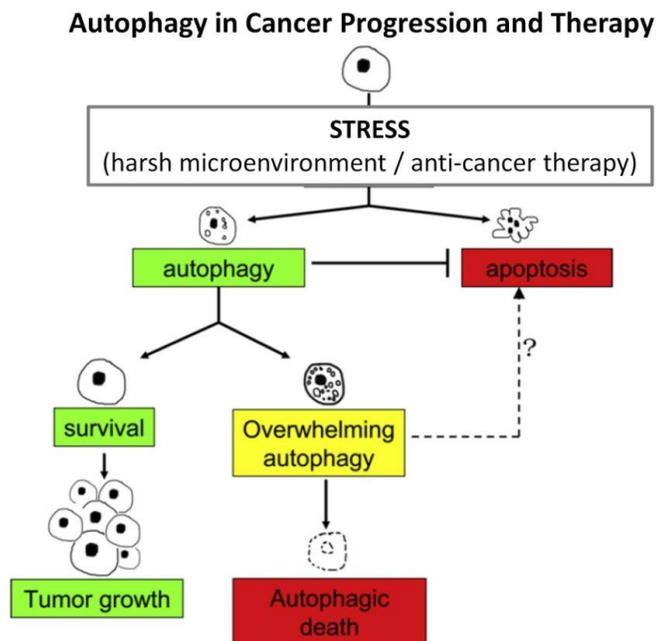
Figure 1.4 Roles of autophagy in cancer progression and therapy.
A variety of stressors can induce autophagy in cancer cells. The process of autophagy may rescue cells from apoptosis and promote survival, enabling tumor growth and cell replication. Alternatively, persistent overwhelming autophagy can result in autophagic cell death (PCDII) independent of apoptosis. Finally, there is believed to be significant cross talk between the processes of autophagy and apoptosis, and if the latter process remains intact, some cells may ultimately undergo apoptosis following prolonged autophagy. Adapted with permission from Elsevier (113).

In summary, autophagy is intricately involved in tumorigenesis and represents an attractive new target for cancer therapy. Current data suggests that, depending on individual tumor characteristics and treatment regimens, either the induction or the inhibition of autophagy may provide therapeutic benefit for patients. Further studies are required to establish the precise role of autophagy during malignant transformation and tumor progression, which may ultimately lead to new therapeutic strategies in cancer.

1.4   Cell Death

Cell death is a normal process that is essential to both the development and homeostasis of multicellular organisms (137). It is tightly regulated since either too much or too little

cell death can lead to pathological defects, such as neurodegeneration or cancer. There

are three major pathways of cell death: apoptosis, necrosis and autophagy, which are

distinguished based on morphologic and molecular features (138) (Figure 1.5). Despite

these classifications, the boundaries between different types of cell death are not strictly

defined and can often overlap. For example, mitochondrial dysfunction is characteristic

of all three forms of cell death, and Bcl-2 proteins regulate both autophagy and apoptosis.

Furthermore, it seems that when one pathway is blocked, others may compensate to

ensure cell death (137). Apoptosis, necrosis and autophagic cell death are described

below, and each is discussed in the context of cancer progression and treatment.

Cell Death Features	Apoptosis (PCD I)	Autophagy (PCD II)	Necrosis
General morphology	Shrink	–	Swell
Chromatin condensation	++	+	–
Vacuolization (Autophagosomes)	–	++	+
Exteriorization of phosphatidylserine	++	+	–
Caspase activation	++	–	–
Processing of LC3	–	++	–
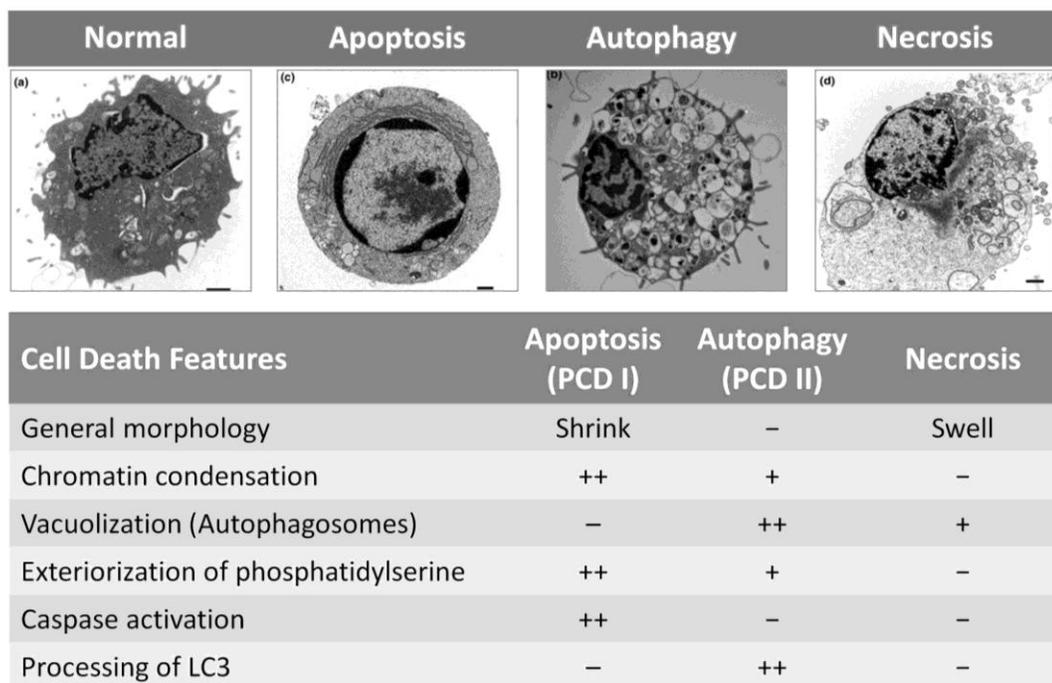
Figure 1.5 Features of autophagic, apoptotic and necrotic cell death.
Electron microscopy images of normal, autophagic, apoptotic and necrotic cells are displayed alongside a summary of the major morphological and molecular features for each type of cell death. Whereas the morphologic features of apoptosis are well defined, the distinction between necrotic and autophagic death is less clear. The bioenergetics catastrophe that culminates in cellular necrosis also stimulates autophagy as the cell tries to correct the decline in ATP levels by catabolizing its constituent molecules. Thus, vacuolation of the cytoplasm is observed in both autophagic and necrotic cells. By contrast, ATP levels are maintained in normal and apoptotic cells consistent with the limited number of autophagic vacuoles in their cytoplasm. The scale bar represents 1 μm. Adapted with permission from Elsevier (139).

1.4.1 Apoptosis

Apoptosis, alternatively referred to as programmed cell death type I (PCDI), is a highly conserved, energy-dependent form of cell death that leads to elimination of cells without activating an inflammatory response. Apoptosis is characterized by cell shrinkage, DNA fragmentation, chromatin condensation, membrane blebbing, externalization of phosphatidylserine and packaging of the cellular contents into apoptotic bodies (138, 139) (Figure 1.5). A defining feature of apoptosis involves the cleavage of cytoskeletal proteins by cysteine-aspartic proteases, or caspases, which are highly conserved throughout evolution (140). Initiator caspases (caspases 2, 8, 9 and 10) are activated by upstream signals and propagate the apoptotic signaling cascade by activating effector caspases through proteolytic cleavage. Activated effector caspases (caspases 3, 6 and 7) cleave a wide variety of substrates, resulting in the collapse of subcellular compartments (137). Termed the "executioners" of apoptosis, caspases can be activated through either the intrinsic mitochondrial pathway or the extrinsic death receptor pathway, as described below and depicted in Figure 1.6.

1.4.1.1 Extrinsic pathway

The extrinsic pathway is activated when cell-surface "death receptors" are bound by members of the TNF (tumor necrosis factor) superfamily (140). For example, death receptors DR4 and DR5 (aka TRAILR1 and TRAILR2) are activated by TRAIL (TNF–related apoptosis-inducing ligand), while Fas (aka CD95 or APO-1) is activated by FasL (Fas-ligand). Ligation induces trimerization of death receptors and recruitment of the adaptor protein FADD (Fas-associated death domain), forming the death-inducing

signaling complex (DISC). FADD in turn recruits procaspase 8, which is activated by

induced proximity in the DISC and ultimately activates caspase 3, the key "executioner"

caspase (137).

1.4.1.2 Intrinsic pathway

The intrinsic or mitochondrial apoptotic pathway is controlled by members of the Bcl-2

family of proteins (141). As discussed in section 1.6, interplay between pro-apoptotic

and anti-apoptotic Bcl-2 family members regulates the permeability of the mitochondrial

membrane. Initiators of the intrinsic pathway include toxic stimuli such as DNA damage,

ROS, or growth-factor withdrawal (137, 140). These stimuli ultimately lead to

mitochondrial membrane permeabilization, promoting the release of pro-apoptotic

mitochondrial proteins such as cytochrome c, Smac/DIABLO (Second Mitochondria-

derived Activator of Caspases/Direct IAP Binding Protein with Low PI), endoG

(endonuclease G), or AIF (apoptosis inducing factor). Cytochrome c interacts with Apaf-

1 (apoptosis protease activating factor 1) and procaspase-9, forming the apoptosome.

Caspase 9 is activated in the apoptosome, and in turn activates caspase 3.

Smac/DIABLO acts to block the action of IAPs (inhibitor of apoptosis proteins), thereby

favoring caspase activation. EndoG and AIF translocate to the nucleus and promote

caspase-independent cell death by mediating DNA fragmentation (137, 140).

There is potential cross-talk between the extrinsic and intrinsic apoptotic pathways,

mediated through t-BID (truncated BID). Caspase 8 cleaves BID to generate t-BID,

which localizes to mitochondria to promote release of pro-apoptotic mitochondrial proteins (140).
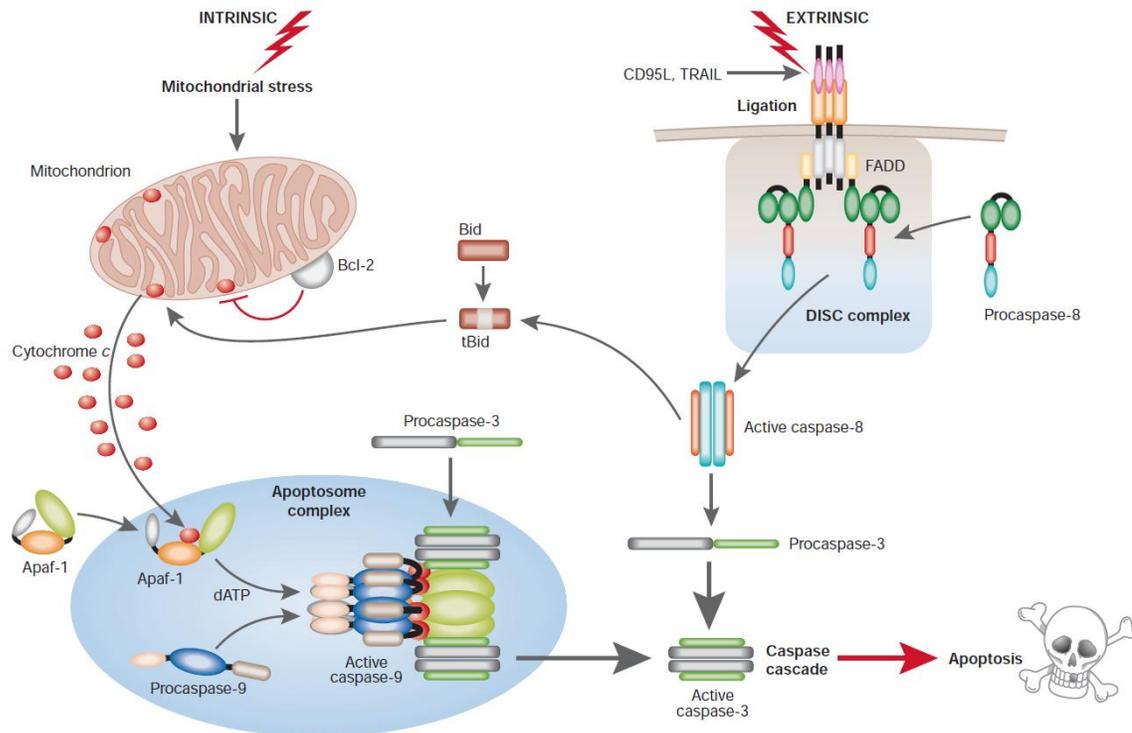
Figure 1.6 Intrinsic and extrinsic apoptosis pathways.
Two major apoptotic pathways are illustrated: one activated via death receptor activation ('extrinsic') and the other by stress-inducing stimuli ('intrinsic'). Triggering of cell surface death receptors of the tumor necrosis factor (TNF) receptor superfamily, including CD95 and TNF-related apoptosis-inducing ligand (TRAIL)-R1/-R2, results in rapid activation of the initiator caspase 8 after its recruitment to a trimerized receptor-ligand complex (DISC) through the adaptor molecule Fas-associated death domain protein (FADD). In the intrinsic pathway, stress-induced apoptosis results in perturbation of mitochondria and the ensuing release of proteins, such as cytochrome c, from the inter-mitochondrial membrane space. The release of cytochrome c, from mitochondria is regulated in part by Bcl-2 family members, with anti-apoptotic (Bcl-2/ Bcl-xL/Mcl-1) and pro-apoptotic (BAX, BAK and t-BID) members inhibiting or promoting the release, respectively. Once released, cytochrome c binds to apoptotic protease-activating factor 1 (Apaf1), which results in formation of the Apaf1–caspase 9 apoptosome complex and activation of the initiator caspase 9. The activated initiator caspases 8 and 9 then activate the effector caspases 3, 6 and 7, which are responsible for the cleavage of important cellular substrates resulting in the classical biochemical and morphological changes associated with the apoptotic phenotype. Reproduced with permission from Nature Publishing Group (142).

1.4.1.3 Apoptosis in cancer

More than half of all tumors exhibit defective apoptosis, representing a major causative factor in the development and progression of cancer (143). Often this is due to altered expression of Bcl-2 proteins, including over-expression of anti-apoptotic family members (through chromosomal translocation, gene amplification, or other epigenetic mechanisms) or defects in the expression of pro-apoptotic family members (through homozygous deletions or inactivating mutations) (144). In addition, apoptosis defects arise through mutations in the tumor suppressor gene TP53, which encodes p53, a transcription factor that regulates the expression of many pro-apoptotic proteins (137, 144). Depending on the sequence of genetic events, such defects may be present in a subset of tumor cells, or they may characterize the tumor as a whole. Many current and experimental cancer therapies aim to induce apoptosis in tumor cells. Examples include Apo2L/TRAIL (a death receptor ligand), apoptin (a caspase activator) and several small molecule inhibitors of anti-apoptotic Bcl-2 proteins (143).

1.4.2 Necrosis

Whereas apoptosis and autophagy are "programmed" modes of cell death, necrosis is generally regarded as a more "accidental" or uncontrolled form of cellular demise (137). Necrosis typically results from metabolic failure with rapid depletion of ATP, usually in response to acute stress or injury such as ischemia. In contrast to the controlled demolition of apoptosis, necrosis is chaotic with swelling and rupture of organelles, vacuolation of the cytoplasm, loss of plasma membrane integrity and spillage of intracellular contents into the extracellular space (138, 139) (Figure 1.5). This includes

31

release of pro-inflammatory cytokines, which trigger inflammation causing further cell

death in neighboring cells (137).

Interestingly, recent evidence suggests that necrosis may not be as disordered as

originally thought – reports of "programmed necrosis" indicate that, like apoptosis,

necrosis can be a highly regulated type of PCD (145). Programmed necrosis allegedly

occurs during normal physiology and development as a consequence of extensive

crosstalk between multiple biochemical and molecular pathways, with calcium ions and

ROS as major effectors of the necrotic process (145). Emerging data on the molecular

mechanisms of programmed necrosis may have significant therapeutic consequences, as

novel therapeutic strategies could aim to exploit necrosis for the killing of apoptosis-

resistant tumor cells, and generation of antitumor immunity (145, 146).

1.4.3   Autophagic Cell Death

As described earlier, autophagy is a lysosomal degradation pathway employed for the

recycling of damaged or nonessential proteins and organelles (49). Autophagy and

autophagic cell death are discussed in detail in section 1.3. Although primarily an

adaptive survival response, severe or sustained autophagy can cause cell death.

Autophagic cell death, or programmed cell death type II (PCD II), is characterized by

morphological and molecular features that are distinct from apoptosis (70).   In apoptosis,

there is early collapse of the cytoskeleton but organelles are initially preserved. In

contrast, autophagic cell death involves early degradation of organelles with initial

preservation of the cytoskeleton. Furthermore, autophagic cell death is caspase-

independent and does not involve DNA fragmentation (70, 139). The hallmark of PCDII is the formation of autophagosomes, which degrade cellular components to a level where normal function is compromised and cell death occurs (138, 139) (Figure 1.5).

Autophagy and autophagic cell death play a significant yet controversial role in malignant transformation and cancer progression (101, 147). As discussed in section 1.3.5.1, autophagy functions in tumor suppression and autophagic cell death represents an alternative cell death pathway for targeting in therapeutic strategies.

In summary, several distinct cell death pathways have been defined, including intrinsic and extrinsic apoptosis, programmed and non-programmed necrosis, and autophagic cell death. The type and intensity of noxious signals, ATP availability, cell type and other factors cooperatively determine how cell death occurs (137). Since deregulation of cell death contributes significantly to the pathophysiology of cancer, detailed knowledge of cell death pathways is critical in the development of novel anticancer therapies.

1.5 Cell Survival

Cellular homeostasis requires a delicate balance between cell death and cell survival signaling pathways, which are constantly influenced by extracellular stimuli. In opposition to the cell death pathways described in the previous section, there exists an equally complex network of cell survival pathways. In addition to the autophagy pathway (discussed in section 1.3), this network comprises multiple growth factor-

activated signaling cascades, including the Ras/MAPK, PI3K/Akt and mTOR signaling pathways, which are frequently deregulated in cancers (Figure 1.7).

1.5.1 Ras/MAPK pathway

The Ras/MAPK signaling pathway couples the activation of cell-surface receptors to intracellular responses including cell proliferation, migration, metabolism and differentiation (148). Initially, ligand binding activates receptor-tyrosine kinases such as EGFR (epidermal growth factor receptor) at the cell surface, facilitating recruitment of intracellular docking proteins such as GRB2 (growth factor receptor-bound protein 2). GRB2 in turn recruits the guanine nucleotide exchange factor SOS (son of sevenless), which binds Ras-GDP and promotes the exchange of GDP for GTP. In the GTP-bound form, Ras is activated and interacts with specific effector proteins, thereby initiating protein kinase cascades involving various members of the MAPK (mitogen-activated protein kinase) family of serine/threonine kinases (148). The best-characterized MAPK signaling cascade is the Ras/Raf/MEK/ERK pathway, where Ras recruits and activates Raf, which phosphorylates and activates MEKs (MAPK and ERK kinases) (149). Activated MEKs in turn phosphorylate ERKs (extracellular regulated kinases), which then translocate to the nucleus and phosphorylate transcription factors such as Elk1 in order to regulate the expression of specific target genes. The cascade is shut down when Ras returns to its inactive state, through intrinsic GTPase activity or with the help of GTPase activating proteins. Other Ras/MAPK signaling cascades are responsible for activating JNK (Jun N-terminal kinase) and NFκB (148).

1.5.2   PI3K/Akt pathway

Cell survival is also regulated by the widely-studied PI3K/Akt pathway (150). Akt, also known as PKB (protein kinase B), is a serine/threonine kinase that stimulates cell proliferation and inhibits apoptosis. Activation of Akt typically begins with ligand binding of receptor tyrosine kinases at the cell membrane, such as IGFR (insulin-like growth factor receptor). Receptor activation facilitates recruitment and activation of PI3K (phosphoinositide 3-kinase), which phosphorylates membrane-bound PIP2 (phosphatidylinositol 3,4-bisphosphate) to generate PIP3 (phosphatidylinositol 3,4,5-trisphosphate). PIP3 subsequently recruits Akt to the plasma membrane where it is phosphorylated by its activating kinase, PDK1 (phosphoinositide-dependent kinase 1) (150). Notably, both PI3K and Akt can be activated by additional mechanisms: for example, PI3K can be activated by Ras (151) and Akt can be activated by integrin signaling, heat shock, and hypoxia (152-154).

Once activated, Akt initiates numerous signaling cascades via its kinase activity, exerting effects on protein synthesis, metabolism, and cell cycle regulation. Akt target proteins include the forkhead (FOX) family of transcription factors, GLUTs (glucose transporters), Chk1 (cell cycle checkpoint kinase 1), BAD, caspase-9, NFκB, mTOR, Raf1 and many others (150). Though diverse, all Akt signaling pathways culminate in anti-apoptosis or pro-survival effects. For example, phosphorylation of FKRH by Akt promotes survival by retaining this transcription factor in the cytoplasm, where it cannot induce the expression of its pro-apoptotic target genes (155). Phosphorylation of BAD

by Akt causes dissociation of the apoptotic BAD/Bcl-xL complex, and phosphorylation of caspase-9 directly inhibits its pro-apoptotic protease activity (156).

1.5.3   mTOR pathway

The mammalian target of rapamycin (mTOR) is a nutrient-sensing kinase that regulates protein synthesis, cell growth, proliferation, motility and survival (157). As described in section 1.3.1, mTOR is also a central regulator of autophagy (158).   The mTOR pathway is regulated by various input signals, including growth factors, hormones, oxidative stress, and nutrient / energy levels. Growth factor activation of mTOR occurs through the PI3K/Akt pathway, where Akt can activate mTOR via direct phosphorylation or by inactivating the TSC1/TSC2 (tuberous sclerosis complex) (159). TSC1/TSC2 inhibits mTOR by promoting GTP hydrolysis of Rheb (Ras homolog enriched in brain), a small GTPase that activates mTOR in its GTP-bound form (157). mTOR also functions as a nutrient/energy sensor through its regulation by AMPK (adenosine 5'-monophosphate activated protein kinase). AMPK is extremely sensitive to changes in the cellular AMP/ATP ratio, which fluctuates according to nutrient availability and energy levels. Increased AMP levels promote AMPK activation, leading to AMPK-mediated phosphorylation and activation of TSC2 and subsequent inhibition of mTOR (159).

mTOR is present as the catalytic subunit of two molecular complexes, mTORC1 and mTORC2, which differ in their regulatory subunits and sensitivity to rapamycin (157). Activation of mTOR results in phosphorylation of several downstream targets, including 4E-BP1 (eukaryotic translation initiation factor-4E-binding protein 1) and the ribosomal

protein S6K (S6 kinase). Non-phosphorylated 4E-BP1 binds tightly to the translation

initiation factor eIF4E, preventing it from recruiting mRNAs to the ribosomal initiation

complex for translation. Upon phosphorylation by mTOR, 4E-BP1 releases eIF4E to

facilitate protein synthesis.   Phosphorylation of S6K by mTOR stimulates further

activation by PDK1, at which point active S6K can stimulate protein synthesis through

activation of S6 ribosomal protein (157). Thus, mTOR effectively senses the appropriate

conditions for cell growth, and relays these signals to stimulate protein synthesis through

multiple signaling pathways.
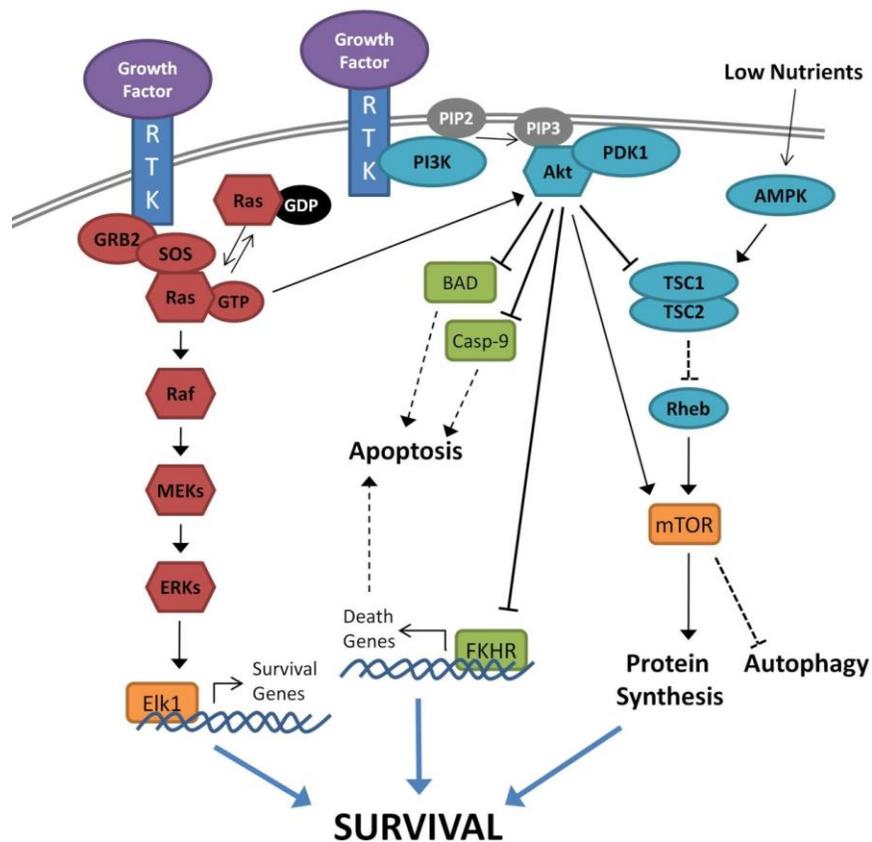
Figure 1.7 Cell survival signaling pathways.
Growth factors activate receptor tyrosine kinases (RTKs) at the cell surface to initiate Ras/MAPK and
PI3K/Akt signaling. Active Ras initiates the Raf/MEK/ERK phosphorylation cascade which regulates the
transcription of multiple pro-survival genes. Active Akt phosphorylates multiple targets in order to inhibit
apoptosis and enhance proliferation and survival. Akt can directly or indirectly activate mTOR to promote
survival and initiate protein synthesis. mTOR is also a central regulator of autophagy.

1.5.4 Survival signaling in cancer

While cell death pathways are often suppressed or defective in cancer cells, survival pathways are often deregulated and over-activated. For example, the Ras-Raf-MEK-ERK pathway features several oncogenes and is deregulated in approximately 30% of all human cancers (149).   Akt and its upstream regulators are similarly deregulated in a wide range of cancers, including over 50% of acute myelogenous leukemias where Akt activation is correlated with poor prognosis (160). Finally, many cancers are characterized by aberrant activation of mTOR (159). Most often, somatic mutations are responsible for malignant aberrations in survival signaling pathways, but germline mutations are also possible. For example, a class of hereditary developmental disorders is caused by germline mutations in genes that encode components of the Ras/MAPK pathway. These syndromes (including Noonan syndrome, LEOPARD syndrome, Neurofibromatosis type I, Costello syndrome, and autoimmune lymphoproliferative syndrome) each exhibit unique phenotypic features owing to different causative mutations; however, a common overlapping feature involves an increased risk of developing cancer (161).

Due to their frequent involvement in malignancy, Raf, PI3K, Akt and mTOR have been heavily targeted in various anti-cancer treatment strategies (162). For example, sorafenib (Nexavar) is a Raf inhibitor approved for the treatment of kidney and liver cancer (163). Metformin is an FDA-approved AMPK activator that ultimately inhibits mTOR, with promising anti-cancer activity (159). Several PI3K and PDK1 inhibitors have also been investigated as cancer therapeutics, exhibiting significant anti-proliferative effects in

cancer cells (164). In addition, preliminary studies have demonstrated anti-cancer activity for a cell-permeable anti-Akt antibody in mouse models (165). Finally, Akt-activating tyrosine kinase receptors such as EGFR and Her2 are frequently altered in cancer and have been successfully targeted by small molecule inhibitors (such as gefitinib) and by monoclonal antibodies (such as Erbitux) (164).

In summary, cell death and cell survival are strictly regulated through a complex network of signaling pathways. Cancers are often characterized by deregulation of these pathways, which are therefore frequently targeted in cancer treatment strategies.

1.6 The Bcl-2 family of proteins

The Bcl-2 family members are crucial mediators of cell fate decisions, a function accomplished through their regulation of mitochondrial membrane integrity (141, 166). Although initially considered as regulators of apoptosis (Figure 1.6), it is now clear that Bcl-2 proteins also participate in the regulation of autophagy and autophagic cell death (141, 167, 168), providing a mechanistic link between these pathways. The Bcl-2 family members are characterized by the presence of one to four Bcl-2 homology (BH) domains, and are functionally classified as either pro-survival or pro-death (Figure 1.8). The balance and interaction of pro-survival and pro-death Bcl-2 proteins dictates survival or commitment to cell death.
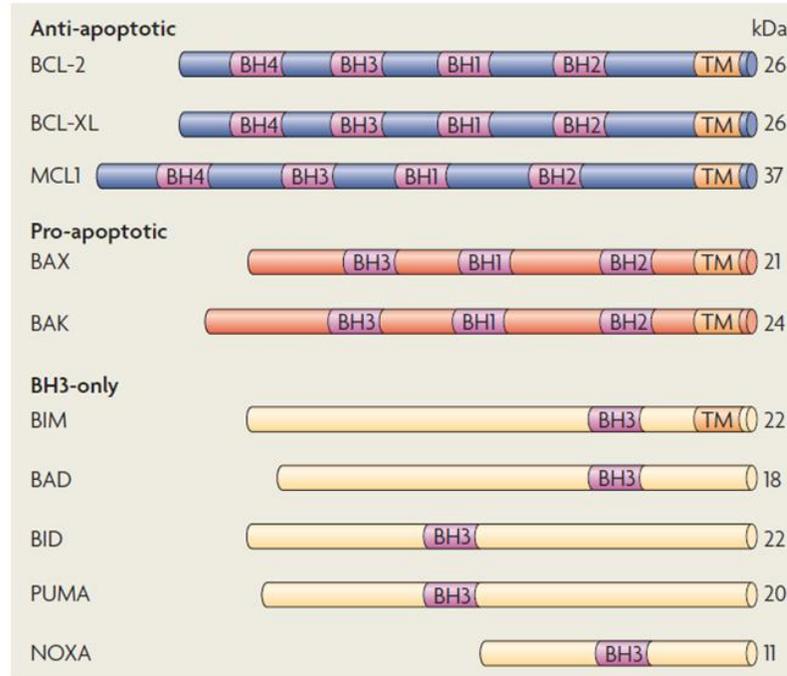
Figure 1.8 Bcl-2 family of proteins.
Bcl-2-family proteins have a crucial role in apoptosis through their ability to regulate mitochondrial membrane integrity. The Bcl-2 family comprises three subfamilies that contain between one and four Bcl-2 homology (BH) domains. The anti-apoptotic subfamily comprises proteins that contain four BH domains. Most members of this subfamily also contain transmembrane domains (TM) and are therefore typically associated with membranes. The pro-apoptotic BAX-like subfamily lacks BH4 domains and promotes apoptosis by forming pores in mitochondrial outer membranes. The BH3-only subfamily is a structurally diverse group of proteins that only display homology within the small BH3 motif. Additional family members are not shown in this diagram. Adapted with permission from Nature Publishing Group (169).

1.6.1 Pro-survival Bcl-2 family members

Pro-survival Bcl-2 proteins contain four BH domains, and are generally integrated within the outer mitochondrial membrane (OMM). The group includes Bcl-2, Bcl-xL (Bcl-2-related gene, long isoform), A1 (Bcl-2-related gene A1), Bcl-w, and Mcl-1. These proteins preserve OMM integrity by directly inhibiting their pro-death counterparts, thereby promoting cell survival (141). In addition to this anti-apoptotic function, Bcl-2 and Bcl-xL can inhibit autophagic cell death though binding to Beclin-1 to inhibit the formation of autophagic vesicles (168).

1.6.2 Pro-death Bcl-2 family members

Pro-death Bcl-2 family members are subdivided into two groups: the multidomain proteins (containing BH1, 2 and 3 domains) and the BH3-only proteins. Upon activation, the multidomain pro-death proteins BAK (Bcl-2 antagonist killer 1) and BAX (Bcl-2-associated x protein) homo-oligomerize to form pores within the OMM, promoting permeabilization and release of pro-apoptotic factors as described in section 1.4.1.2 (141, 166).

The BH3-only proteins are the least homologous amongst all Bcl-2 family members. This sub-family includes BAD (Bcl-2 antagonist of cell death), BID (Bcl-2 interacting domain death agonist), BIM (Bcl-2 interacting mediator of cell death), NOXA and PUMA. All members can directly antagonize pro-survival Bcl-2 proteins through interaction via the conserved BH3 domain. BID, BIM and PUMA can further promote cell death by activating BAX and BAK (141, 166). In addition, BIM, BAD, NOXA and PUMA can promote autophagy through competitive dissociation of Beclin-1 from inhibitory complexes with pro-survival Bcl-2 proteins (168). Due to these functions, the BH3-only proteins are considered as the major sentinels for cellular stress: they are distinctly activated in response to different stress stimuli, and function as "rheostats" to titrate the balance between pro-death and pro-survival cellular signaling (141).

1.6.2.1 BNIP subfamily

BNIP proteins (Bcl-2/E1B-nineteen kilodalton interacting proteins) are a subgroup of the BH3-only subfamily, classified based on limited sequence homology with the BH3

domain and a C-terminal transmembrane domain (170). Members include BNIP1,

BNIP2, BNIP3 and BNIP3L (BNIP3-like protein X, also known as NIX, B5 or BNIP3α).

BNIP 1, 2 and 3 were first identified in a yeast-two-hybrid screen for Bcl-2- and E1B-

19K-interacting proteins (171). The adenovirus E1B 19 kDa protein preserves host cell

viability after viral infection, through a survival-promoting domain homologous to a

discrete sequence motif in Bcl-2 (172). Initial studies indicated that the newly-

discovered BNIP proteins failed to interact with E1B-19K mutants defective in cell death

suppression, suggesting that BNIPs are involved in promoting cell death (171).

BNIP3L/NIX was later cloned from a human placenta cDNA library based on its

homology (56%) to BNIP3 (173). Human BNIP3 maps to chromosome 14q, whereas

NIX is located on chromosome 8q.

BNIP3, a major focus of this dissertation, is the most well-characterized member of the

BNIP group of proteins, and is discussed in detail in section 1.7. BNIP3L/NIX is highly

similar to BNIP3 in terms of structure, function and regulation, and is also discussed in

section 1.7. In comparison, BNIP1 and BNIP2 have not been well studied. Whereas

BNIP3 and BNIP3L localize to mitochondria to induce cell death, BNIP1 and BNIP2

localize to the nuclear envelope and endoplasmic reticulum (171). BNIP1 has been

shown to induce apoptosis via its BH3 domain (174), and based on sequence homology,

may also have phosphodiesterase-like activity (171), although this remains to be proven

empirically. BNIP2 shares significant homology to the Rho GTPase activating protein

(RhoGAP) (171) and indeed, has been shown to possess GTPase-activating activity

towards the small GTPase, Cdc42 (175). Thus, although the BNIP proteins share similar

BH3 and transmembrane domains, as well as the common ability to bind E1B-19K and

Bcl-2, they appear to have very different functional roles within the cell.

1.6.3   Regulation of Bcl-2 family members

Multiple levels of regulation are necessary to tightly control the expression and activity

of Bcl-2 family members as the mediators of cell fate. Regulation occurs through several

pathways, including transcriptional control, post-translational modification, proteolytic

cleavage and dimerization (166, 176).

Transcriptional mechanisms of regulation have been observed for many Bcl-2 family

members. For example, STAT3-mediated transcription of Bcl-2 has been detected in

response to polyamine depletion (177), and interleukin-3 has been shown to activate Mcl-

1 gene transcription (178). Adenovirus E1A activates transcription of NOXA (179), and

transforming growth factor beta stimulates FOXO3-dependent transcription of BIM

(180). In addition, transcriptional repression of Bcl-2 has been reported in cells treated

with imatinib (181) or activator protein-2-alpha (182), while BAX gene transcription was

shown to be repressed by the proto-oncoproteins ETS1 and GFI1 (183).

Post-translational modification is another prominent regulatory mechanism for Bcl-2

family members. For example, dynamic phosphorylation of Bcl-2 is a key modulator of

its stability and activity (184). Mcl-1 is also dynamically phosphorylated, with

phosphorylation at T163 promoting stability (185) and phosphorylation at S159

promoting degradation (186). Phosphorylation of BAD results in cytoplasmic

sequestration and inactivation, and phosphorylation of BAX inhibits its pro-apoptotic

activity (176). Besides phosphorylation, other post-translational modifications also regulate Bcl-2 family members. For example, in addition to phosphorylation, Mcl-1 stability is regulated by ubiquitination and de-ubiquitination (187).

Dimerization is also a key regulatory mechanism for Bcl-2 proteins, since pro-survival and pro-cell death family members form homo- and heterodimers to titrate each other's functions (176). As described above, pro-survival Bcl-2 proteins preserve mitochondrial membrane integrity by sequestering the pro-death "effector" BH3-only proteins (PUMA, BIM, BID) through heterodimerization. During stress, this interaction is disrupted through competitive displacement by the "sensitizer" BH3-only proteins, BAD and NOXA, which liberates the effectors to activate BAX and BAK. Homo-oligomerization is subsequently required for BAX and BAK pro-death activity (166, 176). Thus, the activity of Bcl-2 proteins is highly dependent on complex protein-protein interactions involving both homo- and hetero-dimerization, and homo-oligomerization.

Finally, proteolytic cleavage also regulates some Bcl-2 family members. For example, BID is cleaved into t-BID (truncated BID) by caspase 8 (140). Cleavage allows t-BID to oligomerize and insert into the outer mitochondrial membrane, promoting the release of pro-apoptotic factors. In addition, pro-survival Mcl-1 can be cleaved by caspases to generate a pro-apoptotic fragment (188).

In summary, the expression and activity of Bcl-2 family members is tightly regulated by multiple mechanisms including transcriptional induction and repression, phosphorylation, ubiquitination, homo- and hetero-dimerization, and proteolytic cleavage. Such complex

regulation is required to regulate the interplay between pro-survival and pro-death Bcl-2 family members, which together control critical cell-fate-determining pathways such as autophagy and apoptosis.

1.6.4 Bcl-2 family members in cancer

As described in section 1.4.1.3, more than half of all tumors exhibit defective apoptosis (143), which is often due to deregulation of Bcl-2 proteins (144). This may include over-expression of pro-survival family members (through chromosomal translocation, gene amplification, or other epigenetic mechanisms) or defects in the expression of pro-death family members (through homozygous deletions or inactivating mutations) (144). Indeed, Bcl-2 was first identified based on its involvement in chromosomal translocations observed in non-Hodgkin's lymphoma (189). It has since been proven that most other pro-survival Bcl-2 genes can act as oncogenes, while the pro-death members act as tumor suppressors. Furthermore, the pro-death family members BAX, BID, PUMA and NOXA are direct transcriptional targets of the p53 transcription factor, which is often dysfunctional in tumors (144).

Besides playing a role in tumorigenesis, Bcl-2 family proteins have been linked to patient outcomes and therapy resistance. For example, over-expression of Bcl-2 in lymphoma correlates with chemoresistance and poor prognosis (190). Increased Mcl-1 expression is associated with poor prognosis in ovarian cancer (191), and low expression of BAX predicts poor prognosis in esophageal cancer (192). There is great interest in developing novel therapeutic compounds to modulate the activity of Bcl-2 proteins. One strategy

involves the use of small molecule inhibitors to neutralize pro-survival Bcl-2 proteins, an approach that has shown promise in primary leukemia cells and animal models (193, 194). Another strategy is to use BH3-mimetics to activate BAX and BAK (195).

In summary, the Bcl-2 family proteins play an important role in cancer progression and treatment. Deregulation of Bcl-2 family members is frequently observed in cancer, and often viewed as a causative event in tumorigenesis. Promising new strategies in cancer treatment involve novel mechanisms for neutralizing pro-survival Bcl-2 proteins, or activating pro-death Bcl-2 proteins.

1.7 BNIP3

BNIP3 was first identified in a yeast-two-hybrid screen for Bcl-2- and E1B-19K-interacting proteins (171). As detailed below, BNIP3 is a pro-death member of the BH3-only subfamily of Bcl-2 proteins. Its expression is strongly induced in hypoxia, and mitochondrial localization of BNIP3 has been shown to induce apoptotic, necrotic, or autophagic cell death. Furthermore, BNIP3 appears to play a role in several hypoxia-related pathological conditions, including cancer (196).

1.7.1 BNIP3 structure

BNIP3 is classified as a BH3-only Bcl-2 family member due to its putative BH3 domain (197). The 194 amino acid BNIP3 protein also contains a C-terminal mitochondria-targeting transmembrane (TM) domain, and an N-terminal PEST domain: a peptide sequence rich in proline, glutamic acid, serine and threonine that signals for protein

degradation and is associated with short intracellular half-life. Notably, the BH3 and TM

domains are highly conserved from *Caenorhabditis elegans* to humans (198).
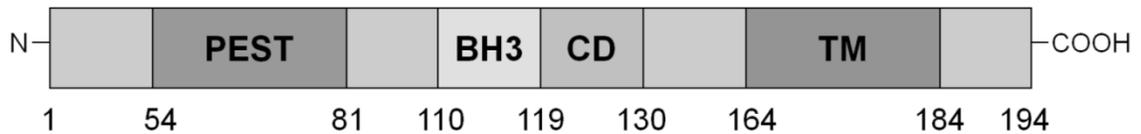
Figure 1.9 Structure of BNIP3 protein.
BNIP3 contains an N-terminal PEST domain that signals for degradation, a Bcl-2 homology 3 (BH3) domain, a conserved domain (CD), and a transmembrane domain (TM) essential for its ability to homodimerize, localize to mitochondria and induce cell death. Amino acid positions are indicated below the diagram.

Unlike most other BH3-only proteins, the cell death activities of BNIP3 are mainly

controlled by the TM domain, rather than the BH3 domain. BH3-only proteins typically

regulate apoptosis through interaction with anti-apoptotic Bcl-2 family members at the

BH3 domain (199); however, BNIP3 interacts with Bcl-2 and Bcl-xL through its TM

domain and its N-terminus (amino acids 1-49) (200). Indeed, while deletion of the TM

domain blocks mitochondrial-localization and cell death, deletion of the BH3 domain

fails to disrupt BNIP3-induced cell death (200).

BNIP3 self-associates at the TM domain, forming homodimers which are resistant to

denaturation by SDS or reducing conditions (201). Biophysical studies indicate that

BNIP3 homodimers form a right-handed parallel helix-helix structure with a continuous

hydrophilic track that can span a lipid bilayer (202). Critical residues in the dimeric

interface include Ser-172 and His-173, part of a conserved glycine zipper motif that has

been proposed to control an acid-sensitive proton channel in the outer mitochondrial

membrane (OMM) (202). This suggests that insertion of BNIP3 homodimers into the

OMM could trigger depolarization of mitochondria, leading to opening of the

mitochondrial permeability transition pore (MPTP) and resulting in cell death as described in section 1.4. In support of this hypothesis, mutation of His-173 to alanine in cardiomyocytes completely inhibited the formation of homodimers, and severely impaired the cell death activity of BNIP3 (203). However, another study showed that while the H173A mutation prevented homodimerization, it did not inhibit the death function (204). Although both studies were performed in cardiomyocytes, the stress conditions used to induce BNIP3 expression were different, suggesting that the importance of homodimerization may be context-dependent.

BNIP3 homodimerization and cell death activity can be abrogated by pro-survival Bcl-2 family members, which compete for binding at the TM domain (200). This was recently demonstrated in malignant glioma cells, where inhibition of Bcl-2 and Bcl-xL with BH3 mimetics and RNA interference enhanced the ability of BNIP3 to induce cell death in anoxia (205).

In summary, BNIP3 is an atypical BH3-only family member with unique structural properties including the ability to homodimerize via its transmembrane domain.

1.7.2   Regulation of BNIP3

1.7.2.1   BNIP3 induction

Although BNIP3 was first identified in 1994 (171), its regulation remained largely unknown until 2000, when subtractive hybridization studies identified BNIP3 as one of the most abundant mRNA transcripts induced in hypoxia (206). This study further

identified a functional HIF-1 response element (HRE) in the BNIP3 promoter, and

demonstrated accumulation of BNIP3 protein after chronic hypoxia. Later studies

confirmed BNIP3 as a direct HIF-1 target, showing that during hypoxia HIF-1α directly

binds to the BNIP3 HRE, and that mutation of the HRE eliminates the hypoxic

responsiveness of the promoter (207). In addition to chronic hypoxia, cyanide has also

been shown to induce BNIP3 expression through stabilization of HIF-1α and activation

of the HRE (208).

Besides HIF-1α, other transcription factors can also regulate the induction of BNIP3

expression. PLAGL2 (pleomorphic adenomas gene-like 2), expressed in response to

hypoxia or iron deficiency, has been shown to activate the BNIP3 promoter independent

of HIF-1 in mouse fibroblasts and neuroblastoma cells, leading to apoptotic cell death

(209). In rat ventricular myocytes, the transcription factor E2F-1 has been shown to

activate the BNIP3 promoter, leading to apoptosis via the intrinsic death pathway (210).

In primary rat cortical neurons, a glucocorticoid response element was shown to mediate

BNIP3 promoter activity, leading to cell death (211). Most recently, BNIP3 was

identified as a FOXO3 target gene along with the autophagy gene LC3 (212). In this

study, BNIP3 was shown to mediate the pro-autophagic activity of FOXO3 in skeletal

muscle.

Several additional stimuli are known to induce BNIP3 expression, although the specific

transcriptional regulators involved are unknown. For example, the neurotoxin manganese

induces BNIP3 expression in neurons, leading to mitochondrial dysfunction and cell

death (213). In addition, nitric oxide (NO) induces BNIP3 expression through the Ras

signaling pathway, leading to cell death in macrophages (214). NO-mediated BNIP3 expression also plays a role in cell death induced by the cytokine TNFα (tumor necrosis factor alpha) (215). Other toxic stimuli known to induce BNIP3 expression include arsenic trioxide, ceramide and amyloid-β (71, 216, 217). Finally, although it does not increase BNIP3 gene transcription, low pH (acidosis) causes accumulation of BNIP3 protein by increasing the half-life of BNIP3 monomers and homodimers (204).

1.7.2.2 BNIP3 repression

Given its pro-death activity, repression of BNIP3 expression is critical to cell survival. For example, during development the embryo experiences hypoxic stress; however, BNIP3 expression is attenuated by pRb/E2F-mediated transcriptional repression, preventing cell death (218). Another mechanism for BNIP3 repression has been elucidated in ventricular myocytes: under basal non-apoptotic conditions, NFκB constitutively occupies and silences BNIP3 gene transcription by competing with E2F-1 for BNIP3 promoter binding (219). The same authors had shown previously that NFκB-mediated repression of BNIP3 expression requires recruitment of HDAC-1 (histone deacetylase 1), since basal BNIP3 gene expression was increased in NFκB-deficient cells, and deletion analysis revealed that canonical NFκB elements in the BNIP3 promoter were important for repression of BNIP3 gene expression by HDAC1 (220).

Additional mechanisms for suppression of BNIP3 expression have been demonstrated in cancer cells. For example, Mahon and colleagues identified S100A4 as a repressor of BNIP3 promoter activity *in vitro*, and demonstrated that siRNA knock-down of S100A4

50

leads to increased BNIP3 expression in pancreatic ductal adenocarcinoma cells (221). In prostate cancer cells, BNIP3 has been identified as a novel target of the transcription factor SIM2s (short isoform of single-minded 2), which attenuates BNIP3 hypoxic induction by interfering with HIF-1 binding at the BNIP3 promoter (222). In addition, silencing of the BNIP3 promoter by hypermethylation has been observed in pancreatic (223), colorectal (224) and haematopoetic cancers (225).

In summary, BNIP3 expression is tightly regulated by multiple mechanisms of induction and repression. BNIP3 is highly induced in hypoxia, by HIF-1, but may also be induced under other stress conditions by additional regulators. Furthermore, there are multiple mechanisms that repress BNIP3 expression, preventing BNIP3-induced cell death under physiological and pathological conditions.

1.7.2.3   Post-translational modification of BNIP3

The N-terminal regions of all BNIP proteins, though divergent, are characterized by the presence of PEST sequences. These regions, rich in proline (P), glutamic acid (E), serine (S) and threonine (T), are typically associated with proteins subjected to high turnover by proteasome-mediated degradation (226). Although regulation of BNIP3 by the ubiquitin-proteasome pathway has not been widely studied, one group has recently shown that treatment with the proteasome inhibitor bortezomib led to accumulation of BNIP3 in breast cancer cells, consistent with inhibition of proteasome-targeted BNIP3 degradation (227).

Thus far, only two other post-translational modifications of BNIP3 have been identified:

O-linked glycosylation and phosphorylation. Manka and Millhorn demonstrated that BNIP3 is glycosylated by O-linked acetylglucosamine in breast cancer cells, where increased glycosylation was associated with increased metastatic dissemination (228). They also observed that glycosylation affected the subcellular localization and cell death activity of BNIP3 (unpublished), suggesting that enhanced O-linked glycosylation confers a survival advantage to cancer cells by silencing BNIP3-mediated cell death.

Phosphorylation of BNIP3 was recently characterized in breast and colorectal cancer cells by Harris and colleagues (227). They demonstrated hyper-phosphorylation of BNIP3 monomers and dimers by a mitotic kinase upon treatment with microtubule inhibitors, showing that phosphorylation increased the stability of BNIP3 protein, but did not affect its subcellular localization. Another study independently reported dynamic phosphorylation of BNIP3 upon simulated ischemia in cardiomyocytes (229). Specific phosphorylation sites have yet to be defined, and will surely be the focus of future studies. A motif search using NetPhos 2.0 (Technical University of Denmark) predicts 25 possible phosphorylation sites, including 10 with prediction scores above 0.99.

In summary, BNIP3 appears to be phosphorylated and/or glycosylated in response to specific pathological conditions or drug treatments. However, more research is required to fully characterize the post-translational regulation of BNIP3.

1.7.2.4 Subcellular localization of BNIP3

The function of BNIP3 is also partially determined by its subcellular localization. In addition to its role in cell death and autophagy (achieved through mitochondrial

localization), BNIP3 can also function in the nucleus as a transcriptional repressor (230). Indeed, several Bcl-2 family members have defined roles in the nucleus (231, 232). Nuclear BNIP3 has been reported in malignant glioma cells and brain tumors (233), in normoxic and reoxygenated hepatocytes (234), and in rat neurons after global brain ischemia (235). In these studies, the subcellular localization of BNIP3 was examined, but its nuclear function was not determined. However, a follow-up study by Burton and colleagues identified a novel transcriptional repression function for BNIP3, showing that nuclear BNIP3 binds to the promoter of the apoptosis-inducing factor (AIF) gene, causing reduced AIF expression and resistance to apoptosis (230). Thus, BNIP3 may serve distinct functional roles depending on its subcellular localization: in addition to its pro-death function at the mitochondrial membrane, BNIP3 may exhibit pro-survival activity by repressing apoptosis gene transcription in the nucleus. Further studies are required to identify additional BNIP3 transcriptional target genes, and to determine whether or not this nuclear function is specific to cancer cells.

1.7.3   BNIP3 and cell death

Forced over-expression of BNIP3 induces cell death that is characterized by localization to the mitochondria, opening of the mitochondrial permeability transition pore (MPTP), loss of mitochondrial membrane potential and reactive oxygen species (ROS) production. Interestingly, at least in transformed cells, this BNIP3-induced cell death is independent of caspase activation and cytochrome c release from the mitochondria (78, 236). Notably, other studies have shown that forced BNIP3 expression is not sufficient to cause cell death in primary, transformed or cancer cells (218, 237). However, since forced

expression may produce non-physiological levels of BNIP3 protein, there is controversy regarding the relevance of results obtained from over-expression studies.

Hypoxic induction of BNIP3 is considered to be a more physiologically-relevant model for the study of BNIP3-mediated cell death, but such studies have also produced confounding results. For example, it has been shown that inhibition of hypoxia-induced BNIP3 expression by RNA interference protects against hypoxia-induced cell death in HEK293 cells (207) and neural precursor cells (238). Yet, others have shown that hypoxia-dependent toxicity is independent of BNIP3 (227, 239). Nevertheless, the first *in vivo* study of BNIP3 function provides strong evidence for its pro-death activity, since loss of BNIP3 in a mouse model was shown to reduce cell death and preserve cardiac function after surgical ischemia/reperfusion (I/R) injury, while conditional over-expression increased apoptosis and infarct size (240).

The following sections will outline the features of BNIP3-mediated cell death, and summarize what is known about the molecular mechanisms involved. Since BNIP3 has been implicated in apoptotic, necrotic and autophagic cell death, its role in each context will be specifically discussed.

1.7.3.1 Features and mechanisms of BNIP3-mediated cell death

BNIP3 is a unique member of the BH3-only proteins since it does not require its BH3 domain for dimerization or pro-death activity (200), and can directly alter mitochondrial membrane potential without the involvement of other Bcl-2 family members (202). The transmembrane (TM) domain is critical for these functions, since BNIP3 deletion mutants

lacking the TM domain fail to homodimerize or localize to mitochondria, and cannot induce cell death (201). Notably, one study has identified a point mutation within the TM domain that prevents homodimerization but does not inhibit the cell death function of BNIP3 in cardiomyocytes, indicating that BNIP3 can induce cell death without dimerization, at least in some cell types (204).

BNIP3 clearly activates cell death at the mitochondrial membrane (Figure 1.10); however, the mechanism of BNIP3-mediated cell death remains poorly defined. In isolated mitochondria, BNIP3 induces mitochondrial permeability transition via its C-terminal tail (including the TM domain), which the authors propose may directly interact with one of the components of the permeability transition pore or with other mitochondrial proteins (241). Mitochondrial dysfunction is generally accepted as the predominant mechanism for BNIP3-mediated cell death; however, several distinct upstream and downstream signaling mechanisms have been reported in different cell types. In cardiomyocytes, localization of BNIP3 to the mitochondria during I/R injury causes release of cytochrome *c* leading to activation of caspases and apoptosis (98, 242). In contrast, caspase-independent, BNIP3-mediated cell death has also been reported in the same cell type (237). A different mechanism has been observed in neurons, where BNIP3 mediates ischemia-induced cell death via mitochondrial release of EndoG (rather than cytochrome *c*), and cell death is caspase-independent (243, 244). BNIP3 over-expression studies in transformed and cancer cells have demonstrated caspase-independent cell death without cytochrome *c* release from mitochondria; however, EndoG release was not examined in these studies (78, 245). Finally, in both primary and

immortalized T lymphocytes, BNIP3 appears to mediate activation-induced cell death by a caspase-independent mechanism (246, 247).

Yet another mechanism for BNIP3-induced cell death has been observed in murine fibroblasts, where over-expressed BNIP3 requires BAX and BAK to induce mitochondrial dysfunction (loss of mitochondrial membrane potential and increased ROS production) and subsequent release of cytochrome c and cell death (248). Although the role of caspases was not examined in this study, the results suggest that BAX and BAK may interact with BNIP3 to induce cell death at the mitochondria. Thus, additional binding partners might also affect BNIP3 function at the mitochondrial membrane. For example, BNIP3 was first identified based on its ability to bind E1B-19K and a homologous domain of Bcl-2 (171), and subsequently Bcl-2 has been shown to counteract BNIP3-induced cell death (201). More recently, Acetyl-Coenzyme A Acyltransferase 2 (ACAA2) has been identified as a functional BNIP3 binding partner, acting at the mitochondrial membrane to block BNIP3-induced cell death in HepG2 and U-2OS cancer cell lines (249). Another potential BNIP3 binding partner in the mitochondrial membrane is Opa1. BNIP3-Opa1 interactions were recently shown to cause mitochondrial fragmentation and apoptosis (250). Thus, functional regulation of BNIP3 involves protein-protein interactions with BAX, BAK, Bcl-2, ACAA2, Opa1, and possibly other unknown binding partners.

In addition to directly regulating mitochondrial dysfunction at the mitochondrial membrane, a recent report suggests that BNIP3 may also remotely regulate mitochondrial membrane potential from the endoplasmic reticulum (ER) (251). In this study, neurons

treated with cyanide induced expression of BNIP3, which localized to both mitochondria and ER. At the ER, BNIP3 stimulated calcium release into the cytosol, ultimately leading to accumulation of mitochondrial calcium and reduction of mitochondrial membrane potential, resulting in caspase-independent cell death.

Taken together, these studies suggest that BNIP3 activates caspase-dependent and caspase-independent cell death through mitochondrial dysfunction, by several different mechanisms which may be cell-type specific and have not yet been fully elucidated. The following sections summarize the evidence implicating BNIP3 in three distinct types of cell death: apoptosis, necrosis and autophagic cell death.

1.7.3.2 BNIP3-mediated apoptosis

Apoptosis is the most well defined type of programmed cell death (see section 1.4.1). Initially, BNIP3 was described as a pro-apoptotic BH3-only protein (201), but more in-depth studies later demonstrated that BNIP3-induced cell death often occurs independent of cytochrome *c* release and caspase activation, two of the hallmark features of apoptosis (78). Nevertheless, there are some recent examples of BNIP3-mediated apoptosis in cardiomyocytes, where BNIP3 has been shown to induce loss of mitochondrial membrane potential, ROS production, DNA condensation, activation of BAX and BAK, and caspase activation (210, 242, 248). In addition, Dorn and colleagues have identified BNIP3 as a major determinant of post-ischemic apoptosis in the heart, since their *in vivo* studies demonstrate that apoptosis is reduced in the myocardium of BNIP3-/- mice after surgical I/R injury (240). Furthermore, they showed that forced cardiac expression of

BNIP3 increases cardiomyocyte apoptosis in unstressed mice. BNIP3-mediated apoptosis has also been demonstrated in hypoxic fibroblast-like synoviocytes, which are important in the pathophysiology of rheumatoid arthritis (252).

1.7.3.3 BNIP3-mediated necrosis

Some reports have described BNIP3-mediated cell death as "non-apoptotic" or "necrosis-like", due to the absence of caspase activity and the presence of certain morphological features. For example, Greenberg and colleagues demonstrated that caspase-independent, BNIP3-mediated cell death involved early plasma membrane permeability, mitochondrial damage, and extensive cytoplasmic vacuolation, yielding a morphotype that is typical of necrosis (78). Another study provides similar ultrastructural evidence for BNIP3-mediated necrosis in *Shigella*-infected nonmyeloid cells (253).

1.7.3.4 BNIP3-mediated autophagy and autophagic cell death

There is strong evidence that BNIP3 induces autophagic cell death. When BNIP3 was first discovered, autophagy had not yet been validated as a distinct form of programmed cell death, but over the last decade it has become clear that BNIP3 is a key regulator of autophagy and autophagic cell death in many contexts and cell types.

Autophagic cell death, described in section 1.4.3, is measured experimentally by observing autophagosomes through ultrastructural analysis, detecting acidic vacuoles with pH-sensitive dyes, and monitoring the localization and processing of LC3, a protein that is recruited to autophagosome membranes during autophagy. These hallmarks of

autophagy have been detected during BNIP3-mediated cell death in multiple cell types

under various stress conditions. For example, malignant glioma cells treated with

hydrogen peroxide, ceramide or arsenic trioxide have been shown to undergo autophagic

cell death dependent on BNIP3 (71, 254, 255). BNIP3-mediated autophagic cell death

has also been demonstrated in primary mouse embryonic fibroblasts treated with hypoxia

mimetics (218). However, others have shown that hypoxia-induced autophagic cell death

is governed by 5'-AMP-activated protein kinase (AMPK), independent of BNIP3 (256).

Finally, increased expression of BNIP3 in skeletal muscle has been shown to induce

autophagy, which contributes to cell death in muscle-wasting disorders (212).

In addition to its role in autophagic cell death, BNIP3 has also been implicated in

protective autophagy signaling. One study demonstrated protective BNIP3-mediated

autophagy in a model of ischemia-reperfusion injury in cardiomyocytes (98), while

another showed that BNIP3-mediated autophagy was required during prolonged hypoxia

to prevent high levels of ROS and cell death in mouse embryonic fibroblasts (257).

The next section will discuss the proposed molecular mechanisms by which BNIP3 may

promote or regulate autophagy and/or autophagic cell death.

1.7.4   Mechanisms of BNIP3-mediated autophagy

The precise mechanism by which BNIP3 regulates autophagy has yet to be fully

elucidated; however, in light of recent evidence, several theories have been developed

(Figure 1.10). One model is based on evidence that BNIP3 competes with Beclin-1 for

interaction with Bcl-2 (257). Beclin-1, a novel BH3-only protein (258), is an essential

autophagy effector that is inhibited when bound at its BH3 domain by Bcl-2 or Bcl-xL (77). Thus, by disrupting this interaction and liberating Beclin-1, BNIP3 can promote autophagy.

BNIP3 may also indirectly promote autophagy by causing mitochondrial dysfunction. As discussed earlier, BNIP3 is targeted to mitochondria where it induces loss of mitochondrial membrane potential and stimulates production of mitochondrial ROS (78, 259). Mitochondrial ROS are potent induces of autophagy (260, 261), signaling for the removal of damaged mitochondria though selective mitochondrial autophagy or "mitophagy" (147). Indeed, mitophagy in hypoxia is BNIP3-dependent both *in vitro* (257) and *in vivo* (262).

Yet another possibility is that BNIP3 induces autophagy via the mTOR signaling pathway. The mammalian target of rapamycin (mTOR) is a central regulator of both cell growth and autophagy (as described in section 1.3.1), and is activated upstream by Rheb, a Ras-related small GTPase (158). Guan and colleagues have shown that BNIP3 directly binds and inactivates Rheb, thereby inhibiting the mTOR pathway, leading to reduced cell growth *in vivo* (263). Although autophagy was not specifically investigated in this study, it is likely that BNIP3-mediated inhibition of mTOR stimulates autophagy, since other mTOR inhibitors (such as rapamycin) are potent inducers of autophagy (52, 93, 158).

Thus, BNIP3 may promote autophagy by at least three independent mechanisms: liberation of the autophagy effector protein Beclin-1 from inhibitory complexes,

stimulation of autophagy-inducing ROS production from damaged mitochondria, and

inhibition of the mTOR pathway (Figure 1.10). However, further studies are required to

fully characterize these and other potential mechanisms of BNIP3-mediated autophagy

and autophagic cell death.
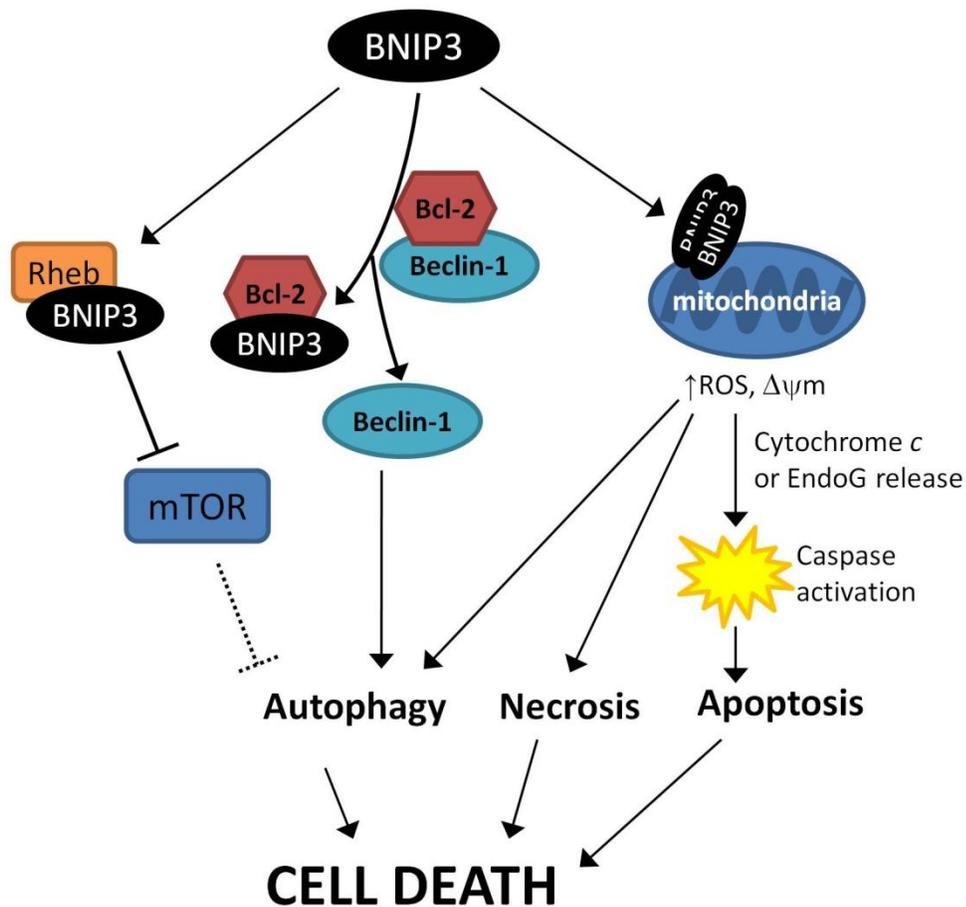
Figure 1.10 Mechanisms of BNIP3-induced cell death.
BNIP3 can induce cell death via autophagic, necrotic or apoptotic mechanisms. BNIP3 homodimers insert into the outer mitochondrial membrane, causing mitochondrial dysfunction characterized by increased reactive oxygen species (ROS) production, opening of the mitochondrial permeability transition pore and subsequent loss of mitochondrial membrane potential ($\Delta\psi$m). Mitochondrial damage can lead to caspase-independent necrotic cell death.   Alternatively, apoptosis will result upon release of mitochondrial apoptotic proteins (cytochrome c or EndoG) and activation of caspases. BNIP3 regulates autophagy and autophagic cell death by three different mechanisms: a) direct binding and inhibition of the mTOR-activating GTPase, Rheb, thereby relieving mTOR's inhibition of the autophagy pathway; b) liberation of the autophagy effector protein, Beclin-1, from an inhibitory complex with Bcl-2 through competitive binding at the BH3 domain; and c) indirect induction of autophagy by BNIP3-mediated mitochondrial ROS. Adapted from (196).

1.7.5   Role of BNIP3 in human disease

BNIP3 has been implicated in several hypoxia-related pathological conditions, including rheumatoid arthritis, liver disease, stroke, and Alzheimer's disease. The role of BNIP3 in heart disease and cancer will be discussed separately in subsequent sections.

Under normal physiologic conditions, BNIP3 expression is restricted to only a few tissues such as skeletal muscle and brain (233). The function of BNIP3 in these tissues has not been well characterized, but could involve repression of transcriptional targets in the nucleus (230), or regulation of basal autophagy (212). However, as discussed earlier in section 1.7.2, BNIP3 is highly upregulated under conditions of hypoxic stress, which are characteristic of several pathological conditions.

Chronic and repetitive episodes of hypoxia are known to play a role in the pathogenesis of rheumatoid arthritis (RA), a disease characterized by inflammation of the synovial joints (31). In a study by El-Gabalawy and colleagues, BNIP3 was found to be highly expressed in the synovium of RA patients, yet RA synoviocytes are characteristically resistant to apoptosis, leading to synovial hyperplasia (252). Over-expression of BNIP3 in cultured fibroblast-like synoviocytes increased apoptosis; however, this effect was inhibited by physiological concentrations of TNFα (tumor necrosis factor alpha) and IL-1β (interleukin 1 beta), two pro-inflammatory cytokines that are found abundantly in RA synovium. Thus, although BNIP3 is widely expressed in RA synovium, its pro-death activity may be inhibited *in vivo* by pro-inflammatory cytokines. Taken together, these

results suggest that increasing BNIP3 expression and/or inhibiting inflammatory cytokines in the synovium could represent a novel treatment approach for RA.

BNIP3 has also been implicated in liver disease, where hypoxia is associated with inflammatory conditions such as ischemia-reperfusion (I/R) and hemorrhagic shock (264, 265). Using RNA interference techniques, Zamora and colleagues have demonstrated that BNIP3 contributes to hypoxia-induced cell death of hepatocytes (234). Furthermore, they used two different models of liver stress (segmental hepatic ischemia and cannulation with controlled bleeding) to demonstrate upregulation of BNIP3 *in vivo*. In another study, BNIP3 upregulation was correlated with liver damage in mice treated with the plant toxin monocrotaline, but the role of BNIP3 was not specifically elucidated in this study (266).

There has also been a role described for BNIP3 in cerebral ischemia (stroke). Stroke results in acute loss of neurons, followed by a second round of delayed neuronal cell death through primarily caspase-independent pathways (267, 268). In a rat model of temporary focal cerebral ischemia, BNIP3 was upregulated and correlated with delayed neuronal death (269). In another study using a model of transient global brain ischemia, BNIP3 was shown to be upregulated and specifically localized to the nucleus of hippocampal neurons, where it was again associated with delayed neuronal death (235). Finally, a third *in vivo* study confirmed that BNIP3 is upregulated in neurons following stroke, but found mitochondrial localization of BNIP3. This study further demonstrated that hypoxia-induced cell death of neurons in culture is BNIP3-dependent (270).

In addition to stroke, hypoxia contributes to many other neurological disorders. This includes Alzheimer's disease, which is characterized by the formation of amyloid-β (Aβ) plaques leading to neuronal cell death and dementia (30). BNIP3 has been implicated in Alzheimer's disease, since Aβ treatment of cultured neurons results in oxidative stress-induced, HIF-1-mediated BNIP3 expression, which contributed to cell death (271). However, another study found that Aβ did not alter the expression of neuronal BNIP3 (272); therefore, further studies will be required to determine whether BNIP3 truly plays a pathological role in the etiology of Alzheimer's disease.

Thus, limited evidence implicates BNIP3 in several hypoxia-related pathological conditions, including rheumatoid arthritis, liver disease, stroke and Alzheimer's disease. More extensive research has detailed the role of BNIP3 in two additional pathological conditions: heart disease and cancer. These will be discussed separately in the following two sections.

1.7.5.1 BNIP3 in heart disease

BNIP3 has been extensively studied in the context of myocardial infarction, or cardiac ischemia and reperfusion (I/R), which is a major underlying cause of clinical heart failure (273). Typically, coronary artery occlusion results in decreased blood flow to the heart (myocardial ischemia) and leads to apoptotic and/or necrotic cell death of cardiomyocytes. Ischemia limits the delivery of oxygen and nutrients to cardiac cells, and is therefore associated with both hypoxia and acidosis (low pH due to lactic acid buildup as a byproduct of increased glycolysis). When reperfusion restores blood flow to

the heart, either spontaneously or through active clinical treatments, the cardiac cells are subject to further damage caused by oxidative stress (274). There is strong evidence implicating BNIP3 in the pathology of I/R injury and myocardial infarction, including many *in vitro* studies of hypoxia-induced cell death in cultured cardiomyocytes, and several *in vivo* studies of I/R injury in animal models.

Using cultured cardiomyocytes, several studies have demonstrated that hypoxia/acidosis-induced cell death is BNIP3-dependent. Experimental evidence shows that BNIP3 expression in cardiomyocytes is induced by hypoxia and persists throughout reoxygenation (237, 242, 275, 276), and that BNIP3 protein is stabilized by acidosis (237, 275). Furthermore, inhibition of BNIP3 by RNA interference or co-expression of a dominant negative mutant blocks hypoxia-induced cell death *in vitro* (98, 237, 242, 275), while over-expression of BNIP3 induces cell death (237, 242).

Several *in vivo* studies have provided further evidence that BNIP3 regulates I/R injury in the heart. Firstly, high levels of BNIP3 protein have been detected in animal models of chronic heart failure (206, 242). In addition, a recent study showed that BNIP3-/- mice experienced 50% less myocardial apoptosis after surgical I/R injury compared to wild type mice (240). Although BNIP3 knockout had no effect on the contractile performance of healthy hearts, BNIP3-/- mice exhibited preserved cardiac output after I/R injury, suggesting myocardial salvage by inhibition of apoptosis. This study also showed that forced cardiac expression of BNIP3 caused myocardial apoptosis and contractile dysfunction in unstressed mice, and further exacerbated post-I/R cardiac damage.

Together, these studies indicate that BNIP3 is a major determinant of post-I/R injury in the heart.

The mechanism of hypoxia-induced, BNIP3-mediated cell death of cardiomyocytes is still under investigation. Over-expression of BNIP3 in cardiomyocytes generally causes cell death characterized by mitochondrial dysfunction; however, some studies report necrosis-like cell death while others report apoptosis. In several studies, BNIP3 failed to activate caspases, and caspase inhibitors were not protective (237, 275). Yet, other studies report that BNIP3 triggered caspase-dependent cell death characterized by hallmarks of apoptosis such as release of cytochrome *c* and caspase 3 cleavage (98, 242). These discrepancies could be attributed to differences in the cell lines tested, or differences in the glucose-content or pH buffering of culture media. In addition, necrotic, autophagic and apoptotic features are known to occur simultaneously, which may confound results. Nevertheless, further investigation is required in order to determine the exact mechanism of BNIP3-induced cell death in the heart.

In summary, there is strong *in vitro* and *in vivo* evidence to implicate BNIP3 as a prominent regulator of cardiac I/R injury, but more research is required to precisely define the role of BNIP3 in ischemic cardiomyopathy and heart failure.

1.7.5.2   BNIP3 in cancer

In addition to the disease conditions discussed in previous sections, hypoxia also contributes significantly to the pathology of cancer (as discussed in section 1.2.3.1). Accordingly, BNIP3 is frequently upregulated in poorly oxygenated regions of solid

tumors. Paradoxically, these tumor cells remain viable. Hypoxic cancer cells have therefore developed mechanisms to evade BNIP3-induced cell death, including sequestration of BNIP3 protein in the nucleus, increased growth factor signalling, and methylation and silencing of the BNIP3 gene, as discussed below.

Increased BNIP3 expression has been observed in human brain tumors, endometrial cancer, cervical tumors, DCIS (ductal carcinoma *in situ*), invasive breast carcinomas, lung tumors, follicular lymphomas, gastric adenocarcinomas, and prostate tumors (reviewed in (196)). In several studies, BNIP3 expression was found to correlate with tumor grade, metastasis or patient outcome. For example, BNIP3 expression was correlated with more advanced clinical stages in cervical tumors (277), increased tumor grade and invasiveness in DCIS (278), increased invasiveness and metastasis in colorectal cancer (279), and poor overall outcome in ependymomas (280), endometrial cancer (281) and non-small cell lung cancer (282).

Thus, despite its pro-death activity, BNIP3 expression in cancer often predicts aggressive disease. This suggests that tumor cells have evolved mechanisms to evade BNIP3-induced cell death. Indeed, this has been proven in several independent studies where BNIP3 is sequestered in the nucleus of cancer cells, such that it cannot activate cell death pathways. Nuclear BNIP3 has been observed in gliomas, non-small cell lung tumors, cervical tumors, breast tumors, and prostate tumors (reviewed in (196)). Nuclear BNIP3 in tumors is associated with poor prognosis and may provide a marker for aggressive disease (233, 282, 283). In glioma cells, nuclear BNIP3 prevents cell death by repressing transcription of the apoptosis-inducing factor (AIF) gene, suggesting a mechanism for the

pro-survival activity of nuclear BNIP3 (230). Another mechanism by which tumors can compensate for increased BNIP3 expression is through increased growth factor (EGF and IGF) signaling, which is known to counteract BNIP3-mediated cell death (207).

Despite the high incidence of hypoxia in solid tumors, corresponding increased BNIP3 expression is not always observed. This is typically accomplished in tumors and cancer cell lines through epigenetic silencing of the BNIP3 promoter. Inactivation of BNIP3 by hypermethylation has been observed in a variety of human cancers including haematopoietic, colorectal, hepatocellular, pancreatic and gastric tumors (284-290). Of these, only two studies analyzed patient outcomes, and both found that BNIP3 silencing correlated with poor prognosis. Friess and colleagues detected BNIP3 silencing in 59% of pancreatic cancer specimens, correlating with a 43% reduction in patient survival (285), while Zochbauer-Muller and colleagues detected BNIP3 silencing in 5.4% of multiple myeloma tumors, correlating with a more than 3-fold reduction in patient survival (290). Notably, normal matched tissue samples from patients with pancreatic, colorectal, and gastric tumors did not exhibit methylation of the BNIP3 promoter (288, 289), suggesting that BNIP3 promoter methylation may be cancer-specific.

Studies have also shown that BNIP3 expression is silenced by hypermethylation in a majority of pancreatic, gastric and colon cancer cell lines, where demethylation restores hypoxia-inducible BNIP3 expression and increases sensitivity to hypoxia-mediated cell death (288, 291). Furthermore, decreased BNIP3 expression in these cell lines has been associated with intrinsic chemoresistance to oxaliplatin (292), 5-fluoro-uracil (285, 293) and gemcitabine (285, 286). This is in agreement with several other studies implicating

BNIP3 in chemotherapy-induced cell death, including ceramide and arsenic-trioxide-induced killing of glioma cells (71, 254), concanavalin A-induced killing of hepatoma cells (294), and bortezomib-induced killing of breast cancer cells (295).

Recently it has been shown that BNIP3 may have opposing functions at different stages of tumor progression: BNIP3 expression was associated with good survival outcome in invasive breast cancer, but with poor outcome in pre-invasive disease.(296) This "dual role" of BNIP3 could potentially be attributed to its role in autophagy. Induction of autophagy through BNIP3 in pre-invasive cancers may provide tumor cells with extra nutrients and promote further tumor progression. However at later stages, BNIP3 expression could promote prolonged autophagy in hypoxic cancer cells, leading to autophagic cell death and better patient outcome.

In summary, down-regulation of BNIP3 allows tumor cells to evade cell death, and is associated with a chemo-resistant phenotype and decreased patient survival. When BNIP3 expression is not effectively repressed, hypoxic tumor cells may counteract the pro-death activity of BNIP3 with increased growth factor signaling or by sequestering BNIP3 in the nucleus. Finally, through its role in regulating autophagy, BNIP3 may have opposing functions at different stages of tumor progression. Due to its role in cancer progression and treatment, BNIP3 may represent an attractive target for novel cancer therapy approaches.

1.7.6 BNIP3 in development

Little is known about the role of BNIP3 in development. BNIP3-/- mice are born in normal Mendelian ratios from heterozygous crosses, and show no increase in mortality or apparent physical abnormalities (240). Thus far, only the cardiac and hematopoietic systems have been characterized in BNIP3-/- mice, and no detectable defects have been identified in unstressed animals (240). Gene expression profiling studies have shown that levels of BNIP3 mRNA, in parallel with Bcl-xL, increase markedly during oligodendrocyte differentiation in an *in vitro* model system (297). This suggests that BNIP3 and Bcl-xL may simultaneously regulate cell survival and cell death during oligodendrocyte differentiation. In agreement with these results, Sandau and Handa have identified BNIP3 as a potential mediator of developmental apoptosis in the postnatal rat brain (298). They found that BNIP3 expression peaked at postnatal day 6.5, correlating with naturally occurring cell death in the neonatal rat cortex and hippocampus. In addition, BNIP3 has been implicated in chondrocyte and osteoclast differentiation, which are known to involve other hypoxia-responsive genes (299, 300).

Controlled cell death is an important aspect of mammalian development, and preliminary evidence suggests that BNIP3 may play a role in this process. However, further studies are required to fully characterize the role of BNIP3 in the development of different organs, tissues and cell types.

1.7.7   BNIP3L/NIX

As described in section 1.6.2.1, the BNIP3L/NIX protein shares 56% homology with BNIP3. NIX has a C-terminal transmembrane domain that is highly homologous to BNIP3, as well as a similar PEST sequence and BH3 domain (301). Similar to BNIP3, NIX is upregulated by hypoxia, localizes to mitochondria and induces cell death in multiple cell lines (301). BNIP3 and NIX are both upregulated in ischemic myocardium (302), and in human breast tumors (303). However, BNIP3 and NIX are regulated by two different pathways in the heart (210, 302), and are differentially correlated with tumor grade in breast cancer (304). Together, these data suggest that BNIP3 and NIX may have both overlapping and distinct functional roles *in vivo*.

1.8 Thesis Rationale and Objectives

1.8.1 Rationale

The solid tumor microenvironment often comprises chronic hypoxia, leading to metastatic changes in tumor cells and resistance to apoptosis (section 1.2.3.1). Current data suggests that autophagy may represent an attractive therapeutic target as an alternative cell death pathway (section 1.3.5.1). Therefore, I sought to determine whether autophagic cell death could be induced in hypoxic cancer cells in the absence of apoptosis.

In order to successfully target autophagic cell death as a cancer treatment strategy, individual target molecules must be identified. Ubiquitous autophagy proteins are not suitable targets since autophagy is a critical pathway for homeostasis in normal cells (section 1.3.3). Therefore, I aimed to determine whether BNIP3 may represent a more cancer-specific autophagy target molecule, since it is specifically induced in hypoxia, and since others have observed autophagic morphology in BNIP3-expressing cells (section 1.7). Since some tumors exhibit resistance to BNIP3-induced cell death (section 1.7.5.2), I also developed a model system for studying the mechanisms of "BNIP3 resistance".

Finally, to further explore the role of BNIP3 in development, autophagy and cell death, I initiated studies using the BNIP3 knockout mouse model. Given the limited evidence implicating BNIP3 in developmental apoptosis and oligodendrocyte differentiation (section 1.7.6), I also sought to further characterize the role of BNIP3 in mammalian brain development.

1.8.2 Hypotheses

BNIP3 mediates autophagic cell death in cancer cells exposed to prolonged hypoxia.

BNIP3 further mediates astrocyte proliferation and brain development *in vivo.*

1.8.3 Objectives

The specific objectives of this project were to:

1) Characterize the mechanism of hypoxia-induced cell death in cancer cells.

2) Determine the role of BNIP3 in hypoxia-induced autophagy and cell death.

3) Identify potential mediators of resistance to BNIP3-induced cell death.

4) Characterize the role of BNIP3 in proliferation and cell cycle progression *in vitro*.

5) Characterize the role of BNIP3 in mouse brain development *in vivo*.

The methods used to accomplish these objectives are described in:

Chapter 2: Materials & Methods.

Results are presented in the following chapters:

Chapter 3: Hypoxic cancer cells can undergo autophagic cell death in the absence of apoptosis.

Chapter 4: BNIP3 plays a pivotal role in hypoxia-induced autophagic cell death.

Chapter 5: Insights into BNIP3 resistance from an inducible expression system.

Chapter 6: A novel role for BNIP3 in cell cycle regulation during brain development.

Finally, these results and their significance are discussed with respect to the relevant scientific literature in:

Chapter 7: Discussion.

Chapter 2: Materials & Methods

2.1   Reagents and chemicals

All chemicals and solvents were of reagent or analytical grade and were obtained from one of the following sources: Sigma-Aldrich (Oakville ON), GIBCO-BRL (Burlington ON), Fisher Scientific (Ottawa ON), Invitrogen (Burlington ON), Calbiochem (San Diego, CA), BIORAD (Mississauga ON), Alexis Biochemicals (San Diego CA), Roche (Mississauga ON), BD Biosciences (Oakville ON), and GE Lifesciences, (Baie d'Urfe QC).

Caspase inhibitor z-VAD-fmk (N-benzyloxycarbonyl-Val-Ala-Asp[O-Me]-fluoromethyl ketone, Calbiochem) was used at 100 μM. 3-methyladenine (Sigma-Aldrich) was used at 2 mM or 5 mM, as indicated. Etoposide (Sigma-Aldrich) was used at 1 mM or 100 μM as indicated. Chloroquine (Sigma-Aldrich) was used at 0.1 mM. The lysosomal inhibitor NH_4Cl was used at 30 mM.

2.2   Antibodies

Antibodies used for Western blot (WB), immunofluorescence (IF), and flow cytometry (FACS) are listed in Table 2.1 (primary antibodies) and Table 2.2 (secondary antibodies).

Table 2.1 Primary Antibodies

Antigen	Host Species	Application (dilution)	Source		
Actin	Rabbit	WB (1:1000)	Sigma-Aldrich	A2066	Oakville, ON
Akt	Rabbit	WB (1:1000)	Cell Signaling	9272	Boston, MA
ATG5	Goat	WB (1:200)	Santa Cruz	sc-8667	Santa Cruz, CA
Beclin 1	Rabbit	WB (1:2000)	Novus	NB 500-249	Burlington, ON
Beclin1	Goat	WB (1:200)	Santa Cruz	sc-10086	Santa Cruz, CA
BNIP3 [mono]	Mouse	WB (1:500)	Dr. A. Greenberg	n/a	University of Manitoba
BNIP3 polyclonal	Rabbit	IF (1:250)	Dr. A. Greenberg	n/a	University of Manitoba
BrdU	Mouse	IF (1:400)	Millipore	MAB4072	Billerica, CA
GFAP	Rabbit	IF (1:1000) WB (1:10,000)	DakoCytomation	Z 0334	Mississauga, ON
HMGB1	Rabbit	IF (1:500)	AbCam	ab18256	Cambridge, MA
LC3	Rabbit	WB (1:200)	Abgent	AP1802b	San Diego, CA
LC3	Mouse	WB (1:300)	Nanotools	0231-100/LC3	Frieburg, Germany
Neurofilament	Rabbit	WB (1:5000)	AbCam	ab9035	Cambridge, MA
Phospho-H2A.X (FITC conjugate)	Mouse	FACS (1:50)	Upstate	16-202A	Billerica, CA

Table 2.2 Secondary Antibodies

Antigen	Host Species	Conjugate (dilution)	Source	
rabbit or mouse IgG	Donkey	Alexa Fluor 488 (1:700)	Molecular Probes	Eugene, OR
rabbit or mouse IgG	Goat	Rhodamine Red (1:700)	Molecular Probes	Eugene, OR
rabbit or mouse IgG goat IgG	Goat Donkey	Horse radish peroxidase (1:3000)	BIORAD	Mississauga, ON
rabbit or mouse IgG	Goat	FITC: fluorescein isothiocyanate (1:200)	Sigma-Aldrich	Oakville, ON

2.3   Plasmids and expression constructs

2.3.1   Constructs for transient and stable over-expression

The GFP-LC3 expression construct (p-EGFP-C1-LC3), originally generated by Kabeya

et al. (305), was provided by Dr. Michael Mowat (Manitoba Institute of Cell Biology).

Empty p-EGFP-C1 vector was obtained from BD Biosciences. The BNIP3 expression

constructs, pcDNA3-BNIP3 and pcDNA3-BNIP3ΔTM, were generated and provided by

Dr. Arnold Greenberg (Manitoba Institute of Cell Biology) {{}}. Empty pcDNA3 vector was obtained from Invitrogen.

2.3.2 Constructs for siRNA expression

Commercially designed siRNA reagents were obtained from Dharmacon (Lafayette, CO), including non-targeting siRNA and siRNA targeted against Beclin-1 and BNIP3. Custom siRNA targeted against ATG5 (5'-GCAACUCUGGAUGGGAUUG-3') was obtained from Sigma-Proligo.

2.3.3 Constructs for TetON inducible expression system

Development of a tetracycline-regulated BNIP3 expression system is described in section 2.5.4. Regulatory (pcDNA6/TR) and inducible-expression (pcDNA4/TO) constructs were obtained from Invitrogen. The pcDNA4/TO-BNIP3 construct was kindly provided by Dr. Adrian Harris (Weatherall Institute of Molecular Medicine). The pcDNA4/TO-LacZ construct was generated by subcloning the LacZ gene from the pSV-β-gal vector (Promega) as described in section 2.5.4.

2.4 Cell culture

Unless otherwise indicated, all cell lines were maintained in a humidified 5% CO_2 environment at 37^oC. Starvation was induced by culturing cells in unsupplemented Earle's Balanced Salt Solution (EBSS, Hyclone). For hypoxia experiments, cells were cultured in less than 1 % oxygen within a hypoxic chamber (Fisher Scientific, Ottawa ON) filled with 5 % CO_2 and 10 % H_2, balanced with N_2.

2.4.1 Human transformed and cancer cell lines

Hypoxia is a critical factor in the development of brain and breast tumors (306, 307), therefore we used a selection of glioma (U87, U251, U373) and breast cancer cell lines (MDA-MB-231, MDA-MB-231M, ZR75, MCF7) for our *in vitro* experiments. In addition we used the transformed human embryonic kidney cell line, HEK293, in several experiments due to the high transfection efficiency achievable in this cell line.

Human transformed and cancer cell lines were cultured in Dulbecco's modified Eagle's medium (DMEM; Invitrogen, Burlington ON) with 100 units/mL penicillin and 100 μg/mL streptomycin (Invitrogen). HEK293 cells (American Type Culture Collection, Rockville MD) were supplemented with 10% bovine calf serum (BCS; Fisher Scientific, Ottawa ON). Human glioblastoma cell lines U251 and U87 (obtained from Dr. V.W. Yong, University of Calgary and Dr. C. Hao, University of Alberta, respectively) and U373 (American Type Culture Collection) were supplemented with 10 % (v/v) fetal bovine serum (FBS; Fisher Scientific, Ottawa ON), 2 mM L-glutamine, and 1 mM MEM sodium pyruvate (Invitrogen). Stable GFP-LC3 clones were selected with Geneticin (3 mg/mL). Human breast cancer cell lines (MDA-MB-231, MDA-MB-231-M) were supplemented with 10% FBS, 2 mM L-glutamine and 1% (v/v) non-essential amino acids (Invitrogen). The human cervical cancer cell line HeLa was supplemented with 5% FBS. The human breast cancer cell line ZR75 was supplemented with 10% FBS, 2 mM L-glutamine, and 1% non-essential amino acids.

2.4.2 Primary mouse astrocytes

Primary mouse astrocytes were cultured in custom astrocyte-selective media:

$CaCl_2 \cdot 2H2O$ (0.256 g/L), $MgSO_4$ (0.96 g/L), KCl (0.402 g/L), NaCl (6.78 g/L), NaH_2PO_4

(0.12 g/L), L-Glutamine (0.294 g/L), Phenol Red (0.02 g/L), D-Glucose (1.352 g/L),

$NaHCO_3$ (2.2 g/L) (all from Sigma-Aldrich, Oakville ON); with the following liquid

supplements from Invitrogen (Burlington, ON): MEM Amino Acids (4% v/v;

Invitrogen), MEM Vitamins (4% v/v; Invitrogen), 33 units/mL penicillin and 33 µg/mL

streptomycin. After isolation in serum-free media, astrocytes were supplemented with

10% or 7% FBS as described in section 2.15.6. Vigorous swirling was used to detach

non-astrocytic cells at the time of passaging and/or changing media.

2.4.3 Mouse embryonic fibroblasts

Mouse embryonic fibroblasts (MEFs) were cultured in DMEM with 100 units/mL

penicillin and 100 µg/mL streptomycin and 10% FBS. Experiments were performed on

MEFs between passages 4 and 8. MEF isolation is described in section 2.15.8.

2.4.4 Passaging and preservation of cells

Typically, cells were passaged at a 1/10 dilution after reaching 80% confluency. Except

for HEK293 (which do not require trypsinization), cells were detached from their culture

plates by incubating with 2.5 % trypsin-EDTA (5 ml per 100 mm plate) for 5 min at room

temperature. The reaction was neutralized by addition of an equal amount of complete

medium, and cells were transferred to a 15 mL conical screw cap tube (Fisher Scientific,

Ottawa ON) and centrifuged at 1200 rpm for 5 min. After centrifugation, the supernatant

was discarded and the cell pellet was resuspended in 10 ml of complete media and then seeded appropriately into new culture plates.

All cell lines were preserved for long-term storage in liquid nitrogen. To prepare cells for freezing, cell pellets were isolated from an 80 % confluent 100 mm plate as described above. Cells were resuspended in 1.5 ml of freezing medium (90 % v/v FBS and 10 % v/v DMSO) and transferred to a labeled Cryovial (Fisher Scientific, Ottawa ON). The vials were then cooled in a Nalgene Cryo freezing container in the -80°C freezer for 24 hrs prior to being transferred to liquid nitrogen for long-term storage.

2.5   Transfection of mammalian cells

2.5.1   DNA transient transfection

For transient transfection experiments, cells were seeded in 6-well dishes 24 to 48 hours prior to transfection in order to achieve approximately 60 % confluence. HEK293 cells were transfected using Lipofectamine 2000 (Invitrogen, Burlington ON), while all other cell lines (U87, U251, MDA-MB-231, U373) were transfected using GenePORTER (Genlantis, Markham ON) as per the manufacturer's instructions. For Lipofectamine 2000 transfections, 1 μg DNA diluted in 200 μL serum-free media was added drop-wise to 12 μl of Lipofectamine reagent diluted in 200 μL serum-free media, and the mixture was incubated for 30 min at room temperature in a microfuge tube. Then, 2.1 ml of serum-free media was added to each well and the DNA/Lipofectamine mixture was added drop-wise. The transfection reagent was incubated with the cells for 5 hrs before being replaced with fresh complete media. For GenePORTER transfections, 2 μg of

DNA, 50 μL of DNA dilutent B, and 10 μL of GenePORTER transfection reagent (per well) were incubated for 30 min at room temperature in a microfuge tube. Then, 1 mL of Opti-MEM serum-free media (Invitrogen) was added to each well and the DNA/GenePORTER mixture was added drop-wise. The transfection reagent was incubated with the cells for 5 hrs and then replaced with fresh complete media. Transfection efficiency (determined by immunofluorescence) was approximately 50% in HEK293 cells, and 15 – 25% in the cancer cell lines.

2.5.2   DNA stable transfection

Transfections were performed as described in section 2.5.1. After 48 hrs the transfected cells were harvested and seeded onto 100 mm tissue culture dishes at a 1/10 dilution. Stably-transfected cells were selected with Geneticin (3 mg/mL) and selection media was changed every 3 days. Once visible at 40x magnification, colonies derived from single cells were reseeded into separate wells of 24-well dishes containing selection media. Stable clones were expanded and tested for over-expression of the gene of interest (GOI), and at least three clones were retained and preserved for each GOI.

2.5.3   siRNA transient transfection

For *beclin-1* and *atg5* silencing, cells at 30% to 50% confluency were transfected with siRNA constructs using Oligofectamine (Invitrogen) according to the manufacturer's instructions. For each transfection, 200 nmol of siRNA was added per 100 mm plate (final concentration 40 nM). Two days post-transfection, cells were seeded into 6-well

plates in preparation for experiments. Knock-down was verified by Western Blot for target gene products as described in section 2.7.

For BNIP3 silencing, cells were seeded in 12-well dishes (5×10^4 cells/well). Cells were transfected at the time of seeding using HiPerfect (QIAGEN) according to the manufacturer's instructions, with a final siRNA concentration of 10 nM. Media was changed after 5 hours. 48 hours post-transfection, cells were transferred to hypoxia or retained in normoxia (control). Knock-down was verified by RT-PCR as described in section 2.8.

2.5.4 Development of a stable tetracycline-regulated BNIP3 expression system

Since BNIP3 is toxic to cells when over-expressed by traditional methods, an inducible tetracycline-regulated BNIP3 expression system was developed using Invitrogen's T-REx™ System. The T-REx™ system consists of two components: the pcDNA6/TR regulatory vector encodes the tetracycline repressor (TR) protein, and the pcDNA4/TO inducible expression vector contains the gene of interest (GOI) controlled by the cytomegalovirus (CMV) promoter and two upstream tetracycline operator sequences (TetO2). When cells are transfected with both components, the TR protein binds to the TetO2 sequence and represses transcription of the GOI. When added to the culture medium, tetracycline (or its more stable analogue, doxycycline) binds and alters the conformation of TR, which is then released from the TetO2 sites, allowing transcription of the GOI.

The BNIP3 gene had previously been subcloned into the pcDNA4/TO inducible expression vector in the laboratory of Dr. Adrian Harris (Weatherall Institute of Molecular Medicine), who kindly provided the vector for our use. The vector was sequenced (Calgary DNA Core Services) and then amplified using a Plasmid Maxi Prep kit (QIAGEN) according to the manufacturer's instructions.

As a control for tetracycline-inducible gene expression, the *LacZ* gene was subcloned into the empty pcDNA4/TO inducible expression vector (*LacZ* encodes for the β-galactosidase, or β-gal, reporter enzyme). First, the *LacZ* gene was cut from the pSV-β-gal vector (Promega) using the restriction enzymes HindIII and BamHI (sequential digestions at 37°C, 1 U enzyme/μg DNA; overnight for HindIII and 1 hour for BamHI). After each digestion, the DNA was purified using the QIAquick PCR Purification Kit (QIAGEN) according to the manufacturer's instructions. In parallel, the pcDNA4/TO vector was similarly digested and purified. Next, the digested and purified pSV-β-gal vector was electrophoresed on a 1% agarose gel with ethidium bromide. The *LacZ* band was excised from the gel and extracted using the Quantum Prep Freeze 'N Squeeze DNA Gel Extraction kit (BioRad). The *LacZ* fragment was then ligated into the digested pcDNA4/TO vector using T4 ligase (NEB) at 14°C overnight. The ligated pcDNA4/TO-β-gal vector was sequenced (Calgary DNA Core Services) and then amplified using a Plasmid Maxi Prep kit (QIAGEN) according to the manufacturer's instructions.

Next, we established stable U87 and HEK293 pcDNA6/TR-expressing cell lines. Transfections were performed as described in section 2.5.1. After 48 hrs the transfected

cells were harvested and seeded onto 100 mm tissue culture dishes at a 1/10 dilution.

Stably-transfected cells were selected with 10 μg/mL blasticidin (Invitrogen) and

selection media was changed every 3 days. For each cell type, 24 colonies (each derived

from a single cell) were reseeded into separate wells of 24-well dishes containing

selection media.

The stable pcDNA6/TR clones were then screened for TR "repressor activity" (Figure

2.1). Each clone was transfected, in duplicate, with the pcDNA4/TO-βgal vector as

described in section 2.5.1. The next day, transfected cells were treated with or without 1

μg/mL doxycycline (Sigma-Aldrich) and incubated for 24 hours to induce βgal

expression. Then, cells were assayed for βgal activity using the βgal Enzyme Assay

System (Promega) according to the manufacturer's instructions. Briefly, 50 μL of cell

lysate was added to an equal volume of 2X assay buffer, containing the substrate ONPG

(o-nitrophenyl-beta-D-galactopyranoside). Samples were incubated for up to 30 min at

37°C to allow for βgal-mediated hydrolysis of the colorless substrate to its colored

product, o-nitrophenyl. Finally, absorbance was read at 420 nm with a SpectraMax M5

multi-mode microplate reader (Molecular Devices, Toronto ON) (Figure 2.1). For each

cell type, the "best repressor clone" (the clone displaying the lowest background β-gal

activity with the highest inducible activity) was retained for use in future experiments.
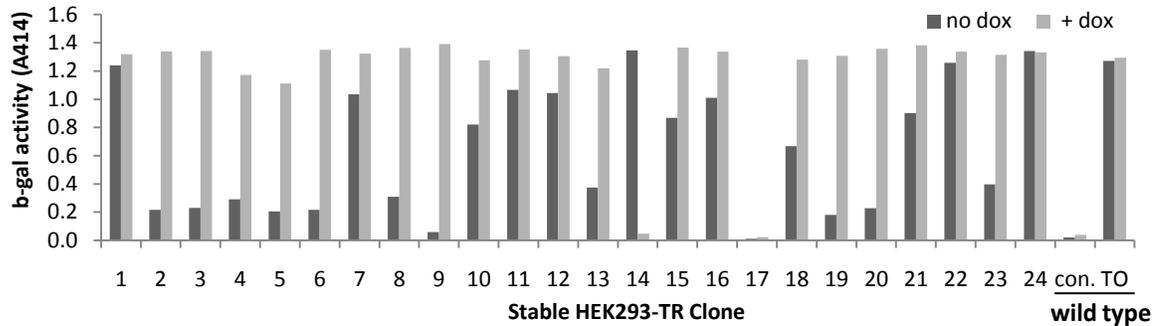
Figure 2.1 B-gal reporter assay for selection of TR repressor clones.
Stable HEK293-TR (pcDNA6/TR) clones were transiently transfected with the pcDNA4/TO-β-gal vector and induced with 1 µg/mL doxycycline (dox) for 24 hours. β-gal activity was then measured using the β-gal Enzyme Assay System (Promega). As a control, β-gal activity was also tested in wild-type cells with or without the reporter vector. Clone 9 was selected as the best repressor clone (low background and high inducible β-gal activity), and was used to generate the stable TetON inducible cell lines. The same procedure was used to select the best U87 repressor clone.

Next, stable inducible cell lines were generated by transfecting the TR clones with pcDNA4/TO inducible expression vectors (empty pcDNA4/TO or pcDNA4/TO-BNIP3 or pcDNA4/TO-βgal) as described in section 2.5.1. After 48 hrs the transfected cells were harvested and seeded onto 100 mm tissue culture dishes at a 1/10 dilution. Stably-transfected cells were selected with blasticidin (10 µg/mL) and zeocin (200 µg/mL for HEK293, 500 µg/mL for U87; Invitrogen) in order to simultaneously select for the regulatory and inducible expression vectors, respectively. Selection media was changed every 3 days. For each cell type, 24 colonies (each derived from a single cell) were reseeded into separate wells of 24-well dishes containing selection media.

The stable inducible clones were then screened for doxycycline-inducible gene expression. Clones were plated in duplicate and treated with or without 1 µg/mL doxycycline for 24 hours. Inducible expression was determined by βgal Enzyme Assay System (for βgal clones, as described above) or by anti-BNIP3 Western Blot (for BNIP3

84

clones, as described in section 2.7). For each cell type (U87-TR and HEK293-TR), a

single pcDNA4/TO clone, two highly-inducible βgal clones, and at least three inducible

BNIP3 clones (low, medium and high induction) were retained for future experiments.

Inducible BNIP3 expression was additionally verified by immunofluorescence as

described in section 2.14.1, and by RT-PCR as described in section 2.8.

2.6   Cell lysis

Cultured cells and frozen tissue samples were lysed for analysis of total proteins. Cell

lines were harvested from the culture dishes as described in section 2.4.4, and centrifuged

to obtain cell pellets. Mouse tissues were harvested and cryo-preserved as described in

section 2.15.2.

2.6.1   Lysis for total proteins from cultured cells

Cell pellets were resuspended in NP40 lysis buffer (1.8 M Hepes pH 7.5, 4 M NaCl, 50

mM $ZnCl_2$, 0.5 M EDTA, 50 mM NaF, 1 % NP40 v/v), including protease inhibitors (1

mM Na ortho-vanadate, 2 mM PMSF). Lysates were vortexed for 15 sec, incubated on

ice for 5 min, vortexed again and incubated for a further 5 min on ice. Samples were then

centrifuged for 5 min at 16000 rpm. The supernatant (total protein lysate) was

transferred to a new microcentrifuge tube and stored at -20°C (short term) or -80°C (long

term).

2.6.2 Lysis for total protein from frozen mouse tissue

Cryo-preserved brain and heart tissue from -80°C storage was cooled further in a thermos filled with liquid nitrogen. A mortar and pestle was also cooled with liquid nitrogen. The tissue was pulverized with the mortar and pestle and scraped into a cooled microfuge tube. RIPA lysis buffer with protease inhibitors was added to the powdered tissue and samples were vortexed for 15s, incubated on ice for 10 min, vortexed again and incubated another 10 min on ice. Samples were then centrifuged at 14000 rpm for 5 min at 4°C. The supernatant (total protein lysate) was transferred to a new microcentrifuge tube and stored at -80°C.

2.7 Western blotting

Protein concentrations were determined by a Bradford assay (BIORAD, Mississauga ON) using BSA (bovine serum albumin) as a standard control and measuring with a DU640 Spectrophotometer (Beckman Coulter, Mississauga ON). Samples were boiled for 5 min in SDS sample buffer (65 mM Tris HCl, pH 6.8, 2 % SDS, 10 % glycerol, 2 % v/v beta-mercaptoethanol, and 0.01 mg bromophenol blue). Proteins were separated on a 10 % acrylamide gel by SDS-PAGE at 100V for approximately 2 hours. The separated proteins were transferred to 0.45 μm nitrocellulose membranes at 24V for 1-2 hours. (Alternatively, for LC3 Western blots, SDS-PAGE was performed using a 16% acrylamide gel with tricine in order to achieve optimal separation of the low molecular weight LC3 isoforms; proteins were transferred to 0.25 μm nitrocellulose membranes and baked at 60°C for 30 minutes prior to blocking.) Membranes were blocked in 5 % skim milk dissolved in TBS-T (20 mM Tris-buffered saline, pH 7.6, 0.1 % Tween 20), and

incubated overnight with primary antibody as indicated in Table 2.1. The next day,

membranes were washed 3 times with TBS-T and incubated with horseradish peroxidase-

linked anti-IgG secondary antibodies for one hour at room temperature, as indicated in

Table 2.2. Finally, the western blots were visualized on autoradiography film (Kodak)

with enhanced chemiluminescence (ECL-plus, NEN-Dupont, Boston MA) as described

by the supplier. Quantitative analysis of protein levels was performed by densitometry

using QuantityOne software (BioRad). When necessary, membranes were stripped for 30

minutes in stripping buffer (Western-Re-Probe, Calbiochem) prior to incubation with a

second primary antibody. Membranes were never re-probed more than twice. Each

western blot is representative of at least three independent experiments.

2.8   Reverse-Transcription and Polymerase Chain Reaction (RT-PCR)

Gene expression was assessed by RT-PCR using the RNAEasy kit (QIAGEN) for RNA

extraction and Superscript III Onestep kit (Invitrogen) for RT-PCR, according to the

manufacturer's instructions. The primers used to amplify mRNA transcripts are listed in

Table 2.3. RT-PCR reactions consisted of 30 minutes at 55°C for cDNA synthesis, 2

minutes at 94°C for denaturation, and 22-28 cycles of [94°C (15 sec), T_M°C (30 sec),

68°C (20 sec)] for amplification, as detailed in Table 2.3. PCR products were separated

on a 2% agarose gel with ethidium bromide (0.1 µg/mL) and visualized with UV

irradiation on a GelDoc2000/ChemiDoc System (Bio-Rad).

Table 2.3 Primers used for RT-PCR gene expression analysis.

Gene	Primer Sequences	Product Size	T_M, Melting Temperature	Cycles
BNIP3	5'-GCA TGA GTC TGG ACG GAG TA-3' 5'-GTT TCA GAA GCC CTG TTG GT-3'	93	58°C	28
GAPDH	5'-ACC CAC TCC TCC ACC TTT G-3' 5'-CTC TTG TGC TCT TGC TGG G-3'	190	58°C	22
CLU (clusterin)	5'-CAG CCC TTC CTT GAG ATG AT-3' 5'-CAT CGT CGC CTT CTC GTA T-3'	109	58°C	22
API5	5'-GCC GAC AGT AGA GGA GCT TT-3' 5'-ATC TTT ATG CTG GCC CAC TT-3'	76	58°C	28
SSAT	5'-CTG CTA GAA GAT GGT TTT GG-3' 5'-ACT GGA CAG ATC AGA AGC AC-3'	330, 440	55°C	28
HSPA1A	5'-TGC GAC AGT CCA CTA CCT TT-3' 5'-AGA AGA GCT CGG TCC TTC C-3'	124	58°C	28

2.9   Microarray analysis of gene expression

Microarray analysis was employed to determine the effect of low-level, leaky expression of BNIP3 in stable inducible cell lines (described in section 2.5.4). RNA was extracted from non-induced HEK293 TO-BNIP3 and TO-βgal stable cell lines using the RNeasy Mini Kit (QIAGEN) according to the manufacturer's instructions. 20 µg of RNA per sample was shipped to the laboratory of Dr. Amadeo Parissenti (Sudbury Regional Hospital), where microarray analysis was performed as described in (308). Briefly, isolated RNA was used as the substrate for cDNA synthesis and Cy3- or Cy5-labeling. Labeled cDNAs were hybridized to H1.7k human cDNA array slides printed at the University Health Network Microarray Centre (Toronto, ON). Hybridized arrays were scanned on an Axon 4000B dual laser scanner (532 nm / 633 nm wavelengths) and the fluorescence intensities for each feature (spot) on the array were determined using GenePix Pro 3.0 software. The results were imported into Microsoft Excel worksheets

where data were normalized and corrected for background. A total of 1,728 genes were surveyed for differential expression between the TO-BNIP3 and TO-βgal samples.

2.10 Flow cytometric analysis of ROS

Reactive oxygen species (ROS) generation was determined by flow cytometry after cells were stained with DHE (dihydroethidium) or CM-H$_2$DCFDA (5-(and-6)-chloromethyl-2′,7′-dichlorodihydrofluofluorescein diacetate, acetyl ester). DHE and CM-H$_2$DCFDA are used to specifically detect the generation of intracellular O$_2^-$ and H$_2$O$_2$, respectively (309). DHE is oxidized to red fluorescent ethidium by O$_2^-$ and CM-H$_2$DCFDA is oxidized to green fluorescent DCF (dichlorofluorescein) by H$_2$O$_2$. Cells were suspended in PBS with 3.2 μM DHE or 5 μM CM-H$_2$DCFDA and incubated at 37°C for 15 min in darkness. Then, the cell suspension was transferred into a 5 ml FACS tube (Falcon) and analyzed on a flow cytometer using CellQuest software within 10 min.

2.11 Cell death assays

2.11.1 Membrane permeability assays for total cell death

Cells were resuspended in 100 μL medium and 2 μL of cell-permeable acridine orange (100 μg/mL), and cell-impermeable ethidium bromide (100 μg/mL) was added. Cells were viewed on an Olympus BX51 fluorescent microscope using the fluorescein filter set. The percentage of dead cells was calculated by counting the number of orange cells (with permeabilized membranes allowing entry of ethidium bromide) in a population of diffused green cells (with intact membranes excluding ethidium bromide). At least 200

cells were counted for each assay. Alternatively, cells were harvested and suspended in

PBS and stained with 0.04% trypan blue (Hartman-Leddon Co., Philadelphia, PA) for 5-

10 min at room temperature. Stained cells were analyzed by flow cytometry using the

FACSscan cytometer and CellQuest software (Becton Dickinson, Mississauga, ON,

Canada). Trypan Blue entering the cell (an indicator of membrane permeabilization) was

measured by the red filter (670 nm, FL3-H) on a log scale (310). Two peaks in the

histograph can be observed: the first peak represents viable cells (impermeable to trypan

blue / dim fluorescence); the second peak represents dead cells (permeable / strong

fluorescence). Through repeat experimentation, we have determined that these two

methods generate similar results in multiple cell lines.

2.11.2 MTT assay for cell viability

Cells were seeded in a 96-well dish (1000 cells /well) on day 1 and transferred to hypoxia

(or retained in normoxia with fresh media) on day 3. Plates were transferred back to

normoxia with fresh media after 24, 48 or 72 hours hypoxia (days 4, 5, or 6,

respectively). The MTT colorimetric assay (311) was performed on day 8: 150 μL of

MTT reagent (3-[4,5-dimethylthiazol-2-yl]-2,5-diphenyl tetrasodium bromide, 1 mg/mL)

in RPMI media was added to each well, and plates were incubated for 1 hour at 37°C in

normoxia. In viable (metabolically active) cells, the yellow MTT reagent is reduced to

insoluble purple formazan by mitochondrial enzymes. After incubation, the plates were

centrifuged at 1500 rpm for 10 min and 125 μL of DMSO was added to each well to

dissolve the purple formazan crystals and the absorbance was read at 540 nm on a

microplate reader.

2.11.3 HMGB1 localization assay for necrosis

HMGB1 (high-mobility group box 1) is normally tightly associated with nuclear chromatin; however, it is specifically released from the nucleus during necrosis (but not autophagy or apoptosis) (312). Cells were fixed, stained using a specific HMGB1 antibody (AbCam), and imaged as described in section 2.14.1. Necrotic cells were identified as cells without nuclear HMGB1 expression.

2.11.4 Apoptosis assays

2.11.4.1 Measurement of sub-G1 peaks with flow-cytometry

Cells were harvested and resuspended in 400 μl of hypotonic PBS with propidium iodide (50 μg/ml), a fluorescent DNA-intercalating agent. After 15 min at room temperature (in the dark), cells were analyzed for DNA content by flow cytometry using the FL2 filter (FACSCaliber, BD Biosciences) and CellQuest Pro software (BD Biosciences, Oakville ON) to resolve the G1 (2N DNA in resting cells), G2 (4N DNA in replicating cells) and sub-G1 peaks. Apoptotic cells are characterized by DNA cleavage, resulting in sub-G1 DNA content. The percentage of cells in the "sub-G1 peak" therefore indicates the percentage of cells undergoing apoptosis (313).

2.11.4.2 Caspase-3 assay

Caspase activity, a hallmark of apoptosis, was measured using the Caspase-3 Apoptosis Detection Kit (sc-4263) from Santa Cruz Biotechnology (Santa Cruz, CA) according to the manufacturer's instructions. Briefly, 20 ug of total cell lysate was diluted in 200 uL

reaction buffer with 10 mM DTT and 5 μL of DEVD-AFC substrate peptide. Reactions

were performed in 96-well plates and incubated for 1 hour at 37°C. The level of free

AFC (cleaved by active caspase 3) was measured using a SpectraMax M5 plate reader

from Molecular Devices (Sunnyvale, CA) with a 400 nm excitation filter and a 505 nm

emission filter.

2.11.4.3 H2A.X phosphorylation assay

The histone H2A.X is phosphorylated at its carboxy-terminal in response to DNA

double-strand breaks during apoptosis. H2A.X phosphorylation was measured using the

H2A.X Phosphorylation Assay Kit (17-344) from Upstate Biotechnology Inc. (Lake

Placid, NY) according to the manufacturer's instructions. Briefly, cells were harvested

and fixed for 20 minutes on ice in fixation solution at a cell density of 2×10^6 per mL. 50

μL of cells were then resuspended in permeabilization solution and incubated for 20

minutes on ice with 3.5 uL of anti-phospho-Histone H2A.X-FITC conjugate. After

washing to remove excess antibody, cells were resuspended in PBS and analyzed by flow

cytometry (FACSCaliber, BD Biosciences) using CellQuest Pro software (BD

Biosciences). Increased H2A.X phosphorylation is visualized as a shift in green

fluorescence.

2.11.4.4 Nuclear condensation assay

To assess nuclear condensation, another hallmark of apoptosis (314), cells were stained

with acridine orange and ethidium bromide as described in section 2.11.1. Cells showing

intense DNA staining in the nucleus were defined as apoptotic versus the diffuse nuclear staining of healthy cells. At least 200 cells were counted per condition.

2.12 Autophagy Assays

2.12.1 Electron microscopy for detection of autophagosomes

Cells were collected and fixed in 2% paraformaldehyde, 0.1% glutaraldehyde in 0.1 M sodium cacodylate for 2 h, postfixed with 1% OsO_4 for 1.5 h, washed and finally stained for 1 h in 3% aqueous uranyl acetate. The samples were then washed again, dehydrated with graded alcohols, and embedded in Epon-Araldite resin (Canemco Inc.). Ultrathin sections were cut on a Reichert ultramicrotome, counterstained with 0.3% lead citrate and examined on a Philips EM420 electron microscope for visual identification of double-membraned autophagosomes (315).

2.12.2 Detection and quantification of AVOs

Autophagy is characterized by the increased production of acidic vesicular organelles (AVOs). Although autophagosomes are not initially acidic, they ultimately fuse with acidic lysosomes at later stages of degradation. AVO detection is not, by itself, a sufficient method for monitoring autophagy; however, it can be an effective indicator in combination with other assays (315). To detect and quantify AVOs, cells were harvested and resuspended in PBS with acridine orange (1 µg/mL), incubated for 10 minutes at room temperature in the dark, and analyzed by flow cytometry (FACSCaliber, BD Biosciences) using CellQuest Pro software (BD Biosciences). Acridine orange is a cell-

permeable, pH-sensitive dye, which stains nuclei and cytoplasm green and any acidic

compartments red. An increase in red fluorescence therefore indicates increased

production of AVOs (315, 316). For each experiment, control (untreated, normoxic) cells

were used to calibrate the baseline level of AVO production to approximately 2%.

2.12.3 GFP-LC3 localization

LC3 is recruited to the autophagosome membrane during autophagy (305). Cells were

transiently transfected with the GFP-LC3 expression vector (305) as described in section

2.5. The next day, cells were incubated in normoxia or hypoxia as indicated. Ultimately

cells were examined under an Olympus BX51 fluorescent microscope to assess GFP-LC3

localization. GFP-LC3 presents a diffuse distribution under control conditions, whereas a

punctate pattern of GFP-LC3 expression is indicative of autophagy. GFP-LC3 stable

clones ("U87-GFP-LC3 cells") were generated in U87 cells after transfection and

selection with Geneticin. The GFP-LC3 expression vector was kindly provided by Drs.

N. Mizushima and T. Yoshimori (Tokyo Medical and Dental University) (305) via Dr.

M. Mowat (Manitoba Institute of Cell Biology).

2.12.4 LC3 processing

In order to be recruited to autophagosome membranes during autophagy, LC3 must be

cleaved and lipidated. This "processed" form of LC3 (LC3-II) can be distinguished from

unprocessed LC3 (LC3-I) by SDS-PAGE (305). Western blotting for LC3-I and LC3-II

was performed as described in section 2.7. LC3-II is continuously degraded during

autophagy, therefore accumulation of LC3-II could signify blockage of lysosomal

degradation rather than increased autophagic flux (315). Therefore, all LC3 processing experiments included control samples that were treated with the lysosomal protease inhibitor, chloroquine (when lysosomal degradation is functioning normally, chloroquine treatment will amplify LC3-II accumulation, permitting distinction between autophagic flux and blockage of lysosomal degradation).

2.13 Cell proliferation assays

2.13.1 Quantification of adherent cells

To compare the rate of cell growth between induced HEK293 TO-BNIP3 and TO-βgal cells, equal numbers of cells were seeded in 6-well dishes in triplicate. After three days, the total number of adherent cells in each well was determined by harvesting the cells in a consistent volume of fresh media and counting a 100 uL aliquot using a Beckman Coulter Counter.

2.13.2 BrdU incorporation

5-bromo-2-deoxyuridine (BrdU) is a synthetic analogue of thymidine, which is incorporated into the newly synthesized DNA of replicating cells during the S phase of the cell cycle (317). Primary cells (grown on glass coverslips) were incubated with 40 μg/mL BrdU for 8 to 72 hours, then immediately fixed in 3.7% formaldehyde for 15 min at room temperature, and stored at 4°C. Immunofluorescence staining for BrdU was performed at room temperature: first, fixed cells were washed twice for 5 min each in PBS. To denature DNA, cells were incubated in 2 M hydrochloric acid for 20 min.

Following neutralization (0.1 M sodium borate in PBS, pH 8.5; 5 min), cells were washed

three times in PBS and then permeabilized (0.2% Tritonx100, 0.5% FBS in PBS; 5 min).

After two more washes in PBS, cells were blocked for 20 min (0.1% NP40, 0.5% FBS in

PBS), and then incubated with anti-BrdU antibody (Chemicon; 1/400 in blocking

solution) for 1 hour. Cells were then washed three times (PBS, 0.1% NP40) and

incubated with FITC-conjugated anti-mouse-IgG antibody (1/200 in blocking solution)

for 1 hour in darkness. After three final washes, stained coverslips were mounted with

DAPI + antifade reagent (Biorad) to counterstain for nuclei. Fluorescence was visualized

and captured as described in section 2.14. BrdU incorporation (317) was scored in a

minimum of 300 cells per sample.

2.13.3 Measurement of G2 peaks with flow-cytometry

As described in section 2.11.4.1, cells were harvested and resuspended in 400 µl of

hypotonic PBS with propidium iodide (50 µg/ml), a fluorescent DNA-intercalating agent.

After 15 min at room temperature (in the dark), cells were analyzed for DNA content by

flow cytometry using the FL2 filter (FACSCaliber, BD Biosciences) and CellQuest Pro

software (BD Biosciences, Oakville ON) to resolve the G1, G2 and sub-G1 peaks

(representing 2N DNA in resting cells, 4N DNA in replicating cells, and cleaved DNA in

apoptotic cells, respectively) (313, 318). The percentage of cells in the G2 peak

represents the percentage of cells with 4N DNA content, achieved through DNA

replication in the S phase of the cell cycle. These cells may either be progressing through

the cell cycle (i.e. proliferating), or experiencing G2/M phase arrest. Therefore, results of

this assay must be interpreted together with additional assays for cell proliferation.

2.13.4 MTT assay for cell viability

As described in section 2.11.2, the MTT assay provides a quantitative measure of cell viability (311). Equal numbers of wild type and BNIP3-/- astrocytes were plated in 96-well dishes on "day 0" (increasing cell densities from 5,000 to 50,000 cells per well, in triplicate). The MTT assay was performed on days 1, 2, 4, 7 and 10 to measure cell proliferation. Briefly, cells were incubated in fresh media containing MTT reagent (0.2 mg/mL) for 1 hour at 37°C to permit metabolism of MTT to formazan in viable cells. After this incubation, media was aspirated and replaced with 125 uL DMSO per well, to dissolve the purple formazan crystals. Absorbance (which is proportional to the number of viable cells in each well) was measured at 540 nm on a microplate reader.

2.14 Immunofluorescence

2.14.1 Immunofluorescence on cultured cells

Cultured cells were either grown on coverslips, or harvested and adhered to glass slides using the ThermoShandon Cytospin 4 apparatus (3 minutes at 200 rpm with medium-low acceleration). In some cases, cells were incubated with 1 uL/mL Mitotracker (Molecular Probes) for 30 minutes prior to harvesting / fixation. Cells on slides or coverslips were fixed in 3.7% formaldehyde in PBS for 15 minutes at room temperature, and stored in fixing solution at 4°C. Following three washes with PBS (0.1 % NP40), slides/slips were incubated with primary antibody in PBS (0.1% NP40, 10% FBS) for 1 hour at room temperature as indicated in Table 2.1. Following three additional washes, slides/slips were incubated with secondary antibody for 1 hour at room temperature in darkness, as

indicated in Table 2.2. After three final washes, slides/slips were mounted with DAPI + antifade reagent (Biorad) to counterstain for nuclei. Fluorescence was visualized and captured using a Zeiss Axiophot microscope with a cooled charge-coupled device camera, or with an Olympus BX51 fluorescent microscope with a Photometrics Cool Snap CF camera and an Olympus IX70 inverted confocal laser microscope using Fluoview 2.0 software.

2.14.2 Immunofluorescence on cryopreserved brain tissue

Brain cryosections (described in section 2.15.4) were removed from -80°C storage and air-dried at room temperature for 15 min. Slides were incubated with 150 uL blocking buffer (PBS with 5% goat serum, 0.2% TritonX 100, 0.02% sodium azide, 1mg/mL BSA) for two hours at room temperature in a humid chamber. After blocking, slides were incubated with 100 uL primary antibody diluted in blocking buffer (as indicated in Table 2.1) overnight at 4°C. The next day, after three 5-min washes (PBS with 0.1% NP40), slides were incubated with 100 uL fluorescent-conjugated secondary antibody diluted in blocking buffer (as indicated in Table 2.2) for 1.5 hours at room temperature in the dark. After three final washes, coverslips were mounted with DAPI + antifade reagent (Biorad) to counterstain for nuclei. Fluorescence was visualized and captured as described above in section 2.14.1.

2.14.3 Immunofluorescence on paraffin-embedded brain tissue

Paraffin-embedded brain sections (described in section 2.15.5) were baked in an oven (60 ^{o}C) for 20 min. The slides were deparaffinized in coplin jars filled with xylene for 10

min, and rehydrated by sequential incubation in 100, 95, 85, 75, and 50 % ethanol for 2 min each. After two 5-min washes in ddH$_2$O, antigen presentation was performed by microwaving the slides in a pressure cooker filled with citrate buffer (10 mM citric acid monohydrate, pH 6.0) for 20 min on high power. The slides were removed, cooled to room temperature (RT), and then washed three times for 5 min in PBS-T (0.5 % Triton X100). Blocking solution (PBS, 0.2 % Triton X100, 0.02 % sodium azide, 5 % goat serum and 0.1 % bovine serum albumin) was added to each slide and incubated in a humidity chamber for 2 hrs at RT. Primary antibodies (Table 2.1) were diluted in blocking solution and added to the slides for overnight incubation at 4 $^{\circ}$C. The next day, slides were washed 3X with PBS-T and the appropriate secondary antibody (Table 2.2) was prepared in blocking solution and added to the slides for 2 hrs at RT in the dark. After three final washes in PBS-T, coverslips were mounted with SlowFade Gold antifade mounting reagent with DAPI stain (Invitrogen). Fluorescence was visualized and captured using an Olympus BX51 fluorescent microscope with a Photometrics Cool Snap CF camera.

2.15 BNIP3-/- mouse model

All animal protocols were conducted in accordance with guidelines set by the Canadian Council on Animal Care and the University of Manitoba Animal Care Committee. The BNIP3-null mouse model was kindly provided by Dr. Gerald Dorn (Washington University School of Medicine). The BNIP3-null allele was generated by replacing exons 2 and 3 of the BNIP3 gene with a neomycin resistance cassette through homologous recombination (240). This insertion truncates the BNIP3 protein prior to its

critical BH3 and transmembrane domains. The BNIP3-null allele was validated by Dorn and colleagues, who showed by Northern blot and immunoblot assays that neither BNIP3 RNA nor BNIP3 protein were detectable in homozygous BNIP3-null mice (240). Unless otherwise specified, heterozygotes were crossed to generate all wild type and BNIP3-null mice studied.

2.15.1 Genotyping and identification

Mice were ear-punched and genotyped between 3 and 4 weeks of age. Individual mice were identified using a simple cage-numbering and ear-punch system, with no more than four mice to a cage (no punch "0" / left ear punch "L"/ right ear punch "R"/ both ears punched "B"). Cages were numbered in sequence according to birth date; female cages were assigned odd numbers and male cages were assigned even numbers. Genomic DNA was extracted from tail clippings using the *prep*GEM™ extraction kit (Zygem, Solana Beach CA) according to the manufacturer's instructions. PCR was then performed using 3 primers (5′-TGTGGCTGAGAGTCAGTGGTC-3′; 5′-TTGCAAGTCTAGGAGTCAGTT-3′; 5′-GTGGATGTGGAATGTGTGCG-3′) to generate a 435-bp wild type allele product and a 220-bp BNIP3-null allele product under the following conditions: 94°C for 30 seconds, 60°C for 30 seconds, 72°C for 90 seconds; 33 cycles. PCR products were separated on a 1.8% agarose gel with ethidium bromide (125 V, 40 min) and visualized on a UV transilluminometer with QuantityOne imaging software (BioRad).

2.15.2 Tissue collection and cryopreservation

Adult mice were sacrificed by cervical dislocation (asphyxiation was not used due to the oxygen-sensitive nature of this research), and the heart and brain were immediately removed and separately transferred to labeled cryovials on ice. As soon as possible, the tissue-containing cryovials were immersed in liquid nitrogen to cryo-preserve the tissue. Samples were then stored at -80°C.

2.15.3 Tissue fixation by trans-cardiac perfusion

Adult mice were anesthetized with a lethal dose of avertin (1 mg/g delivered by intraperitoneal injection, Sigma-Aldrich). Mice were closely monitored to ensure complete anesthesia. After surgically retracting the rib cage to expose the beating heart, the right atrium was cut open with fine surgical scissors to allow for drainage of blood and perfusion fluid. An 18-guage cannula was immediately inserted into the left ventricle, and the mouse was slowly perfused with 30 mL of phosphate buffer (0.1 M, pH 7.4) to remove all traces of blood. Next, the mouse was perfused with approximately 30 mL of fresh paraformaldehyde fixative (4% in 0.1M phosphate buffer, pH 7.4) until the tissues were adequately fixed and the mouse became generally stiff. At this point the cannula was removed from the heart and the brain was carefully removed and immersed in fixative for post-fixation at 4°C overnight. The next day, the fixed brain was processed for paraffin embedding or cryo-preservation, as described below.

2.15.4 Whole brain cryopreservation, sectioning and cresyl violet staining

Fixed whole brains were cytoprotected in a sucrose gradient: brains were carefully transferred to 13 mL round-bottom snap-cap tubes and submerged in 10 mL of a 20% sucrose solution (20% v/v in 0.1 M phosphate buffer), and incubated on a rocking platform at 4°C until the tissue sunk to the base of the tube (usually overnight). This procedure was repeated in 30% sucrose solution. Then, half of the sucrose solution was replaced with OCT compound (optimal cutting temperature compound, Tissue-Tek) and the tissue was incubated for a further 60 min. Next, the brains were embedded in OCT over dry ice: working over a tray of dry ice, labeled plastic OCT molds (1 inch^3) were filled half-way with OCT and placed in a 100 mm plastic culture dish containing 15 mL of 2-methylbutane. As the OCT began to freeze from the bottom-up, the brain was carefully placed into the mold, using forceps to maneuver the brain into the desired orientation. Additional OCT was added to completely cover the tissue. Once the entire tissue-containing, OCT-filled mold was frozen (about 10 min), it was placed in an airtight bag and stored at -80°C until sectioning.

Cryosectioning was performed on a Shandon Cryotome SME Cryostat (Thermo Fisher Scientific). The tissue-containing OCT block was transferred from -80°C storage to the cryostat. The orientation of the tissue was marked with ink prior to discarding the plastic mold. The frozen OCT/tissue block was then allowed to equilibrate to -20°C in the cryostat for 1 hour prior to sectioning. At this point, the block was mounted onto the chuck with fresh OCT and using the "cryobar boost" setting. The top layer of OCT was cut away in 25 μm sections. Upon reaching the tissue, coronal sections were cut at 12

μm and every second section was discarded. Retained sections were mounted on pre-

labeled Superfrost PLUS glass slides (Fisherbrand) and kept inside the cryostat at -20°C.

Slides were ultimately transferred to plastic storage boxes and kept at -80°C.

Every 10th slide was removed and allowed to dry at room temperature, to be stained by

cresyl violet for morphological analysis and to serve as a reference section. After air-

drying at room temperature, sections were stained in 0.5% cresyl violet acetate (Sigma-

Aldrich) for 30 sec, washed in ddH$_2$0 (2 x 2 min), and then dehydrated in increasingly

pure ethanol: 50%, 75%, 85%, 95% (2 min each) and 100% (2 x 2 min). Next, the

sections were cleared with xylene (2 x 2 min) in a fumehood, and finally coverslips were

applied with mounting medium (Richard-Allen Scientific). After drying for at least 2

hours, images of the stained sections were obtained using an Olympus S2X12

stereomicroscope equipped with a SPOT digital camera (Diagnostic Instruments Inc.).

The resulting images were used to create a "reference chart" for each cryosectioned brain

(Figure 2.2). Anatomical regions were identified based on comparison with the online

High Resolution Mouse Brain Atlas (www.hms.harvard.edu/research/brain/atlas.html).
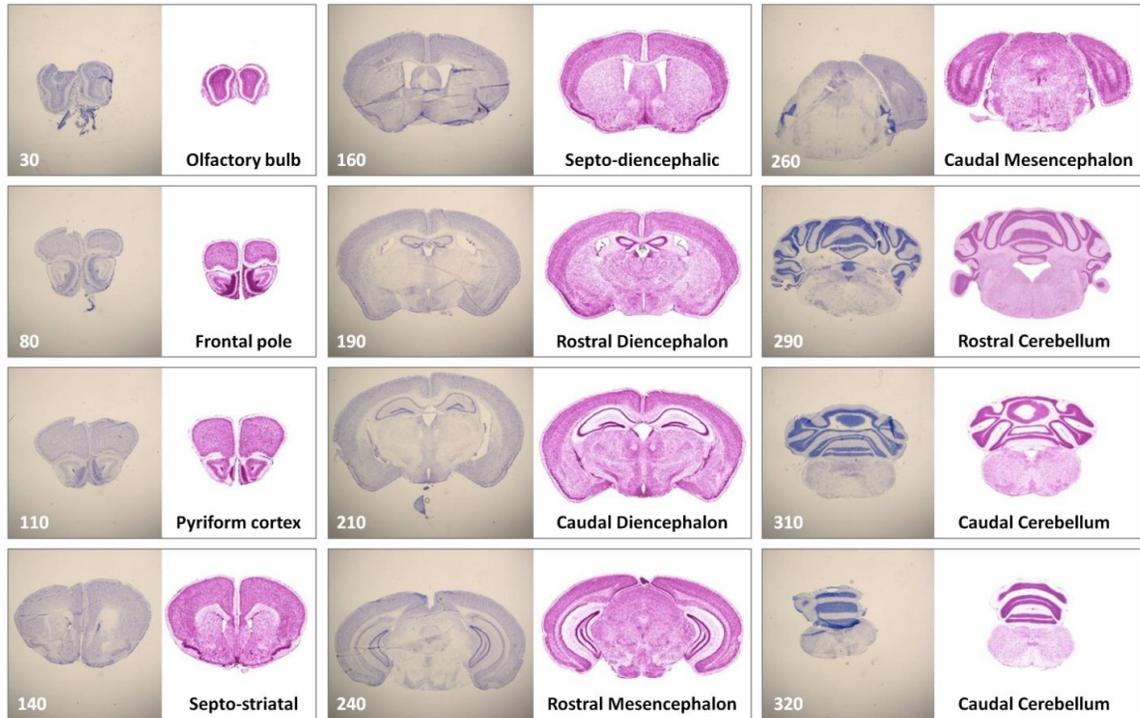
Figure 2.2 Representative mouse brain reference chart.
For each cryo-preserved mouse brain, select cryosections were stained with cresyl violet to construct a reference chart. To facilitate accurate identification of anatomical brain regions, reference sections (left panels) were matched to equivalent sections (right panels) from Harvard University's online High Resolution Mouse Brain Atlas (www.hms.harvard.edu/research/brain/atlas.html). Reference slide numbers are indicated in white.

2.15.5 Whole brain paraffin-embedding, sectioning and H&E staining

Paraffin-embedding and sectioning of perfusion-fixed whole brains was performed as a contract service by the Manitoba Breast Tumor Bank. Every 50 μm, two 10 μm horizontal sections were retained and mounted on separate glass slides; one was processed for hematoxylin and eosin (H&E) staining by the Tumor Bank, while the other was stored for future use. Matched stained and unstained sections were stored together in plastic slide boxes at room temperature.

2.15.6 Brain morphology and cellularity analysis on H&E-stained sections

Images of H&E-stained sections were captured on an Olympus BX51 microscope

equipped with the Olympus DP70 Digital Camera System and used to compare gross

brain morphology in matched wild type and BNIP3-null specimens. Anatomical features

were identified using the online High Resolution Mouse Brain Atlas

(www.hms.harvard.edu/research/brain/atlas.html). Cellularity in anatomically-matched

sections was determined by analyzing 200x and 400x images with the "counter" function

in Image Pro Plus 5.0 software. At least eight different areas (selected to cover a variety

of anatomical brain regions) were analyzed and compared in each brain, as shown in

Figure 2.3. Three pairs of adult wild type and BNIP3-/- littermates were compared, in

addition to four E18.5 embryos (2 wild type and 2 BNIP3-/-) from a single heterozygous

cross.
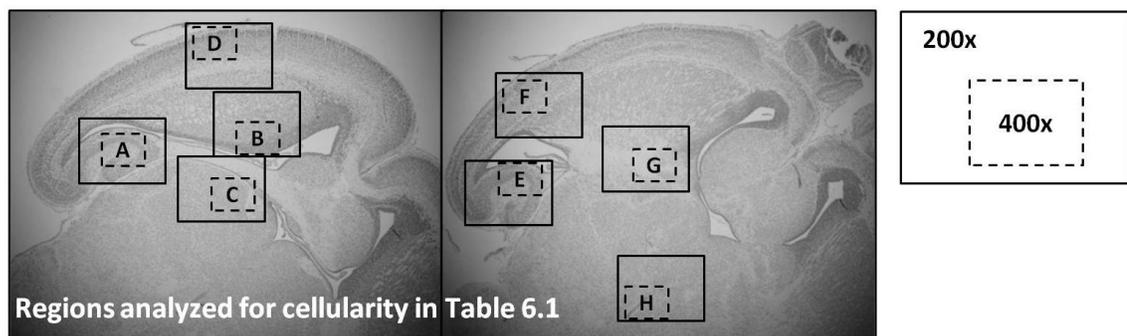
Figure 2.3 Brain regions analyzed for cellularity.
Fixed and paraffin-embedded mouse brains were sectioned and H&E-stained for morphological analysis. Cellularity was determined in eight regions (A-H) of each brain, as depicted here. A) hippocampus, B) striatum, C) thalamus, D) somatosensory cortex, E) hippocampus, F) secondary auditory cortex, G) stria terminalis, H) paraventricular thalamic nucleus.

2.15.7 Isolation of primary astrocytes from neonates

Primary astrocytes were isolated from newborn mice (less than 48-hours old) resulting from homozygous wild type or null crosses. Mice were sacrificed by decapitation and whole brains were immediately removed and placed in ice-cold serum-free astrocytes culture medium (see section 2.4.2). Under a Leica MZ6 stereomicroscope, extra-fine forceps were used to carefully dissect each brain, removing the meninges and retaining the astrocyte-rich cortexes while discarding the remaining tissue (olfactory bulbs, brain stem, cerebellum, hippocampus, etc.) The cortexes were transferred to a fresh dish of ice-cold serum-free culture media and transferred to a sterile biosafety cabinet. Cortexes from each litter were combined and chopped into small pieces ($<1mm^3$) and then transferred to a 50 mL conical centrifuge tube with 15 mL of serum-free culture media. The tissue was mechanically dissociated by vortexing (45 seconds full speed) and then filtered through 70 μm and 10 μm sterile spectra/mesh nylon filters (Spectrum) in sequence, to achieve a single-cell suspension. Cells were seeded in astrocyte culture media with 10% FBS at a density of 6×10^5 cells/mL. Media was changed after 3 days and then twice per week (with vigorous swirling prior to removal of media, to encourage detachment of the less adherent, non-astrocyte cells). After reaching 100% confluency (approximately 10 – 14 days after isolation), FBS was reduced to 7% and cells were cultured for an additional two weeks in order to reach functional maturity before experimentation. "Mature" astrocyte cultures were tested for purity by immunofluorescence staining for the astrocyte-specific marker protein GFAP (glial fibrillary acidic protein). When necessary, astrocyte cultures were passaged and cryo-

preserved as described in section 2.4.4, though never more than once (hence, p0 or p1 astrocytes were used in all experiments).

2.15.8   Isolation of embryonic fibroblasts

Mouse embryonic fibroblasts (MEFs) were derived from E12 – E14 mouse embryos generated from heterozygous crosses. Mothers were sacrificed by cervical dislocation and the uterus was immediately removed and placed in sterile PBS. Embryos were individually dissected (the head and organs were removed and retained for genotyping as described above), chopped into small pieces ($<1mm^3$) and further dissociated by trypsin digestion (5 – 7 minutes in 5 mL 2.5 % trypsin-EDTA at room temperature). Then, 10 mL of DMEM with 10% FBS was added and the cell suspension was transferred to a 100 mm culture dish. Media was changed twice per week and cells were passaged as described in section 2.4.4.   The initial three passages were used to increase MEF cell purity, and experiments were performed on cells from passages 3 – 8 (after 8 passages cell proliferation slowed considerably).

Chapter 3: Hypoxic cancer cells can undergo autophagic cell death in the absence of apoptosis.

3.1 Rationale

Hypoxia is a physiological stress encountered during various pathologies including cancer, myocardial infarction, and stroke (section 1.2). Cells deprived of oxygen will initially employ adaptive and survival strategies; however, severe or sustained hypoxia ultimately leads to cell death. The precise mechanisms of hypoxia-induced cell death remain unclear as apoptosis, necrosis and autophagy have all been reported in response to hypoxic stress (7-9).

Autophagy is a conserved lysosomal degradation pathway required for basic cellular homeostasis (section 1.3). Although generally regarded as a survival mechanism, it has recently been shown that autophagy can sometimes promote cell death. However, this has mainly been demonstrated in systems where apoptosis is artificially inhibited (168, 319, 320).

Chronic hypoxia is typical of tumor development, leading to metastatic changes and resistance to apoptosis. Indeed, the extent of tumor hypoxia correlates with neoplastic aggression, resistance to therapy, and reduced survival (33). Therefore, it is important to understand the cell death mechanisms involved (and evaded) during hypoxia in order to develop improved cancer treatment strategies. Thus, we sought to determine whether autophagic cell death could be induced in hypoxic cancer cells, independent of apoptosis.

3.2   Hypoxia induces autophagy in cancer cells.

Autophagy is best characterized as a response to nutrient deprivation, an energy-limiting cellular stress (321). Hypoxia is another energy-limiting stress, known to decrease ATP levels via inhibition of the oxidative phosphorylation pathway (322). Previously, "metabolic stress" (hypoxia combined with nutrient deprivation) has been shown to induce autophagy (7). To determine whether hypoxia alone can induce autophagy, we exposed seven human cell lines to prolonged hypoxia ($< 1\%$ O_2, 24 to 72 hours). Since tumor hypoxia is especially prevalent in gliomas and breast tumors (48, 307), we studied three glioma cell lines (U87, U373, U251) and three breast cancer cell lines (ZR75, MDA-MB-231, MDA-MB-231-M), in addition to one embryonic cell line (HEK293). We found that, in all cell lines tested, autophagy was induced by hypoxia. Using electron microscopy, we identified double-membraned autophagosomes in U87 cells under hypoxic conditions. These structures were absent under normal conditions (Figure 3.1).
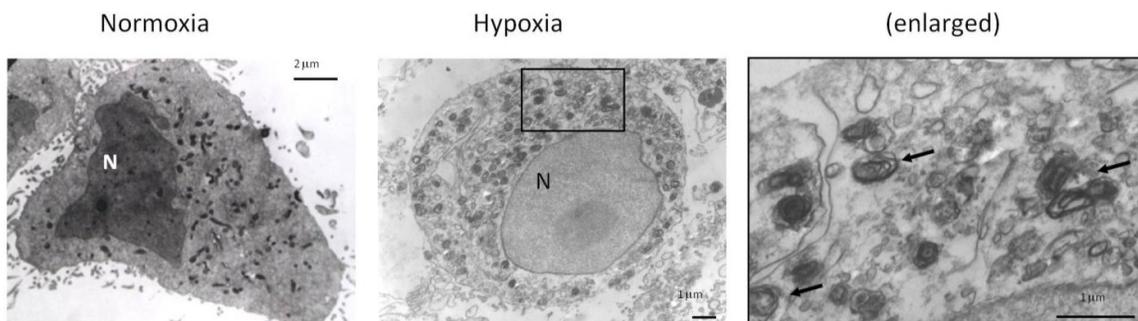
Figure 3.1 Detection of hypoxia-induced autophagosomes by electron microscopy.
U87 cells were incubated in normoxia or hypoxia for 24 hours followed by ultrastructural analysis by electron microscopy. Arrows indicate double-membraned autophagic vacuoles, in some cases containing mitochondria.

We also transfected cells with the widely-used autophagy marker GFP-LC3. LC3 (mammalian ATG8), is recruited to the autophagosome membrane during autophagy

(305). Under normoxia, GFP-LC3 was diffusely fluorescent whereas under hypoxia

GFP-LC3 became punctate, indicating formation of autophagosomes (Figure 3.2A). The

extent of GFP-LC3 punctate staining in the different cell lines ranged from 23% to 76%

after 48 hours of hypoxia, compared to 3% to 12% in normoxia (Figure 3.2C). Notably,

strong induction of GFP-LC3 puncta was observed as quickly as 1 hour after exposure to

hypoxia (Figure 3.2B). In order to be recruited to autophagosome membranes, cytosolic

LC3 (LC3-I) is conjugated to phosphatidyl-ethanolamine. This processed form (LC3-II)

migrates faster than the unlipidated form (LC3-I) on SDS-PAGE, and is detected more

readily by Western blot. We observed a drastic increase in LC3 processing in U87 cells

under hypoxia (Figure 3.3A). To verify that hypoxia-induced accumulation of LC3-II is

due to autophagic flux, and not blockage of lysosomal degradation, we repeated this

experiment in HEK293 cells in the presence or absence of the lysosomal protease

inhibitor, chloroquine. Hypoxia-induced accumulation of LC3-II was amplified in the

presence of chloroquine (Figure 3.3B). Thus, LC3-II is induced and degraded in

lysosomes during hypoxia, an indication of autophagic flux.
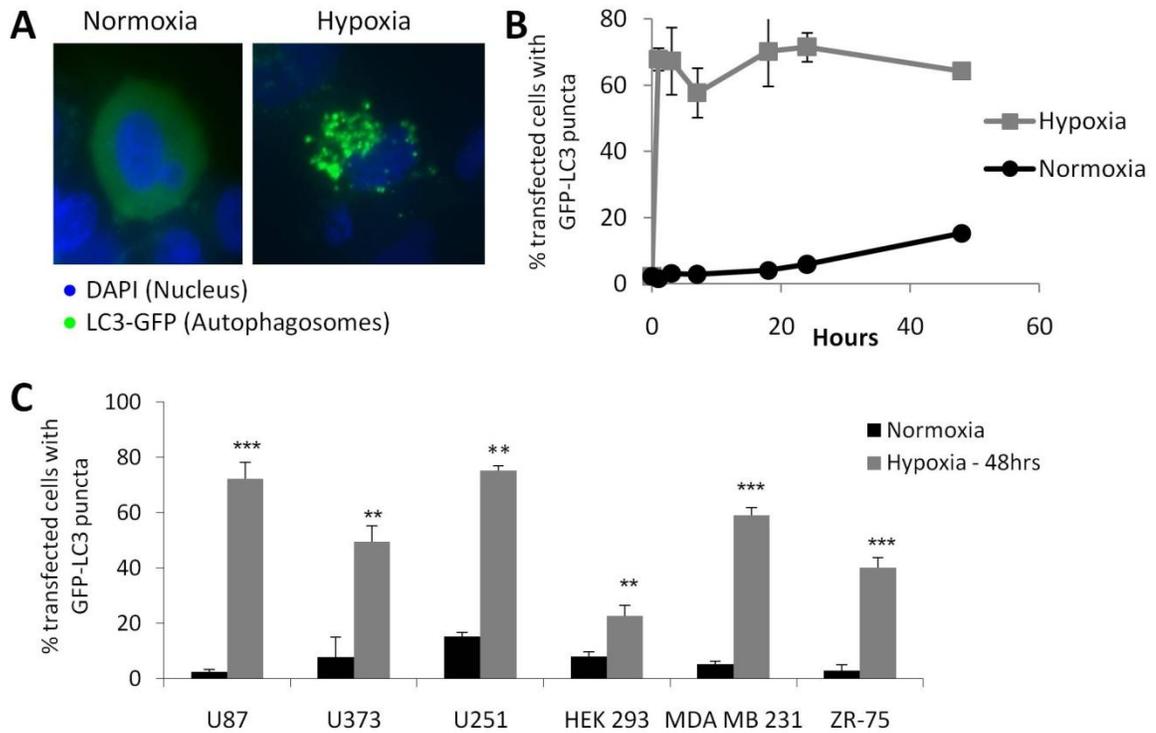
Figure 3.2 Detection of hypoxia-induced autophagy by GFP-LC3 distribution.
Cells transiently expressing GFP-LC3 were incubated in normoxia or hypoxia for 24 hours. (A) GFP-LC3 displayed diffuse intracellular localization under normoxic conditions, while membrane translocation (punctate localization) indicative of autophagy was observed in hypoxic cells. Images were obtained using identical microscope settings, exposure times, and manipulations for brightness and contrast.   (B) Quantification of GFP-LC3 translocation in transiently-transfected normoxic and hypoxic U87 cells. (C) Quantification of GFP-LC3 translocation in transiently-transfected normoxic and hypoxic cells. 200 cells per sample were counted for punctate versus diffuse staining (representative of three independent experiments). Error bars indicate standard deviation and statistical analysis was by unpaired student's t-test: *p<.05, **p<.01, ***p<.001.
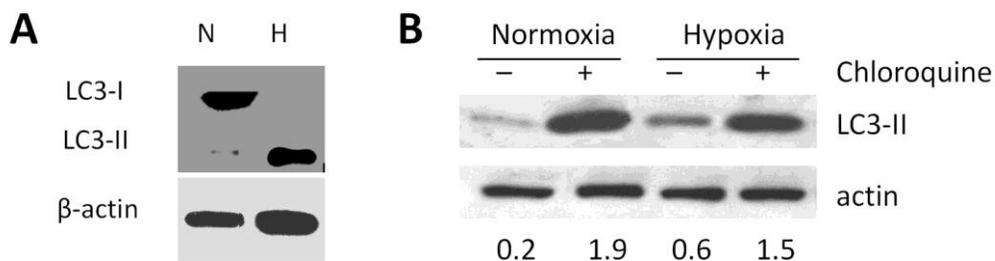
Figure 3.3 Detection of hypoxia-induced autophagy by LC3 processing.
U87 cells were incubated in normoxia (N) or 24 hours hypoxia (H). Total cell lysates were prepared and analyzed by Western Blot as described in Materials & Methods. (A) LC3-II, which is produced during autophagy, migrates faster on SDS-PAGE. (B) Autophagic flux and LC3-II turnover in hypoxia. HEK293 cells were exposed to 24 hours hypoxia or normoxia, in the presence or absence of the lysosomal protease inhibitor chloroquine (0.1 mM), followed by Western blotting for LC3-II. Results were quantified by densitometry analysis (values represent LC3-II/actin ratios).

Finally, we assessed the production of acidic vesicular organelles (AVOs). AVOs include lysosomes as well as autophagolysosomes, which are characteristic of autophagy and can be detected and quantified by acridine orange staining and flow cytometry (323). In U87 cells, AVO production was increased from 1.8% in normoxia to 18.7% in hypoxia (Figure 3.4A). Similar increases were observed in the other cell lines, corresponding with increased GFP-LC3 punctate staining and LC3 processing (Figure 3.4B). Taken together, these results clearly demonstrate the induction of autophagy as a response to chronic hypoxia in multiple cancer cell lines, and HEK293 fibroblasts.
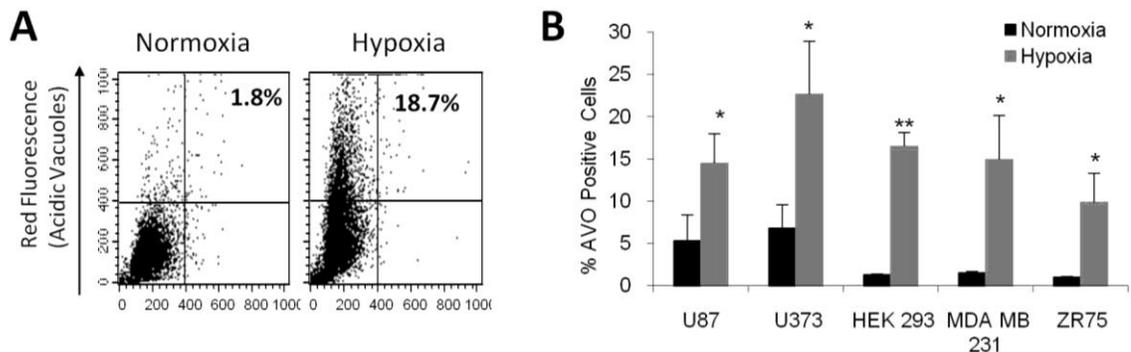
Figure 3.4 Detection of hypoxia-induced autophagy by AVO production.
(A) U87 cells incubated in normoxia or hypoxia for 48 hours were stained with acridine orange (1 μg/mL) and analyzed by flow cytometry to measure acid vacuole (AVO) production. Cytoplasm and nuclei fluoresce green while AVO / autophagosomes fluoresce red. (B) Quantification of AVO production in normoxic and hypoxic cells (representative of three independent experiments). Error bars indicate standard deviation and statistical analysis was by unpaired student's t-test: *p<.05, **p<.01, ***p<.001.

3.3 Prolonged hypoxia can induce autophagic cell death without apoptosis.

To determine whether the autophagy observed in hypoxic cancer cells contributes to cell death, we used the autophagy inhibitor 3-methyladenine (3-MA), which blocks autophagosome formation through inhibition of the Class III PI3K/Beclin-1 complex (324, 325). To further determine whether apoptosis contributes to hypoxia-induced cell

death, we used the caspase inhibitor z-VAD-fmk. We confirmed the specificity of these inhibitors by measuring cell death and GFP-LC3 puncta induced by classic apoptotic and autophagic stimuli (Figure 3.5). Only z-VAD blocked etoposide-induced apoptotic cell death, and only 3-MA blocked the formation of starvation- and hypoxia-induced autophagosomes, visualized as GFP-LC3 puncta. Notably, z-VAD did not completely inhibit etoposide-induced cell death, possibly due to the contribution of necrosis as a compensating cell death mechanism. Similarly, 3-MA did not completely inhibit hypoxia-induced autophagy, likely because this inhibitor must be used at moderate levels to avoid off-target affects: 3-MA targets both class I and class III PI3Ks, resulting in a net inhibition of autophagy at moderate concentrations. However, at high concentrations, severe inhibition of class I PI3K interferes with critical signaling pathways and leads to cell death (315).
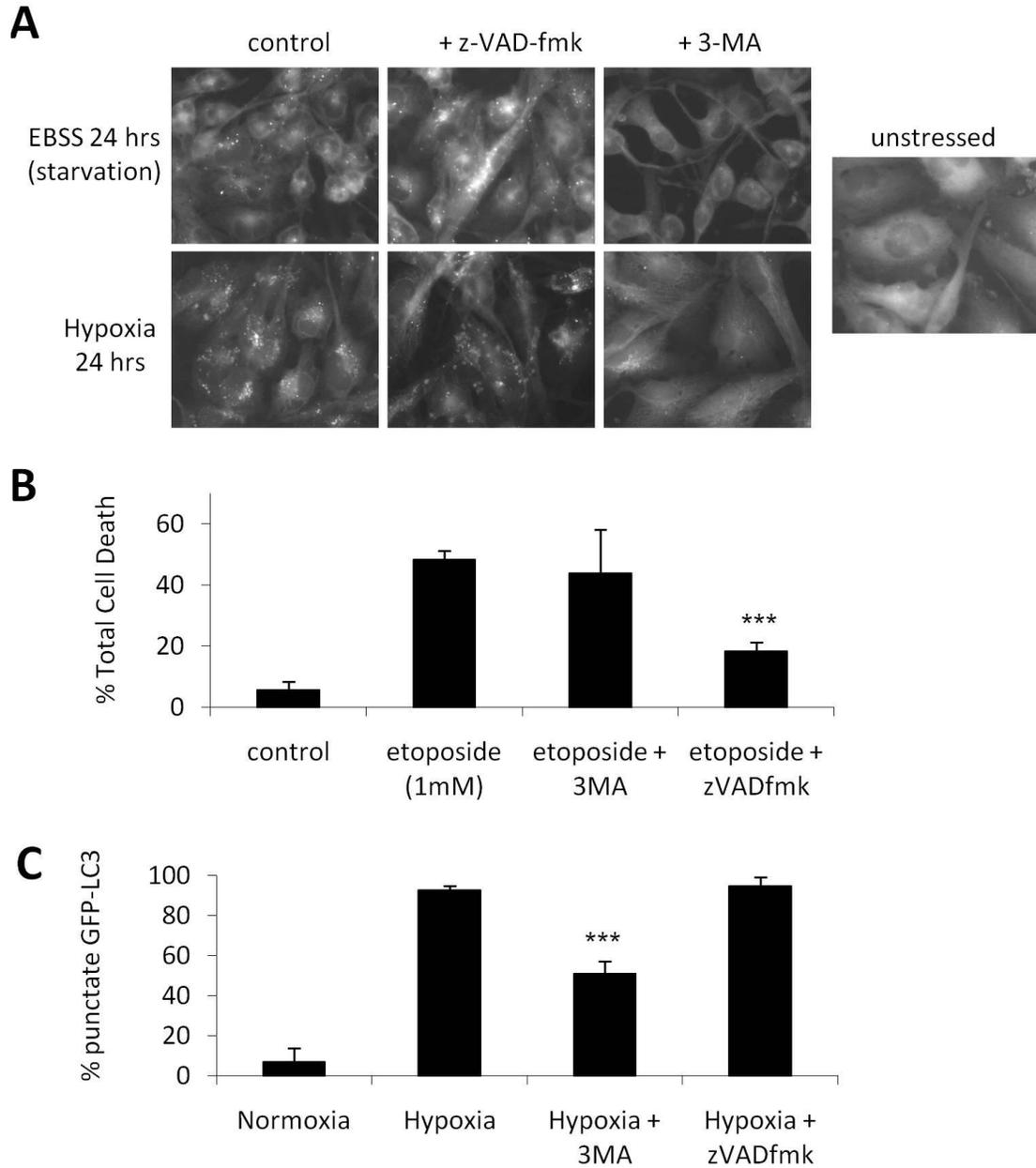
Figure 3.5 Specificity of apoptosis and autophagy inhibitors.
(A) Stable U251-GFP-LC3 cells were unstressed, or treated with EBSS (starvation), or exposed to hypoxia for 24 hours in the presence or absence of specific inhibitors for autophagy (PI3-Kinase inhibitor 3-MA) or apoptosis (caspase inhibitor z-VAD-fmk). 3-MA reduced the formation of GFP-LC3 puncta whereas z-VAD-fmk had no effect. (B) HEK293 cells were treated with the apoptosis inducer etoposide (1mM) for 48 hours with or without 3-MA or z-VAD-fmk.   Total cell death was determined by membrane permeability assay; z-VAD-fmk reduced etoposide-induced cell death whereas 3-MA had no effect. (C) U87-GFP-LC3 cells were incubated for 24 hours in normoxia or hypoxia, with or without 3-MA or z-VAD-fmk.   3-MA reduced hypoxia-induced GFP-LC3 puncta whereas z-VAD-fmk had no effect.   Results represent 3 independent experiments, error bars indicate standard deviation.   Statistical analysis was by unpaired t-test: ***$p<.001$ compared to etoposide (B) or hypoxia (C).

Next, we confirmed that prolonged hypoxia induces cell death in cancer cells. Cells were cultured in hypoxia over a 72-hour time course and the amount of total cell death was determined by membrane permeability assay and MTT viability assay. In all cell lines tested, hypoxia induced significant cell death by 48 hours (Figure 3.6), representing a delay compared to the induction of autophagy which occurred as early as 1 hour (Figure 3.2B). We then used 3-MA and z-VAD-fmk to determine the mechanism of hypoxia-induced cell death in each cell line (Figure 3.7). Interestingly, 3-MA was protective against hypoxia-induced cell death in some cell lines (indicating autophagic cell death), whereas z-VAD-fmk was protective in others (indicating apoptosis). For example, in U251 cells, 48 hours of hypoxia induced 45% cell death. 3-MA treatment had no effect (42% cell death), while z-VAD-fmk treatment offered significant protection (17% cell death), indicating apoptosis. Similar results were observed in MDA-MB-231-M cells, indicating that hypoxia-induced cell death is apoptotic in these two cell lines. By contrast, hypoxia-induced cell death in ZR75 cells was unchanged by z-VAD-fmk (49% vs. 51% cell death), but significantly reduced by 3-MA (28% cell death). Similar results in U87, U373, HEK293 and MDA-MB-231 cells indicate autophagic cell death. Furthermore, the failure of z-VAD-fmk to protect these cell lines from hypoxia-induced cell death suggests that autophagic cell death occurred independent of apoptosis (Figure 3.7).
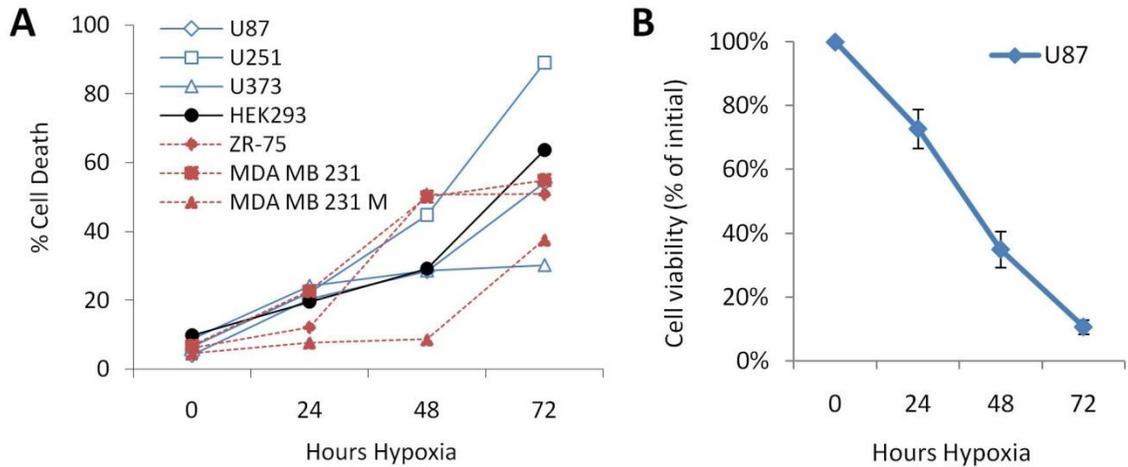
Figure 3.6 Prolonged hypoxia induces cell death in cancer cells.
Cells were cultured in hypoxia over a 72-hour time course. (A) Total cell death was determined by acridine orange membrane permeability assay as described in Materials and Methods. Compared to normoxic cells (time zero), cell death in hypoxic cells (48 and 72 hours) was significantly increased in all seven cell types ($p<.05$, 1-tailed t-test). (B) The MTT viability assay was performed as described in Materials and Methods. Experiments were performed in triplicate; error bars indicate standard error of three independent experiments.
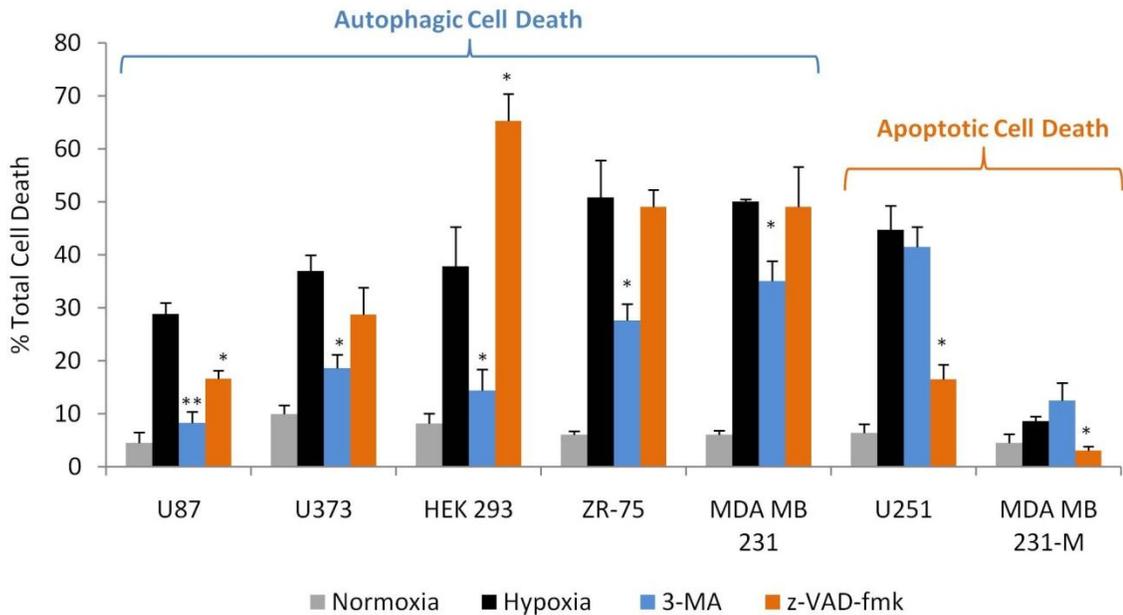
Figure 3.7 Effect of autophagy and apoptosis inhibitors on hypoxia-induced cell death.
Cells were incubated in hypoxia for 48 hours in the presence or absence of the autophagy inhibitor 3-MA, or the apoptosis inhibitor z-VAD-fmk. Total cell death was determined by membrane permeability assay. For cell lines where 3-MA was protective, hypoxia-induced cell death was classified as autophagic. For cell lines where z-VAD-fmk was protective, hypoxia-induced cell death was classified as apoptotic. All results represent three independent experiments and error bars indicate standard error. Statistical analysis was by one-way ANOVA and post-hoc unpaired t-tests: *$p<.05$, **$p<.01$ (relative to hypoxia alone for each cell line).

Notably, hypoxia-induced cell death was only partially suppressed by 3-MA in ZR75 and

MDA-MB-231 cells (Figure 3.7), possibly because 3-MA only partially inhibited

hypoxia-induced autophagy (Figure 3.5). Alternatively, the remaining cell death after 3-

MA treatment could be necrotic (but not apoptotic, since z-VAD-fmk was not protective

in these cells). Indeed, we observed that the nuclear protein HMGB1, which is

specifically released during necrosis, exhibited nuclear staining in normoxic cells but was

released in a proportion of hypoxic cells (Figure 3.8).

Surprisingly, in the case of HEK293 cells, hypoxia-induced cell death was enhanced by

caspase inhibition: cell death was 38% in untreated cells, reduced to 14% by 3-MA, and

increased to 65% by z-VAD-fmk (Figure 3.7). Although unexpected, this response is in

agreement with previous reports that caspase inhibitors can promote alternative death

pathways including both necrosis and autophagic cell death (326).
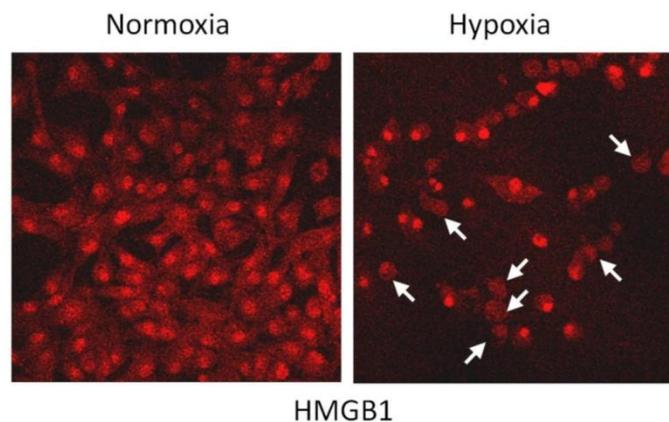
Figure 3.8 Cellular localization of HMGB1 in hypoxic cells.
U87 cells were incubated for 48 hours in normoxia or hypoxia, then stained for HMGB1. This protein is normally tightly associated with nuclear chromatin; however, it is specifically released from the nucleus during necrosis (but not autophagy or apoptosis). While HMGB1 staining was primarily nuclear in normoxic cells, a proportion of hypoxic cells showed release of HMGB1 (white arrows), indicating necrosis.

To further confirm that autophagy is a mechanism for hypoxia-induced cell death, at least in some cell lines, we used siRNA to knock-down the autophagy proteins Beclin-1 and ATG5. Beclin-1 (mammalian ATG6) is a regulator of the Class III PI3K complex involved in autophagosome formation (105) while ATG5 is part of a ubiquitin-like pathway required for the formation of autophagic vesicles (327). As expected, siRNA against Beclin-1 or ATG5 strongly reduced the expression of the corresponding gene products in HEK293 cells, compared to control (non-targeting) siRNA (Figure 3.9A). In addition, siRNA knock-down of Beclin-1 and ATG5 significantly reduced hypoxia-induced autophagy as determined by AVO production in HEK293 cells (Figure 3.9B). As shown previously in Figure 3.4, AVO production in all tested cell lines correlated with induction of autophagy as demonstrated by other detection methods (GFP-LC3 localization, LC3 processing and detection of autophagosomes by electron microscopy). More importantly, we found that knock-down of Beclin-1 or ATG5 significantly reduced hypoxia-induced cell death as determined by trypan blue membrane permeability assay (Figure 3.9C). In control cells we observed 60% cell death, whereas Beclin-1 and ATG5 knock-down reduced cell death to 28% and 18%, respectively (Figure 3.9D). Non-targeting siRNA failed to prevent hypoxia-induced cell death, indicating that hypoxia-induced cell death is dependent on the autophagy proteins Beclin-1 and ATG5. Collectively, these results show that prolonged hypoxia can induce autophagic cell death without apoptosis in multiple transformed and cancer cell lines.
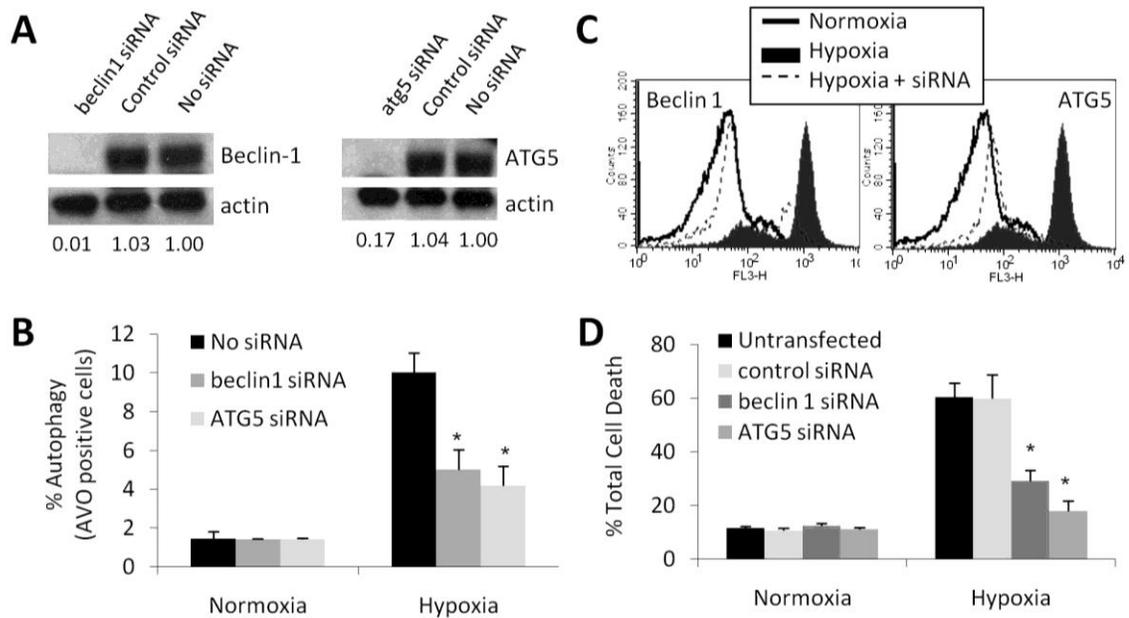
Figure 3.9 Hypoxia-induced cell death is blocked by knock-down of Beclin-1 and ATG5.
HEK293 cells were untransfected (control) or transiently transfected with siRNA against *beclin-1* or *ATG5*, or a non-targeting control siRNA. (A) Western blot analysis with β-actin as a loading control at 72 hours post-transfection. Numerical values indicate protein quantification by densitometry, normalized to β-actin. (B) 72 hours post-transfection, cells were incubated in normoxia or hypoxia for a further 48 hours. Autophagy was assessed by detection of AVOs. (C) Total cell death was determined by trypan blue membrane permeability assay using flow cytometry as described in Materials and Methods. Red fluorescence yields two observable peaks, representing viable cells (first peak – weak fluorescence) and dead cells (second peak, unable to exclude the dye and therefore strongly fluorescent). (D) Quantification of trypan blue assay using CellQuest software, representing four independent experiments. Error bars indicate standard deviation; statistical analysis was by unpaired student's t-test: *p<.001.

3.4 Cancer cell lines undergoing hypoxia-induced autophagic cell death are competent for apoptosis.

It has been reported that oxygen deprivation can induce apoptosis (8), and that autophagy may promote or occur simultaneously with apoptosis (328). Therefore, we investigated the apoptotic response to hypoxia in the cell lines tested above. Since U251 and MDA-MB-231-M cells had already demonstrated their apoptotic capacity during hypoxia-induced cell death (Figure 3.7), we specifically investigated the five "autophagic" cell lines (U87, U373, HEK293, ZR75, and MDA-MB-231). To first confirm that these cells are competent for apoptosis, we used the anti-cancer drug etoposide, a DNA damaging

119

agent and known apoptotic stimulus (329). In all five cell lines, nuclear condensation (a

hallmark of apoptosis) was detected after etoposide treatment, but not after 48 hours

hypoxia (Figure 3.10A), even though considerable cell death was observed (Figure 3.6).

Depending on the cell line, nuclear condensation occurred in 30% to 85% of etoposide-

treated cells compared to just 2% to 7% of hypoxia-treated cells, which did not differ

significantly from control cells (3% to 8%).

We also determined the level of caspase activity (another hallmark of apoptosis) using a

fluorescently-labeled peptide substrate for caspase 3 (DEVD-AFC). Caspase activation

was detected following etoposide treatment in all five cell lines (ranging from 160 to

2071 relative units). However, hypoxia failed to significantly activate caspases after 48

hours (40 to 130 relative units, compared to between 25 and 83 for controls) (Figure

3.10B). By contrast, U251 cells exhibited significant caspase activity upon both

etoposide and hypoxia treatment (719 and 2147 relative units, respectively). This

confirms our earlier finding that U251 cells induce apoptotic cell death in hypoxia,

whereas the other cell lines do not (Figure 3.7). Notably, U87, U373 and HEK293 cells

had reduced (but significant) caspase activation upon etoposide treatment compared to

ZR-75 and MDA MB 231 cells, correlating with the level of nuclear condensation

detected.

Another marker for apoptosis is the occurrence of DNA double strand breaks, where

phosphorylation of histone H2A.X occurs (330). Using antibodies specific to

phosphorylated H2A.X, we determined the level of H2A.X phosphorylation by flow

cytometry. In the autophagic cell lines, we found that etoposide treatment induced

H2A.X phosphorylation whereas hypoxia did not (Figure 3.10C). As expected, U251

cells exhibited H2A.X phosphorylation in response to both etoposide and hypoxia.
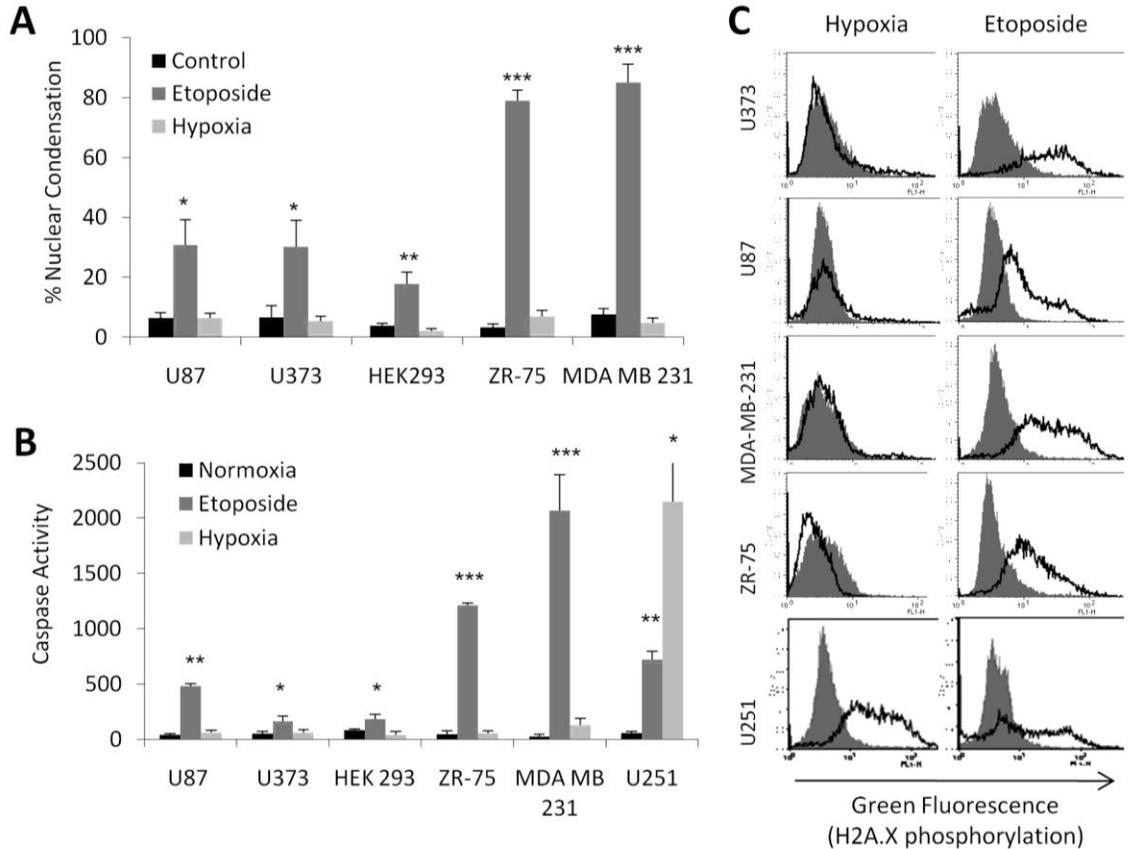
Figure 3.10 Hypoxia fails to induce apoptosis in apoptosis-competent cells.
(A) Cells were untreated or treated with etoposide (100 μM) or incubated in hypoxia for 48 hours. Nuclear condensation was assessed by acridine orange and ethidium bromide staining as described in Materials and Methods.   Results represent three independent experiments. (B) Caspase activity was measured by a fluorometric caspase 3 substrate cleavage assay as described in Materials and Methods. Results represent three independent experiments. (C) Permeabilized whole cell lysates were incubated with a FITC-tagged anti-phospho-H2A.X antibody, followed by flow cytometry. Solid curve represents untreated cells and empty curve represents hypoxia or etoposide treated cells. The figure is representative of three independent experiments. Error bars indicate standard deviation; statistical significance was determined by unpaired t-test (*$p<.05$, **$p<.01$, ***$p<.001$).

Taken together, these results show that hypoxia fails to induce apoptosis in multiple

apoptosis-competent cell lines (U87, U373, HEK293, ZR-75, MDA-MB-231), yet

successfully triggers apoptosis in others (U251, MDA-MB-231-M). The mechanism for

preference between hypoxia-induced apoptosis or autophagic cell death is currently

unknown, but should be the focus of future research since hypoxia-induced cell death

pathways are important in many pathologies including cancer.

3.5 Chapter summary

In summary, the results in this chapter demonstrate the following:

- Hypoxia universally induces autophagy in transformed and cancer cell lines (U87, U373, HEK293, ZR75, MDA-MB-231, U251 and MDA-MB-231-M).

- Prolonged (48 hours) hypoxia induces cell death in transformed and cancer cell lines.

- Hypoxia induces apoptosis in select cell lines (U251 and MDA-MB-231-M), but fails to induce apoptosis in others (U87, U373, HEK293, ZR75, and MDA-MB-231), despite robust apoptotic capacity in all cell lines tested.

- Hypoxia induces autophagic cell death, without apoptosis, in several apoptosis-competent cell lines (U87, U373, HEK293, ZR75, MDA-MB-231).

- In addition to autophagic cell death, necrosis may contribute to hypoxia-induced cell death in some cell lines.

The mechanism for the preference between autophagy and apoptosis under hypoxia in specific cells is unknown. Nevertheless, these results suggest that hypoxic cancer cells can undergo autophagic cell death in the absence of apoptosis. These are significant findings which contribute to the understanding of cell death mechanisms in hypoxia, and provide evidence for physiologically relevant autophagic cell death in apoptosis-competent cells. Furthermore, this research supports the hypothesis that targeting autophagy as an alternative cell death pathway may lead to promising new cancer treatment strategies.

Chapter 4: BNIP3 plays a pivotal role in hypoxia-induced autophagic cell death.

4.1 Rationale

In order to successfully target autophagic cell death as a cancer treatment strategy, individual target molecules must be identified. Ubiquitous autophagy proteins are not suitable targets since autophagy is a critical pathway for homeostasis in normal cells (section 1.3). We hypothesized that BNIP3 may represent a more "cancer-specific" autophagy target molecule, since it is selectively induced during hypoxia (207), and since others have observed autophagic morphology in BNIP3-expressing cells (78).

BNIP3 is a pro-death Bcl-2 family member that is upregulated under hypoxic conditions (section 1.7). In transformed and cancer cells, forced over-expression of BNIP3 induces 'non-apoptotic' cell death that is characterized by localization to the mitochondria, opening of the permeability transition pore, loss of membrane potential and ROS production (78). In these cells, BNIP3-induced cell death is independent of caspase activation and cytochrome *c* release from the mitochondria. However, in other cell types BNIP3 can induce cell death via apoptosis (242, 248) or through a necrotic mechanism (253). BNIP3 has also been implicated in ceramide- and arsenic trioxide-induced autophagy (71, 254) and in hypoxia-induced cell death (207). Thus, we aimed to determine whether BNIP3 plays a role in hypoxia-induced autophagic cell death in cancer cells.

4.2   BNIP3 plays a role in the hypoxia-induced autophagic cell death of transformed and cancer cells.

BNIP3 is a direct HIF-1α target gene (207).   Accordingly, we found that BNIP3 mRNA and protein levels were elevated in HEK293, U87 and U251 cells at 48 and 72 hours hypoxia (Figure 4.1), time points that correspond with increased cell death (Figure 3.6). Since forced over-expression of BNIP3 is known to induce a 'non-apoptotic' form of cell death (78), and since arsenic trioxide-induced autophagic cell death involves upregulation of BNIP3 (71), we investigated whether BNIP3 is also involved hypoxia-induced autophagic cell death.
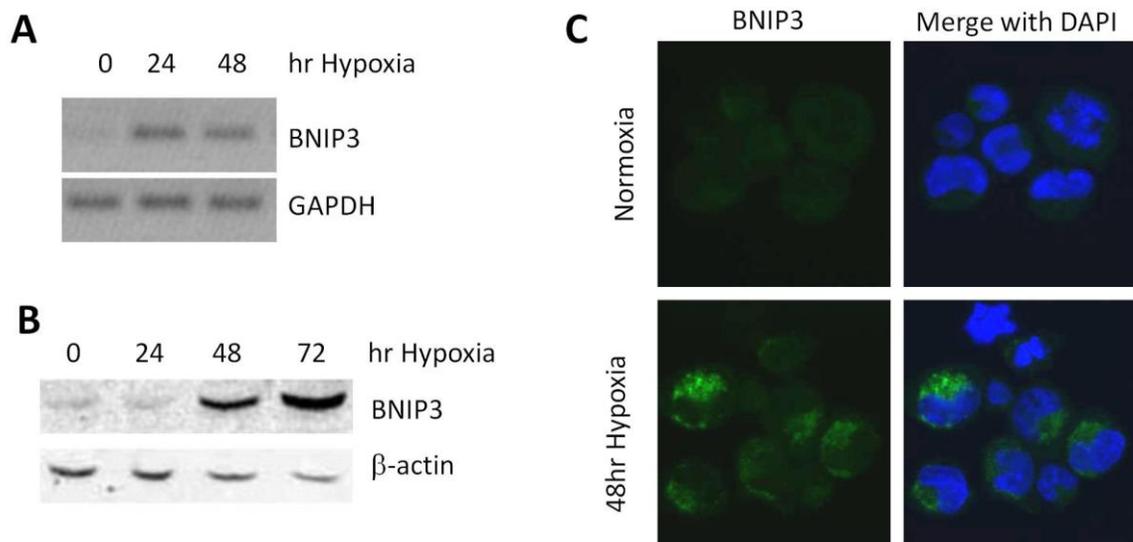
Figure 4.1 Hypoxic induction of BNIP3
(A) RT-PCR analysis of BNIP3 gene expression in U87 cells cultured in normoxia or hypoxia for up to 48 hours, with GAPDH as a loading control. (B) Western blot analysis of BNIP3 protein expression in total cell lysates from HEK293 cells cultured in normoxia or hypoxia for up to 72 hours, with actin as a loading control. (C) Immunofluorescence for BNIP3 expression in U251 cells exposed to normoxia or 48 hours hypoxia.

First, we examined the effect of forced BNIP3 over-expression in HEK293 and U87 cells. We found that BNIP3 induced an autophagic response in both cell types: GFP-LC3

punctate staining increased from 2% or 3% in cells transfected with empty vector, to 81% or 56% in cells transfected with BNIP3 (Figure 4.2A&B). Furthermore, BNIP3 appeared to co-localize with GFP-LC3, suggesting involvement with autophagosomes (Figure 4.2C). There was no increase in GFP-LC3 punctate staining in cells transfected with the dominant-negative mutant BNIP3ΔTM, indicating that the TM domain (which targets BNIP3 to mitochondria) is critical for BNIP3's ability to induce autophagy (Figure 4.2B). By electron microscopy, we observed the formation of double-membraned autophagosomes upon BNIP3 expression in HEK293 cells (Figure 4.2D).

As expected, BNIP3 over-expression also induced cell death. We found that BNIP3-induced cell death was reduced by the autophagy inhibitor 3-MA (from 71% to 45%), but was unchanged by the caspase inhibitor z-VAD-fmk (Figure 4.2E). Our results suggest that in these cells, BNIP3-induced cell death is autophagic and not apoptotic.
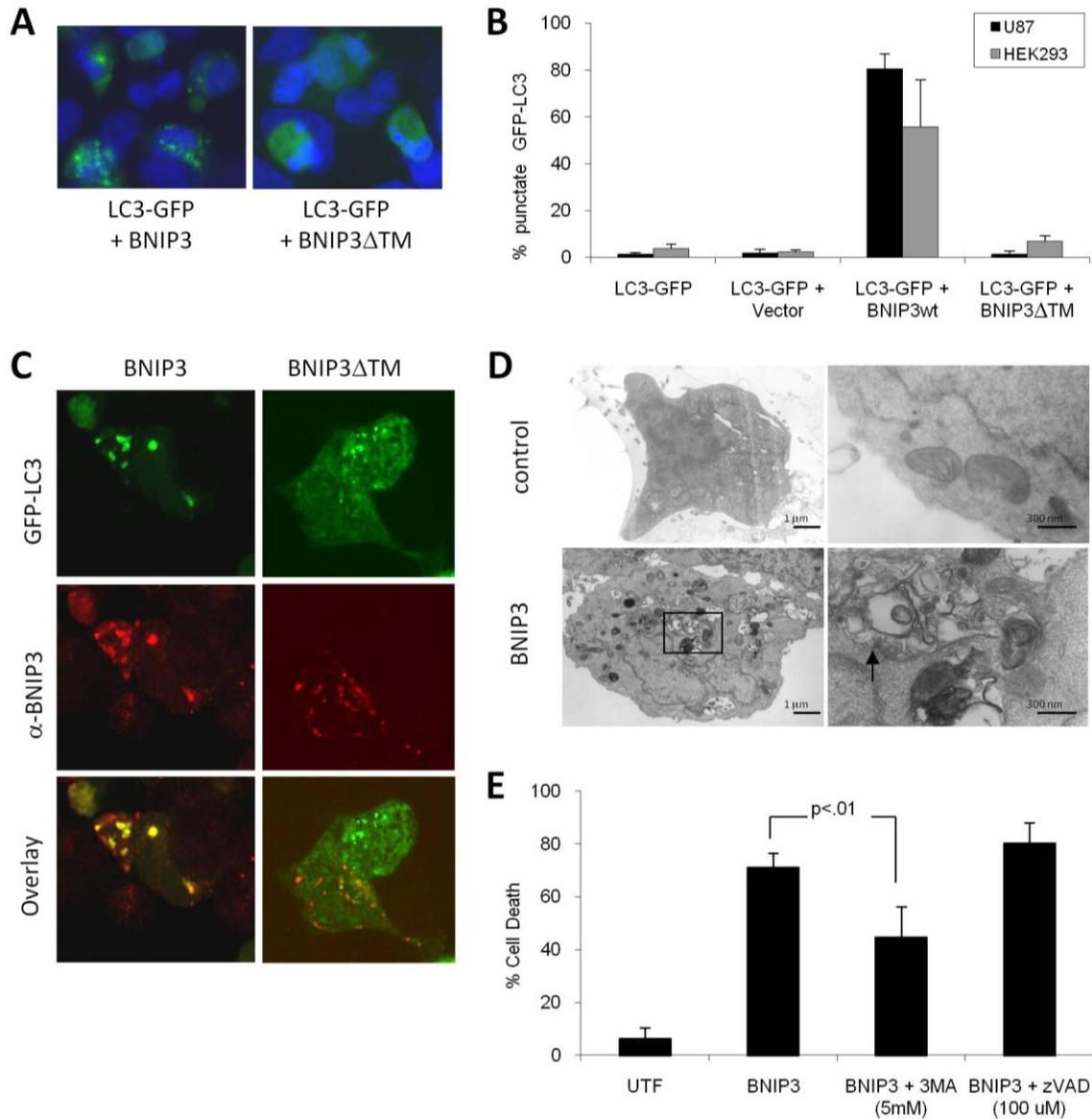
Figure 4.2 BNIP3 induces TM-dependent autophagic cell death.
HEK293 and U87 cells were transiently transfected with the autophagy marker GFP-LC3, alone or with pcDNA3 (empty vector) or pcDNA3-BNIP3 or pcDNA3-BNIP3ΔTM (a dominant-negative, transmembrane-domain-deleted mutant). (A) Representative images showing GFP-LC3 localization in HEK293 cells transfected with BNIP3 or BNIP3ΔTM. (B) GFP-LC3 distribution (in co-transfected cells only) was assessed and quantified. Error bars indicate standard deviation of three independent experiments. (C) HEK293 cells were transiently co-transfected with GFP-LC3 and BNIP3 or BNIP3ΔTM under normoxic conditions. Cells were stained with anti-BNIP3 antibodies and co-localization with GFP-LC3 was assessed by confocal microscopy. (D) HEK293 cells were untransfected (control) or transfected with BNIP3. Cells were analyzed by electron microscopy for detection of autophagosomes. (E) HEK293 cells were untransfected (UTF) (control) or transfected with BNIP3. Cells were untreated or treated with 3-MA (5 mM) or z-VAD-fmk (100 μM) for 24 hours post-transfection. Immunofluorescence for BNIP3 was performed and cell death in BNIP3-positive cells was determined by assessing nuclear morphology. Error bars indicate standard deviation of three independent experiments. Statistical significance was determined by a two-tailed t-test.

Next, we investigated the role of BNIP3 in hypoxia-induced autophagy and cell death. It

has previously been shown that hypoxia-induced cell death is partially blocked by

expression of the dominant-negative BNIP3ΔTM mutant or by knock-down of the BNIP3

gene (207). Our results show that hypoxia-induced autophagy is also reduced by

BNIP3ΔTM or by BNIP3 knock-down, while it is enhanced by over-expression of wild

type BNIP3: GFP-LC3 punctate staining at 24 hours hypoxia was 53% for empty vector

cells, reduced to 34% in BNIP3ΔTM-expressing cells, and increased to 86% for BNIP3-

expressing cells (Figure 4.3A). Additionally, BNIP3 knock-down by siRNA reduced

hypoxia-induced AVO production from 32% to 23%, compared to cells transfected with

control siRNA (Figure 4.3B&C). This represents a statistically significant (p=.002) yet

incomplete reduction in hypoxia-induced AVO production, since normoxic levels were 5-

6%. Whether this difference is biologically significant remains to be determined, and

should ideally be tested with an alternative approach since this assay is confounded by

the increase in AVO production caused by the transfection process (compared to

untransfected cells, control siRNA-transfected cells exhibited a 2.5-fold increase in

hypoxia-induced AVOs, which can only be attributed to the transfection process or the

general presence of siRNA).

Finally, BNIP3 knock-down did not affect the formation of hypoxia-induced GFP-LC3

puncta in stable GFP-LC3 clones (Figure 4.3D); however, this is likely because siRNA

transfection itself induced autophagy (Figure 4.3C&D: control siRNA induces autophagy

in normoxia), perhaps to an extent that masks the effect of BNIP3 knock-down in this

particular assay. Taken together, our results indicate that hypoxia-induced BNIP3 plays

an important role in hypoxia-induced autophagy, and that the TM domain is critical for

this function.
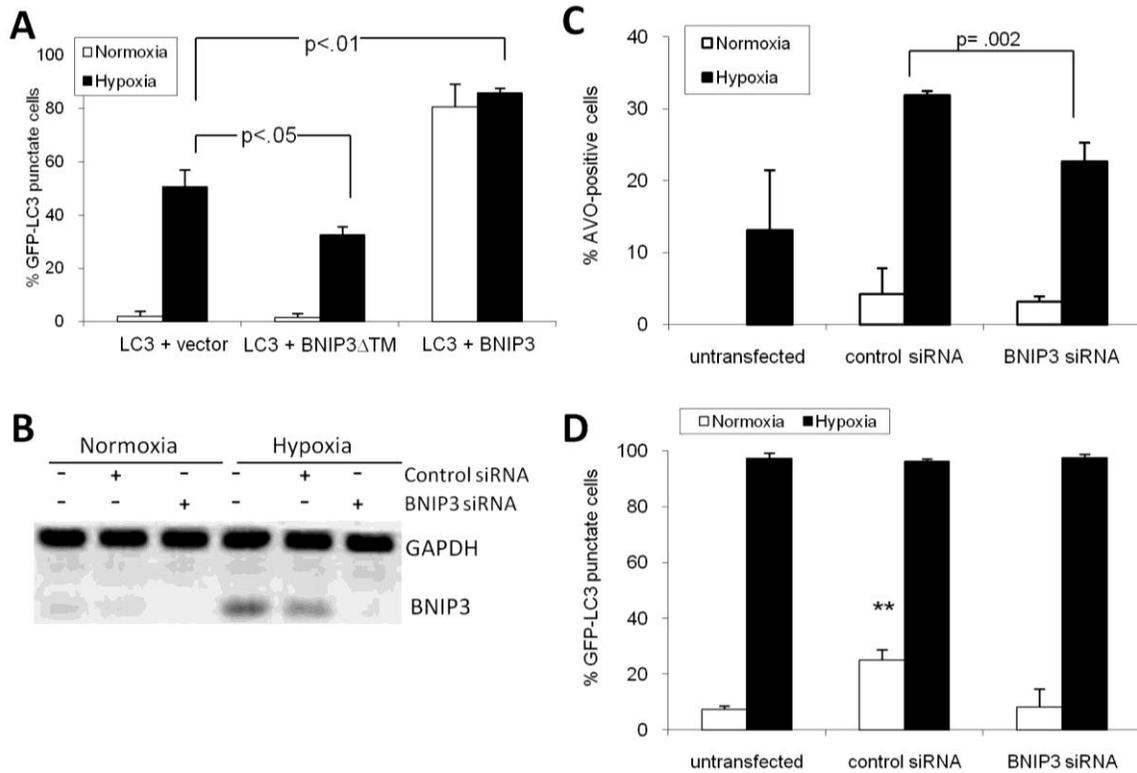
Figure 4.3 BNIP3 plays a role in hypoxia-induced autophagic cell death.
(A) HEK293 cells were transfected with GFP-LC3 plus empty vector, BNIP3 or BNIP3ΔTM, and
incubated in normoxia or hypoxia for 24-hours post-transfection. GFP-LC3 distribution (in co-transfected
cells only) was assessed and quantified. (B) U87 cells were untransfected, or transfected with control
siRNA or BNIP3 siRNA and silencing of gene expression was verified by RT-PCR analysis as described in
Materials and Methods. (C) Two days after siRNA silencing, U87 cells were retained in normoxia or
exposed to 24 hours hypoxia, and AVO production was measured by flow-cytometry. (D) Two days after
siRNA silencing, U87-GFP-LC3 cells were retained in normoxia or exposed to 24 hours hypoxia, and GFP-
LC3 distribution was assessed and quantified. Error bars indicate standard deviation of three independent
experiments.   Statistical significance was determined by an unpaired t-test: **p<.01 (compared to
untransfected, normoxia).

4.3 BNIP3 plays a role in hypoxia-induced cell death in primary astrocytes and fibroblasts.

To further confirm the role of BNIP3 in hypoxia-induced cell death, we used primary cells derived from BNIP3-null mice. These cells provide a truly BNIP3-null model system, in contrast to siRNA knock-down and dominant-negative mutant studies, where complete inhibition of BNIP3 is difficult to achieve. The BNIP3-/- mouse model was kindly provided by Dr. Gerald Dorn at the Washington University School of Medicine (section 2.15). Dorn and colleagues generated the BNIP3-/- mouse model using conventional gene targeting through homologous recombination. Their targeting vector introduced a neomycin cassette in place of exons 2 and 3 of the BNIP3 gene, thereby truncating the protein prior to the critical BH3 and transmembrane domains (240). In agreement with Dorn and colleagues, we found that homozygous BNIP3-null mice were born from heterozygous crosses at normal Mendelian ratios (of 96, 25 were BNIP3+/+, 41 were BNIP3+/- and 30 were BNIP3-/-) and showed no increase in mortality or apparent physical abnormalities during follow-up for over 10 months.

To determine the role of BNIP3 in primary cells under hypoxic stress, we isolated astrocytes and embryonic fibroblasts from wild type and BNIP3-/- mice. Astrocytes were isolated from the cerebral cortices of newborn mice as described in section 2.15.6. A high level of culture purity was achieved, since our primary astrocyte cultures expressed the astrocyte marker GFAP (glial fibrillary acidic protein), but not the neuronal marker neurofilament (Figure 4.4). Mouse embryonic fibroblasts (MEFs) were isolated from E12.5 – E14.5 embryos as described in section 2.15.8.
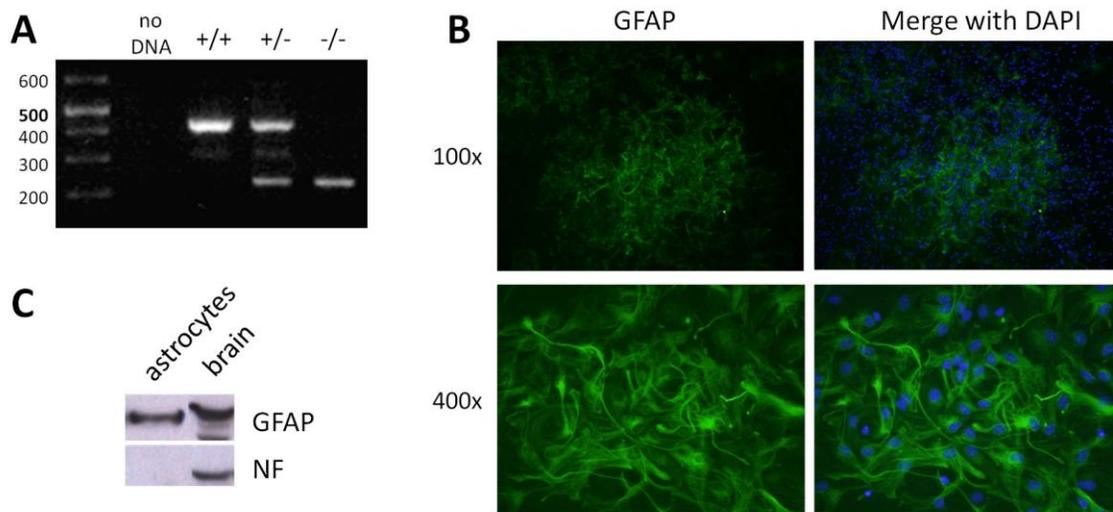
Figure 4.4 BNIP3-/- mouse model: genotyping and culture of primary astrocytes.
(A) PCR was employed for genotyping BNIP3-null, wild-type and heterozygous mice. As described in Materials & Methods, three primers were used to generate a 435-bp WT allele product and a 220-bp BNIP3-null allele product. One upstream primer anneals to the intron between exons 2 and 3, while the other anneals to the neomycin cassette, which replaces exons 2 and 3 in the BNIP3-null allele. The third primer binds downstream of the targeting vector insertion site, recognizing both the wild-type and BNIP3-null alleles. (B) Primary astrocytes were isolated from newborn wild-type and BNIP3-/- mice as described in Materials & Methods. Cultured astrocytes were grown on coverslips and the astrocyte marker GFAP was detected by immunofluorescence. Nuclei were counterstained with DAPI. This representative image depicts wild type astrocytes. (C) As a measure of purity, total cell lysates from cultured wild type astrocytes were Western blotted for the astrocyte marker GFAP and the neuronal marker Neurofilament (NF). Whole brain tissue was used as a control since both astrocytes and neurons are present in brain tissue.

Similar to cancer cells, wild type MEFs and astrocytes induced high levels of BNIP3

protein expression upon exposure to hypoxia (Figure 4.5A&B). Interestingly, wild type

astrocytes expressed low levels of BNIP3 protein even under normoxic conditions, as

detected by Western blot (Figure 4.5A). Multiple bands detected by Western blot suggest

post-translational modification of BNIP3, however this remains to be directly proven.

Although we could not detect BNIP3 by immunofluorescence in these cells to determine

its subcellular localization, this finding is in agreement with previous reports that nuclear

BNIP3 is expressed in normal human astrocytes (233). Significant cell death occurred by

24 hours hypoxia in primary astrocytes (53% cell death), and by 40 hours hypoxia in

131

MEFs (42% cell death). It is tempting to speculate that primary astrocytes are inherently

more sensitive to hypoxia due to their basal expression of BNIP3 (which was not

observed in the less sensitive MEFs); however, this was not directly tested and there are

surely many other potentially responsible molecular differences between astrocytes and

MEFs. Nevertheless, loss of BNIP3 was significantly protective in both cell types:

hypoxia-induced cell death was reduced to 19% in BNIP3-/- astrocytes, and 10%, and in

BNIP3-/- MEFs (Figure 4.5D&E). Ultimately, after extended hypoxia, all primary

cultures attained 100% cell death. It is likely that the wild type cultures attained

complete cell death earlier than BNIP3-/- cultures; however, this can only be confirmed

by a more rigorous analysis with additional time points in the late stages of hypoxic

exposure.
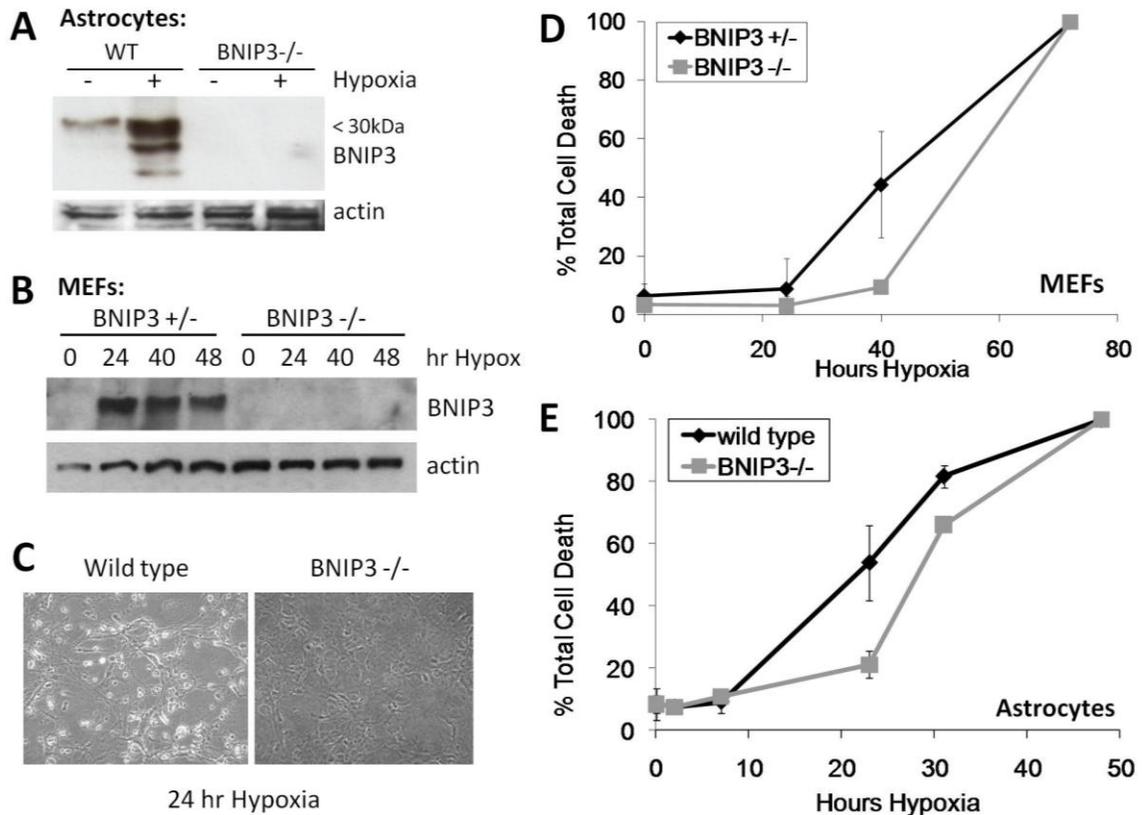
Figure 4.5 Loss of BNIP3 is protective against hypoxia-induced cell death in primary cells.
Wild-type, heterozygous and BNIP3-/- primary mouse astrocytes and MEFs were cultured in normoxia or hypoxia for up to 72 hours. Total cell lysates from astrocytes (A) and MEFs (B) were analyzed by Western blot for expression of BNIP3. (C) Images of wild type and BNIP3-/- astrocytes after 24 hours hypoxia. The majority of wild type cells were detached from the culture plate while BNIP3-/- cells remained adherent. Total cell death was measured by membrane permeability assay in MEFs (D) and astrocytes (E). Loss of BNIP3 was protective against hypoxia-induced cell death in both cell types. Error bars indicate standard deviation of three independent experiments.

Together, these results provide the first conclusive evidence from a BNIP3-null model

system to confirm that BNIP3 plays a role in promoting hypoxia-induced cell death.

4.4 Chapter summary

In summary, the results in this chapter demonstrate the following:

- Hypoxia induces BNIP3 expression in primary and cancer cells.

- BNIP3 induces TM-domain-dependent autophagic cell death.

- Hypoxia-induced autophagic cell death in transformed and cancer cells occurs through a mechanism involving BNIP3.

- Primary mouse astrocytes express low levels of BNIP3 under normoxic conditions.

- Loss of BNIP3 is partially protective against hypoxic stress in mouse astrocytes and fibroblasts, causing significant delay in hypoxia-induced cell death.

Collectively, these findings identify BNIP3 as an important mediator of hypoxia-induced autophagic cell death. Previous BNIP3 knock-down studies have been met with skepticism in the fields of hypoxia and cell death research. For the first time, we have used the BNIP3-null mouse model to provided conclusive evidence for the role of BNIP3 in hypoxia-induced autophagy and cell death. The results presented in Chapter 3 indicate that hypoxic cancer cells can undergo autophagic cell death in the absence of apoptosis, thereby supporting the emerging theory that autophagy can serve as a killing mechanism in hypoxic and/or apoptosis-resistant tumors. The results presented in this chapter further identify BNIP3 as a potential target molecule in this pathway. Further research will be required to elucidate the mechanism of BNIP3-mediated autophagy in hypoxic cancer cells, and to establish methods of targeting BNIP3 in this pathway for therapeutic benefit.

Chapter 5: Insights into BNIP3 resistance from an inducible expression system.

5.1   Rationale

To further characterize the functional role of BNIP3, we endeavored to perform additional over-expression studies. Previously, we and others had studied BNIP3-induced cell death by over-expressing BNIP3 protein through transient transfection (78, 201, 207, 243, 246, 249, 251, 254, 270). However, it can be difficult to achieve high transfection efficiency in some cell types, and the process of transfection itself can cause cellular stress and induce autophagy (315, 331). Use of stable cell lines can circumvent these problems; however, proteins such as BNIP3 cannot be stably expressed because they promote cell death. Therefore, we developed an inducible BNIP3 expression system, with unexpected results.

5.2   Doxycycline-inducible BNIP3 fails to induce cell death: a model for BNIP3 resistance.

Using Invitrogen's TREx™ System, we established stable U87 and HEK293 cell lines with tetracycline-regulated BNIP3 (as described in Materials & Methods, section 2.5.4). In these "TetON" cells (TO-BNIP3 cells), BNIP3 expression is highly induced by doxycycline (a stable analogue of tetracycline), as detected by immunofluorescence, Western blot and RT-PCR (Figure 5.1A-C). Phosphatase treatment of TO-BNIP3 cell lysates revealed that the induced BNIP3 dimer was phosphorylated (Figure 5.1D), which is in agreement with several recent studies that have shown dynamic BNIP3 phosphorylation (227, 229). To control for the effects of doxycycline treatment and

massive induction of protein synthesis, we also generated stable TO-βgal cells to use as

experimental controls (Figure 5.1E). These cells express the same regulatory and

expression vectors as TO-BNIP3 cells, with inducible (non-toxic) β-galactosidase instead

of BNIP3.
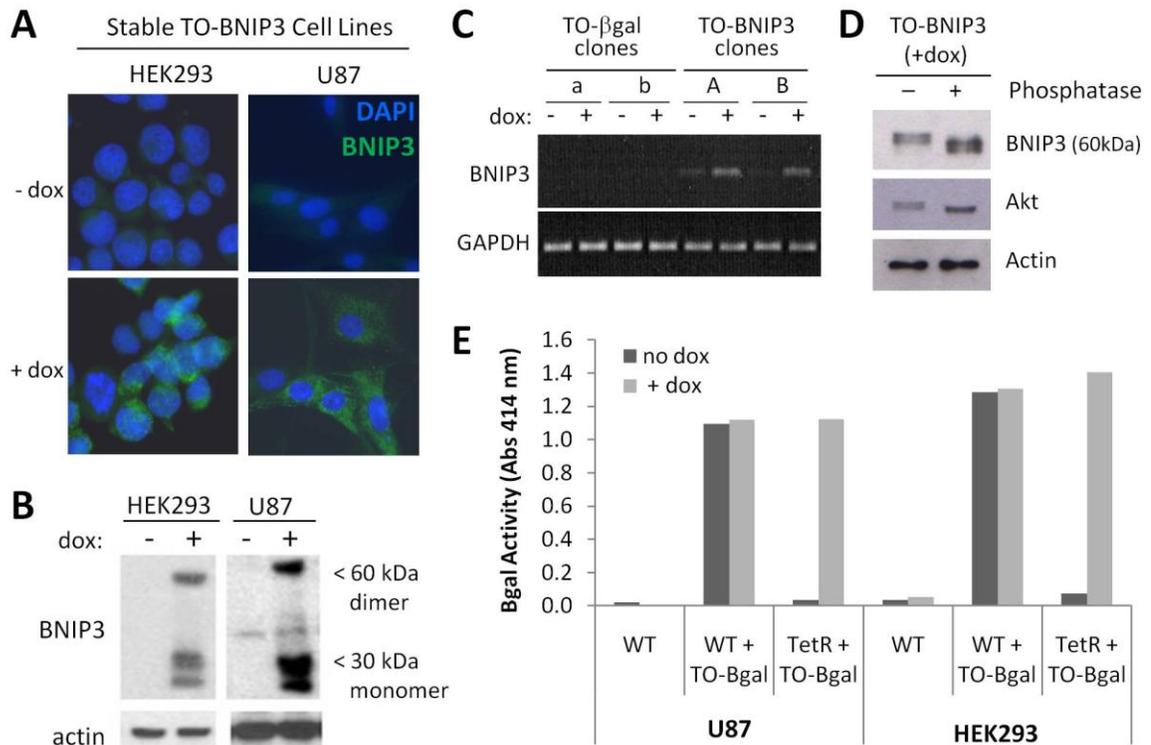
Figure 5.1 Stable doxycycline-inducible expression of BNIP3 and β-galactosidase.
HEK293 and U87 cells were engineered to stably co-express the Tet Repressor protein (TR) and tetracycline-inducible BNIP3 (TO-BNIP3) or β-galactosidase (TO-βgal) as described in Materials & Methods. Multiple clones were established for each cell line. Addition of the tetracycline analog, doxycycline (dox), for 24 hours relieves TR repression and induces BNIP3 expression as detected by immunofluorescence (A), Western blot (B) and RT-PCR (C, HEK293 clones). (D) Induced BNIP3 is phosphorylated. HEK293 TO-BNIP3 clone A cells were treated with doxycycline to induce BNIP3 expression, and whole cell lysates were treated or untreated with calf intestine alkaline phosphatase (CIP; 1U/μg protein) prior to Western blotting for BNIP3, Akt (phosphorylation control) and actin (loading control). Downshift upon CIP treatment indicates removal of phosphate groups. The BNIP3 60 kDa dimer was therefore observed to be phosphorylated in induced TO-BNIP3 cells. (E) βgal activity is induced by doxycycline in TR/TO-βgal cells. Inducible βgal activity is not exhibited by wild type cells, or wild type cells expressing TO-βgal without the TR regulatory vector.

We and others have previously shown that BNIP3 triggers mitochondrial ROS production and autophagy (71, 78, 213, 218, 253) and (Figure 4.2). As expected, induced BNIP3 expression in TO-BNIP3 cells led to increased ROS production and autophagy, which was not observed after βgal induction (Figure 5.2A&B). Unexpectedly, BNIP3 induction did not result in cell death, even after 48 hours. In both U87 and HEK293 TO-BNIP3 cell lines, cell death remained unchanged at 9-12% regardless of the level of BNIP3 induction, which was comparable to TO-βgal cells with or without induction (6-13%) (Figure 5.2C). Since we routinely observe over 60% cell death in BNIP3 transient transfection experiments by 24 hours (Figure 4.2E), this suggests that our TO-BNIP3 cells may have developed resistance to BNIP3-induced cell death. Since others have demonstrated the cytotoxicity of phospho-BNIP3 (229), the observed phosphorylation of induced BNIP3 (Figure 5.1D) is unlikely to be responsible for the absence of BNIP3-induced cell death.
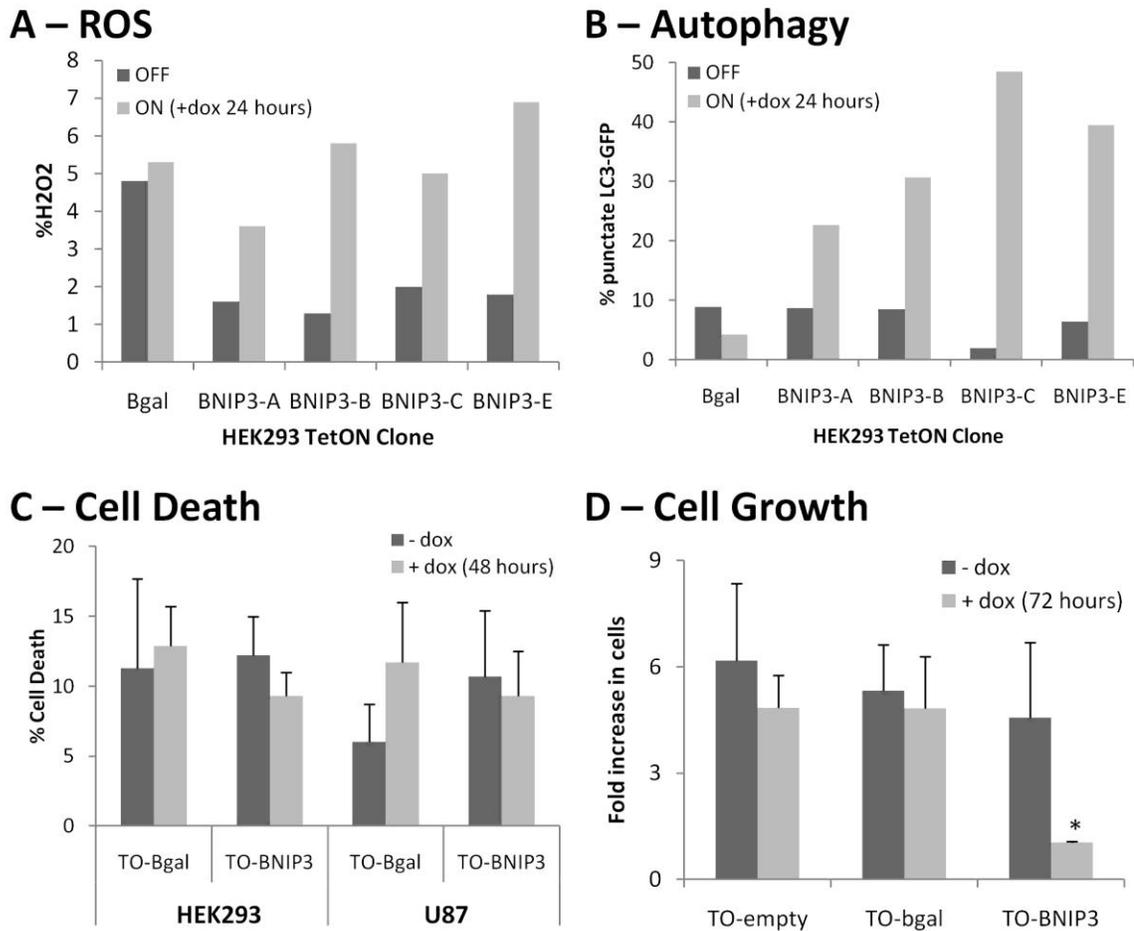
Figure 5.2 Effects of BNIP3 induction in TO-BNIP3 cells.
HEK293 and U87 cells were engineered to stably co-express the Tet Repressor protein (TR) and tetracycline-inducible BNIP3 (TO-BNIP3) or β-galactosidase (TO-βgal) as described in Materials & Methods. Cells were untreated or treated with doxycycline (1 μg/mL) to induce gene expression. (A) Reactive oxygen species (ROS) production was increased upon BNIP3 (but not βgal) induction. ROS were detected using the dye CM-H$_2$DCFDA, which is oxidized to green fluorescent DCF (dichlorofluorescein) by hydrogen peroxide.   (B) Autophagy was also increased upon BNIP3 (but not βgal) induction, as determined by GFP-LC3 localization. TO-cells were in transiently transfected with GFP-LC3. 24 hours after transfection, cells were untreated or treated with doxycycline for an additional 24 hours. (C) Cell death was not induced upon BNIP3 or βgal induction, as determined by membrane permeability assay. (D) Cell growth was severely restricted upon BNIP3 (but not βgal) induction in HEK293 cells. For each cell type, 1.5x10^5 cells were seeded in one well of a 6-well culture dish, with or without doxycycline (gene induction). Three days later, the number of adherent cells in each well was determined using a Beckman Coulter Counter. The fold-increase represents the ratio of cells on day three compared to the number of cells originally seeded.   Results represent the average of three independent experiments; error bars represent standard deviation. A&B, n=1. C&D, n=3. *p<.01 by t-test.

Chronic exposure to BNIP3 could elicit a resistance phenotype, but the TREx™ system is designed to repress BNIP3 expression until induction is stimulated with doxycycline. In practice, however, we detected "leaky" expression of BNIP3 in un-induced TO-BNIP3

138

cells. Leaky BNIP3 expression was not detectable by immunofluorescence or Western blot (likely due to low antibody sensitivity); however, RT-PCR analysis clearly showed increased BNIP3 expression in uninduced TO-BNIP3 clones compared to TO-βgal clones (Figure 5.1C). This subtle but persistent BNIP3 expression in uninduced TO-BNIP3 cells could be sufficient to induce cell death and select for a BNIP3-resistant phenotype. Hence, while these findings preclude the use of TO-BNIP3 cells for studying BNIP3-induced cell death as originally intended, they highlight an opportunity to study "BNIP3 resistance".

Notably, although cell death was not induced upon BNIP3 expression, proliferation appeared to be severely restricted (Figure 5.2D). Three days after seeding, the number of TO-βgal cells had increased 5.3-fold, which was unchanged (4.8-fold) in the presence of doxycycline. Proliferation of TO-BNIP3 cells was comparable in the absence of doxycycline (4.6-fold increase over three days); however, doxycycline treatment (i.e. BNIP3 induction) at the time of seeding restricted proliferation almost completely (1.05-fold increase). This finding is consistent with a previous study that reported a rapamycin-sensitive growth advantage in BNIP3-knockdown tumor xenografts, suggesting that BNIP3 inhibits cell growth by suppressing the mTOR pathway (263). Additional methods must be employed to confirm decreased proliferation in TO-BNIP3 cells (for example, MTT or colony-forming assays), and the involvement of mTOR signaling remains to be tested. Nevertheless, our results suggest that while TO-BNIP3 cells have developed resistance to BNIP3-induced cell death, the mechanisms by which they accomplish resistance may either directly inhibit cell growth, or indirectly restrict

proliferation by diverting energy and resources from growth-promoting signaling
pathways.

Finally, it remains possible that BNIP3 may be necessary but not sufficient for
autophagic cell death, requiring additional cellular stress (for example, hypoxia, acidosis
or DNA damage) to achieve cytotoxicity. While the transient overexpression studies
described in section 4.2 appear to indicate that BNIP3 is sufficient to induce autophagic
cell death, the process of transient transfection in these experiments could be a source of
accompanying cellular stress, perhaps required for BNIP3-mediated cytotoxicity. Such
"transient transfection stress" would be absent in the stable induction system described
here. Further research is required to address this possibility.

5.3   Identification of potential mediators of BNIP3 resistance.

In cancer, hypoxic tumor cells frequently express BNIP3 yet remain viable ((230, 296,
332)). Thus, our TO-BNIP3 cell lines, which remain viable upon significant BNIP3
induction, represent a model system of BNIP3 resistance that may be physiologically
relevant to cancer. To characterize the mechanism of BNIP3-resistance in TO-BNIP3
cells, we performed a microarray analysis comparing gene expression in uninduced
HEK293 TO-BNIP3-clone-A and TO-βgal-clone-A cells (Table 5.1). Of the 1,728 genes
surveyed, 22 were found to be differentially regulated, including 6 genes where the
change in expression was greater than 2-fold and/or the expression was sufficiently high
as to achieve significance with less than 2-fold difference (Figure 5.3). Five of these six
genes were up-regulated in TO-BNIP3 cells compared to TO-βgal cells: IFI30

140

(interferon gamma-inducible protein 30), HSPA1A (heat shock 70kDa protein 1A), SSAT (spermidine/spermine N1-acetyltransferase), CLU (clusterin), and CD44 antigen. One gene, API5 (apoptosis inhibitor 5, aka antiapoptois clone 11/AAC-11), was down-regulated.

Further research is required in order to validate the "BNIP3-resistance" phenotype, to confirm the differential expression of our candidate genes, and to determine their functional significance. Based on previous studies of these genes and their gene products (discussed further in section 7.6), we believe that three in particular may warrant further investigation. CLU is abnormally upregulated in numerous cancers and is a key contributor to chemoresistance (333). The SSAT enzyme is highly inducible, participating in adaptive responses to environmental stress (334), and a hypoxia-inducible isoform has been identified and implicated in tumor progression (335). Finally, HSPA1A is a member of the HSP70 family of "stress response" genes which have been shown to protect against ischemic brain injury in rats (336) and increase the survival of Drosophila under acute and intermittent hypoxia (337). API5 is also an intriguing candidate, as the only down-regulated gene identified in TO-BNIP3 cells. API5 has been characterized as an anti-apoptosis gene, but its down-regulation in BNIP3-TO cells suggests that it may have other, yet-to-be defined functions in autophagy or cell survival.

Thus, using a potentially novel model system of BNIP3 resistance, we have identified several possible mediators of resistance to BNIP3-induced cell death, including CLU, SSAT and HSP70.

Table 5.1 Differential gene expression in TO-βgal and TO-BNIP3 cells.
mRNA was extracted from non-induced HEK293 TO-BNIP3 and TO-βgal cells. Microarray analysis was performed, surveying a total of 1,728 genes. Average gene expression, expressed in relative fluorescence units (FU), and standard error (%SE) are shown. Twenty-two genes, listed here, were found to be differentially expressed, including six (listed first) with especially high confidence.

GenBank Accession ID	Gene Symbol	Gene Name	TO-βgal		TO-BNIP3		Ratio BNIP3/βgal
			Avg FU	%SE	Avg FU	%SE	
BG387747	API5	apoptosis inhibitor 5	7391	11%	4604	10%	0.62
W24688	IFI30	interferon, gamma-inducible protein 30	560	12%	1008	13%	1.80
T74240	HSPA1A	heat shock 70kDa protein 1A	329	6%	689	5%	2.09
AA056280	SSAT	spermidine/spermine N1-acetyltransferase 1	661	9%	1494	8%	2.26
W68191	CLU	clusterin	3256	10%	8199	11%	2.52
N28294	CD44	CD44 molecule	93	11%	255	8%	2.76
R61009	ADCY8	adenylate cyclase 8	44	14%	54	16%	1.22
AA136799	GADD45A	growth arrest and DNA-damage-inducible, alpha	1476	13%	2169	10%	1.47
T65096	ARFRP1	ADP-ribosylation factor related protein 1	34	17%	50	18%	1.47
R66676	ETV5	ets variant 5	237	13%	356	19%	1.50
R32409	PLA2G5	phospholipase A2, group V	124	11%	187	19%	1.51
H53477	COL2A1	collagen, type II, alpha 1	1237	6%	1875	7%	1.52
W88806	UROS	uroporphyrinogen III synthase	557	10%	845	9%	1.52
R06555	PTPRU	protein tyrosine phosphatase, receptor type, U	120	13%	182	16%	1.52
W58696	GAS1	growth arrest specific 1	37	22%	57	23%	1.52
W37704	EPCAM	epithelial cell adhesion molecule	1306	13%	2010	11%	1.54
R33892	HOXB5	homeobox B5	537	13%	827	16%	1.54
H92049	LRBA	LPS-responsive vesicle trafficking, beach and anchor	1721	11%	2702	8%	1.57
BF965177	TMSB4X	thymosin beta 4, X-linked	358	10%	619	13%	1.73
AA135957	ABCB1	ATP-binding cassette, sub-family B (MDR/TAP) 1	307	14%	533	15%	1.74
N31222	DPP4	dipeptidyl-peptidase 4	494	9%	890	9%	1.80
BI669347	SEPP1	selenoprotein P, plasma, 1	280	11%	507	12%	1.81
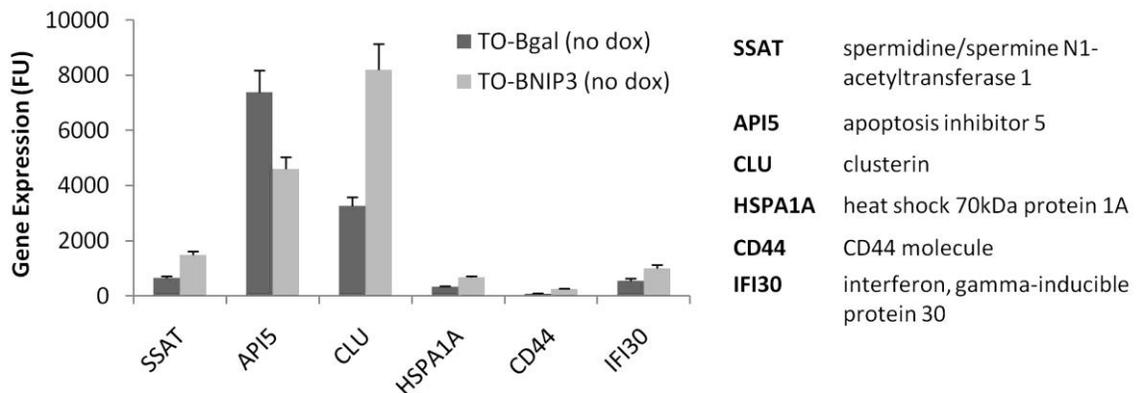
Figure 5.3 Differential gene expression in TO-BNIP3 cells: potential mediators of BNIP3 resistance. Graphical representation of the top six differentially-regulated genes in TO-BNIP3 cells compared to TO-βgal cells, identified by microarray analysis as detailed in Table 5.1.

5.4   Chapter summary

In summary, the results in this chapter demonstrate the following:

- We have successfully generated stable HEK293 and U87 cell lines expressing tetracycline-regulated β-galactosidase (TO-βgal) or BNIP3 (TO-BNIP3).

- Induced expression of BNIP3 in TO-BNIP3 cells leads to ROS production, autophagy and impaired proliferation, but fails to induce cell death.

- Resistance to BNIP3-induced cell death in TO-BNIP3 cells may be attributable to leaky BNIP3 expression in uninduced cells (remains to be proven).

- Using uninduced TO-BNIP3 cells as a model for BNIP3 resistance, we have tentatively identified 23 genes which are differentially regulated compared to TO-βgal cells, representing potential mediators of BNIP3 resistance.

- Based on gene expression analysis combined with current knowledge of their cellular functions, we have identified 3 promising candidate mediators of BNIP3 resistance: CLU (clusterin), HSP70 (heat shock 70kDa protein), and SSAT (spermidine/spermine N(1)-acetyltransferase).

These findings have important physiological implications, since hypoxic tumor cells often express BNIP3 yet remain viable and exhibit chemoresistance (section 1.7.5.2). Albeit unintentionally, we have developed a potentially novel model system for studying BNIP3 resistance. While further studies are required to confirm and characterize the role of our candidate proteins in BNIP3 resistance, this research could ultimately establish the foundation for new therapeutic strategies targeting BNIP3 resistance in tumors.

Chapter 6: A novel role for BNIP3 in cell cycle regulation during brain development.

6.1 Rationale

Besides serving as a source of primary cells for *in vitro* experiments (as described in Chapter 4), the BNIP3-/- mouse model presents an opportunity to study the role of BNIP3 *in vivo*. Ultimately our goal is to study hypoxia-related pathologies in BNIP3-null mice, to determine how BNIP3 contributes to disease processes such as tumorigenesis and ischemic injury. However, before this research can be undertaken it is essential to determine whether any relevant baseline differences exist between BNIP3-/- mice and their wild type counterparts. Since BNIP3 has previously been implicated in the pathophysiology of brain tumors (230), neurodegeneration (217), and ischemic stroke (269, 270), we specifically aimed to characterize the effect of BNIP3 knockout in the mouse brain. Just as Dorn and colleagues characterized the cardiovascular and hematopoietic systems of BNIP3-/- mice prior to studying myocardial infarction (240), we endeavored to characterize the healthy BNIP3-null mouse brain prior to studying hypoxia-related brain pathologies.

Currently, little is known about the role of BNIP3 in normal brain function and development. The BNIP3-/- mouse model has not yet been extensively studied, and the only report thus far focuses exclusively on the heart and cardiovascular system (240). However, limited evidence has implicated BNIP3 in oligodendrocyte differentiation (297) and developmental apoptosis in the postnatal rat brain (298). In addition, hypoxia and HIF-1 are established mediators of embryogenesis (22), and regulated cell death is an

important aspect of mammalian development. Accordingly, as a HIF-1 target gene and cell death mediator, BNIP3 is a likely candidate for the regulation of hypoxia-driven developmental processes. Thus, we sought to determine the effect of BNIP3 knockout on normal mouse brain function and development *in vivo*.

6.2   BNIP3 knockout causes increased cellularity in the mouse brain

As described in section 4.3, we found that homozygous BNIP3-null mice were born from heterozygous crosses at normal Mendelian ratios and showed no increase in mortality or apparent physical abnormalities. In agreement with previous studies (233, 298) , we detected moderate BNIP3 expression in unstressed wild type brain (Figure 6.1) and cultured astrocytes (Figure 4.5A), suggesting that BNIP3 may play a functional role in brain physiology and development.
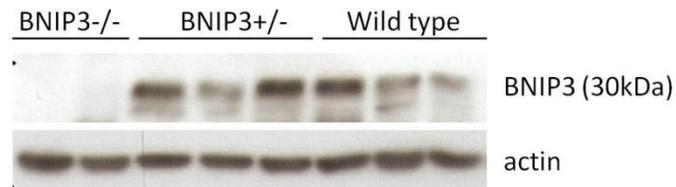
Figure 6.1 BNIP3 protein expression in mouse brain.
Total cell lysates were generated from cryo-preserved brain tissue extracted from wild type, heterozygous and BNIP3-null adult mice. Lysates were analyzed for BNIP3 expression by Western blot, with actin as a loading control; each lane represents a different mouse. Mice were sacrificed by cervical dislocation to minimize hypoxia at the time of death, and brain tissue was removed within 5 minutes.

Initially, we examined the gross brain morphology of unstressed adult mice. Wild type and BNIP3-/- littermates were sacrificed at 8 weeks of age (n = 3 pairs, each pair from a different litter). Brain tissue was fixed by cardiac perfusion and overnight immersion in paraformaldehyde. After paraffin-embedding, sectioning and hematoxylin and eosin

staining, overall morphology and cellularity were assessed. Since BNIP3-/- mice do not exhibit any obvious neurological impairment, we were not surprised to find that BNIP3-/- brains were grossly normal. Upon closer inspection, however, the BINP3-/- brains appeared more cellular compared to wild type (Figure 6.2). Although the difference was modest and did not reach statistical significance in adults (average increase = 5%, 95%CI = -1% to 13%), it was consistently observed in multiple areas of the brain, including the cerebellum, hippocampus, cortex and inferior colliculus (Figure 6.2). In this preliminary study, only one section was analyzed per anatomical region. Future research will aim to confirm the observed differential cellularity through the analysis of additional brain sections.
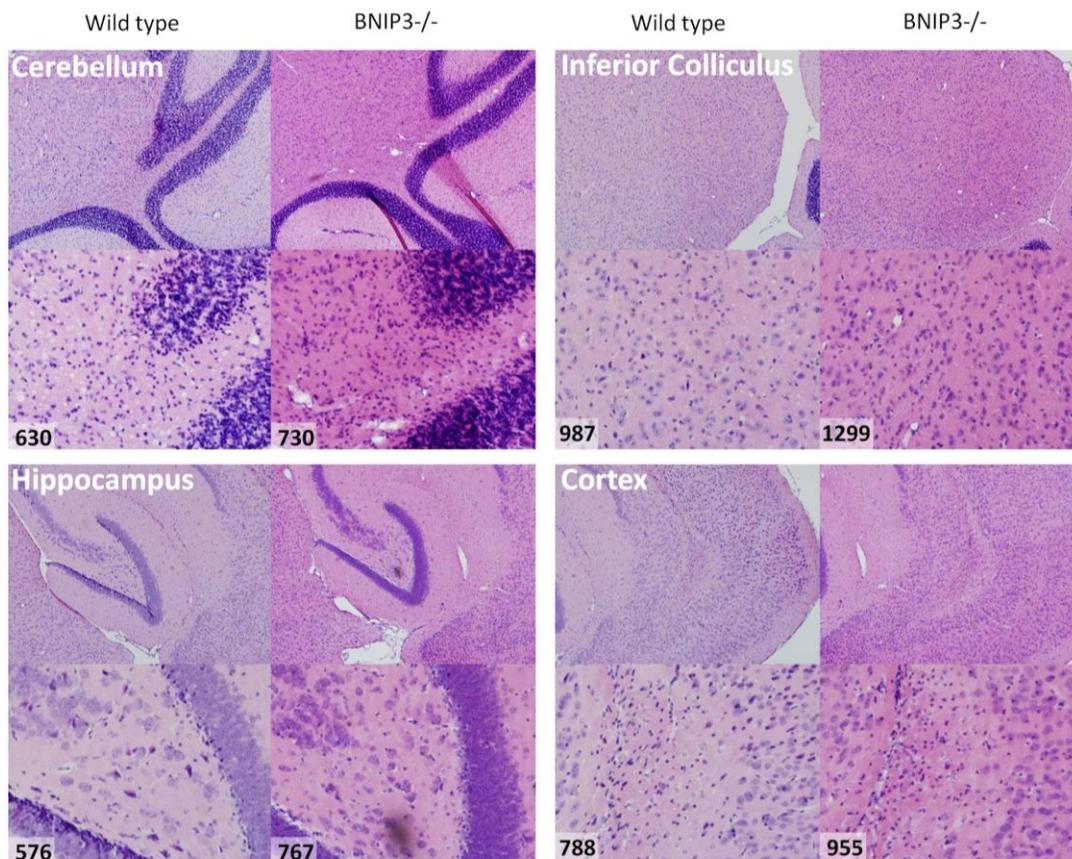
Figure 6.2 Morphology and cellularity of adult wild type and BNIP3-/- brains.
Whole brains from unstressed 8-week old wild type and BNIP3-/- mice were fixed by cardiac perfusion and overnight immersion in paraformaldehyde (n = 3 pairs of littermates from different heterozygous crosses). Brains were embedded in paraffin, sectioned and stained with hematoxylin and eosin as described in Materials & Methods. Images were captured at 100x and 400x magnification and cell counting was performed using Image Pro Plus 5.0 software. These representative images depict the morphology of the cerebellum, hippocampus, cortex and inferior colliculus, with cell counts for the 400x images indicating increased cellularity in BNIP3-/- brains.

We additionally examined brain morphology and cellularity in E18.5 embryos (n = 4 littermates, 2 wild type and 2 BNIP3-/-). Similar to adults, gross morphology appeared normal in BNIP3-/- embryonic brains and moderately increased cellularity was observed (Figure 6.3). In this case, differential cellularity was statistically significant: E18.5 BNIP3-/- brains were 11% more cellular compared to wild type (95% confidence interval: 5.0 – 17.1%). Once again, increased cellularity was observed in multiple areas of the brain, including: the hippocampus, striatum, thalamus, cortex, stria terminalis, and paraventricular thalamic nucleus (

Table 6.1). In agreement with these results, we found that during primary astrocyte isolation, cortices from BNIP3-/- neonates contained more cells compared to wild type; however, this trend failed to reach statistical significance (2.68×10^5 cells/BNIP3-null cortex vs. 2.09×10^5 cells/wild-type cortex; n = 5 litters per genotype, representing 74 neonates in total; p = 0.10).
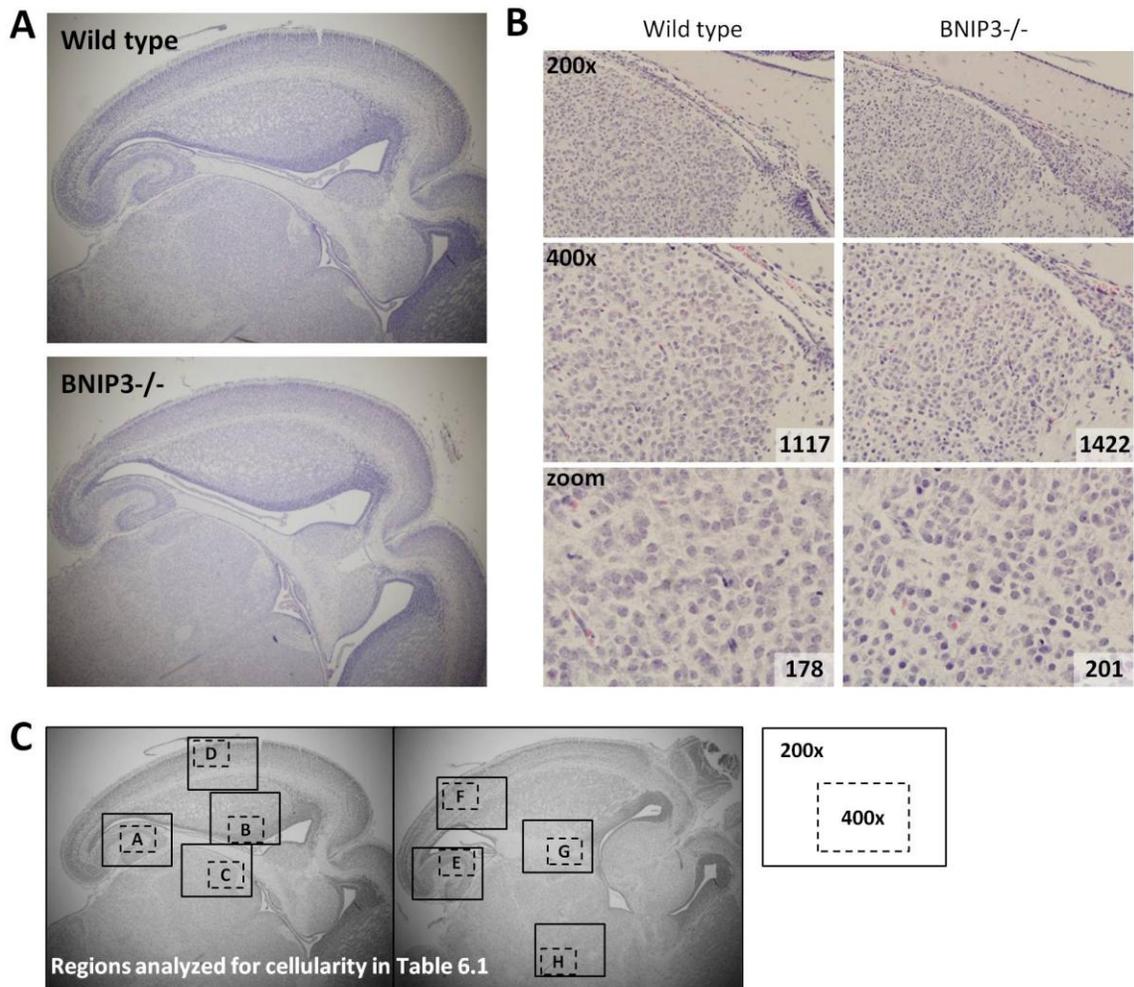
Figure 6.3 Morphology and cellularity of E18.5 wild type and BNIP3-/- mice.
E18.5 embryos were obtained from a single heterozygous cross. Brains were fixed by overnight immersion in paraformaldehyde, followed by paraffin embedding, horizontal sectioning and staining with hematoxylin and eosin. Images captured at 40x magnification revealed no significant difference in general morphology; representative images are shown in (A). Images captured at 200x and 400x magnification were analyzed with Image Pro Plus 5.0 to determine cellularity; representative images with cell counts are shown in (B). These images correspond to region "C" in panel (C), which depicts the 8 regions analyzed for cellularity in each brain. A = hippocampus, B = striatum, C = thalamus, D = somatosensory cortex, E = hippocampus, F = secondary auditory cortex, G = stria terminalis, H = paraventricular thalamic nucleus.

Table 6.1 Cellularity of wild type and BNIP3-/- E18.5 brains.
Whole brain sections from E18.5 embryos were prepared and analyzed as in Figure 6.3 (n = 4 littermates, 2 wild type and 2 BNIP3-/-). Average cell counts and percent standard deviation were calculated for 8 brain regions as depicted in Figure 6.3C. In this preliminary study, one section was analyzed per anatomical region.

| Region and Magnification | | Wild Type | | BNIP3-/- | | Ratio: |
		Avg	% SD	Avg	% SD	null/WT
A Hippocampus	20x	2410	11.0	2875	1.6	1.19
	40x	916	6.4	1284	5.9	1.40
B Striatum	20x	3365	5.4	4057	9.6	1.21
	40x	1432	18.7	1577	1.0	1.10
C Thalamus	20x	1954	20.0	2039	3.6	1.04
	40x	1221	12.0	1493	6.7	1.22
D Somatosensory cortex	20x	2976	7.5	3798	4.8	1.28
	40x	1225	6.9	1275	4.6	1.04
E Hippocampus	20x	3202	3.6	3223	0.8	1.01
	40x	1141	3.3	1179	8.0	1.03
F Secondary auditory cortex	20x	3371	4.5	3286	5.3	0.97
	40x	1375	3.4	1287	5.9	0.94
G Stria terminalis	20x	2641	3.9	3057	n/a	1.16
	40x	646	2.8	688	4.7	1.07
H Paraventricular thalamic nucleus	20x	2888	n/a	3144	5.4	1.09
	40x	1308	5.1	1336	2.2	1.02
Overall Average						**1.11** **(95%CI: 1.05-1.17)**

To determine which cell type(s) account for the increased cellularity in BNIP3-/- brains, we performed immunofluorescence and Western blot analyses to detect neurons and glia, the two major classes of cells in the mammalian brain (Figure 6.4). To detect neurons, we assayed for expression of the neuronal marker, NF-L (68kDa light neurofilament subunit). To detect astrocytes, the most abundant type of macroglial cell, we assayed for expression of the astrocyte marker, GFAP (glial fibrillary acidic protein). By immunofluorescence, GFAP expression appeared to be reduced in BNIP3-/- brains compared to wild type (Figure 6.4A). However by Western blot, GFAP expression did not differ significantly between wild type and BNIP3-/- mice, although expression

appeared to increase with age from 8 to 32 weeks in both genotypes (Figure 6.4B).

While our NF-L antibody was inadequate for immunofluorescence, we detected similar

levels of NF-L protein in wild type and BNIP3-/- brains by Western blot (Figure 6.4B).

Thus, further research is required to fully characterize the altered cellular composition of

the BNIP3-null brain. These studies could be facilitated through acquisition of additional

antibodies for immunofluorescence, and should include qRT-PCR analysis. Additional

cell types should also be investigated, such as oligodendrocytes and microglia, and other

neuroanatomic regions of the developing and adult brains.
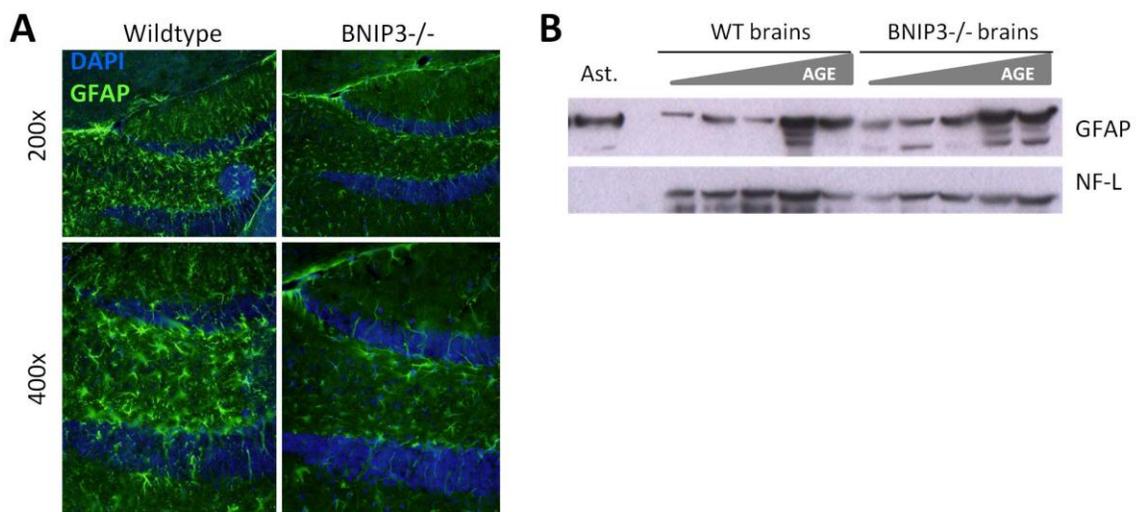
Figure 6.4 Expression of neuronal and astrocyte markers in wild type and BNIP3-/- mouse brain.
Wildtype and BNIP3-/- mice were sacrificed at 8 – 32 weeks of age and brains were cryopreserved as
described in Materials and Methods. (A) Detection of the astrocyte marker GFAP (glial fibrillary acidic
protein) in adult (8 week) mouse brain by immunofluorescence. (B) Detection of GFAP and the neuronal
marker NF-L (68kDa light neurofilament subunit) in cultured astrocytes (Ast.) and adult (8 - 32 week)
mouse brains. To control for loading, the Bradford protein assay was performed on all lysates and an equal
amount of total protein was loaded in each lane.

Taken together, these results show that loss of BNIP3 in the developing mouse brain

appears to cause increased cellularity, which persists into adulthood. The mechanism,

composition and functional significance of increased cellularity in the BNIP3-null brain

remains to be determined.

6.3   BNIP3 knockout causes differential growth patterns *in vitro*

The observed increase in brain cellularity after BNIP3 knockout *in vivo* could be the result of reduced cell death and/or increased cell proliferation during development. Indeed, BNIP3 is a proven mediator of cell death in several contexts (196), and at least one report has implicated BNIP3 as a negative regulator of cell growth through suppression of mTOR signaling (263). In the BNIP3-null model system, we have already shown that loss of BNIP3 leads to reduced hypoxia-induced cell death in embryonic fibroblasts and astrocytes *in vitro* (Figure 4.5). To determine if BNIP3 knockout also affects the proliferation of these cells, we analyzed cell cycle progression by measuring the rate of BrdU incorporation and the proportion of cells with 4N DNA content (Figure 6.5). BrdU is specifically incorporated into the nuclei of proliferating cells during DNA replication (S phase), and can be detected with specific antibodies. After DNA replication and before cell division (G2 phase), cells have 4N DNA content which can be detected through propidium iodide staining and flow cytometry. Interestingly, these two assays generated potentially conflicting results. We detected decreased BrdU incorporation in BNIP3-/- astrocytes compared to wild type (10.3% vs. 17.0%, p<.05), suggesting decreased proliferation (Figure 6.5A). By contrast, the proportion of 4N cells was increased in BNIP3-/- cultures compared to wild type (26.2% vs. 21.2%, p<.02), suggesting either increased proliferation or G2/M cell cycle arrest (Figure 6.5B). There appeared to be no difference in the overall rate of proliferation as measured by the MTT viability assay (Figure 6.5C); however, additional methods must be employed to confirm this finding.
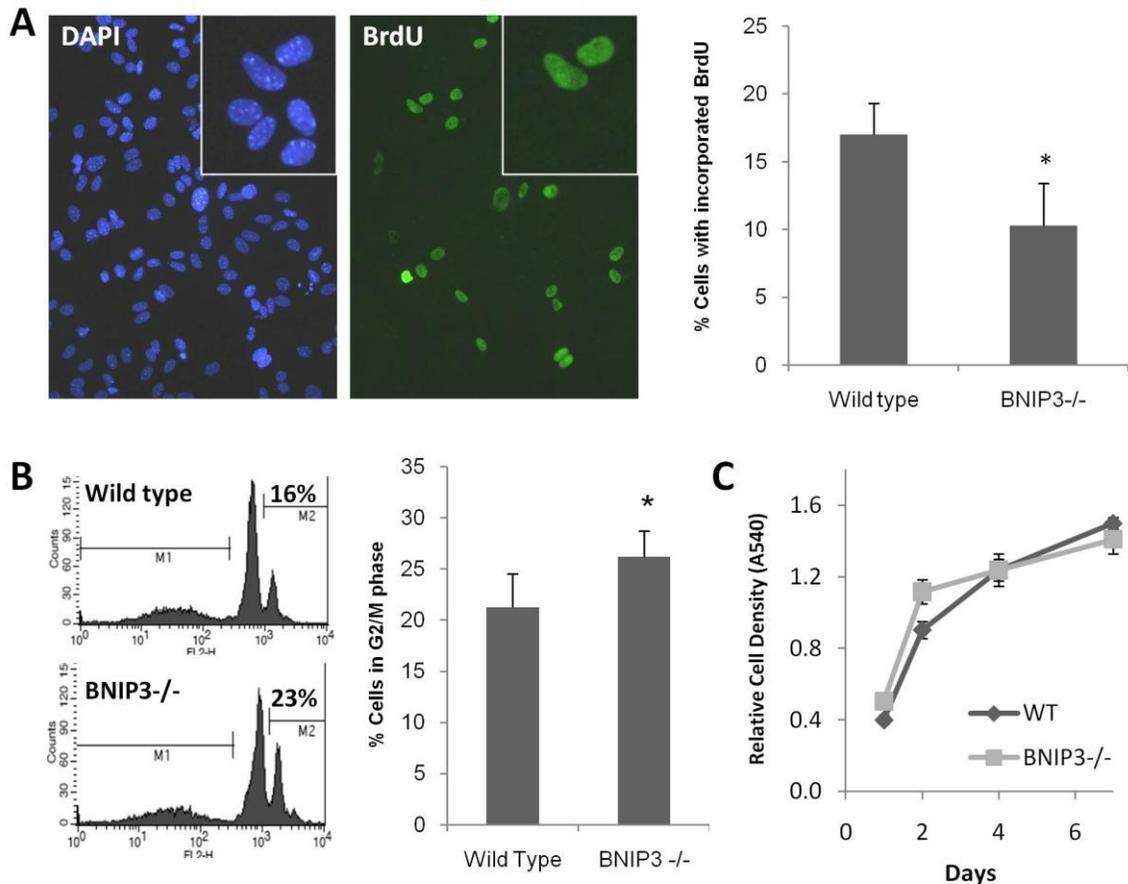
Figure 6.5 Loss of BNIP3 causes differential cell cycle progression in cultured primary astrocytes.
(A) Cultured primary astrocytes were incubated with BrdU for 48 hours. BrdU is specifically incorporated into the DNA of replicating cells. BrdU incorporation was detected by immunofluorescence with BrdU-specific antibodies. At least 200 cells per sample were scored for BrdU incorporation. Results represent three independent experiments and error bars indicate standard deviation, *p<.05. (B) The DNA content of cultured astrocytes was analyzed by PI staining and flow cytometry. The proportion of cells in the G2/M phase (4N DNA content) was quantified in 11 independent experiments representing 5 separate isolations of WT and BNIP3-/- cells. (C) Equivalent amounts of WT and BNIP3-/- astrocytes were plated in triplicate in 96-well plates and allowed to replicate for 1 to 6 days. Relative cell density was measured by quantifying the amount of MTT reagent metabolized to purple formazan in each well by colorimetric assay.

Together, these results indicate that BNIP3-/- astrocytes have a decreased rate of DNA replication and may also progress more slowly through the G2/M phase of cell division; however, these changes do not appear to significantly affect the rate of astrocyte proliferation *in vitro*. The rate of cell death, which was not specifically addressed in these experiments, could also be a contributing factor and will be addressed in future studies.

6.4   Chapter summary

In summary, the results presented in this chapter demonstrate the following:

- BNIP3-null mice are born at normal Mendelian ratios and show no increase in mortality or apparent physical abnormalities up to 10 months of age.
- BNIP3-/- adult and embryonic brains are grossly normal, but appear to exhibit a moderate increase in cellularity across multiple brain regions.
- BNIP3-/- astrocytes have a decreased rate of DNA replication and may progress more slowly through the G2/M phase of cell division; however, these changes do not significantly affect the rate of proliferation *in vitro*.

Collectively, these results identify a potentially novel role for BNIP3 in the regulation of cell cycle progression and mammalian brain development. While it has been widely studied as a mediator of cell death (section 1.7.3), BNIP3 has never before been implicated in cell growth or proliferation. Further studies are required to fully elucidate the role of BNIP3 in proliferation *in vivo* and in different cell types, and to determine how BNIP3 may regulate DNA replication or promote cell division. Besides providing new insights into mammalian development, these findings may ultimately have therapeutic implications if BNIP3-mediated proliferative pathways are found to play a role in BNIP3-related pathologies such as ischemic injury or cancer.

Chapter 7: Discussion

7.1   Autophagy in hypoxia: pro-survival or pro-death?

Although autophagy has been characterized in many contexts, our studies were among the first to specifically investigate this pathway in hypoxic cancer cells. Prior to the publication of our results (338), hypoxia-induced autophagy in cancer cells had not been conclusively demonstrated, let alone functionally characterized. In fact, little was known about hypoxia-induced autophagy in any context. Ischemia-hypoxia had been shown to induce autophagic cell death in the brain (339), while protective autophagy was shown to occur after ischemic injury in the heart (9). With respect to cancer, limited evidence suggested that autophagy could protect against "metabolic stress" (hypoxia combined with nutrient deprivation) in tumor cells (7). Thus, our results have contributed significantly to the understanding of autophagy in hypoxia, showing that prolonged hypoxia-induced autophagy can contribute to cancer cell death.

Since we published our findings in 2008, several new studies have demonstrated both pro-death and pro-survival roles for hypoxia-induced autophagy in various contexts (340). For example, protective autophagy has been demonstrated in MEFs subjected to prolonged hypoxia, where mitochondrial autophagy is necessary to prevent toxic production of ROS (257). Similarly, autophagy was shown to be protective against toxic ROS in tumor cells exposed to cycling hypoxia and reoxygenation (341). Autophagy has also been described as a renoprotective mechanism during ischemia-reperfusion renal injury *in vivo* (342). By contrast, hypoxia was shown to induce autophagic cell death in

154

the developing fetal liver of RB-null mice (218) and in neonatal ischemic brain injury (343).

There have also been several new reports of hypoxia-induced autophagy in cancer subsequent to our 2008 publication. In agreement with our findings, Wouters and colleagues showed that hypoxia induces autophagy in cancer cells and human xenograft tumors; however, they determined that autophagy was primarily pro-survival since blockade of hypoxia-induced autophagy sensitized cells to hypoxia and tumors to treatment (344). Interestingly, this group further demonstrated that hypoxia-induced autophagy was mediated by the unfolded protein response (UPR), through PKR-like ER kinase (PERK)-mediated upregulation of LC3 and ATG5. Jaakkola and colleagues have similarly reported protective hypoxia-induced autophagy in cancer cells (345). They demonstrated that hypoxia-induced autophagy promotes degradation of p62 (sequestosome 1), permitting elevated Ras/ERK signaling which may protect cancer cells against hypoxic stress. Finally, Denko and colleagues have also demonstrated hypoxia-induced autophagy in cancer cells (346). Similar to our findings, and in contrast to Wouters and Jaakola, they determined that autophagy contributed to cancer cell death, since ablation of autophagy caused increased survival in hypoxic environments and accelerated xenograft tumor growth.

Thus, our research contributes to a growing body of evidence that implicates hypoxia-induced autophagy in multiple pathophysiological conditions including cancer, through both protective and destructive mechanisms. Existing evidence suggests that hypoxia-

155

induced autophagy is mediated through HIF, mTOR and UPR signaling (21); however, further research is required to fully elucidate the specific mechanisms involved.

7.2 Autophagy as a distinct mechanism of cell death

Previously, autophagic cell death has often been observed alongside apoptosis (131, 132, 347, 348), while apoptosis-independent autophagic cell death has frequently been described in systems using caspase inhibitors or genetic manipulation to directly block apoptosis (5, 7, 136, 168, 319). Our results convincingly demonstrate that hypoxia induces apoptosis-independent autophagic cell death in apoptosis-competent cancer cells.

It is widely recognized that autophagy occurs at low basal levels to maintain cellular homeostasis. For example, neurodegenerative disorders are detected in animal models where the autophagy proteins ATG7 or ATG5 are eliminated from neurons, suggesting a role for autophagy in maintaining normal neuronal function (62, 349). It is also accepted that autophagy can be transiently induced by stress, such as nutrient deprivation, as a survival response (49). This concept has been illustrated many times at the cellular level, and more recently in an animal model of ATG5-deficient mice. These mice, although nearly normal at birth, could not survive the early neonatal starvation period since they failed to induce autophagy (67). Thus, autophagy contributes to homeostasis and cell survival functions in various physiological contexts.

The role of autophagy as a form of programmed cell death (PCD type II) has also been established, but remains controversial – especially in cancer. As described in section

1.3.4, autophagy has been observed to promote or activate apoptosis in some cases (68-70). However, prolonged autophagy leading to apoptosis-independent PCDII has been demonstrated in multiple contexts, including arsenic trioxide treatment of glioma cells (71), hydroxychloroquine treatment of human dermal fibroblasts (73), ganglioside treatment of astrocytes (74), and in response to a "autophagonizer", a novel small molecule inducer of autophagy (75). Our results provide additional evidence that autophagy can function as a distinct mechanism for programmed cell death. We have presented a clear demonstration of prolonged autophagy contributing to hypoxia-induced cell death, without induction of apoptosis, in cancer cells that are otherwise fully competent to induce apoptosis in response to a DNA damaging agent.

The apparently contradictory functions for autophagy could be explained by a time-dependent "dual role" for autophagy in cell survival and cell death: early induction of autophagy may contribute to a protective response, whereas prolonged autophagy could lead to cell death. Indeed, we found that autophagy was strongly induced in viable cells as quickly as 1 hour following acute hypoxia. Since this rapid onset of autophagy occurred nearly 24 hours before cell death was detectable, it likely occurred as an initial survival strategy. Thus, our results are consistent with a model whereby rapidly-induced autophagy could initially offer protection against hypoxic stress, while prolonged autophagy in hypoxia functions as a distinct mechanism of cell death, independent of apoptosis.

7.3 Autophagy in cancer: an alternative cell death pathway with therapeutic potential

As discussed in section 1.3.5.1, there is evidence that autophagy may be protective or destructive to tumor cells, depending on the cellular context and conditions. For example, autophagy may be employed by cancer cells to promote survival in the harsh tumor microenvironment, which commonly inflicts metabolic and oxidative stress (7, 65, 66). However, autophagy also represents an important tumor-suppressive mechanism, blocking tumorigenesis by preventing oxidative damage and mutagenesis through the removal of damaged mitochondria (51, 350). Recent evidence suggests that, similar to apoptosis, autophagy is suppressed in many cancers (351). This conflicting evidence has inspired the theory that autophagy may serve different functional roles in cancer according to the stage of malignancy, limiting tumor formation early in the process and promoting cancer cell survival and invasion at later stages of progression (328).

The two-faced role of autophagy in cancer presents an interesting therapeutic dilemma: should autophagy be induced, or inhibited during cancer treatment? Evidence exists to support both strategies, since many anticancer therapies induce protective autophagy (which can be inhibited to improve therapeutic efficacy), while other therapies induce destructive autophagy (which enhances or directly mediates cytotoxicity). The role of autophagy in specific cancer therapies is discussed in section 1.3.5.1, and in several recent reviews (112-114, 351, 352). Despite the dual role of autophagy in cancer cell survival and cell death, there is a consensus that autophagy should be considered as a new target for anticancer therapy. Our research provides strong evidence for autophagy as a distinct mechanism of cell death in hypoxic cancer cells, thereby supporting the emerging

158

theory that autophagy could be effectively targeted as an alternative cell death pathway in novel treatment strategies. The challenge going forward will be to determine when to stimulate, and when to inhibit autophagy for therapeutic benefit, based on treatment-specific anticancer mechanisms and individual tumor characteristics such as stage of malignancy, apoptotic and autophagic capacity.

7.4   BNIP3 in hypoxia: pro-survival or pro-death?

The role of BNIP3 in the hypoxia response has proven difficult to define and remains controversial. While some studies have implicated BNIP3 as an inducer of cell death (78, 201, 207, 236), others have failed to detect pro-death BNIP3 activity in hypoxia (218, 227, 239, 353). In addition, BNIP3 has been identified as a mediator of hypoxia-induced autophagy in both pro-survival (98, 218, 257, 353, 354) and pro-death (222, 338) contexts. For example, Bellot et al. have shown that BNIP3 knockdown suppresses hypoxia-induced autophagy and triggers cell death in normal and cancer cells (353), while Farrall et al. have conversely shown that SIM2-mediated BNIP3 repression attenuates hypoxia-induced autophagic cell death in prostate cancer cells (222). In contrast, at least three studies have shown that hypoxia-induced autophagy can occur independent of BNIP3 (256, 344, 355). Finally, whereas BNIP3 exerts its pro-death activity at the mitochondrial membrane, recent studies have defined a protective role for nuclear BNIP3 (section 1.7.2.4).

Our data support BNIP3 as a mediator of hypoxia-induced autophagic cell death; however, it is likely that the role of BNIP3 is cell-type specific, and may also depend on

159

the severity and duration of hypoxia. Indeed, Tracy and Macleod have suggested that BNIP3 may initially allow survival in hypoxia by promoting autophagy to prevent ATP depletion and eliminate damaged mitochondria, yet its function could be subverted to induce cell death under conditions of acidosis that arise following prolonged hypoxia and anaerobic glycolysis (356). Further research is required to determine the molecular mechanisms responsible for BNIP3-mediated autophagy in both pro-survival and pro-death contexts, which could ultimately reveal opportunities for exploiting BNIP3 and autophagy in therapeutic strategies for treating hypoxic tumors.

7.5   BNIP3 as a potential "cancer-specific" target in the autophagy pathway

In order to successfully target autophagic cell death as a cancer treatment strategy, individual target molecules must be identified. Ubiquitous autophagy proteins cannot be easily targeted since autophagy mediates energy homeostasis and protein turnover in normal cells (section 1.3). We have identified BNIP3 as a potential "cancer-specific" autophagy target molecule.

BNIP3 is a pro-death Bcl-2 family member that is not generally expressed in unstressed normal cells; however, it is strongly upregulated under hypoxic conditions including poorly oxygenated regions of solid tumors (section 1.7). Different studies have shown that BNIP3 can induce cell death with features of autophagy (78), apoptosis (242, 248), or necrosis (253). BNIP3 has also been separately implicated in autophagy induced by ceramide, arsenic trioxide and hydrogen peroxide (71, 254, 255) and in hypoxia-induced cell death (207). We have now demonstrated that BNIP3 plays a key role in the hypoxia-

induced autophagic cell death of cancer cells. Furthermore, since the role of BNIP3 in

hypoxia-induced cell death and survival is controversial (340), we used primary BNIP3-

null cells to provide conclusive evidence for the role of BNIP3 in promoting hypoxia-

induced autophagy and cell death.

Recently, it has been shown that BNIP3 may have opposing functions at different stages

of tumor progression: BNIP3 expression was associated with good survival outcome in

invasive breast cancer, but with poor outcome in pre-invasive disease (296). This "dual

role" for BNIP3 may be attributable to its opposing functions in the nucleus versus the

cytoplasm, since previous studies have shown that nuclear BNIP3 is pro-survival,

whereas cytoplasmic BNIP3 – upon localization to mitochondria – is pro-death (196,

230). Studies addressing the localization of BNIP3 at different stages of tumor

development would be required to validate this hypothesis. Another possibility is that

BNIP3 contributes to both cell survival and cell death through its role in autophagy. Our

data confirm that BNIP3 expression is a strong inducer of autophagy and demonstrate

that BNIP3 is important for hypoxia-induced autophagic cell death. Induction of

autophagy through BNIP3 in pre-invasive cancers may provide tumor cells with extra

nutrients and promote further tumor progression. However at later stages, BNIP3

expression could promote prolonged autophagy in hypoxic cancer cells, leading to

autophagic cell death and better patient outcome. In a recent study, RB-/- MEF cells had

increased HIF-1-mediated BNIP3 expression, contributing to increased autophagy and

cell death (218). Moreover, in glioma cells BNIP3 has been identified as having a pivotal

role in both ceramide- and arsenic trioxide-induced autophagic cell death (71, 254).

Thus, together with previous studies, our research suggests that BNIP3 may be an important therapeutic target in the autophagy pathway.

In theory, BNIP3 could be safely targeted without adverse effects since it is preferentially expressed during hypoxic stress, which is characteristic of tumors but not normal tissues. As well, the BNIP3-null mouse is viable, fertile and otherwise phenotypically normal under normoxic conditions. Further research will be required to elucidate the mechanism of BNIP3-mediated autophagy in hypoxic cancer cells, and to establish methods of targeting BNIP3 in this pathway for therapeutic benefit.

7.6   Mediators of BNIP3 resistance as targets for cancer therapy

Hypoxic tumor cells often express BNIP3 yet remain viable and exhibit chemoresistance (section 1.7.5.2). Albeit unintentionally, we have developed a novel model system for studying such "BNIP3 resistance": our TO-BNIP3 cell lines, which remain viable upon significant BNIP3 induction, represent a model system of BNIP3 resistance that may be physiologically relevant to cancer.

Microarray analysis identified 22 differentially-regulated genes that may participate in achieving cell death resistance in TO-BNIP3 cells. Further research is required in order to confirm the "BNIP3 resistance" phenotype, and to validate the differential expression of these genes and to determine their functional significance in BNIP3 resistance; however speculation is possible based on current knowledge of these genes and their gene products. As discussed below, we believe that three candidates particularly warrant

further investigation as potential mediators of BNIP3 resistance: CLU, SSAT and HSPA1A.

CLU encodes for two protein isoforms (a cytoplasmic/secreted glycoprotein and a truncated nuclear form) with opposing functions in cell death, tumor progression and neurodegenerative disorders (333, 357). Cytoplasmic CLU is abnormally upregulated in numerous cancers and is a key contributor to chemoresistance, since it can block apoptosis by binding and inhibiting the pro-death Bcl-2 protein BAX (333). CLU is also reported to act as an extremely sensitive biosensor of ROS, protecting against oxidative injury (357). While our results are preliminary, they are consistent with CLU-mediated protection against BNIP3-induced cell death, possibly through direct protein-protein interaction or inhibition of BNIP3-induced oxidative stress.

SSAT is another interesting candidate gene in BNIP3 resistance. The protein encoded by this gene is a rate-limiting enzyme in the catabolism of polyamines, which are critical mediators of normal and neoplastic growth (334). The SSAT enzyme is highly inducible, participating in adaptive responses to environmental stress by acetylating the polyamines spermidine and spermine, thereby targeting them for export or degradation (334). Spermidine was recently shown to induce autophagy (86); therefore, SSAT-mediated degradation of spermidine could represent a mechanism for reducing BNIP3-induced autophagy to manageable (non-destructive) levels. Interestingly, a hypoxia-inducible isoform of SSAT has been identified, and was shown to promote cell survival and tumor progression (335). The mechanism of SSAT-mediated survival in hypoxia has not yet been determined, but given our preliminary results, it is tempting to predict that hypoxia-

induced SSAT may promote survival through direct or indirect inhibition of BNIP3-mediated hypoxic cell death.

According to our results, HSPA1A may also be involved in BNIP3 resistance. A member of the HSP70 family of "stress response" genes, HSPA1A encodes a 70kDa heat shock protein (HSP). Induced to protect against various forms of cellular stress, HSPs are molecular chaperones which stabilize existing proteins against aggregation and mediate the folding of newly translated proteins (358). Interestingly, HSP70 has been shown to protect against ischemic brain injury in rats by reducing protein aggregation, apoptosis, and necrosis (336). Although it is a known regulator of ischemia-induced neuronal cell death, the role of BNIP3 was not examined in this study. Our preliminary data raise the possibility that HSP70-mediated protection against ischemic brain injury may occur through inhibition of BNIP3-mediated neuronal cell death. Another study recently found that HSP70 expression increases the survival of Drosophila under acute and intermittent hypoxia (337). The mechanism of HSP70-mediated survival in hypoxia was not determined, but our preliminary results are consistent with the hypothesis that induction of HSP70 could promote survival in hypoxia by direct or indirect inhibition of BNIP3-mediated hypoxic cell death.

Thus, using a novel model system we have identified several potential mediators of BNIP3 resistance, including CLU, SSAT and HSP70. While further studies are required to confirm and characterize the role of our candidate proteins in BNIP3 resistance, this research could ultimately establish the foundation for new therapeutic strategies targeting BNIP3 resistance in tumors.

7.7   BNIP3 in brain development and cell cycle progression

Regulated cell death is an important aspect of mammalian brain development, and preliminary evidence suggests that BNIP3 may play a role in this process. For example, a systematic evaluation of Bcl-2 family gene expression showed that BNIP3 is significantly upregulated during oligodendrocyte differentiation in an *in vitro* model (297). In this study, differentiation of primary oligodendroglial progenitor cells was induced by withdrawal of trophic factors and gene expression was measured by real-time PCR at three developmental stages. Levels of BNIP3 and BNIP3L mRNA were increased more than four-fold during differentiation, corresponding with increased apoptosis *in vitro*, which is thought to mimic the physiological apoptotic pruning of superfluous immature oligodendrocytes seen during development *in vivo.*

Similarly, *in vivo* BNIP3 expression has been correlated with naturally occurring cell death in the postnatal rat brain (298). In this study, BNIP3 mRNA expression was localized and quantified by in situ hybridization and real-time PCR at different stages of postnatal development. BNIP3 expression was detected in the neonatal cortex, hippocampus, habenula and thalamus, with the highest levels of expression occurring at postnatal day 6.5. This timing correlates with the previously described period of developmental apoptosis in the neonatal rat brain (359, 360). Thus, two independent studies have identified BNIP3 as a mediator of developmental apoptosis in the mammalian brain, which is further supported by our results. We have demonstrated that knockout of BNIP3 in the mouse brain results in increased cellularity, consistent with a role for BNIP3 in promoting developmental apoptosis.

The mechanism, composition and functional significance of increased cellularity in the BNIP3-null brain remains to be determined. Thus far, no obvious neurological impairments have been reported in BNIP3-/- mice, nor have we observed any such defects. However, we have not performed any specific tests for neurological function. It may be informative to perform a behavioral analysis, such as the SHIRPA protocol (361), which includes tests for neurological functions including balance, coordination, pain perception, acoustic response, anxiety, learning and memory. Notably, studies in the BNIP3-null mouse showed that while BNIP3 has no essential function in the unstressed mouse heart, it is significantly involved in the pathophysiology of myocardial infarction (240). Thus, it is possible that BNIP3 may have no essential function in the unstressed brain, but could be an important mediator of pathologies such as ischemic stroke, neurodegenerative disease or tumorigenesis. Further studies are required to address these hypotheses. Finally, it must also be considered that BNIP3L could partially compensate for BNIP3 in the knockout mouse model, especially since BNIP3L expression was shown to increase in parallel with BNIP3 during oligodendrocyte differentiation (297).

In addition to providing supportive evidence for BNIP3's role in brain development, our work has also identified a related and potentially novel role for BNIP3 in the regulation of cell cycle progression. While previous studies have suggested that BNIP3 is involved in development through its established role in cell death (297, 298), our results indicate that BNIP3 may additionally regulate cell growth and proliferation. We showed that BNIP3-/- astrocytes have a decreased rate of DNA replication and may progress more slowly through the G2/M phase of cell division. Since these changes did not significantly affect the overall rate of astrocyte proliferation *in vitro*, our results collectively suggest

166

that the observed cellularity increase in BNIP3-null brains most likely results from a deficit in cell death during development, which may over-compensate for a possible deficit in cell cycle progression. It is also possible that the rate of astrocyte proliferation is mediated by BNIP3 *in vivo*, but not *in vitro*, due to contributions from the *in situ* microenvironment, or cell-cell interactions, which are absent in two-dimensional cell culture conditions. Nevertheless, we have identified a potentially novel role for BNIP3 in cell cycle progression, warranting further study in additional cell types and physiological contexts.

Thus, our research is consistent with previous claims that BNIP3 is a mediator of mammalian brain development, and further identifies a potentially novel role for BNIP3 in cell cycle regulation. Additional studies are required to fully elucidate the role of BNIP3 in brain development and cell cycle progression, and to determine how BNIP3 may regulate DNA replication or promote cell division. Besides providing new insights into mammalian development, these findings may ultimately have therapeutic implications if BNIP3-mediated proliferative pathways are found to play a role in BNIP3-related pathologies such as ischemic injury or cancer.

7.8   Future Directions

The research presented in this dissertation has inspired several new experimental aims in the broad areas of hypoxia-induced cell death, BNIP3 resistance, BNIP3-mediated autophagy, and BNIP3 in proliferation, brain development, and brain pathologies (Figure 7.1).

7.8.1   Hypoxia-induced cell death

We determined that hypoxia differentially induces apoptosis and autophagic cell death in different cancer cell lines, all of which are competent for etoposide-induced apoptosis. Future studies will aim to determine the mechanism responsible for this differential induction of cell death pathways in hypoxia, with important implications for cancer therapy since knowledge of specific mechanisms of cell death and survival in hypoxic tumor cells is critical to the design of effective new anticancer drugs.

Microarray analysis could be employed to generate gene expression profiles for "autophagic" versus "apoptotic" cell lines, with the goal of identifying genes that are differentially expressed between the two groups. Candidate genes could then be functionally characterized and studied in the context of hypoxia-induced autophagy and cell death. In addition, concurrent studies should focus on the MDA-MB-231 breast cancer cell line (autophagic) and the related metastatic subclone, MDA-MB-231-M (apoptotic). These cell lines have evolved from a common lineage yet they exhibit differential induction of cell death pathways in hypoxia. It will be informative to

determine whether the same molecular adaptations that facilitate metastasis are also responsible for dictating the mechanism of hypoxia-induced cell death.

Another potential line of investigation could focus on the three glioma cell lines characterized in our initial studies, since they exhibit differential induction of cell death pathways in hypoxia as well as differential mutation status for the tumor suppressors PTEN and p53 – both of which are implicated in autophagy regulation (106, 107, 362). U87 (PTEN-mutant, p53-wt) and U373 (PTEN-mutant, p53-mutant) both exhibit autophagic cell death in hypoxia, while U251 (PTEN-mutant, p53-mutant) exhibits apoptotic cell death. It may be particularly interesting to study the role of p53 in hypoxia-induced autophagic cell death, since its mutational status differs between the three glioma cell lines. Others have shown that nuclear p53 transactivates proautophagic genes, while cytoplasmic p53 can repress autophagy through a distinct mechanism at the mitochondria (362). However, in the case of hypoxia-induced autophagic cell death, additional factors are likely to be involved since p53 mutations are found in both U373 (autophagic) and U251 (apoptotic) cells. Nevertheless, such studies could provide valuable insight into the role of p53 as a "master regulator" of autophagy – a phenomenon that is still poorly understood.

In each of these proposed experimental approaches, the ultimate goal will be to identify biomarkers or gene signatures that can distinguish tumors susceptible to apoptosis from those susceptible to autophagic cell death, a distinction that would be extremely helpful in assigning treatment protocols. Furthermore, this research could potentially identify novel anti-cancer drug targets: while apoptosis has repeatedly been targeted in various

treatment strategies, autophagic cell death remains to be fully explored and exploited as a target pathway in cancer.

In addition to characterizing the hypothetical apoptosis/autophagy "switch" in hypoxia, it will be important to characterize the transition from protective to destructive autophagic activity in cells under hypoxic stress. We detected autophagy induction after as little as 1 hour of hypoxia (likely triggered as a survival response), yet sustained hypoxia caused autophagic cell death. If autophagy is to be successfully targeted for cancer therapy, it is critical to understand how this pathway is being utilized by tumor cells. Therefore, hypoxia-induced autophagy should be systematically characterized at regular intervals to determine the specific signalling molecules involved at each stage of progression. The expression and activity of "autophagy proteins" such as Beclin-1, LC3I/II, mTOR, and ATG5 should be carefully monitored with the goal of identifying and characterizing the threshold that marks the transition from protective to destructive autophagy in hypoxia. By understanding this critical transition, therapeutic manipulation may be possible such that protective autophagy can be driven to induce cell death.

Finally, in order to more closely approximate the tumor microenvironment, it will be important to characterize the response of cancer cells to various levels and durations of hypoxia. Thus far, we have mainly studied chronic hypoxia (24 to 72 hours), and we have not been able to strictly control the extent of hypoxia due to equipment limitations. Future studies should examine the full spectrum of physiological hypoxia, including acute, chronic and cycling exposures over a range of oxygen levels (0.02% to 4%).

7.8.2   BNIP3 resistance

We have developed a novel model system for studying resistance to BNIP3-induced cell death, which is physiologically relevant to cancer since tumor cells often express BNIP3 yet remain viable.   Using this model system, we have identified several candidate mediators of BNIP3 resistance (CLU, SSAT and HSPA1A). Future studies will aim to confirm the "BNIP3 resistance" phenotype, identify additional candidates, and then confirm and characterize their role in BNIP3 resistance.

To confirm that our tetracycline-inducible (TO)-BNIP3 clones are indeed resistant to BNIP3-induced cell death, two critical experiments must be performed: measurement of cell death after transient overexpression of BNIP3 and after exposure to hypoxia (where BNIP3 is an established mediator of cell death). If the TO-BNIP3 clones exhibit resistance compared to control (TO-βgal) clones, then the "BNIP3 resistance" phenotype will be validated and can be further investigated, as described below.

First, a more comprehensive microarray analysis should be performed to assess a wider array of genes in multiple clones before determining which candidate genes warrant follow-up study. Our initial analysis (completed in early 2007) was performed on a now-retired, relatively small 1.7k array comprising only 1,728 genes. The University Health Network Microarray Centre now offers a 34.6k array, and even larger arrays are commercially available (for example, the Affymetrix GeneChip Human Genome U133 Plus 2.0 Array analyzes over 47,000 transcripts). To increase reliability, the analysis should include multiple independent RNA preparations from several different clones of

TO-BNIP3 and TO-βgal cells. In addition, it would be interesting to analyze uninduced (-DOX) versus induced (+DOX) samples for each clone tested. This more comprehensive analysis should identify a promising list of candidate genes for further study.

Next, differential gene and protein expression must be validated by RT-PCR and Western blot. Then, mechanistic studies including overexpression and knock-down of candidate genes must be performed in models of BNIP3-induced cell death. Overexpression of candidate genes could be achieved by stable or transient transfection, while knock-down could be achieved by siRNA or shRNA transfection. The effect on BNIP3-induced cell death *in vitro* could then be assessed either directly (BNIP3 overexpression) or indirectly (hypoxic induction of BNIP3). If these experiments provide evidence for candidate-mediated resistance to BNIP3-induced cell death, then further investigation of the molecular mechanisms involved will be warranted. For example, co-immunoprecipitation studies could be performed to determine if BNIP3 directly interacts with any of the candidate proteins. If direct interaction is not detected, further experiments could examine the effect of candidate proteins on specific aspects of BNIP3-induced cell death such as autophagy, ROS production, and mitochondrial dysfunction.

The localization of BNIP3 in TO-BNIP3 cells should also be investigated. Although our preliminary results indicate that induced BNIP3 expression is cytoplasmic (Figure 5.1), it will be important to confirm the presence or absence of nuclear BNIP3 in these cells. Since nuclear BNIP3 is known to regulate gene transcription (230), it could possibly contribute to the "BNIP3 resistance" phenotype through a transcriptional mechanism.

Finally, since we have detected phosphorylation of BNIP3 in our model system, it would be worthwhile to investigate how phosphorylation affects the pro-death and/or pro-survival activity of BNIP3, and to determine whether phosphorylation is affected by the candidate mediators of BNIP3 resistance.

7.8.3 BNIP3-mediated autophagy

As discussed in sections 1.7.4 and 7.4, BNIP3 has been shown to mediate autophagy by several distinct mechanisms in both pro-death and pro-survival contexts. Here, we have identified BNIP3 as a mediator of hypoxia-induced autophagic cell death; however, the mechanism of BNIP3-mediated autophagy in this context is unknown. Future studies will investigate whether BNIP3 mediates hypoxia-induced autophagy by affecting mitochondrial dysfunction, Beclin-1 availability, mTOR activity, or other yet-to-be identified pathways.

To determine whether mitochondrial dysfunction is a critical determinant of BNIP3-mediated autophagy in hypoxia, cells could be treated with tiron or bongkrekic acid during hypoxic exposure. Tiron is a ROS scavenger, while bongkrekic acid is an inhibitor of the mitochondrial PT pore. These reagents can therefore suppress the downstream effects of mitochondrial dysfunction, revealing whether these processes are crucial to hypoxia-induced autophagy.

To determine whether BNIP3 modulates Beclin-1 availability to induce autophagy in hypoxia, co-immunoprecipitation studies could be performed on normoxic versus hypoxic cancer cells. While the overall expression of Beclin-1 may not change, its

availability could be altered since hypoxia-induced BNIP3 may compete with Beclin-1 for Bcl-2 binding. By immunoprecipitating Bcl-2 and immunoblotting for Beclin-1 and BNIP3, it would be possible to determine whether BNIP3 is competing with Beclin-1 for Bcl-2 binding, thus liberating Beclin-1 to facilitate autophagy. This has previously been demonstrated in MEFs (257), but it has never been confirmed in cancer cells.

Finally, to determine whether BNIP3 induces autophagy in hypoxic cancer cells through interaction with the mTOR activator Rheb, co-immunoprecipitation of endogenous Rheb and BNIP3 could be performed. This interaction has been demonstrated in mouse liver and HEK293 cells (263), but remains to be shown in human tumors or cancer cell lines. In addition, mTOR activity could be measured by assessing phosphorylation of its target proteins S6K and/or 4EBP1, for which phospho-specific antibodies are commercially available. By performing this experiment in cancer cells with or without BNIP3 knock-down, the role of BNIP3 in hypoxia-induced mTOR inhibition could be determined.

Eventually, once the mechanism of BNIP3-mediated autophagy in hypoxia has been characterized, additional studies may focus on methods of targeting BNIP3 in this pathway for therapeutic benefit.

7.8.4   BNIP3 in proliferation

We have determined that BNIP3-/- astrocytes exhibit altered cell cycle progression. Future research will aim to confirm and characterize the role of BNIP3 in cell cycle regulation, both *in vitro* and *in vivo*, in different cell types.

Initially, owing to our results thus far, studies will focus on the role of BNIP3 in DNA replication and G2/M-arrest. As a marker of DNA replication, BrdU incorporation should be assessed in additional cell types (besides astrocytes and MEFs). This could include additional primary cell cultures from wild type and BNIP3-/- mice, such as myoblasts, germ cells, cardiomyocytes, osteoblasts or hepatocytes. Similar experiments could be performed in human transformed or cancer cell lines using gene overexpression and knock-down techniques. BrdU incorporation could also be studied *in vivo* by injecting wild type or BNIP3-/- mice or pregnant mothers prior to sacrifice. If BNIP3 is confirmed as a mediator of DNA replication, the mechanism could be initially characterized through co-immunoprecipitation studies to determine if BNIP3 interacts with any of the DNA replication "machinery" such as DNA polymerases, ligases, helicases, or topoisomerases.

If BNIP3 is not directly implicated in DNA replication, it could be investigated in the broader context of cell cycle regulation. Initial studies should focus on confirming our preliminary observation that BNIP3-/- cells exhibit increased G2/M cell-cycle arrest. If this finding can be replicated in additional cell types, then it will be worthwhile to further investigate the expression and activity of cell-cycle regulatory proteins, such as cyclins and cyclin-dependent kinases (CDKs), in wild-type and BNIP3-/- cells. Expression levels could be assessed by Western blot or ELISA, and CDK activity could initially be measured using commercially available kits.

It will also be worth revisiting whether or not BNIP3-null cells proliferate at a similar rate compared to wild type cells. Using the MTT assay we did not detect a difference in

cell growth rate; however, the MTT assay is only a surrogate for cell growth since it actually measures metabolic activity, specifically assaying mitochondrial reductase enzymes. Additional studies should be performed to more directly assess cell growth, such as direct cell counting (using a Coulter counter or hemacytometer) or the colorimetric crystal violet growth assay. Especially in the case of primary astrocytes, it would be ideal to measure cell growth beginning immediately from the day of isolation.

Finally, the role of BNIP3 in proliferation could also be studied using our TO-BNIP3 system, since we have observed dramatically reduced proliferation in induced TO-BNIP3 cells. Additional methods should be employed to confirm this finding (such as MTT or clonogenic assays), followed by further analysis of the molecular mechanisms involved. Guan and colleagues have previously shown that BNIP3 inhibits cell growth *in vivo* by suppressing the mTOR pathway (263), so it will be interesting to determine whether mTOR activity is altered upon BNIP3 induction in our Tet-ON system. Thus, in addition to modeling "BNIP3 resistance", the TO-BNIP3 system may present an opportunity for studying the role of BNIP3 in cell growth and proliferation, which is poorly understood at present.

7.8.5 BNIP3 in brain development

We have shown that BNIP3 knockout may cause increase cellularity in the mouse brain *in vivo*. Future research will aim to confirm this preliminary finding, and to fully characterize the altered cellular composition of the BNIP3-null brain. First, cellularity assessment should be performed on additional brain sections from the adult mice and

E18.5 embryos analyzed in our preliminary study, in order to achieve a total of 3 sections per anatomical region for each animal. Thus far, we have analyzed 3 pairs of adult littermates (one wild type and one BNIP3-/- per pair) from different heterozygous crosses. Additional pairs may be required to achieve statistically significant data. We have also analyzed four E18.5 littermates (two wt and two BNIP3-/-) from a single heterozygous cross. At least two more embryos of each genotype, from a separate heterozygous cross, should be analyzed before drawing final conclusions. Additionally, it would be useful to compare brain weights in wild type versus BNIP3-/- animals as a surrogate measure of brain cellularity.

If confirmed, the increased cellularity of the BNIP3-null brain will be characterized through comprehensive analysis of multiple cell types including astrocytes, neurons, microglia and oligodendrocytes. These can be identified in whole brain sections by immunohistochemistry or immunofluorescence using antibodies for cell-type specific markers such as (but not limited to): GFAP (astrocytes), neurofilament (neurons), lectin/RCA-1 (microglia), and ABCA2 (oligodendrocytes). In addition, the functional significance of increased brain cellularity in BNIP3-/- mice should be determined through behavioral analysis and testing for neurological function. Initially, it may be useful to perform a comprehensive phenotype assessment such as the SHIRPA protocol (361), which includes tests for neurological functions including balance, coordination, pain perception, acoustic response, anxiety, learning and memory. Additional studies could then be designed to focus on any identified abnormalities.

7.8.6 BNIP3 in brain pathologies

Complete characterization of the unstressed BNIP3-null brain will facilitate future studies of hypoxia-related brain pathologies in the BNIP3-/- mouse model. This research may include collaborative studies on cerebral ischemia (stroke), neurodegeneration, and/or tumorigenesis.

We will initiate a collaborative *in vivo* study on the role of BNIP3 in focal brain ischemia and reperfusion. After temporary surgical occlusion of the left middle cerebral artery (a routinely-used stroke model), the pathophysiology, recovery and survival of wild type and BNIP3-/- mice will be examined and compared. The BNIP3-null mouse model could also be used to study the role of BNIP3 in neurodegeneration: since multiple transgenic models of Alzheimer's disease and Parkinson's disease have been developed in recent years (363), there is the potential for cross-breeding to generate BNIP3-null versions of these models. Neurological symptoms, brain morphology and overall survival could then be assessed and compared in BNIP3-wt and BNIP3-null animals. Since BNIP3 has been implicated as a mediator of neuronal cell death and neurodegeneration (217, 235, 269, 270), we anticipate that BNIP3-null animals may experience improved recovery after stroke, or reduced neurological symptoms in models of neurodegenerative disease.

Finally, the BNIP3-null mouse model could be used to study the role of BNIP3 in brain tumorigenesis in two fundamental ways: cross-breeding with established transgenic brain tumor mouse models, or viral delivery of oncogenes to the BNIP3-/- brain.   Both methods have been used extensively for *in vivo* modeling of brain tumors (364). For

example, brain tumors develop in mice with engineered loss of the tumor suppressor genes NF1 and TP53 (365), and in mice injected with a murine retrovirus encoding PDGF (366). Combining these or other models with the BNIP3-null background would provide valuable insight into the role of BNIP3 in brain tumor initiation, formation, progression and metastasis. Specific variables to be measured and compared include: tumor incidence, size, histopathology, hypoxia and autophagic capacity, as well as metastasis and overall animal survival.

These experiments will be critical to establishing the role of BNIP3 in tumor progression, since conflicting evidence currently implicates BNIP3 in both pro-survival and pro-death signaling pathways (section 7.4). Thus, it could reasonably be hypothesized that BNIP3 knockout will confer a survival advantage to tumors (due to the absence of BNIP3-mediated cell death), yet it could equally be surmised that BNIP3-null tumors will fail to thrive (due to a lack of BNIP3-mediated autophagy). One must also consider that the BNIP3-null model eliminates both cytoplasmic and nuclear BNIP3, which are known to serve distinct cellular functions. Tumor modeling studies in the BNIP3-null model will therefore be extremely informative in characterizing the complex role of BNIP3 in cancer.

7.8.7 Summary of Future Directions

In summary, the research presented in this dissertation has not only produced several important findings with implications for cancer therapy, but it has additionally laid the foundation for future research with even more far-reaching implications for several

fundamental signalling pathways, as well as brain development and multiple brain

pathologies (Figure 7.1).
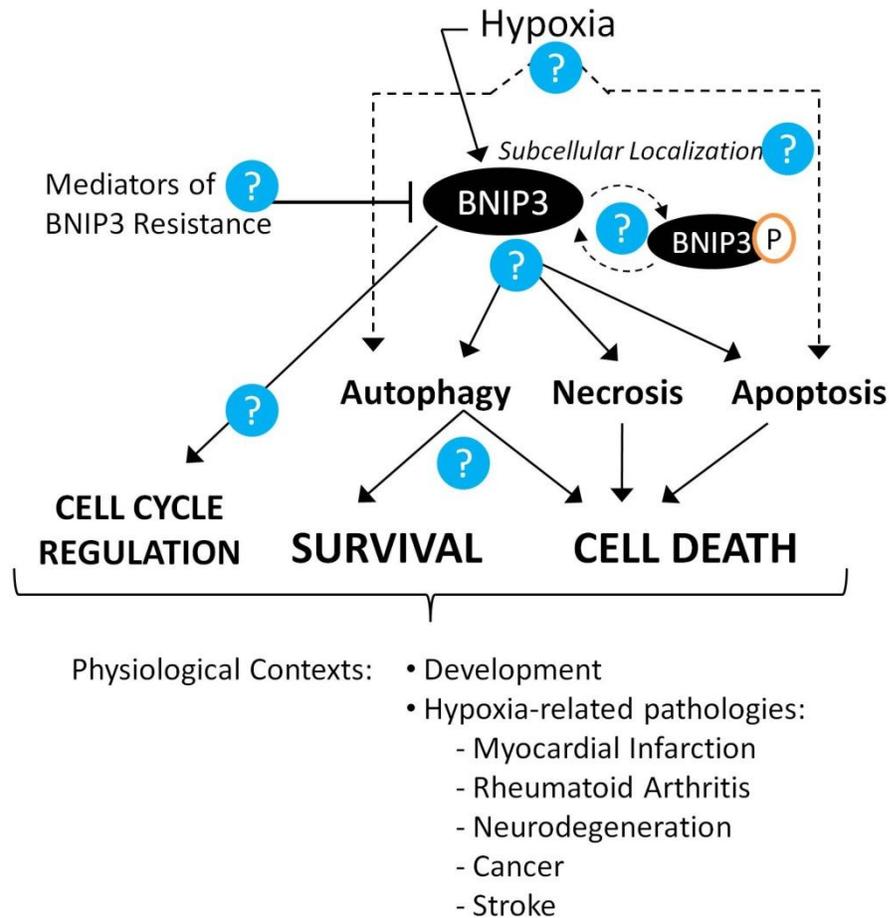
Figure 7.1 Future directions for BNIP3 and autophagy research.
The known functions of BNIP3 (which have been partially established through our work) are depicted here, along with potential themes for future research (blue question marks). Induced in hypoxia, BNIP3 can mediate necrotic or apoptotic cell death, as well as protective or destructive autophagy. Hypoxia can also induce autophagy and apoptosis independent of BNIP3. BNIP3's function is partially regulated by its subcellular localization (nuclear vs. cytoplasmic). BNIP3 can be dynamically phosphorylated, and may function in cell cycle regulation. We have also identified several candidate mediators of BNIP3 resistance. Future studies will focus on: characterizing the differential hypoxic induction of autophagy and apoptosis in different cell lines; identifying and characterizing mediators of BNIP3 resistance; determining the role of BNIP3 phosphorylation; elucidating the role of BNIP3 in cell cycle regulation; determining the mechanism of BNIP3-mediated autophagy in hypoxia; characterizing the mechanism and significance of BNIP3 subcellular localization, and understanding how protective autophagy transitions to autophagic cell death during prolonged hypoxia. These future studies have potential implications in multiple physiological contexts including development and hypoxia-related pathologies such as cancer.

7.9   Final Conclusions

Our investigation of BNIP3 and hypoxia-induced autophagy in cancer cells has contributed significantly to the fields of molecular cell biology and oncology. Specifically, we have demonstrated that hypoxic cancer cells (which are notoriously difficult to target with conventional therapies) can undergo autophagic cell death in the absence of apoptosis. This work provides support to the emerging theory that autophagy represents an alternative cell death pathway that could be effectively targeted in novel anticancer treatment strategies. Furthermore, we have identified BNIP3 as a potential "cancer-specific" target molecule in the autophagy signaling pathway. We have also established a novel model system for studying BNIP3 resistance, which commonly occurs in solid tumors. Finally, we have implicated BNIP3 in mammalian brain development and identified a potentially novel function for BNIP3 in cell cycle progression.

Examined in context with the current literature, our results highlight the dual roles of both BNIP3 and autophagy in cell survival and cell death. We have shown that BNIP3 may play an important role in normal brain development, including cell cycle progression and proliferation. In contrast, BNIP3 appears to mediate cell death in hypoxic cancer cells. Although it remains to be proven, we postulate that BNIP3 mediates these opposing cellular processes through its role in the regulation of autophagy, a pathway with established roles in both cell survival and cell death.

Taken together, this research advances the current understanding of autophagy signaling and its role in hypoxia, cell death and cancer progression – concepts which are highly controversial at present. In addition, our work contributes to the body of knowledge surrounding the complex function of BNIP3, a cell death mediator with additional roles in autophagy, cancer and development. Comprehensive characterization of autophagy and BNIP3 will ultimately identify new targets for cancer therapy, and our research contributes significantly to this important goal.

Chapter 8: References

1.   Hanahan D, Weinberg RA. The hallmarks of cancer. Cell 2000; 100(1):57-70.

2.   Munger K. Disruption of oncogene/tumor suppressor networks during human carcinogenesis. Cancer Invest 2002; 20(1):71-81.

3.   Ruan K, Song G, Ouyang G. Role of hypoxia in the hallmarks of human cancer. J Cell Biochem 2009; 107(6):1053-62.

4.   Giaccia AJ, Simon MC, Johnson R. The biology of hypoxia: The role of oxygen sensing in development, normal function, and disease. Genes Dev 2004; 18(18):2183-94.

5.   Pouyssegur J, Dayan F, Mazure NM. Hypoxia signalling in cancer and approaches to enforce tumour regression. Nature 2006; 441(7092):437-43.

6.   Bristow RG, Hill RP. Hypoxia and metabolism. hypoxia, DNA repair and genetic instability. Nat Rev Cancer 2008; 8(3):180-92.

7.   Degenhardt K, Mathew R, Beaudoin B, et al. Autophagy promotes tumor cell survival and restricts necrosis, inflammation, and tumorigenesis. Cancer Cell 2006; 10(1):51-64.

8.   Brunelle JK, Chandel NS. Oxygen deprivation induced cell death: An update. Apoptosis 2002; 7(6):475-82.

9.   Hamacher-Brady A, Brady NR, Gottlieb RA. Enhancing macroautophagy protects against ischemia/reperfusion injury in cardiac myocytes. J Biol Chem 2006; 281(40):29776-87.

10.   Webb JD, Coleman ML, Pugh CW. Hypoxia, hypoxia-inducible factors (HIF), HIF hydroxylases and oxygen sensing. Cell Mol Life Sci 2009; 66(22):3539-54.

11.   Mazure NM, Brahimi-Horn MC, Berta MA, et al. HIF-1: Master and commander of the hypoxic world. A pharmacological approach to its regulation by siRNAs. Biochem Pharmacol 2004; 68(6):971-80.

12.   Klimova T, Chandel NS. Mitochondrial complex III regulates hypoxic activation of HIF. Cell Death Differ 2008; 15(4):660-6.

13.   Wenger RH. Cellular adaptation to hypoxia: O2-sensing protein hydroxylases, hypoxia-inducible transcription factors, and O2-regulated gene expression. FASEB J 2002; 16(10):1151-62.

14.   Hill RP, Marie-Egyptienne DT, Hedley DW. Cancer stem cells, hypoxia and metastasis. Semin Radiat Oncol 2009; 19(2):106-11.

15.   Subarsky P, Hill RP. Graded hypoxia modulates the invasive potential of HT1080 fibrosarcoma and MDA MB231 carcinoma cells. Clin Exp Metastasis 2008; 25(3):253-64.

16. Mansfield KD, Guzy RD, Pan Y, et al. Mitochondrial dysfunction resulting from loss of cytochrome c impairs cellular oxygen sensing and hypoxic HIF-alpha activation. Cell Metab 2005; 1(6):393-9.

17. Guzy RD, Hoyos B, Robin E, et al. Mitochondrial complex III is required for hypoxia-induced ROS production and cellular oxygen sensing. Cell Metab 2005; 1(6):401-8.

18. Brunelle JK, Bell EL, Quesada NM, et al. Oxygen sensing requires mitochondrial ROS but not oxidative phosphorylation. Cell Metab 2005; 1(6):409-14.

19. Wenger RH. Cellular adaptation to hypoxia: O2-sensing protein hydroxylases, hypoxia-inducible transcription factors, and O2-regulated gene expression. FASEB J 2002; 16(10):1151-62.

20. Chen W, Ostrowski RP, Obenaus A, Zhang JH. Prodeath or prosurvival: Two facets of hypoxia inducible factor-1 in perinatal brain injury. Exp Neurol 2009; 216(1):7-15.

21. Wouters BG, Koritzinsky M. Hypoxia signalling through mTOR and the unfolded protein response in cancer. Nat Rev Cancer 2008; 8(11):851-64.

22. Dunwoodie SL. The role of hypoxia in development of the mammalian embryo. Dev Cell 2009; 17(6):755-73.

23. Krishnan J, Ahuja P, Bodenmann S, et al. Essential role of developmentally activated hypoxia-inducible factor 1alpha for cardiac morphogenesis and function. Circ Res 2008; 103(10):1139-46.

24. Compernolle V, Brusselmans K, Franco D, et al. Cardia bifida, defective heart development and abnormal neural crest migration in embryos lacking hypoxia-inducible factor-1alpha. Cardiovasc Res 2003; 60(3):569-79.

25. Amarilio R, Viukov SV, Sharir A, Eshkar-Oren I, Johnson RS, Zelzer E. HIF1alpha regulation of Sox9 is necessary to maintain differentiation of hypoxic prechondrogenic cells during early skeletogenesis. Development 2007; 134(21):3917-28.

26. Millman JR, Tan JH, Colton CK. The effects of low oxygen on self-renewal and differentiation of embryonic stem cells. Curr Opin Organ Transplant 2009; 14(6):694-700.

27. Burke AP, Virmani R. Pathophysiology of acute myocardial infarction. Med Clin North Am 2007; 91(4):553, 72; ix.

28. Shi H. Hypoxia inducible factor 1 as a therapeutic target in ischemic stroke. Curr Med Chem 2009; 16(34):4593-600.

29. Peers C, Dallas ML, Boycott HE, Scragg JL, Pearson HA, Boyle JP. Hypoxia and neurodegeneration. Ann N Y Acad Sci 2009; 1177:169-77.

30. Ogunshola OO, Antoniou X. Contribution of hypoxia to Alzheimer's disease: Is HIF-1alpha a mediator of neurodegeneration? Cell Mol Life Sci 2009; 66(22):3555-63.

31. Taylor PC, Sivakumar B. Hypoxia and angiogenesis in rheumatoid arthritis. Curr Opin Rheumatol 2005; 17(3):293-8.

32. Brahimi-Horn MC, Chiche J, Pouyssegur J. Hypoxia and cancer. J Mol Med 2007; 85(12):1301-7.

33. Vaupel P. The role of hypoxia-induced factors in tumor progression. Oncologist 2004; 9 Suppl 5:10-7.

34. Semenza GL. Defining the role of hypoxia-inducible factor 1 in cancer biology and therapeutics. Oncogene 2010; 29(5):625-34.

35. Knisely JP, Rockwell S. Importance of hypoxia in the biology and treatment of brain tumors. Neuroimaging Clin N Am 2002; 12(4):525-36.

36. Yu JL, Rak JW, Coomber BL, Hicklin DJ, Kerbel RS. Effect of p53 status on tumor response to antiangiogenic therapy. Science 2002; 295(5559):1526-8.

37. Rofstad EK, Galappathi K, Mathiesen B, Ruud EB. Fluctuating and diffusion-limited hypoxia in hypoxia-induced metastasis. Clin Cancer Res 2007; 13(7):1971-8.

38. Cairns RA, Kalliomaki T, Hill RP. Acute (cyclic) hypoxia enhances spontaneous metastasis of KHT murine tumors. Cancer Res 2001; 61(24):8903-8.

39. Heddleston JM, Li Z, Lathia JD, Bao S, Hjelmeland AB, Rich JN. Hypoxia inducible factors in cancer stem cells. Br J Cancer 2010; 102(5):789-95.

40. Prowse AH, Webster AR, Richards FM, et al. Somatic inactivation of the VHL gene in von hippel-lindau disease tumors. Am J Hum Genet 1997; 60(4):765-71.

41. Moeller BJ, Richardson RA, Dewhirst MW. Hypoxia and radiotherapy: Opportunities for improved outcomes in cancer treatment. Cancer Metastasis Rev 2007; 26(2):241-8.

42. Brown JM, Wilson WR. Exploiting tumour hypoxia in cancer treatment. Nat Rev Cancer 2004; 4(6):437-47.

43. Marcu L, Olver I. Tirapazamine: From bench to clinical trials. Curr Clin Pharmacol 2006; 1(1):71-9.

44. Chen JK, Hu LJ, Wang J, Lamborn KR, Kong EL, Deen DF. Hypoxia-induced BAX overexpression and radiation killing of hypoxic glioblastoma cells. Radiat Res 2005; 163(6):644-53.

45. Potter C, Harris AL. Hypoxia inducible carbonic anhydrase IX, marker of tumour hypoxia, survival pathway and therapy target. Cell Cycle 2004; 3(2):164-7.

46. Bache M, Kappler M, Said HM, Staab A, Vordermark D. Detection and specific targeting of hypoxic regions within solid tumors: Current preclinical and clinical strategies. Curr Med Chem 2008; 15(4):322-38.

47. Holland JP, Lewis JS, Dehdashti F. Assessing tumor hypoxia by positron emission tomography with cu-ATSM. Q J Nucl Med Mol Imaging 2009; 53(2):193-200.

48. Jensen RL. Brain tumor hypoxia: Tumorigenesis, angiogenesis, imaging, pseudoprogression, and as a therapeutic target. J Neurooncol 2009; 92(3):317-35.

49. Levine B. Eating oneself and uninvited guests: Autophagy-related pathways in cellular defense. Cell 2005; 120(2):159-62.

50. Suzuki K, Ohsumi Y. Molecular machinery of autophagosome formation in yeast, saccharomyces cerevisiae. FEBS Lett 2007; 581(11):2156-61.

51. Jin S, White E. Role of autophagy in cancer: Management of metabolic stress. Autophagy 2007; 3(1):28-31.

52. Pattingre S, Espert L, Biard-Piechaczyk M, Codogno P. Regulation of macroautophagy by mTOR and beclin 1 complexes. Biochimie 2008; 90(2):313-23.

53. Arsham AM, Neufeld TP. Thinking globally and acting locally with TOR. Curr Opin Cell Biol 2006; 18(6):589-97.

54. Arico S, Petiot A, Bauvy C, et al. The tumor suppressor PTEN positively regulates macroautophagy by inhibiting the phosphatidylinositol 3-kinase/protein kinase B pathway. J Biol Chem 2001; 276(38):35243-6.

55. Ohsumi Y. Molecular dissection of autophagy: Two ubiquitin-like systems. Nat Rev Mol Cell Biol 2001; 2(3):211-6.

56. Tolkovsky AM. Mitophagy. Biochim Biophys Acta 2009; 1793(9):1508-15.

57. Manjithaya R, Nazarko TY, Farre JC, Subramani S. Molecular mechanism and physiological role of pexophagy. FEBS Lett 2010; 584(7):1367-73.

58. Komatsu M, Ichimura Y. Physiological significance of selective degradation of p62 by autophagy. FEBS Lett 2010; 584(7):1374-8.

59. Moscat J, Diaz-Meco MT. P62 at the crossroads of autophagy, apoptosis, and cancer. Cell 2009; 137(6):1001-4.

60. Pankiv S, Clausen TH, Lamark T, et al. p62/SQSTM1 binds directly to Atg8/LC3 to facilitate degradation of ubiquitinated protein aggregates by autophagy. J Biol Chem 2007; 282(33):24131-45.

61. Komatsu M, Waguri S, Ueno T, et al. Impairment of starvation-induced and constitutive autophagy in Atg7-deficient mice. J Cell Biol 2005; 169(3):425-34.

62. Komatsu M, Waguri S, Chiba T, et al. Loss of autophagy in the central nervous system causes neurodegeneration in mice. Nature 2006; 441(7095):880-4.

63. Tsukada M, Ohsumi Y. Isolation and characterization of autophagy-defective mutants of saccharomyces cerevisiae. FEBS Lett 1993; 333(1-2):169-74.

64. Doelling JH, Walker JM, Friedman EM, Thompson AR, Vierstra RD. The APG8/12-activating enzyme APG7 is required for proper nutrient recycling and senescence in arabidopsis thaliana. J Biol Chem 2002; 277(36):33105-14.

65. Boya P, Gonzalez-Polo RA, Casares N, et al. Inhibition of macroautophagy triggers apoptosis. Mol Cell Biol 2005; 25(3):1025-40.

66.	Lum JJ, Bauer DE, Kong M, et al. Growth factor regulation of autophagy and cell survival in the absence of apoptosis. Cell 2005; 120(2):237-48.

67.	Kuma A, Hatano M, Matsui M, et al. The role of autophagy during the early neonatal starvation period. Nature 2004; 432(7020):1032-6.

68.	Cui Q, Tashiro S, Onodera S, Minami M, Ikejima T. Autophagy preceded apoptosis in oridonin-treated human breast cancer MCF-7 cells. Biol Pharm Bull 2007; 30(5):859-64.

69.	Gonzalez-Polo RA, Boya P, Pauleau AL, et al. The apoptosis/autophagy paradox: Autophagic vacuolization before apoptotic death. J Cell Sci 2005; 118(Pt 14):3091-102.

70.	Maiuri MC, Zalckvar E, Kimchi A, Kroemer G. Self-eating and self-killing: Crosstalk between autophagy and apoptosis. Nat Rev Mol Cell Biol 2007; 8(9):741-52.

71.	Kanzawa T, Zhang L, Xiao L, Germano IM, Kondo Y, Kondo S. Arsenic trioxide induces autophagic cell death in malignant glioma cells by upregulation of mitochondrial cell death protein BNIP3. Oncogene 2005; 24(6):980-91.

72.	Reef S, Zalckvar E, Shifman O, et al. A short mitochondrial form of p19ARF induces autophagy and caspase-independent cell death. Mol Cell 2006; 22(4):463-75.

73.	Ramser B, Kokot A, Metze D, Weiss N, Luger TA, Bohm M. Hydroxychloroquine modulates metabolic activity and proliferation and induces autophagic cell death of human dermal fibroblasts. J Invest Dermatol 2009; 129(10):2419-26.

74.	Hwang J, Lee S, Lee JT, et al. Gangliosides induce autophagic cell death in astrocytes. Br J Pharmacol 2010; 159(3):586-603.

75.	Choi IK, Cho YS, Jung HJ, Kwon HJ. Autophagonizer, a novel synthetic small molecule, induces autophagic cell death. Biochem Biophys Res Commun 2010; 393(4):849-54.

76.	Bras M, Queenan B, Susin SA. Programmed cell death via mitochondria: Different modes of dying. Biochemistry (Mosc) 2005; 70(2):231-9.

77.	Pattingre S, Tassa A, Qu X, et al. Bcl-2 antiapoptotic proteins inhibit beclin 1-dependent autophagy. Cell 2005; 122(6):927-39.

78.	Vande Velde C, Cizeau J, Dubik D, et al. BNIP3 and genetic control of necrosis-like cell death through the mitochondrial permeability transition pore. Mol Cell Biol 2000; 20(15):5454-68.

79.	Eskelinen EL, Saftig P. Autophagy: A lysosomal degradation pathway with a central role in health and disease. Biochim Biophys Acta 2009; 1793(4):664-73.

80.	Rajawat YS, Hilioti Z, Bossis I. Aging: Central role for autophagy and the lysosomal degradative system. Ageing Res Rev 2009; 8(3):199-213.

81. Vellai T, Takacs-Vellai K, Sass M, Klionsky DJ. The regulation of aging: Does autophagy underlie longevity? Trends Cell Biol 2009; 19(10):487-94.

82. Donati A, Cavallini G, Paradiso C, et al. Age-related changes in the autophagic proteolysis of rat isolated liver cells: Effects of antiaging dietary restrictions. J Gerontol A Biol Sci Med Sci 2001; 56(9):B375-83.

83. Jia K, Levine B. Autophagy is required for dietary restriction-mediated life span extension in C. elegans. Autophagy 2007; 3(6):597-9.

84. Hansen M, Chandra A, Mitic LL, Onken B, Driscoll M, Kenyon C. A role for autophagy in the extension of lifespan by dietary restriction in C. elegans. PLoS Genet 2008; 4(2):e24.

85. Melendez A, Talloczy Z, Seaman M, Eskelinen EL, Hall DH, Levine B. Autophagy genes are essential for dauer development and life-span extension in C. elegans. Science 2003; 301(5638):1387-91.

86. Eisenberg T, Knauer H, Schauer A, et al. Induction of autophagy by spermidine promotes longevity. Nat Cell Biol 2009; 11(11):1305-14.

87. Deretic V, Levine B. Autophagy, immunity, and microbial adaptations. Cell Host Microbe 2009; 5(6):527-49.

88. Iwasaki A. Role of autophagy in innate viral recognition. Autophagy 2007; 3(4):354-6.

89. Nakagawa I, Amano A, Mizushima N, et al. Autophagy defends cells against invading group A streptococcus. Science 2004; 306(5698):1037-40.

90. Gutierrez MG, Master SS, Singh SB, Taylor GA, Colombo MI, Deretic V. Autophagy is a defense mechanism inhibiting BCG and mycobacterium tuberculosis survival in infected macrophages. Cell 2004; 119(6):753-66.

91. Schmid D, Pypaert M, Munz C. Antigen-loading compartments for major histocompatibility complex class II molecules continuously receive input from autophagosomes. Immunity 2007; 26(1):79-92.

92. Winslow AR, Rubinsztein DC. Autophagy in neurodegeneration and development. Biochim Biophys Acta 2008; 1782(12):723-9.

93. Ravikumar B, Vacher C, Berger Z, et al. Inhibition of mTOR induces autophagy and reduces toxicity of polyglutamine expansions in fly and mouse models of huntington disease. Nat Genet 2004; 36(6):585-95.

94. Spencer B, Potkar R, Trejo M, et al. Beclin 1 gene transfer activates autophagy and ameliorates the neurodegenerative pathology in alpha-synuclein models of parkinson's and lewy body diseases. J Neurosci 2009; 29(43):13578-88.

95. Martinet W, Agostinis P, Vanhoecke B, Dewaele M, De Meyer GR. Autophagy in disease: A double-edged sword with therapeutic potential. Clin Sci (Lond) 2009; 116(9):697-712.

96.   Nakai A, Yamaguchi O, Takeda T, et al. The role of autophagy in cardiomyocytes in the basal state and in response to hemodynamic stress. Nat Med 2007; 13(5):619-24.

97.   Tannous P, Zhu H, Nemchenko A, et al. Intracellular protein aggregation is a proximal trigger of cardiomyocyte autophagy. Circulation 2008; 117(24):3070-8.

98.   Hamacher-Brady A, Brady NR, Logue SE, et al. Response to myocardial ischemia/reperfusion injury involves Bnip3 and autophagy. Cell Death Differ 2007; 14(1):146-57.

99.   Takemura G, Miyata S, Kawase Y, Okada H, Maruyama R, Fujiwara H. Autophagic degeneration and death of cardiomyocytes in heart failure. Autophagy 2006; 2(3):212-4.

100.   Klionsky DJ. Autophagy: From phenomenology to molecular understanding in less than a decade. Nat Rev Mol Cell Biol 2007; 8(11):931-7.

101.   Hippert MM, O'toole PS, Thorburn A. Autophagy in cancer: Good, bad, or both? Cancer Res 2006; 66(19):9349-51.

102.   Espina V, Mariani BD, Gallagher RI, et al. Malignant precursor cells pre-exist in human breast DCIS and require autophagy for survival. PLoS One 2010; 5(4):e10240.

103.   Qu X, Yu J, Bhagat G, et al. Promotion of tumorigenesis by heterozygous disruption of the beclin 1 autophagy gene. J Clin Invest 2003; 112(12):1809-20.

104.   Yue Z, Jin S, Yang C, Levine AJ, Heintz N. Beclin 1, an autophagy gene essential for early embryonic development, is a haploinsufficient tumor suppressor. Proc Natl Acad Sci U S A 2003; 100(25):15077-82.

105.   Liang XH, Jackson S, Seaman M, et al. Induction of autophagy and inhibition of tumorigenesis by beclin 1. Nature 1999; 402(6762):672-6.

106.   Feng Z, Zhang H, Levine AJ, Jin S. The coordinate regulation of the p53 and mTOR pathways in cells. Proc Natl Acad Sci U S A 2005; 102(23):8204-9.

107.   Arico S, Petiot A, Bauvy C, et al. The tumor suppressor PTEN positively regulates macroautophagy by inhibiting the phosphatidylinositol 3-kinase/protein kinase B pathway. J Biol Chem 2001; 276(38):35243-6.

108.   Maiuri MC, Le Toumelin G, Criollo A, et al. Functional and physical interaction between bcl-X(L) and a BH3-like domain in beclin-1. EMBO J 2007.

109.   Lefranc F, Facchini V, Kiss R. Proautophagic drugs: A novel means to combat apoptosis-resistant cancers, with a special emphasis on glioblastomas. Oncologist 2007; 12(12):1395-403.

110.   Mathew R, Karp CM, Beaudoin B, et al. Autophagy suppresses tumorigenesis through elimination of p62. Cell 2009; 137(6):1062-75.

111.   Dalby KN, Tekedereli I, Lopez-Berestein G, Ozpolat B. Targeting the prodeath and prosurvival functions of autophagy as novel therapeutic strategies in cancer. Autophagy 2010; 6(3).

112. White E, DiPaola RS. The double-edged sword of autophagy modulation in cancer. Clin Cancer Res 2009; 15(17):5308-16.

113. Coates JM, Galante JM, Bold RJ. Cancer therapy beyond apoptosis: Autophagy and anoikis as mechanisms of cell death. J Surg Res 2009.

114. Kondo Y, Kondo S. Autophagy and cancer therapy. Autophagy 2006; 2(2):85-90.

115. Amaravadi RK, Yu D, Lum JJ, et al. Autophagy inhibition enhances therapy-induced apoptosis in a myc-induced model of lymphoma. J Clin Invest 2007; 117(2):326-36.

116. Abedin MJ, Wang D, McDonnell MA, Lehmann U, Kelekar A. Autophagy delays apoptotic death in breast cancer cells following DNA damage. Cell Death Differ 2007; 14(3):500-10.

117. Yang C, Kaushal V, Shah SV, Kaushal GP. Autophagy is associated with apoptosis in cisplatin injury to renal tubular epithelial cells. Am J Physiol Renal Physiol 2008.

118. Claerhout S, Verschooten L, Van Kelst S, et al. Concomitant inhibition of AKT and autophagy is required for efficient cisplatin-induced apoptosis of metastatic skin carcinoma. Int J Cancer 2010.

119. Sivaprasad U, Basu A. Inhibition of ERK attenuates autophagy and potentiates tumor necrosis factor-alpha-induced cell death in MCF-7 cells. J Cell Mol Med 2008.

120. Sun SY. Enhancing perifosine's anticancer efficacy by preventing autophagy. Autophagy 2010; 6(1):184-5.

121. Carew JS, Nawrocki ST, Kahue CN, et al. Targeting autophagy augments the anticancer activity of the histone deacetylase inhibitor SAHA to overcome bcr-abl-mediated drug resistance. Blood 2007.

122. Wu WK, Cho CH, Lee CW, et al. Macroautophagy and ERK phosphorylation counteract the antiproliferative effect of proteasome inhibitor in gastric cancer cells. Autophagy 2010; 6(2):228-38.

123. Pan J, Cheng C, Verstovsek S, Chen Q, Jin Y, Cao Q. The BH3-mimetic GX15-070 induces autophagy, potentiates the cytotoxicity of carboplatin and 5-fluorouracil in esophageal carcinoma cells. Cancer Lett 2010.

124. Krmpot AJ, Janjetovic KD, Misirkic MS, et al. Protective effect of autophagy in laser-induced glioma cell death in vitro. Lasers Surg Med 2010; 42(4):338-47.

125. Robert G, Ben Sahra I, Puissant A, et al. Acadesine kills chronic myelogenous leukemia (CML) cells through PKC-dependent induction of autophagic cell death. PLoS One 2009; 4(11):e7889.

126. Puissant A, Robert G, Fenouille N, et al. Resveratrol promotes autophagic cell death in chronic myelogenous leukemia cells via JNK-mediated p62/SQSTM1 expression and AMPK activation. Cancer Res 2010; 70(3):1042-52.

127. Fu J, Shao CJ, Chen FR, Ng HK, Chen ZP. Autophagy induced by valproic acid is associated with oxidative stress in glioma cell lines. Neuro Oncol 2010; 12(4):328-40.

128. Kanzawa T, Germano IM, Komata T, Ito H, Kondo Y, Kondo S. Role of autophagy in temozolomide-induced cytotoxicity for malignant glioma cells. Cell Death Differ 2004; 11(4):448-57.

129. Chau YP, Lin SY, Chen JH, Tai MH. Endostatin induces autophagic cell death in EAhy926 human endothelial cells. Histol Histopathol 2003; 18(3):715-26.

130. Du J, Martin SM, Levine M, et al. Mechanisms of ascorbate-induced cytotoxicity in pancreatic cancer. Clin Cancer Res 2010; 16(2):509-20.

131. Duan W, Jin X, Li Q, Tashiro SI, Onodera S, Ikejima T. Silibinin induced autophagic and apoptotic cell death in HT1080 cells through a reactive oxygen species pathway. J Pharmacol Sci 2010.

132. Huang SW, Liu KT, Chang CC, et al. Imiquimod simultaneously induces autophagy and apoptosis in human basal cell carcinoma cells. Br J Dermatol 2010.

133. Xue LY, Chiu SM, Oleinick NL. Atg7 deficiency increases resistance of MCF-7 human breast cancer cells to photodynamic therapy. Autophagy 2010; 6(2):248-55.

134. Ji HT, Chien LT, Lin YH, Chien HF, Chen CT. 5-ALA mediated photodynamic therapy induces autophagic cell death via AMP-activated protein kinase. Mol Cancer 2010; 9(1):91.

135. Zois CE, Koukourakis MI. Radiation-induced autophagy in normal and cancer cells: Towards novel cytoprotection and radio-sensitization policies? Autophagy 2009; 5(4):442-50.

136. Kim KW, Moretti L, Mitchell LR, Jung DK, Lu B. Endoplasmic reticulum stress mediates radiation-induced autophagy by perk-eIF2alpha in caspase-3/7-deficient cells. Oncogene 2010.

137. Hotchkiss RS, Strasser A, McDunn JE, Swanson PE. Cell death. N Engl J Med 2009; 361(16):1570-83.

138. Galluzzi L, Maiuri MC, Vitale I, et al. Cell death modalities: Classification and pathophysiological implications. Cell Death Differ 2007; 14(7):1237-43.

139. Edinger AL, Thompson CB. Death by design: Apoptosis, necrosis and autophagy. Curr Opin Cell Biol 2004; 16(6):663-9.

140. Fulda S, Debatin KM. Extrinsic versus intrinsic apoptosis pathways in anticancer chemotherapy. Oncogene 2006; 25(34):4798-811.

141. Chipuk JE, Moldoveanu T, Llambi F, Parsons MJ, Green DR. The BCL-2 family reunion. Mol Cell 2010; 37(3):299-310.

142. MacFarlane M, Williams AC. Apoptosis and disease: A life or death decision. EMBO Rep 2004; 5(7):674-8.

143. Ghobrial IM, Witzig TE, Adjei AA. Targeting apoptosis pathways in cancer therapy. CA Cancer J Clin 2005; 55(3):178-94.

144. Yip KW, Reed JC. Bcl-2 family proteins and cancer. Oncogene 2008; 27(50):6398-406.

145. Festjens N, Vanden Berghe T, Vandenabeele P. Necrosis, a well-orchestrated form of cell demise: Signalling cascades, important mediators and concomitant immune response. Biochim Biophys Acta 2006; 1757(9-10):1371-87.

146. Sasi N, Hwang M, Jaboin J, Csiki I, Lu B. Regulated cell death pathways: New twists in modulation of BCL2 family function. Mol Cancer Ther 2009; 8(6):1421-9.

147. Jin S. Autophagy, mitochondrial quality control, and oncogenesis. Autophagy 2006; 2(2):80-4.

148. Orton RJ, Sturm OE, Vyshemirsky V, Calder M, Gilbert DR, Kolch W. Computational modelling of the receptor-tyrosine-kinase-activated MAPK pathway. Biochem J 2005; 392(Pt 2):249-61.

149. Kolch W. Ras/Raf signalling and emerging pharmacotherapeutic targets. Expert Opin Pharmacother 2002; 3(6):709-18.

150. Song G, Ouyang G, Bao S. The activation of Akt/PKB signaling pathway and cell survival. J Cell Mol Med 2005; 9(1):59-71.

151. Bradley EW, Ruan MM, Vrable A, Oursler MJ. Pathway crosstalk between Ras/Raf and PI3K in promotion of M-CSF-induced MEK/ERK-mediated osteoclast survival. J Cell Biochem 2008; 104(4):1439-51.

152. Loufrani L, Retailleau K, Bocquet A, et al. Key role of alpha(1)beta(1)-integrin in the activation of PI3-kinase-akt by flow (shear stress) in resistance arteries. Am J Physiol Heart Circ Physiol 2008; 294(4):H1906-13.

153. Wei H, Vander Heide RS. Ischemic preconditioning and heat shock activate akt via a focal adhesion kinase-mediated pathway in langendorff-perfused adult rat hearts. Am J Physiol Heart Circ Physiol 2010; 298(1):H152-7.

154. Tseng WP, Yang SN, Lai CH, Tang CH. Hypoxia induces BMP-2 expression via ILK, akt, mTOR, and HIF-1 pathways in osteoblasts. J Cell Physiol 2010; 223(3):810-8.

155. Burgering BM, Medema RH. Decisions on life and death: FOXO forkhead transcription factors are in command when PKB/Akt is off duty. J Leukoc Biol 2003; 73(6):689-701.

156. Fujita E, Jinbo A, Matuzaki H, Konishi H, Kikkawa U, Momoi T. Akt phosphorylation site found in human caspase-9 is absent in mouse caspase-9. Biochem Biophys Res Commun 1999; 264(2):550-5.

157. Wullschleger S, Loewith R, Hall MN. TOR signaling in growth and metabolism. Cell 2006; 124(3):471-84.

158. Jung CH, Ro SH, Cao J, Otto NM, Kim DH. mTOR regulation of autophagy. FEBS Lett 2010; 584(7):1287-95.

159. Memmott RM, Dennis PA. Akt-dependent and -independent mechanisms of mTOR regulation in cancer. Cell Signal 2009; 21(5):656-64.

160. Kornblau SM, Womble M, Qiu YH, et al. Simultaneous activation of multiple signal transduction pathways confers poor prognosis in acute myelogenous leukemia. Blood 2006; 108(7):2358-65.

161. Tidyman WE, Rauen KA. The RASopathies: Developmental syndromes of Ras/MAPK pathway dysregulation. Curr Opin Genet Dev 2009; 19(3):230-6.

162. Carnero A. The PKB/AKT pathway in cancer. Curr Pharm Des 2010; 16(1):34-44.

163. Hasskarl J. Sorafenib. Recent Results Cancer Res 2010; 184:61-70.

164. Cheng JQ, Lindsley CW, Cheng GZ, Yang H, Nicosia SV. The Akt/PKB pathway: Molecular target for cancer drug discovery. Oncogene 2005; 24(50):7482-92.

165. Shin I, Edl J, Biswas S, Lin PC, Mernaugh R, Arteaga CL. Proapoptotic activity of cell-permeable anti-akt single-chain antibodies. Cancer Res 2005; 65(7):2815-24.

166. Wong WW, Puthalakath H. Bcl-2 family proteins: The sentinels of the mitochondrial apoptosis pathway. IUBMB Life 2008; 60(6):390-7.

167. Pattingre S, Levine B. Bcl-2 inhibition of autophagy: A new route to cancer? Cancer Res 2006; 66(6):2885-8.

168. Shimizu S, Kanaseki T, Mizushima N, et al. Role of bcl-2 family proteins in a non-apoptotic programmed cell death dependent on autophagy genes. Nat Cell Biol 2004; 6(12):1221-8.

169. Taylor RC, Cullen SP, Martin SJ. Apoptosis: Controlled demolition at the cellular level. Nat Rev Mol Cell Biol 2008; 9(3):231-41.

170. Zhang HM, Cheung P, Yanagawa B, McManus BM, Yang DC. BNips: A group of pro-apoptotic proteins in the bcl-2 family. Apoptosis 2003; 8(3):229-36.

171. Boyd JM, Malstrom S, Subramanian T, et al. Adenovirus E1B 19 kDa and bcl-2 proteins interact with a common set of cellular proteins. Cell 1994; 79(2):341-51.

172. Subramanian T, Boyd JM, Chinnadurai G. Functional substitution identifies a cell survival promoting domain common to adenovirus E1B 19 kDa and bcl-2 proteins. Oncogene 1995; 11(11):2403-9.

173. Matsushima M, Fujiwara T, Takahashi E, et al. Isolation, mapping, and functional analysis of a novel human cDNA (BNIP3L) encoding a protein homologous to human NIP3. Genes Chromosomes Cancer 1998; 21(3):230-5.

174. Yasuda M, Chinnadurai G. Functional identification of the apoptosis effector BH3 domain in cellular protein BNIP1. Oncogene 2000; 19(19):2363-7.

175. Low BC, Lim YP, Lim J, Wong ES, Guy GR. Tyrosine phosphorylation of the bcl-2-associated protein BNIP-2 by fibroblast growth factor receptor-1 prevents its binding to Cdc42GAP and Cdc42. J Biol Chem 1999; 274(46):33123-30.

176. Chipuk JE, Moldoveanu T, Llambi F, Parsons MJ, Green DR. The BCL-2 family reunion. Mol Cell 2010; 37(3):299-310.

177. Bhattacharya S, Ray RM, Johnson LR. STAT3-mediated transcription of bcl-2, mcl-1 and c-IAP2 prevents apoptosis in polyamine-depleted cells. Biochem J 2005; 392(Pt 2):335-44.

178. Wang JM, Chao JR, Chen W, Kuo ML, Yen JJ, Yang-Yen HF. The antiapoptotic gene mcl-1 is up-regulated by the phosphatidylinositol 3-kinase/Akt signaling pathway through a transcription factor complex containing CREB. Mol Cell Biol 1999; 19(9):6195-206.

179. Flinterman M, Guelen L, Ezzati-Nik S, et al. E1A activates transcription of p73 and noxa to induce apoptosis. J Biol Chem 2005; 280(7):5945-59.

180. Wildey GM, Howe PH. Runx1 is a co-activator with FOXO3 to mediate transforming growth factor beta (TGFbeta)-induced bim transcription in hepatic cells. J Biol Chem 2009; 284(30):20227-39.

181. Bonovolias ID, Tsiftsoglou AS. Hemin counteracts the repression of bcl-2 and NrF2 genes and the cell killing induced by imatinib in human bcr-abl(+) CML cells. Oncol Res 2009; 17(11-12):535-47.

182. Wajapeyee N, Britto R, Ravishankar HM, Somasundaram K. Apoptosis induction by activator protein 2alpha involves transcriptional repression of bcl-2. J Biol Chem 2006; 281(24):16207-19.

183. Nakazawa Y, Suzuki M, Manabe N, et al. Cooperative interaction between ETS1 and GFI1 transcription factors in the repression of bax gene expression. Oncogene 2007; 26(24):3541-50.

184. Ruvolo PP, Deng X, May WS. Phosphorylation of Bcl2 and regulation of apoptosis. Leukemia 2001; 15(4):515-22.

185. Zhao J, Xin M, Wang T, Zhang Y, Deng X. Nicotine enhances the antiapoptotic function of mcl-1 through phosphorylation. Mol Cancer Res 2009; 7(12):1954-61.

186. Maurer U, Charvet C, Wagman AS, Dejardin E, Green DR. Glycogen synthase kinase-3 regulates mitochondrial outer membrane permeabilization and apoptosis by destabilization of MCL-1. Mol Cell 2006; 21(6):749-60.

187. Schwickart M, Huang X, Lill JR, et al. Deubiquitinase USP9X stabilizes MCL1 and promotes tumour cell survival. Nature 2010; 463(7277):103-7.

188. Le Gouill S, Podar K, Harousseau JL, Anderson KC. Mcl-1 regulation and its role in multiple myeloma. Cell Cycle 2004; 3(10):1259-62.

189. Tsujimoto Y, Cossman J, Jaffe E, Croce CM. Involvement of the bcl-2 gene in human follicular lymphoma. Science 1985; 228(4706):1440-3.

190. Gascoyne RD, Adomat SA, Krajewski S, et al. Prognostic significance of bcl-2 protein expression and bcl-2 gene rearrangement in diffuse aggressive non-hodgkin's lymphoma. Blood 1997; 90(1):244-51.

191. Shigemasa K, Katoh O, Shiroyama Y, et al. Increased MCL-1 expression is associated with poor prognosis in ovarian carcinomas. Jpn J Cancer Res 2002; 93(5):542-50.

192. Kang SY, Han JH, Lee KJ, et al. Low expression of bax predicts poor prognosis in patients with locally advanced esophageal cancer treated with definitive chemoradiotherapy. Clin Cancer Res 2007; 13(14):4146-53.

193. Mason KD, Khaw SL, Rayeroux KC, et al. The BH3 mimetic compound, ABT-737, synergizes with a range of cytotoxic chemotherapy agents in chronic lymphocytic leukemia. Leukemia 2009; 23(11):2034-41.

194. Mason KD, Vandenberg CJ, Scott CL, et al. In vivo efficacy of the bcl-2 antagonist ABT-737 against aggressive myc-driven lymphomas. Proc Natl Acad Sci U S A 2008; 105(46):17961-6.

195. Oh KJ, Barbuto S, Pitter K, Morash J, Walensky LD, Korsmeyer SJ. A membrane-targeted BID BCL-2 homology 3 peptide is sufficient for high potency activation of BAX in vitro. J Biol Chem 2006; 281(48):36999-7008.

196. Burton TR, Gibson SB. The role of bcl-2 family member BNIP3 in cell death and disease: NIPping at the heels of cell death. Cell Death Differ 2009; 16(4):515-23.

197. Yasuda M, Theodorakis P, Subramanian T, Chinnadurai G. Adenovirus E1B-19K/BCL-2 interacting protein BNIP3 contains a BH3 domain and a mitochondrial targeting sequence. J Biol Chem 1998; 273(20):12415-21.

198. Cizeau J, Ray R, Chen G, Gietz RD, Greenberg AH. The C. elegans orthologue ceBNIP3 interacts with CED-9 and CED-3 but kills through a BH3- and caspase-independent mechanism. Oncogene 2000; 19(48):5453-63.

199. Lomonosova E, Chinnadurai G. BH3-only proteins in apoptosis and beyond: An overview. Oncogene 2008; 27 Suppl 1:S2-19.

200. Ray R, Chen G, Vande Velde C, et al. BNIP3 heterodimerizes with bcl-2/Bcl-X(L) and induces cell death independent of a bcl-2 homology 3 (BH3) domain at both mitochondrial and nonmitochondrial sites. J Biol Chem 2000; 275(2):1439-48.

201. Chen G, Ray R, Dubik D, et al. The E1B 19K/Bcl-2-binding protein Nip3 is a dimeric mitochondrial protein that activates apoptosis. J Exp Med 1997; 186(12):1975-83.

202. Bocharov EV, Pustovalova YE, Pavlov KV, et al. Unique dimeric structure of BNip3 transmembrane domain suggests membrane permeabilization as a cell death trigger. J Biol Chem 2007; 282(22):16256-66.

203. Kubli DA, Quinsay MN, Huang C, Lee Y, Gustafsson AB. Bnip3 functions as a mitochondrial sensor of oxidative stress during myocardial ischemia and reperfusion. Am J Physiol Heart Circ Physiol 2008; 295(5):H2025-31.

204. Frazier DP, Wilson A, Graham RM, Thompson JW, Bishopric NH, Webster KA. Acidosis regulates the stability, hydrophobicity, and activity of the BH3-only protein Bnip3. Antioxid Redox Signal 2006; 8(9-10):1625-34.

205. Hetschko H, Voss V, Senft C, Seifert V, Prehn JH, Kogel D. BH3 mimetics reactivate autophagic cell death in anoxia-resistant malignant glioma cells. Neoplasia 2008; 10(8):873-85.

206. Bruick RK. Expression of the gene encoding the proapoptotic Nip3 protein is induced by hypoxia. Proc Natl Acad Sci U S A 2000; 97(16):9082-7.

207. Kothari S, Cizeau J, McMillan-Ward E, et al. BNIP3 plays a role in hypoxic cell death in human epithelial cells that is inhibited by growth factors EGF and IGF. Oncogene 2003; 22(30):4734-44.

208. Zhang L, Li L, Liu H, et al. HIF-1alpha activation by a redox-sensitive pathway mediates cyanide-induced BNIP3 upregulation and mitochondrial-dependent cell death. Free Radic Biol Med 2007; 43(1):117-27.

209. Yang YS, Yang MC, Guo Y, Williams OW, Weissler JC. PLAGL2 expression-induced lung epithelium damages at bronchiolar alveolar duct junction in emphysema: BNip3- and SP-C-associated cell death/injury activity. Am J Physiol Lung Cell Mol Physiol 2009; 297(3):L455-66.

210. Yurkova N, Shaw J, Blackie K, et al. The cell cycle factor E2F-1 activates Bnip3 and the intrinsic death pathway in ventricular myocytes. Circ Res 2008; 102(4):472-9.

211. Sandau US, Handa RJ. Glucocorticoids exacerbate hypoxia-induced expression of the pro-apoptotic gene Bnip3 in the developing cortex. Neuroscience 2007; 144(2):482-94.

212. Mammucari C, Milan G, Romanello V, et al. FoxO3 controls autophagy in skeletal muscle in vivo. Cell Metab 2007; 6(6):458-71.

213. Prabhakaran K, Chapman GD, Gunasekar PG. BNIP3 up-regulation and mitochondrial dysfunction in manganese-induced neurotoxicity. Neurotoxicology 2009; 30(3):414-22.

214. An HJ, Maeng O, Kang KH, et al. Activation of ras up-regulates pro-apoptotic BNIP3 in nitric oxide-induced cell death. J Biol Chem 2006; 281(45):33939-48.

215. Ghavami S, Eshraghi M, Kadkhoda K, et al. Role of BNIP3 in TNF-induced cell death--TNF upregulates BNIP3 expression. Biochim Biophys Acta 2009; 1793(3):546-60.

216. Daido S, Kanzawa T, Yamamoto A, Takeuchi H, Kondo Y, Kondo S. Pivotal role of the cell death factor BNIP3 in ceramide-induced autophagic cell death in malignant glioma cells. Cancer Res 2004; 64(12):4286-93.

217. Zhang S, Zhang Z, Sandhu G, et al. Evidence of oxidative stress-induced BNIP3 expression in amyloid beta neurotoxicity. Brain Res 2007; 1138:221-30.

218. Tracy K, Dibling BC, Spike BT, Knabb JR, Schumacker P, Macleod KF. BNIP3 is an RB/E2F target gene required for hypoxia-induced autophagy. Mol Cell Biol 2007; 27(17):6229-42.

219. Shaw J, Yurkova N, Zhang T, et al. Antagonism of E2F-1 regulated Bnip3 transcription by NF-kappaB is essential for basal cell survival. Proc Natl Acad Sci U S A 2008; 105(52):20734-9.

220. Shaw J, Zhang T, Rzeszutek M, et al. Transcriptional silencing of the death gene BNIP3 by cooperative action of NF-kappaB and histone deacetylase 1 in ventricular myocytes. Circ Res 2006; 99(12):1347-54.

221. Mahon PC, Baril P, Bhakta V, et al. S100A4 contributes to the suppression of BNIP3 expression, chemoresistance, and inhibition of apoptosis in pancreatic cancer. Cancer Res 2007; 67(14):6786-95.

222. Farrall AL, Whitelaw ML. The HIF1alpha-inducible pro-cell death gene BNIP3 is a novel target of SIM2s repression through cross-talk on the hypoxia response element. Oncogene 2009; 28(41):3671-80.

223. Okami J, Simeone DM, Logsdon CD. Silencing of the hypoxia-inducible cell death protein BNIP3 in pancreatic cancer. Cancer Res 2004; 64(15):5338-46.

224. Bacon AL, Fox S, Turley H, Harris AL. Selective silencing of the hypoxia-inducible factor 1 target gene BNIP3 by histone deacetylation and methylation in colorectal cancer. Oncogene 2007; 26(1):132-41.

225. Murai M, Toyota M, Satoh A, et al. Aberrant DNA methylation associated with silencing BNIP3 gene expression in haematopoietic tumours. Br J Cancer 2005; 92(6):1165-72.

226. Rogers S, Wells R, Rechsteiner M. Amino acid sequences common to rapidly degraded proteins: The PEST hypothesis. Science 1986; 234(4774):364-8.

227. Mellor HR, Rouschop KM, Wigfield SM, Wouters BG, Harris AL. Synchronised phosphorylation of BNIP3, bcl-2 and bcl-xL in response to microtubule-active drugs is JNK-independent and requires a mitotic kinase. Biochem Pharmacol 2010; 79(11):1562-72.

228. Manka D, Millhorn DE. A potential molecular link between aerobic glycolysis and cancer. Cell Cycle 2006; 5(4):343-4.

229. Graham RM, Thompson JW, Wei J, Bishopric NH, Webster KA. Regulation of Bnip3 death pathways by calcium, phosphorylation, and hypoxia-reoxygenation. Antioxid Redox Signal 2007; 9(9):1309-15.

230. Burton TR, Eisenstat DD, Gibson SB. BNIP3 (bcl-2 19 kDa interacting protein) acts as transcriptional repressor of apoptosis-inducing factor expression preventing cell death in human malignant gliomas. J Neurosci 2009; 29(13):4189-99.

231. Kamer I, Sarig R, Zaltsman Y, et al. Proapoptotic BID is an ATM effector in the DNA-damage response. Cell 2005; 122(4):593-603.

232. Massaad CA, Portier BP, Taglialatela G. Inhibition of transcription factor activity by nuclear compartment-associated bcl-2. J Biol Chem 2004; 279(52):54470-8.

233. Burton TR, Henson ES, Baijal P, Eisenstat DD, Gibson SB. The pro-cell death bcl-2 family member, BNIP3, is localized to the nucleus of human glial cells: Implications for glioblastoma multiforme tumor cell survival under hypoxia. Int J Cancer 2006; 118(7):1660-9.

234. Metukuri MR, Beer-Stolz D, Namas RA, et al. Expression and subcellular localization of BNIP3 in hypoxic hepatocytes and liver stress. Am J Physiol Gastrointest Liver Physiol 2009; 296(3):G499-509.

235. Schmidt-Kastner R, Aguirre-Chen C, Kietzmann T, Saul I, Busto R, Ginsberg MD. Nuclear localization of the hypoxia-regulated pro-apoptotic protein BNIP3 after global brain ischemia in the rat hippocampus. Brain Res 2004; 1001(1-2):133-42.

236. Guo K, Searfoss G, Krolikowski D, et al. Hypoxia induces the expression of the pro-apoptotic gene BNIP3. Cell Death Differ 2001; 8(4):367-76.

237. Kubasiak LA, Hernandez OM, Bishopric NH, Webster KA. Hypoxia and acidosis activate cardiac myocyte death through the bcl-2 family protein BNIP3. Proc Natl Acad Sci U S A 2002; 99(20):12825-30.

238. Walls KC, Ghosh AP, Ballestas ME, Klocke BJ, Roth KA. Bcl-2/Adenovirus E1B 19-kd interacting protein 3 (BNIP3) regulates hypoxia-induced neural precursor cell death. J Neuropathol Exp Neurol 2009; 68(12):1326-38.

239. Papandreou I, Krishna C, Kaper F, Cai D, Giaccia AJ, Denko NC. Anoxia is necessary for tumor cell toxicity caused by a low-oxygen environment. Cancer Res 2005; 65(8):3171-8.

240. Diwan A, Krenz M, Syed FM, et al. Inhibition of ischemic cardiomyocyte apoptosis through targeted ablation of Bnip3 restrains postinfarction remodeling in mice. J Clin Invest 2007; 117(10):2825-33.

241. Kim JY, Cho JJ, Ha J, Park JH. The carboxy terminal C-tail of BNip3 is crucial in induction of mitochondrial permeability transition in isolated mitochondria. Arch Biochem Biophys 2002; 398(2):147-52.

242. Regula KM, Ens K, Kirshenbaum LA. Inducible expression of BNIP3 provokes mitochondrial defects and hypoxia-mediated cell death of ventricular myocytes. Circ Res 2002; 91(3):226-31.

243. Zhao ST, Chen M, Li SJ, et al. Mitochondrial BNIP3 upregulation precedes endonuclease G translocation in hippocampal neuronal death following oxygen-glucose deprivation. BMC Neurosci 2009; 10:113.

244. Zhang Z, Yang X, Zhang S, Ma X, Kong J. BNIP3 upregulation and EndoG translocation in delayed neuronal death in stroke and in hypoxia. Stroke 2007; 38(5):1606-13.

245. Guo K, Searfoss G, Krolikowski D, et al. Hypoxia induces the expression of the pro-apoptotic gene BNIP3. Cell Death Differ 2001; 8(4):367-76.

246. Wan J, Martinvalet D, Ji X, et al. The bcl-2 family pro-apoptotic molecule, BNIP3 regulates activation-induced cell death of effector cytotoxic T lymphocytes. Immunology 2003; 110(1):10-7.

247. Lamy L, Ticchioni M, Rouquette-Jazdanian AK, et al. CD47 and the 19 kDa interacting protein-3 (BNIP3) in T cell apoptosis. J Biol Chem 2003; 278(26):23915-21.

248. Kubli DA, Ycaza JE, Gustafsson AB. Bnip3 mediates mitochondrial dysfunction and cell death through bax and bak. Biochem J 2007; 405(3):407-15.

249. Cao W, Liu N, Tang S, et al. Acetyl-coenzyme A acyltransferase 2 attenuates the apoptotic effects of BNIP3 in two human cell lines. Biochim Biophys Acta 2008; 1780(6):873-80.

250. Landes T, Emorine LJ, Courilleau D, Rojo M, Belenguer P, Arnaune-Pelloquin L. The BH3-only Bnip3 binds to the dynamin Opa1 to promote mitochondrial fragmentation and apoptosis by distinct mechanisms. EMBO Rep 2010.

251. Zhang L, Li L, Leavesley HW, Zhang X, Borowitz JL, Isom GE. Cyanide-induced apoptosis of dopaminergic cells is promoted by BNIP3 and bax modulation of endoplasmic reticulum-mitochondrial Ca2+ levels. J Pharmacol Exp Ther 2010; 332(1):97-105.

252. Kammouni W, Wong K, Ma G, Firestein GS, Gibson SB, El-Gabalawy HS. Regulation of apoptosis in fibroblast-like synoviocytes by the hypoxia-induced bcl-2 family member bcl-2/adenovirus E1B 19-kd protein-interacting protein 3. Arthritis Rheum 2007; 56(9):2854-63.

253. Carneiro LA, Travassos LH, Soares F, et al. Shigella induces mitochondrial dysfunction and cell death in nonmyleoid cells. Cell Host Microbe 2009; 5(2):123-36.

254. Daido S, Kanzawa T, Yamamoto A, Takeuchi H, Kondo Y, Kondo S. Pivotal role of the cell death factor BNIP3 in ceramide-induced autophagic cell death in malignant glioma cells. Cancer Res 2004; 64(12):4286-93.

255. Byun YJ, Kim SK, Kim YM, Chae GT, Jeong SW, Lee SB. Hydrogen peroxide induces autophagic cell death in C6 glioma cells via BNIP3-mediated suppression of the mTOR pathway. Neurosci Lett 2009; 461(2):131-5.

256. Papandreou I, Lim AL, Laderoute K, Denko NC. Hypoxia signals autophagy in tumor cells via AMPK activity, independent of HIF-1, BNIP3, and BNIP3L. Cell Death Differ 2008; 15(10):1572-81.

257. Zhang H, Bosch-Marce M, Shimoda LA, et al. Mitochondrial autophagy is an HIF-1-dependent adaptive metabolic response to hypoxia. J Biol Chem 2008; 283(16):10892-903.

258. Oberstein A, Jeffrey PD, Shi Y. Crystal structure of the bcl-XL-beclin 1 peptide complex: Beclin 1 is a novel BH3-only protein. J Biol Chem 2007; 282(17):13123-32.

259. Chen G, Ray R, Dubik D, et al. The E1B 19K/Bcl-2-binding protein Nip3 is a dimeric mitochondrial protein that activates apoptosis. J Exp Med 1997; 186(12):1975-83.

260. Scherz-Shouval R, Shvets E, Fass E, Shorer H, Gil L, Elazar Z. Reactive oxygen species are essential for autophagy and specifically regulate the activity of Atg4. EMBO J 2007; 26(7):1749-60.

261. Scherz-Shouval R, Elazar Z. ROS, mitochondria and the regulation of autophagy. Trends Cell Biol 2007; 17(9):422-7.

262. Band M, Joel A, Hernandez A, Avivi A. Hypoxia-induced BNIP3 expression and mitophagy: In vivo comparison of the rat and the hypoxia-tolerant mole rat, spalax ehrenbergi. FASEB J 2009; 23(7):2327-35.

263. Li Y, Wang Y, Kim E, et al. Bnip3 mediates the hypoxia-induced inhibition on mammalian target of rapamycin by interacting with rheb. J Biol Chem 2007; 282(49):35803-13.

264. Lemaster JJ, Thurman RG. Hypoxia and reperfusion injury to liver. Prog Liver Dis 1993; 11:85-114.

265. McCloskey CA, Kameneva MV, Uryash A, Gallo DJ, Billiar TR. Tissue hypoxia activates JNK in the liver during hemorrhagic shock. Shock 2004; 22(4):380-6.

266. Copple BL, Rondelli CM, Maddox JF, Hoglen NC, Ganey PE, Roth RA. Modes of cell death in rat liver after monocrotaline exposure. Toxicol Sci 2004; 77(1):172-82.

267. Didenko VV, Ngo H, Minchew CL, Boudreaux DJ, Widmayer MA, Baskin DS. Caspase-3-dependent and -independent apoptosis in focal brain ischemia. Mol Med 2002; 8(7):347-52.

268. Dijkhuizen RM, Knollema S, van der Worp HB, et al. Dynamics of cerebral tissue injury and perfusion after temporary hypoxia-ischemia in the rat: Evidence for region-specific sensitivity and delayed damage. Stroke 1998; 29(3):695-704.

269. Althaus J, Bernaudin M, Petit E, Toutain J, Touzani O, Rami A. Expression of the gene encoding the pro-apoptotic BNIP3 protein and stimulation of hypoxia-inducible factor-1alpha (HIF-1alpha) protein following focal cerebral ischemia in rats. Neurochem Int 2006; 48(8):687-95.

270. Zhang Z, Yang X, Zhang S, Ma X, Kong J. BNIP3 upregulation and EndoG translocation in delayed neuronal death in stroke and in hypoxia. Stroke 2007; 38(5):1606-13.

271. Zhang S, Zhang Z, Sandhu G, et al. Evidence of oxidative stress-induced BNIP3 expression in amyloid beta neurotoxicity. Brain Res 2007; 1138:221-30.

272. Yao M, Nguyen TV, Pike CJ. Beta-amyloid-induced neuronal apoptosis involves c-jun N-terminal kinase-dependent downregulation of bcl-w. J Neurosci 2005; 25(5):1149-58.

273. Dorn GW,2nd, Kirshenbaum LA. Cardiac reanimation: Targeting cardiomyocyte death by BNIP3 and NIX/BNIP3L. Oncogene 2008; 27 Suppl 1:S158-67.

274. Jennings RB, Steenbergen C,Jr, Reimer KA. Myocardial ischemia and reperfusion. Monogr Pathol 1995; 37:47-80.

275. Graham RM, Frazier DP, Thompson JW, et al. A unique pathway of cardiac myocyte death caused by hypoxia-acidosis. J Exp Biol 2004; 207(Pt 18):3189-200.

276. Pitts KR, Derry JM, Kerkof K, Lawrence WA, Toombs CF. Differentially regulated functional gene clusters identified during ischemia and reperfusion in isolated cardiac myocytes using coverslip hypoxia. J Pharmacol Toxicol Methods 2008; 57(1):42-51.

277. Leo C, Horn LC, Hockel M. Hypoxia and expression of the proapoptotic regulator BNIP3 in cervical cancer. Int J Gynecol Cancer 2006; 16(3):1314-20.

278. Sowter HM, Ferguson M, Pym C, et al. Expression of the cell death genes BNip3 and NIX in ductal carcinoma in situ of the breast; correlation of BNip3 levels with necrosis and grade. J Pathol 2003; 201(4):573-80.

279. Koukourakis MI, Giatromanolaki A, Polychronidis A, et al. Endogenous markers of hypoxia/anaerobic metabolism and anemia in primary colorectal cancer. Cancer Sci 2006; 97(7):582-8.

280. Lukashova-v Zangen I, Kneitz S, Monoranu CM, et al. Ependymoma gene expression profiles associated with histological subtype, proliferation, and patient survival. Acta Neuropathol 2007; 113(3):325-37.

281. Giatromanolaki A, Koukourakis MI, Gatter KC, Harris AL, Sivridis E. BNIP3 expression in endometrial cancer relates to active hypoxia inducible factor 1alpha pathway and prognosis. J Clin Pathol 2008; 61(2):217-20.

282. Giatromanolaki A, Koukourakis MI, Sowter HM, et al. BNIP3 expression is linked with hypoxia-regulated protein expression and with poor prognosis in non-small cell lung cancer. Clin Cancer Res 2004; 10(16):5566-71.

283. Ishida M, Sunamura M, Furukawa T, et al. Elucidation of the relationship of BNIP3 expression to gemcitabine chemosensitivity and prognosis. World J Gastroenterol 2007; 13(34):4593-7.

284. Calvisi DF, Ladu S, Gorden A, et al. Mechanistic and prognostic significance of aberrant methylation in the molecular pathogenesis of human hepatocellular carcinoma. J Clin Invest 2007; 117(9):2713-22.

285. Erkan M, Kleeff J, Esposito I, et al. Loss of BNIP3 expression is a late event in pancreatic cancer contributing to chemoresistance and worsened prognosis. Oncogene 2005; 24(27):4421-32.

286. Akada M, Crnogorac-Jurcevic T, Lattimore S, et al. Intrinsic chemoresistance to gemcitabine is associated with decreased expression of BNIP3 in pancreatic cancer. Clin Cancer Res 2005; 11(8):3094-101.

287. Murai M, Toyota M, Satoh A, et al. Aberrant DNA methylation associated with silencing BNIP3 gene expression in haematopoietic tumours. Br J Cancer 2005; 92(6):1165-72.

288. Murai M, Toyota M, Suzuki H, et al. Aberrant methylation and silencing of the BNIP3 gene in colorectal and gastric cancer. Clin Cancer Res 2005; 11(3):1021-7.

289. Okami J, Simeone DM, Logsdon CD. Silencing of the hypoxia-inducible cell death protein BNIP3 in pancreatic cancer. Cancer Res 2004; 64(15):5338-46.

290. Heller G, Schmidt WM, Ziegler B, et al. Genome-wide transcriptional response to 5-aza-2'-deoxycytidine and trichostatin a in multiple myeloma cells. Cancer Res 2008; 68(1):44-54.

291. Abe T, Toyota M, Suzuki H, et al. Upregulation of BNIP3 by 5-aza-2'-deoxycytidine sensitizes pancreatic cancer cells to hypoxia-mediated cell death. J Gastroenterol 2005; 40(5):504-10.

292. Tang H, Liu YJ, Liu M, Li X. Establishment and gene analysis of an oxaliplatin-resistant colon cancer cell line THC8307/L-OHP. Anticancer Drugs 2007; 18(6):633-9.

293. de Angelis PM, Fjell B, Kravik KL, et al. Molecular characterizations of derivatives of HCT116 colorectal cancer cells that are resistant to the chemotherapeutic agent 5-fluorouracil. Int J Oncol 2004; 24(5):1279-88.

294. Chang CP, Yang MC, Liu HS, Lin YS, Lei HY. Concanavalin A induces autophagy in hepatoma cells and has a therapeutic effect in a murine in situ hepatoma model. Hepatology 2007; 45(2):286-96.

295. Periyasamy-Thandavan S, Jackson WH, Samaddar JS, et al. Bortezomib blocks the catabolic process of autophagy via a cathepsin-dependent mechanism, affects endoplasmic reticulum stress and induces caspase-dependent cell death in antiestrogen-sensitive and resistant ER+ breast cancer cells. Autophagy 2010; 6(1):19-35.

296. Tan EY, Campo L, Han C, et al. BNIP3 as a progression marker in primary human breast cancer; opposing functions in in situ versus invasive cancer. Clin Cancer Res 2007; 13(2 Pt 1):467-74.

297. Itoh T, Itoh A, Pleasure D. Bcl-2-related protein family gene expression during oligodendroglial differentiation. J Neurochem 2003; 85(6):1500-12.

298. Sandau US, Handa RJ. Localization and developmental ontogeny of the pro-apoptotic Bnip3 mRNA in the postnatal rat cortex and hippocampus. Brain Res 2006; 1100(1):55-63.

299. Chen L, Fink T, Zhang XY, Ebbesen P, Zachar V. Quantitative transcriptional profiling of ATDC5 mouse progenitor cells during chondrogenesis. Differentiation 2005; 73(7):350-63.

300. Knowles HJ, Athanasou NA. Hypoxia-inducible factor is expressed in giant cell tumour of bone and mediates paracrine effects of hypoxia on monocyte-osteoclast differentiation via induction of VEGF. J Pathol 2008; 215(1):56-66.

301. Chen G, Cizeau J, Vande Velde C, et al. Nix and Nip3 form a subfamily of pro-apoptotic mitochondrial proteins. J Biol Chem 1999; 274(1):7-10.

302. Galvez AS, Brunskill EW, Marreez Y, et al. Distinct pathways regulate proapoptotic nix and BNip3 in cardiac stress. J Biol Chem 2006; 281(3):1442-8.

303. Sowter HM, Ratcliffe PJ, Watson P, Greenberg AH, Harris AL. HIF-1-dependent regulation of hypoxic induction of the cell death factors BNIP3 and NIX in human tumors. Cancer Res 2001; 61(18):6669-73.

304. Sowter HM, Ferguson M, Pym C, et al. Expression of the cell death genes BNip3 and NIX in ductal carcinoma in situ of the breast; correlation of BNip3 levels with necrosis and grade. J Pathol 2003; 201(4):573-80.

305. Kabeya Y, Mizushima N, Ueno T, et al. LC3, a mammalian homologue of yeast Apg8p, is localized in autophagosome membranes after processing. EMBO J 2000; 19(21):5720-8.

306. Jensen RL. Brain tumor hypoxia: Tumorigenesis, angiogenesis, imaging, pseudoprogression, and as a therapeutic target. J Neurooncol 2009; 92(3):317-35.

307. Lundgren K, Holm C, Landberg G. Hypoxia and breast cancer: Prognostic and therapeutic implications. Cell Mol Life Sci 2007; 64(24):3233-47.

308. Villeneuve DJ, Hembruff SL, Veitch Z, Cecchetto M, Dew WA, Parissenti AM. cDNA microarray analysis of isogenic paclitaxel- and doxorubicin-resistant breast tumor cell lines reveals distinct drug-specific genetic signatures of resistance. Breast Cancer Res Treat 2006; 96(1):17-39.

309. Rothe G, Valet G. Flow cytometric analysis of respiratory burst activity in phagocytes with hydroethidine and 2',7'-dichlorofluorescin. J Leukoc Biol 1990; 47(5):440-8.

310. Chen Y, McMillan-Ward E, Kong J, Israels SJ, Gibson SB. Oxidative stress induces autophagic cell death independent of apoptosis in transformed and cancer cells. Cell Death Differ 2008; 15(1):171-82.

311. Holt PS, Buckley S, Deloach JR. Detection of the lethal effects of T-2 mycotoxin on cells using a rapid colorimetric viability assay. Toxicol Lett 1987; 39(2-3):301-12.

312. Scaffidi P, Misteli T, Bianchi ME. Release of chromatin protein HMGB1 by necrotic cells triggers inflammation. Nature 2002; 418(6894):191-5.

313. Nicoletti I, Migliorati G, Pagliacci MC, Grignani F, Riccardi C. A rapid and simple method for measuring thymocyte apoptosis by propidium iodide staining and flow cytometry. J Immunol Methods 1991; 139(2):271-9.

314. Wyllie AH, Beattie GJ, Hargreaves AD. Chromatin changes in apoptosis. Histochem J 1981; 13(4):681-92.

315. Klionsky DJ, Abeliovich H, Agostinis P, et al. Guidelines for the use and interpretation of assays for monitoring autophagy in higher eukaryotes. Autophagy 2008; 4(2):151-75.

316. Paglin S, Hollister T, Delohery T, et al. A novel response of cancer cells to radiation involves autophagy and formation of acidic vesicles. Cancer Res 2001; 61(2):439-44.

317. Gratzner HG. Monoclonal antibody to 5-bromo- and 5-iododeoxyuridine: A new reagent for detection of DNA replication. Science 1982; 218(4571):474-5.

318. Krishan A. Rapid flow cytofluorometric analysis of mammalian cell cycle by propidium iodide staining. J Cell Biol 1975; 66(1):188-93.

319. Xu Y, Kim SO, Li Y, Han J. Autophagy contributes to caspase-independent macrophage cell death. J Biol Chem 2006.

320. Yu L, Alva A, Su H, et al. Regulation of an ATG7-beclin 1 program of autophagic cell death by caspase-8. Science 2004; 304(5676):1500-2.

321. Mizushima N, Yamamoto A, Matsui M, Yoshimori T, Ohsumi Y. In vivo analysis of autophagy in response to nutrient starvation using transgenic mice expressing a fluorescent autophagosome marker. Mol Biol Cell 2004; 15(3):1101-11.

322. Kristian T. Metabolic stages, mitochondria and calcium in hypoxic/ischemic brain damage. Cell Calcium 2004; 36(3-4):221-33.

323. Paglin S, Hollister T, Delohery T, et al. A novel response of cancer cells to radiation involves autophagy and formation of acidic vesicles. Cancer Res 2001; 61(2):439-44.

324. Seglen PO, Gordon PB. 3-methyladenine: Specific inhibitor of autophagic/lysosomal protein degradation in isolated rat hepatocytes. Proc Natl Acad Sci U S A 1982; 79(6):1889-92.

325. Wu YT, Tan HL, Shui G, et al. Dual role of 3-methyladenine in modulation of autophagy via different temporal patterns of inhibition on class I and III phosphoinositide 3-kinase. J Biol Chem 2010; 285(14):10850-61.

326. Vandenabeele P, Vanden Berghe T, Festjens N. Caspase inhibitors promote alternative cell death pathways. Sci STKE 2006; 2006(358):pe44.

327. Mizushima N, Yamamoto A, Hatano M, et al. Dissection of autophagosome formation using Apg5-deficient mouse embryonic stem cells. J Cell Biol 2001; 152(4):657-68.

328. Gozuacik D, Kimchi A. Autophagy as a cell death and tumor suppressor mechanism. Oncogene 2004; 23(16):2891-906.

329. Mizumoto K, Rothman RJ, Farber JL. Programmed cell death (apoptosis) of mouse fibroblasts is induced by the topoisomerase II inhibitor etoposide. Mol Pharmacol 1994; 46(5):890-5.

330. Fillingham J, Keogh MC, Krogan NJ. GammaH2AX and its role in DNA double-strand break repair. Biochem Cell Biol 2006; 84(4):568-77.

331. Kuma A, Matsui M, Mizushima N. LC3, an autophagosome marker, can be incorporated into protein aggregates independent of autophagy: Caution in the interpretation of LC3 localization. Autophagy 2007; 3(4):323-8.

332. Lee H, Paik SG. Regulation of BNIP3 in normal and cancer cells. Mol Cells 2006; 21(1):1-6.

333. Djeu JY, Wei S. Clusterin and chemoresistance. Adv Cancer Res 2009; 105:77-92.

334. Pegg AE. Spermidine/spermine-N(1)-acetyltransferase: A key metabolic regulator. Am J Physiol Endocrinol Metab 2008; 294(6):E995-1010.

335. Kim K, Ryu JH, Park JW, Kim MS, Chun YS. Induction of a SSAT isoform in response to hypoxia or iron deficiency and its protective effects on cell death. Biochem Biophys Res Commun 2005; 331(1):78-85.

336. Giffard RG, Xu L, Zhao H, et al. Chaperones, protein aggregation, and brain protection from hypoxic/ischemic injury. J Exp Biol 2004; 207(Pt 18):3213-20.

337. Azad P, Haddad GG. Survival in acute and severe low o environment: Use of a genetic model system. Ann N Y Acad Sci 2009; 1177:39-47.

338. Azad MB, Chen Y, Henson ES, et al. Hypoxia induces autophagic cell death in apoptosis-competent cells through a mechanism involving BNIP3. Autophagy 2008; 4(2):195-204.

339. Adhami F, Liao G, Morozov YM, et al. Cerebral ischemia-hypoxia induces intravascular coagulation and autophagy. Am J Pathol 2006; 169(2):566-83.

340. Mazure NM, Pouyssegur J. Hypoxia-induced autophagy: Cell death or cell survival? Curr Opin Cell Biol 2010; 22(2):177-80.

341. Rouschop KM, Ramaekers CH, Schaaf MB, et al. Autophagy is required during cycling hypoxia to lower production of reactive oxygen species. Radiother Oncol 2009; 92(3):411-6.

342. Jiang M, Liu K, Luo J, Dong Z. Autophagy is a renoprotective mechanism during in vitro hypoxia and in vivo ischemia-reperfusion injury. Am J Pathol 2010; 176(3):1181-92.

343. Uchiyama Y, Koike M, Shibata M. Autophagic neuron death in neonatal brain ischemia/hypoxia. Autophagy 2008; 4(4):404-8.

344. Rouschop KM, van den Beucken T, Dubois L, et al. The unfolded protein response protects human tumor cells during hypoxia through regulation of the autophagy genes MAP1LC3B and ATG5. J Clin Invest 2010; 120(1):127-41.

345. Pursiheimo JP, Rantanen K, Heikkinen PT, Johansen T, Jaakkola PM. Hypoxia-activated autophagy accelerates degradation of SQSTM1/p62. Oncogene 2009; 28(3):334-44.

346. Papandreou I, Lim AL, Laderoute K, Denko NC. Hypoxia signals autophagy in tumor cells via AMPK activity, independent of HIF-1, BNIP3, and BNIP3L. Cell Death Differ 2008; 15(10):1572-81.

347. Lee CY, Clough EA, Yellon P, Teslovich TM, Stephan DA, Baehrecke EH. Genome-wide analyses of steroid- and radiation-triggered programmed cell death in drosophila. Curr Biol 2003; 13(4):350-7.

348. Gorski SM, Chittaranjan S, Pleasance ED, et al. A SAGE approach to discovery of genes involved in autophagic cell death. Curr Biol 2003; 13(4):358-63.

349. Hara T, Nakamura K, Matsui M, et al. Suppression of basal autophagy in neural cells causes neurodegenerative disease in mice. Nature 2006; 441(7095):885-9.

350. Qu X, Yu J, Bhagat G, et al. Promotion of tumorigenesis by heterozygous disruption of the beclin 1 autophagy gene. J Clin Invest 2003; 112(12):1809-20.

351. Hait WN, Jin S, Yang JM. A matter of life or death (or both): Understanding autophagy in cancer. Clin Cancer Res 2006; 12(7 Pt 1):1961-5.

352. Bacon AL, Harris AL. Hypoxia-inducible factors and hypoxic cell death in tumour physiology. Ann Med 2004; 36(7):530-9.

353. Bellot G, Garcia-Medina R, Gounon P, et al. Hypoxia-induced autophagy is mediated through hypoxia-inducible factor induction of BNIP3 and BNIP3L via their BH3 domains. Mol Cell Biol 2009; 29(10):2570-81.

354. Zeng X, Kinsella TJ. BNIP3 is essential for mediating 6-thioguanine- and 5-fluorouracil-induced autophagy following DNA mismatch repair processing. Cell Res 2010; 20(6):665-75.

355. Wilkinson S, O'Prey J, Fricker M, Ryan KM. Hypoxia-selective macroautophagy and cell survival signaled by autocrine PDGFR activity. Genes Dev 2009; 23(11):1283-8.

356. Tracy K, Macleod KF. Regulation of mitochondrial integrity, autophagy and cell survival by BNIP3. Autophagy 2007; 3(6):616-9.

357. Trougakos IP, Gonos ES. Chapter 9: Oxidative stress in malignant progression: The role of clusterin, a sensitive cellular biosensor of free radicals. Adv Cancer Res 2009; 104:171-210.

358. Gupta SC, Sharma A, Mishra M, Mishra RK, Chowdhuri DK. Heat shock proteins in toxicology: How close and how far? Life Sci 2010; 86(11-12):377-84.

359. Ferrer I, Tortosa A, Blanco R, et al. Naturally occurring cell death in the developing cerebral cortex of the rat. evidence of apoptosis-associated internucleosomal DNA fragmentation. Neurosci Lett 1994; 182(1):77-9.

360. Spreafico R, Frassoni C, Arcelli P, Selvaggio M, De Biasi S. In situ labeling of apoptotic cell death in the cerebral cortex and thalamus of rats during development. J Comp Neurol 1995; 363(2):281-95.

361. Rogers DC, Fisher EM, Brown SD, Peters J, Hunter AJ, Martin JE. Behavioral and functional analysis of mouse phenotype: SHIRPA, a proposed protocol for comprehensive phenotype assessment. Mamm Genome 1997; 8(10):711-3.

362. Maiuri MC, Galluzzi L, Morselli E, Kepp O, Malik SA, Kroemer G. Autophagy regulation by p53. Curr Opin Cell Biol 2010; 22(2):181-5.

363. Jankowsky JL, Savonenko A, Schilling G, Wang J, Xu G, Borchelt DR. Transgenic mouse models of neurodegenerative disease: Opportunities for therapeutic development. Curr Neurol Neurosci Rep 2002; 2(5):457-64.

364. Fomchenko EI, Holland EC. Mouse models of brain tumors and their applications in preclinical trials. Clin Cancer Res 2006; 12(18):5288-97.

365. Reilly KM, Loisel DA, Bronson RT, McLaughlin ME, Jacks T. Nf1; Trp53 mutant mice develop glioblastoma with evidence of strain-specific effects. Nat Genet 2000; 26(1):109-13.

366. Uhrbom L, Hesselager G, Nister M, Westermark B. Induction of brain tumors in mice using a recombinant platelet-derived growth factor B-chain retrovirus. Cancer Res 1998; 58(23):5275-9.